BINDING STUDIES OF ACHIRAL AND CHIRAL METAL COMPLEXES WITH CT DNA AND NUCLEOTIDES

ABSTRACT

OF THE

THESIS

SUBMITTED FOR THE AWARD OF DEGREE OF

Doctor of Philosophy

IN

CHEMISTRY

BY

FATIMA SAYEED

Under the Supervision of

Dr. (Mrs.) Farukh Arjmand

DEPARTMENT OF CHEMISTRY
ALIGARH MUSLIM UNIVERSITY
ALIGARH (INDIA)

2010

Abstract

Abstract

There is a considerable interest in small molecules that bind to DNA because of their potential use in chemotherapeutics, regulators of gene expression and tools for molecular biology and nanotechnology. Transition metal complexes, which provide high stability, structural versatility and unique spectroscopic and redox properties, are explored largely for DNA binding studies. These metal complexes are capable of binding to DNA by multitude of interactions via, DNA intercalation, DNA groove binding or external electrostatic or covalent linkage and cleavage of DNA by virtue of their intrinsic chemical, electrochemical or photochemical reactivities. Metal-nucleic acid chemistry has gained momentum after Rosenberg's discovery of cisplatin- cis-diamminedichloroplatinum(II) and its subsequent clinical use for treating solid tumors (testicular and ovarian cancers). DNA has been identified as the possible primary molecular target of both cisplatin and other metal based drugs. The clinical use of cisplatin, however, is severely limited by its toxic side effects, its limited applicability to relatively narrow range of tumors and acquired or inherent resistance. This has spurred research for the development of new non-platinum metal-based anticancer agents which are more efficacious, less toxic and can overcome resistance. Therefore, alternate strategies based on different metal ions, ligand functionality, shape or geometric requirement and stereoselectivity were opted to design these new cancer drug therapeutics. In the majority of complexes studied, the metal usually serves as the redox center and the ligand is responsible for DNA recognition, nevertheless metals are also used as building blocks for well defined, three dimensional constructs. The modular approach of optimising the design by the use of coordinating ligands, which themselves are active pharmacophores, offers to fine-tune metals properties and in this manner tailored

multifunctional ligand can assist to achieve target selectivity/improved solubility. The mechanism of cytotoxic action which is related to DNA binding affinity can also vary accordingly, as the biological activity is strongly dependent on structure-activity relationship. This optimization based on shape selectivity is introduced by chiral ligands which interact with DNA- an inherently chiral biomolecule in a site-specific manner. Furthermore, chirality may enhance the pharmacological behaviour of complexes, by adopting a specific conformation; thereby improving the DNA-binding affinity to provide recognition elements in the metal nucleobase recognition process. The interaction of metal complexes with nucleobases and/or nucleotides is very well established, and is now known to be the basis of antitumor drug action. The metal complexes, which are favoured as effective drug candidates are molecules that; damage DNA; block DNA synthesis indirectly through inhibition of nucleic acid precursor biosynthesis; disrupt hormonal stimulation of cell growth; must recognize nucleic acid particularly in sequence specific fashion and then bind to DNA in a way that alters their function.

The characterization of DNA recognition by aromatic metal complexes has been substantially aided by studying the DNA cleavage activity. Literature reveals that double strand breaks in duplex DNA are thought to be more significant sources of cell lethality as compared to single strand breaks, as they are less readily repaired by DNA repair mechanism. A number of copper(II) complexes are exceptional candidates for mediation of strand scission of duplex DNA. The metal complex DNA interaction has been investigated using a host of biophysical methods like electronics absorption, fluorescence spectroscopy, cyclic voltammetry, circular dichroic studies, NMR dynamics with nucleotides, hydrodynamic measurements

such as viscosity and cleavage reaction have been assayed using agarose gel electrophoresis.

The present work stems from our interest to design DNA-binding drug candidates which can be explored as antitumor chemotherapeutics. In view of this rationale, we present in this thesis four series of novel metal-based drug candidates employing *de novo* synthetic strategy (by the variation of ligand scaffold and the metal ions: transition, copper(II)/zinc(II) and non-transition, organotin(IV) metal ions). Their *in vitro* binding studies with CT-DNA and nucleotides viz 5′-GMP, 5′-TMP, 5′-AMP, 5′-CMP were carried out to evaluate their DNA binding potential and thereby, their therapeutic potency.

The development of new heterobimetallic complexes $[C_6H_{24}N_4O_6CuSn_2Cl_4]Cl_2$ and $[C_6H_{24}N_4O_6ZnSn_2Cl_4]Cl_2$ from their monometallic analogues $[C_6H_{20}N_4O_2Cu]Cl_2$ and $[C_6H_{20}N_4O_2Zn]Cl_2$, incorporating both transition {copper(II) and zinc(II)} and non-transition {tin(IV)} metal ions, were synthesized with the aim to synergize effects of two metal ions possessing preferential selectivity towards biomolecules. The heterobimetallic complexes show novelty due to dual binding modes in comparison to their monometallic analogues and thus exhibit greater binding propensity with DNA. These complexes were thoroughly characterized by spectroscopic (IR, ^{1}H, ^{13}C and ^{119}Sn NMR, EPR, UV-vis., ESI-MS) and analytical methods. The comparative interaction of monometallic complexes and their heterobimetallic analogues with CT-DNA in Tris-buffer were studied by various biophysical methods such as electronic absorption titration, fluorescence titration, cyclic voltammetry and viscosity measurements. To quantify the extent binding of complexes with DNA, the intrinsic binding constant K_b of complexes were determined, which follows the

order; $[C_6H_{24}N_4O_6ZnSn_2Cl_4]Cl_2$>$[C_6H_{24}N_4O_6CuSn_2Cl_4]Cl_2$>$[C_6H_{20}N_4O_2Zn]Cl_2$> $[C_6H_{20}N_4O_2Cu]Cl_2$, thus, revealing a pronounced DNA binding of the heterobimetallic complexes in comparison to their respective monometallic analogues. Furthermore, the interaction of transition metal ions of heterobimetallic complexes with 5'-GMP and 5'-TMP was ascertained by absorption titration of the heterobimetallic complexes with these nucleotides which clearly shows selective preference of 5'-GMP with the copper(II) complex while zinc(II) complex preferring selective interactions with 5'-TMP. The results of spectroscopic, viscometric and cyclic voltammetric studies of the heterobimetallic complexes with CT-DNA suggested electrostatic mode of binding with the phosphate backbone of DNA double helix. Heterobimetallic complexes $[C_6H_{24}N_4O_6CuSn_2Cl_4]Cl_2$ and $[C_6H_{24}N_4O_6ZnSn_2Cl_4]Cl_2$ when subjected to gel electrophoresis with supercoiled pBR322 DNA, demonstrate significant cleavage activity under physiologically relevant conditions.

As a means of further exploring the chiral preference of potential drug candidates, a new series of chiral modulated organotin antitumor drug (S)/(R)-$[C_{15}H_{21}NO_2Sn]$ and (S)/(R)-$[C_{10}H_{16}NOSnCl]$ derived from S- and R- enantiomers of [4-(2-hydroxy-1-phenylethylimino)pent-2-ol] and 2-amino-2-phenylethanol, respectively, were synthesized and characterized by various physicochemical and spectroscopic methods. Chiral modulation of the drug is responsible for its high binding affinity towards DNA (primary pharmacological target) as the efficacy of most of the chiral drugs is based on enantioselectivity. In order to establish the enantiomeric selectivity in drug-DNA binding, preliminary complex-DNA interaction studies employing UV-visible, fluorescence, circular dichroic and viscosity measurements were

elucidated revealing preference of binding for S-enantiomer of the complexes towards the ultimate drug target DNA. Nevertheless, both isomers displayed higher K_b values than that of cisplatin drug. Furthermore, interaction studies of complex (S)-[$C_{15}H_{21}NO_2Sn$] with 5'-GMP using ^{1}H and ^{31}P NMR again verifies electrostatic binding mode of the complex. The less effective cleavage pattern demonstrated by these complexes (S)-[$C_{15}H_{21}NO_2Sn$] and (S)-[$C_{10}H_{16}NOSnCl$] at micromolar concentration suggested a strand scission of plasmid pBR322 DNA from its supercoiled Form I to open circular Form II. Moreover, significant binding exhibited by the S-enantiomer of both the complexes [$C_{15}H_{21}NO_2Sn$] and [$C_{10}H_{16}NOSnCl$] in comparison to their R-enantiomeric analogues led us to investigate their *in vitro* antitumor potential via Sulforhodamine-B (SRB) assay to assess cellular proliferation against five human cell lines of different histological origin viz. Hop62 (human lung), DWD (human oral), K562 (human leukemia), DU145 (human prostrate) and MCF-7 (human breast). The complex (S)-[$C_{15}H_{21}NO_2Sn$] displayed remarkably pronounced and specific activity for K562 (Human leukemia) while complex (S)-[$C_{10}H_{16}NOSnCl$] exhibited significant activity towards Hop62 (Human lung), DWD (Human oral), DU145 (Human prostrate) and MCF-7 (Human breast).

Benzimidazoles are important subunits of biologically relevant ligands owing to their broad spectrum of biological and chemotherapeutic potential. The biological relevance of these heterocyclic aromatic building blocks is due to their structural similarity with nucleobases. Additionally, benzimidazole derived drugs have received much attention owing to the fact that benzimidazole residue is a constituent of Vitamin B_{12}, which supports their potential use as therapeutics. Thus, the benzimidazole ligand [$C_{16}H_{14}N_4O_2$] exhibits coordination mode with an oxygen

atom of alcohol group directed towards the metal ion and another –OH group with different molecular axis directed away from the metal center. These complexes, $[C_{18}H_{19}N_4O_2SnCl]$ and $[C_{52}H_{42}N_4O_2Sn_2]$ exhibit a pentacoordinate geometry while the complex $[C_{28}H_{23}N_4O_2SnCl]$ reveals hexacoordinated environment around the tin(IV) metal ions as evidenced by ^{119}Sn NMR studies.

The DNA binding ability of benzimidazole ligand $[C_{16}H_{14}N_4O_2]$ and their organotin(IV) complexes $[C_{18}H_{19}N_4O_2SnCl]$, $[C_{28}H_{23}N_4O_2SnCl]$ and $[C_{52}H_{42}N_4O_2Sn_2]$ were examined by means of different biophysical methods. The effects of varying substituents of organotin(IV) metal ions both aliphatic and aromatic was studied as it is well known that the biological effects of organotins depends on both the nature and number of organic groups bound to tin(IV) cation. The absorption titration of the complexes with CT-DNA reveal significant "hyperchromic" effect together with strong bathochromic shift of 4-5 nm which infer substantial binding of the complexes with CT-DNA. The intrinsic binding constant K_b values of the complexes $[C_{18}H_{19}N_4O_2SnCl]$, $[C_{28}H_{23}N_4O_2SnCl]$ and $[C_{52}H_{42}N_4O_2Sn_2]$ were found to be $2.16 \pm 0.04 \times 10^4$, $3.47 \pm 0.04 \times 10^4$ and $4.60 \pm 0.04 \times 10^3$ M^{-1} respectively, suggesting pronounced binding of complex $[C_{28}H_{23}N_4O_2SnCl]$ with DNA double helix, among the other complexes. These spectral changes reflect the different binding propensity of the complexes with CT-DNA due to different structural constraints and suggest an electrostatic binding of the complexes with partial intercalative interactions. Although the cationic core of tin(IV) lack base specificity in DNA binding, the hexacoordinated $[C_{28}H_{23}N_4O_2SnCl]$ with labile Cl group promotes higher binding of this complex towards DNA exhibiting a multifaceted binding of the complex probably due to

differential conformational effects induced by planar ligands towards CT-DNA. The mechanism of binding of the complexes was further ascertained by the interaction studies of these complexes with nucleotides (5′-GMP and 5′-TMP) using absorption spectroscopy suggesting a clear preference for 5′-GMP binding which was further authenticated by NMR (^{1}H and ^{31}P NMR) studies.

In addition to the importance of the metal ions in DNA-binding regime, the optimization and structure activity relationship of various ligands with CT-DNA plays an eminent role in governing the DNA binding interactions. In this context, novel Schiff base ligand derived from the condensation reaction of 2-amino-3-formylchromone with 2-amino-2-phenylethanol, [$C_{18}H_{16}N_2O_3$] was synthesized and characterized which involves combination element of ammine functionality and naturally occurring heterocyclic chromone, 4H-benzopyran-4-one compounds which modulates their biological activity to a large extent. Subsequently, their transition metal complexes [$C_{36}H_{34}N_4O_7Cu$]$(NO_3)_2$ and [$C_{36}H_{32}N_4O_6Zn$]$(NO_3)_2$ were also prepared. The DNA-binding studies of the ligand and complexes with CT-DNA by employing different biophysical methods. The UV-visible titrations of both ligand and complexes, exhibit concurrent increase in the absorption intensity with a red shift of 2-3 nm illustrate electrostatic association of the complexes with CT-DNA by subsequent stabilization of the DNA helical structure. This "hyperchromic effect" was explained on the basis of two phenomena via, electrostatic interactions primarily by groove binding and effect of the coordination geometry around the central metal ion on CT-DNA binding. In order to quantify the binding extent of both ligand and complexes, binding constant K_b values were determined which display a higher propensity of [$C_{36}H_{34}N_4O_7Cu$]$(NO_3)_2$ complex to bind with CT-DNA compared to

$[C_{36}H_{32}N_4O_6Zn](NO_3)_2$ complex. Moreover, the complexes exhibit higher binding for CT-DNA as compared to classical cisplatin drug. Furthermore, the absorption studies with mononucleotides (5′-GMP, 5′-TMP, 5′-AMP and 5′-CMP) were also monitored to examine the base specific interactions of the transition metal complexes $[C_{36}H_{34}N_4O_7Cu](NO_3)_2$ and $[C_{36}H_{32}N_4O_6Zn](NO_3)_2$. The extent of interaction of nucleotides with the complexes follows the order; 5′-GMP > 5′-TMP > 5′-CMP > 5′-AMP for $[C_{36}H_{34}N_4O_7Cu](NO_3)_2$ and 5′-TMP > 5′-GMP > 5′-CMP > 5′-AMP for the $[C_{36}H_{32}N_4O_6Zn](NO_3)_2$ complex thus, supporting a higher propensity of copper(II) complex towards 5′-GMP and for zinc(II) complex towards 5′-TMP. To further support these findings, the interaction of complex $[C_{36}H_{32}N_4O_6Zn](NO_3)_2$ with 5′-GMP and 5′-TMP, was ascertained by ^1H and ^{31}P NMR studies which confirms higher binding propensity of the complex towards 5′-TMP as compared to 5′-GMP. The binding studies performed using fluorescence, circular dichroism, viscosity further conclude a groove binding mechanism of the complexes towards DNA. The DNA cleavage activity of the complex $[C_{36}H_{34}N_4O_7Cu](NO_3)_2$ using agarose gel electrophoresis in presence of increasing concentration of complex shows an excellent cleavage revealing the conversion of supercoiled Form I to open circular Form II and then to linearized Form III. The cleavage of DNA by the complex in presence of activators follows the order; H_2O_2 > MPA >GSH >Asc. The mechanistic pathway followed by the complex in the presence of various radical scavengers such as NaN_3, DMSO, tert-butyl alcohol, NaN_3 and SOD suggested cleave of plasmid DNA via, oxidative mechanism. Furthermore, the major groove binding ability of the complex was ascertained on the basis of cleavage pattern of plasmid in presence of minor and major groove binding agents such as DAPI and methyl green.

BINDING STUDIES OF ACHIRAL AND CHIRAL METAL COMPLEXES WITH CT DNA AND NUCLEOTIDES

THESIS

SUBMITTED FOR THE AWARD OF THE DEGREE OF

Doctor of Philosophy

IN

CHEMISTRY

BY

FATIMA SAYEED

Under the Supervision of

Dr. (Mrs.) Farukh Arjmand

DEPARTMENT OF CHEMISTRY
ALIGARH MUSLIM UNIVERSITY
ALIGARH (INDIA)

2010

Dedicated

to my Beloved Parents

Dr. (Mrs.) Farukh Arjmand
Department of Chemistry
Aligarh Muslim University, Aligarh-202002, India

Phone No. 0571-2703893
E-mail: farukh_arjmand@yahoo.co.in

Certificate

The work embodied in this thesis entitled "**Binding studies of chiral and chiral metal complexes with CT DNA and nucleotides**" is the result of original researches carried out by **Mrs. Fatima Sayeed** under my supervision and is suitable for the award of Ph.D. degree.

Farukh Arjmand

Dr. (Mrs) Farukh Arjmand

CONTENTS

Acknowledgements

ACKNOWLEDGEMENTS

The whole period during which this experimental work was undertaken, was highly educative and in a way on the personal front, made me a better student to learn with more insight into the subject.

My gratitude and heartfelt emotions which cannot be expressed in words are for my most respected teacher and supervisor ***Dr. (Mrs.) Farukh Arjmand,*** Reader, Department of Chemistry. Her personal interest in every case and her ever helping and almost all the time presence in the Department to guide me deserve special mention. ***Dr. Arjmand*** personal and proper counseling in carving my personality and achieving some thing excellent turned me to a great extent. I will remain indebted to her for the rest of my life.

Prof. Sartaj Tabassum, Department of Chemistry, in spite of his very busy academic schedule guided me on every corner. It needs a special mention for his valuable suggestion, encouragement and constant cooperation during the whole course of my Ph.D. work.

At this juncture of my life I wish to thank my beloved parents and my husband Mohammad Abdullah for their inspiration and the innumerable sacrifices, the unmatched love, sincerity and for encouraging me to accomplish this task and provided me the self-confidence. I would also acknowledge the support and love of my dear brothers Rayhan Sayeed and Ahmad Omer for all the strength and support they have given me during my Ph.D. My special thanks are reserved for my most loved Ammi Jaani (grand mother) to whom I see as apostle of my life.

Also I would do injustice if I fail to mention here the support and care shown by all the lab mates and my friends for encouraging and sharing me on every crucial moment.

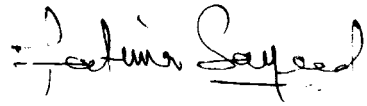

FATIMA SAYEED

Publications

Publications

1. Synthesis, characterization and DNA-binding studies of mono and heterobimetallic complexes Cu-Sn_2/Zn-Sn_2 and their DNA cleavage activity.

   Farukh Arjmand and ***Fatima Sayeed***, **J. Mol. Str.**, (2010), 965, 14.

2. *In vitro* DNA binding studies of chiral [4-(2-hydroxy-1-phenylethylimino)pent-2-ol]dimethyltin(IV) and 2-(chlorodimethylstannyloxy)-1-phenylethanamine: Antitumor activity of their S-enantiomer against human tumor cell lines.

   Farukh Arjmand, ***Fatima Sayeed*** and Sartaj Tabassum, **J. Inorg. Biochem.**, (2010), *(Manuscript under revision).*

3. *In vitro* binding studies of chiral organotin(IV) complexes of 1,2-bis-2(-1H-benzimidazol-2-yl)-1,2-ethanediol with CT-DNA and nucleotides (5′-GMP and 5′-TMP): Effect of the ancillary ligand on binding propensity.

   Farukh Arjmand, ***Fatima Sayeed***, **Eur. J. Med. Chem.**, *(Communicated).*

4. Synthesis of new chiral heterocyclic Schiff base modulated Cu(II)/Zn(II) complexes: Their comparative binding studies with CT-DNA and mononucleotides (5′-GMP, 5′-TMP, 5′-AMP and 5′-CMP) and cleavage activity.

   Farukh Arjmand and ***Fatima Sayeed,*** **Photochem. Photobiol. A: Chem.,** *(Communicated)*

5. *De novo* design of chiral organotin(IV) cancer drug candidate: Validation of enantiopreferential binding to molecular target DNA and 5′-GMP by UV-visible, fluorescence, ^{1}H and ^{31}P NMR.

   Farukh Arjmand, Girish Chandra Sharma, ***Fatima Sayeed,*** Mohd. Muddassir, Sartaj Tabassum, **Bioorg. Med. Chem.**, (2010), *(Communicated).*

Abstract

Abstract

There is a considerable interest in small molecules that bind to DNA because of their potential use in chemotherapeutics, regulators of gene expression and tools for molecular biology and nanotechnology. Transition metal complexes, which provide high stability, structural versatility and unique spectroscopic and redox properties. are explored largely for DNA binding studies. These metal complexes are capable of binding to DNA by multitude of interactions via, DNA intercalation, DNA groove binding or external electrostatic or covalent linkage and cleavage of DNA by virtue of their intrinsic chemical, electrochemical or photochemical reactivities. Metal-nucleic acid chemistry has gained momentum after Rosenberg's discovery of cisplatin- cis-diamminedichloroplatinum(II) and its subsequent clinical use for treating solid tumors (testicular and ovarian cancers). DNA has been identified as the possible primary molecular target of both cisplatin and other metal based drugs. The clinical use of cisplatin, however, is severely limited by its toxic side effects, its limited applicability to relatively narrow range of tumors and acquired or inherent resistance. This has spurred research for the development of new non-platinum metal-based anticancer agents which are more efficacious, less toxic and can overcome resistance. Therefore, alternate strategies based on different metal ions, ligand functionality, shape or geometric requirement and stereoselectivity were opted to design these new cancer drug therapeutics. In the majority of complexes studied, the metal usually serves as the redox center and the ligand is responsible for DNA recognition, nevertheless metals are also used as building blocks for well defined, three dimensional constructs. The modular approach of optimising the design by the use of coordinating ligands, which themselves are active pharmacophores, offers to fine-tune metals properties and in this manner tailored

multifunctional ligand can assist to achieve target selectivity/improved solubility. The mechanism of cytotoxic action which is related to DNA binding affinity can also vary accordingly, as the biological activity is strongly dependent on structure-activity relationship. This optimization based on shape selectivity is introduced by chiral ligands which interact with DNA- an inherently chiral biomolecule in a site-specific manner. Furthermore, chirality may enhance the pharmacological behaviour of complexes, by adopting a specific conformation; thereby improving the DNA-binding affinity to provide recognition elements in the metal nucleobase recognition process. The interaction of metal complexes with nucleobases and/or nucleotides is very well established, and is now known to be the basis of antitumor drug action. The metal complexes, which are favoured as effective drug candidates are molecules that; damage DNA; block DNA synthesis indirectly through inhibition of nucleic acid precursor biosynthesis; disrupt hormonal stimulation of cell growth; must recognize nucleic acid particularly in sequence specific fashion and then bind to DNA in a way that alters their function.

The characterization of DNA recognition by aromatic metal complexes has been substantially aided by studying the DNA cleavage activity. Literature reveals that double strand breaks in duplex DNA are thought to be more significant sources of cell lethality as compared to single strand breaks, as they are less readily repaired by DNA repair mechanism. A number of copper(II) complexes are exceptional candidates for mediation of strand scission of duplex DNA. The metal complex DNA interaction has been investigated using a host of biophysical methods like electronics absorption, fluorescence spectroscopy, cyclic voltammetry. circular dichroic studies, NMR dynamics with nucleotides, hydrodynamic measurements

such as viscosity and cleavage reaction have been assayed using agarose gel electrophoresis.

The present work stems from our interest to design DNA-binding drug candidates which can be explored as antitumor chemotherapeutics. In view of this rationale, we present in this thesis four series of novel metal-based drug candidates employing *de novo* synthetic strategy (by the variation of ligand scaffold and the metal ions; transition, copper(II)/zinc(II) and non-transition, organotin(IV) metal ions). Their *in vitro* binding studies with CT-DNA and nucleotides viz 5′-GMP, 5′-TMP, 5′-AMP, 5′-CMP were carried out to evaluate their DNA binding potential and thereby, their therapeutic potency.

The development of new heterobimetallic complexes $[C_6H_{24}N_4O_6CuSn_2Cl_4]Cl_2$ and $[C_6H_{24}N_4O_6ZnSn_2Cl_4]Cl_2$ from their monometallic analogues $[C_6H_{20}N_4O_2Cu]Cl_2$ and $[C_6H_{20}N_4O_2Zn]Cl_2$, incorporating both transition {copper(II) and zinc(II)} and non-transition {tin(IV)} metal ions, were synthesized with the aim to synergize effects of two metal ions possessing preferential selectivity towards biomolecules. The heterobimetallic complexes show novelty due to dual binding modes in comparison to their monometallic analogues and thus exhibit greater binding propensity with DNA. These complexes were thoroughly characterized by spectroscopic (IR, ^{1}H, ^{13}C and ^{119}Sn NMR, EPR, UV-vis., ESI-MS) and analytical methods. The comparative interaction of monometallic complexes and their heterobimetallic analogues with CT-DNA in Tris-buffer were studied by various biophysical methods such as electronic absorption titration, fluorescence titration, cyclic voltammetry and viscosity measurements. To quantify the extent binding of complexes with DNA, the intrinsic binding constant K_b of complexes were determined, which follows the

order; $[C_6H_{24}N_4O_6ZnSn_2Cl_4]Cl_2$>$[C_6H_{24}N_4O_6CuSn_2Cl_4]Cl_2$>$[C_6H_{20}N_4O_2Zn]Cl_2$> $[C_6H_{20}N_4O_2Cu]Cl_2$, thus, revealing a pronounced DNA binding of the heterobimetallic complexes in comparison to their respective monometallic analogues. Furthermore, the interaction of transition metal ions of heterobimetallic complexes with 5′-GMP and 5′-TMP was ascertained by absorption titration of the heterobimetallic complexes with these nucleotides which clearly shows selective preference of 5′-GMP with the copper(II) complex while zinc(II) complex preferring selective interactions with 5′-TMP. The results of spectroscopic, viscometric and cyclic voltammetric studies of the heterobimetallic complexes with CT-DNA suggested electrostatic mode of binding with the phosphate backbone of DNA double helix. Heterobimetallic complexes $[C_6H_{24}N_4O_6CuSn_2Cl_4]Cl_2$ and $[C_6H_{24}N_4O_6ZnSn_2Cl_4]Cl_2$ when subjected to gel electrophoresis with supercoiled pBR322 DNA, demonstrate significant cleavage activity under physiologically relevant conditions.

As a means of further exploring the chiral preference of potential drug candidates, a new series of chiral modulated organotin antitumor drug (S)/(R)-$[C_{15}H_{21}NO_2Sn]$ and (S)/(R)-$[C_{10}H_{16}NOSnCl]$ derived from S- and R- enantiomers of [4-(2-hydroxy-1-phenylethylimino)pent-2-ol] and 2-amino-2-phenylethanol, respectively, were synthesized and characterized by various physicochemical and spectroscopic methods. Chiral modulation of the drug is responsible for its high binding affinity towards DNA (primary pharmacological target) as the efficacy of most of the chiral drugs is based on enantioselectivity. In order to establish the enantiomeric selectivity in drug-DNA binding, preliminary complex-DNA interaction studies employing UV-visible, fluorescence, circular dichroic and viscosity measurements were

elucidated revealing preference of binding for S-enantiomer of the complexes towards the ultimate drug target DNA. Nevertheless, both isomers displayed higher K_b values than that of cisplatin drug. Furthermore, interaction studies of complex (S)-[$C_{15}H_{21}NO_2Sn$] with 5'-GMP using ^1H and ^{31}P NMR again verifies electrostatic binding mode of the complex. The less effective cleavage pattern demonstrated by these complexes (S)-[$C_{15}H_{21}NO_2Sn$] and (S)-[$C_{10}H_{16}NOSnCl$] at micromolar concentration suggested a strand scission of plasmid pBR322 DNA from its supercoiled Form I to open circular Form II. Moreover, significant binding exhibited by the S-enantiomer of both the complexes [$C_{15}H_{21}NO_2Sn$] and [$C_{10}H_{16}NOSnCl$] in comparison to their R-enantiomeric analogues led us to investigate their *in vitro* antitumor potential via Sulforhodamine-B (SRB) assay to assess cellular proliferation against five human cell lines of different histological origin viz, Hop62 (human lung), DWD (human oral), K562 (human leukemia), DU145 (human prostrate) and MCF-7 (human breast). The complex (S)-[$C_{15}H_{21}NO_2Sn$] displayed remarkably pronounced and specific activity for K562 (Human leukemia) while complex (S)-[$C_{10}H_{16}NOSnCl$] exhibited significant activity towards Hop62 (Human lung), DWD (Human oral), DU145 (Human prostrate) and MCF-7 (Human breast).

Benzimidazoles are important subunits of biologically relevant ligands owing to their broad spectrum of biological and chemotherapeutic potential. The biological relevance of these heterocyclic aromatic building blocks is due to their structural similarity with nucleobases. Additionally, benzimidazole derived drugs have received much attention owing to the fact that benzimidazole residue is a constituent of Vitamin B_{12}, which supports their potential use as therapeutics. Thus, the benzimidazole ligand [$C_{16}H_{14}N_4O_2$] exhibits coordination mode with an oxygen

atom of alcohol group directed towards the metal ion and another –OH group with different molecular axis directed away from the metal center. These complexes, $[C_{18}H_{19}N_4O_2SnCl]$ and $[C_{52}H_{42}N_4O_2Sn_2]$ exhibit a pentacoordinate geometry while the complex $[C_{28}H_{23}N_4O_2SnCl]$ reveals hexacoordinated environment around the tin(IV) metal ions as evidenced by ^{119}Sn NMR studies.

The DNA binding ability of benzimidazole ligand $[C_{16}H_{14}N_4O_2]$ and their organotin(IV) complexes $[C_{18}H_{19}N_4O_2SnCl]$, $[C_{28}H_{23}N_4O_2SnCl]$ and $[C_{52}H_{42}N_4O_2Sn_2]$ were examined by means of different biophysical methods. The effects of varying substituents of organotin(IV) metal ions both aliphatic and aromatic was studied as it is well known that the biological effects of organotins depends on both the nature and number of organic groups bound to tin(IV) cation. The absorption titration of the complexes with CT-DNA reveal significant "hyperchromic" effect together with strong bathochromic shift of 4-5 nm which infer substantial binding of the complexes with CT-DNA. The intrinsic binding constant K_b values of the complexes $[C_{18}H_{19}N_4O_2SnCl]$, $[C_{28}H_{23}N_4O_2SnCl]$ and $[C_{52}H_{42}N_4O_2Sn_2]$ were found to be $2.16 \pm 0.04x10^4$, $3.47 \pm 0.04x10^4$ and $4.60 \pm 0.04x10^3$ M^{-1} respectively, suggesting pronounced binding of complex $[C_{28}H_{23}N_4O_2SnCl]$ with DNA double helix, among the other complexes. These spectral changes reflect the different binding propensity of the complexes with CT-DNA due to different structural constraints and suggest an electrostatic binding of the complexes with partial intercalative interactions. Although the cationic core of tin(IV) lack base specificity in DNA binding, the hexacoordinated $[C_{28}H_{23}N_4O_2SnCl]$ with labile Cl group promotes higher binding of this complex towards DNA exhibiting a multifaceted binding of the complex probably due to

differential conformational effects induced by planar ligands towards CT-DNA. The mechanism of binding of the complexes was further ascertained by the interaction studies of these complexes with nucleotides (5′-GMP and 5′-TMP) using absorption spectroscopy suggesting a clear preference for 5′-GMP binding which was further authenticated by NMR (^{1}H and ^{31}P NMR) studies.

In addition to the importance of the metal ions in DNA-binding regime, the optimization and structure activity relationship of various ligands with CT-DNA plays an eminent role in governing the DNA binding interactions. In this context, novel Schiff base ligand derived from the condensation reaction of 2-amino-3-formylchromone with 2-amino-2-phenylethanol, [$C_{18}H_{16}N_2O_3$] was synthesized and characterized which involves combination element of ammine functionality and naturally occurring heterocyclic chromone, 4H-benzopyran-4-one compounds which modulates their biological activity to a large extent. Subsequently, their transition metal complexes [$C_{36}H_{34}N_4O_7Cu$](NO_3)$_2$ and [$C_{36}H_{32}N_4O_6Zn$](NO_3)$_2$ were also prepared. The DNA-binding studies of the ligand and complexes with CT-DNA by employing different biophysical methods. The UV-visible titrations of both ligand and complexes, exhibit concurrent increase in the absorption intensity with a red shift of 2-3 nm illustrate electrostatic association of the complexes with CT-DNA by subsequent stabilization of the DNA helical structure. This "hyperchromic effect" was explained on the basis of two phenomena via, electrostatic interactions primarily by groove binding and effect of the coordination geometry around the central metal ion on CT-DNA binding. In order to quantify the binding extent of both ligand and complexes, binding constant K_b values were determined which display a higher propensity of [$C_{36}H_{34}N_4O_7Cu$](NO_3)$_2$ complex to bind with CT-DNA compared to

$[C_{36}H_{32}N_4O_6Zn](NO_3)_2$ complex. Moreover, the complexes exhibit higher binding for CT-DNA as compared to classical cisplatin drug. Furthermore, the absorption studies with mononucleotides (5′-GMP, 5′-TMP, 5′-AMP and 5′-CMP) were also monitored to examine the base specific interactions of the transition metal complexes $[C_{36}H_{34}N_4O_7Cu](NO_3)_2$ and $[C_{36}H_{32}N_4O_6Zn](NO_3)_2$. The extent of interaction of nucleotides with the complexes follows the order; 5′-GMP > 5′-TMP > 5′-CMP > 5′-AMP for $[C_{36}H_{34}N_4O_7Cu](NO_3)_2$ and 5′-TMP > 5′-GMP > 5′-CMP > 5′-AMP for the $[C_{36}H_{32}N_4O_6Zn](NO_3)_2$ complex thus, supporting a higher propensity of copper(II) complex towards 5′-GMP and for zinc(II) complex towards 5′-TMP. To further support these findings, the interaction of complex $[C_{36}H_{32}N_4O_6Zn](NO_3)_2$ with 5′-GMP and 5′-TMP, was ascertained by ^{1}H and ^{31}P NMR studies which confirms higher binding propensity of the complex towards 5′-TMP as compared to 5′-GMP. The binding studies performed using fluorescence, circular dichroism, viscosity further conclude a groove binding mechanism of the complexes towards DNA. The DNA cleavage activity of the complex $[C_{36}H_{34}N_4O_7Cu](NO_3)_2$ using agarose gel electrophoresis in presence of increasing concentration of complex shows an excellent cleavage revealing the conversion of supercoiled Form I to open circular Form II and then to linearized Form III. The cleavage of DNA by the complex in presence of activators follows the order; H_2O_2 > MPA >GSH >Asc. The mechanistic pathway followed by the complex in the presence of various radical scavengers such as NaN_3, DMSO, tert-butyl alcohol, NaN_3 and SOD suggested cleave of plasmid DNA via, oxidative mechanism. Furthermore, the major groove binding ability of the complex was ascertained on the basis of cleavage pattern of plasmid in presence of minor and major groove binding agents such as DAPI and methyl green.

Abbreviations

AMP	adenosine monophosphate
CD	circular dichroism
CMP	cytidine monophosphate
CT-DNA	calf thymus DNA
DAPI	4′,6-diamidino-2-phenylindole
DMSO	dimethylsulfoxide
EDTA	ethylenediaminetetraacetic acid
EPR	electron parmagentic resonance
ESI	electrospray ionization
EthBr	ethidium bromide
GMP	guanosine monophosphate
IL	intra ligand
LNT	liquid nitrogen temperature
MPA	mercaptopropionic acid
NMR	nuclear magnetic resonance
SRB	sulphorhodamine B
TMP	thymidine monophosphate
Tris	tris(hydroxymethyl)aminomethane
UV	ultra-violet

CHAPTER I

Introduction

Introduction

Medicinal inorganic chemistry - an interdisciplinary area of science emerged from the burgeoning field of bioinorganic chemistry which includes metal-based drugs, metal sequestering or mobilizing agents, metal-containing diagnostic aids, and the medicinal recruitment of endogenous metal ions. It combines various aspect of inorganic chemistry and chemical biology of living system. Because small molecules can affect biochemical function, there is a clear link between chemical biology, pharmacology and medicine [1]. While small molecules usually imply organic compounds [2], inorganic small molecules have long history in both biology and medicine.

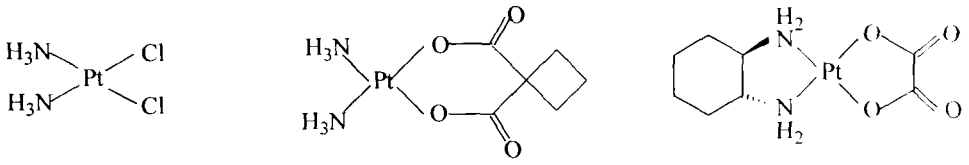

Figure 1. *Platinum(II) complexes in clinical use for cancer chemotherapy, cisplatin (left), carboplatin (middle), oxaliplatin (right).*

The use of metal complexes as therapeutic agents can be traced back to 3500 B.C [3]. Copper and gold have been used since antiquity in metal based therapies [4,5]. Medicinal inorganic chemistry in particular, after the prototypical success story of cisplatin- an archetypical inorganic antitumor drug used for the treating several solid malignancies such as testicular, ovarian, bladder and neck cancers [6,7] (Figure 1). However the clinical efficacy of this drug is well established yet, it exhibits only a narrow spectrum of activity and has been associated with severe side effects such as nephrotoxicity, neurotoxicity, and emetogenesis as well as inherent or acquired resistance [8-10]. Therefore, new drug design strategies have been applied to

inorganic metal complexes, such as finding pharmacologically active ligand scaffolds, attachment of intercalating agents or other ancillary functional groups and introduction of chiral motifs in order to modulate or optimise the detrimental properties of these metal complexes leading to the development of more efficacious drug candidates with pronounced anticancer potential acting via, specific reaction pathway in the biological system [11].

Inorganic elements play a crucial role in biological and biomedical processes [12], and it is evident that many organic compounds used in medicine do not have purely organic mode of action; some are activated or biotransformed by metal ions including metalloenzymes [13], others have a direct or indirect effect on metal ion metabolism. Metal ions are also very important for the structure and function of nucleic acids. Both essential and non-essential metals can be used in therapy and diagnosis. Thus, diversity of the properties of inorganic elements makes them versatile for many applications viz. for therapy [14], diagnosis [15], catalysis [16], molecular magnets [17], molecular light switches [18-20] etc. Brief summary of the general chemical properties of metals as outlined in several books of bioinorganic chemistry [12,21,22] is given below

1. Charge. Metal ions are positively charged in aqueous solution, but that charge can be manipulated depending on the coordination environment so that a metal complexed by ligands can be cationic, anionic, or neutral.

2. Interactions with ligands. Metal ions bind to ligands via, interactions that are often strong and selective. The ligands impart their own functionality and can fine tune properties of the overall complex that are unique from those of the individual ligand or metal.

3. Structure and bonding. Metal ligand complexes span a range of coordination geometries that give them unique shapes compared with organic molecules. The bond lengths, bond angles, and number of coordination sites can vary depending on the metal and its oxidation state.

4. Lewis acid character. Metal ions with high electron affinity can significantly polarize groups that are coordinated to them, facilitating hydrolysis reactions.

5. Partially filled d-shell. For the transition metals, the variable number of electrons in the d-shell orbitals imparts interesting electronic and magnetic properties to transition metal complexes.

6. Redox activity. Coupled with the variability of electrons in the d-shell is the ability for many transition metals to undergo one-electron oxidation and reduction reactions.

Transition metal complexes stand out as exceptional candidates for artificial nucleases of DNA due to their ability to recognize and react selectively with individual target sites [23-28]. Stable, inert, water soluble, versatile structures as well as spectroscopically and electrochemically active metal centers constitute the unique signatures of transition metal complexes, which make them sensitive diagnostic agents [29].

Additionally, transition metal complexes exhibit significant modulation effects, which can tune the mode of binding and their reactivity towards biomolecules. A vast number of ligands can be readily 'plugged' in and out of a wide variety of metal centers. This unique attribute of metal complexes provides system that utilizes strength of both synthetic organic chemistry and transition metal complexes. Any

metal ion or complex is subject to the potential limitations in the Bertrand diagram. (Figure 2) which is usually used in discussing the essentiality of elements [30].

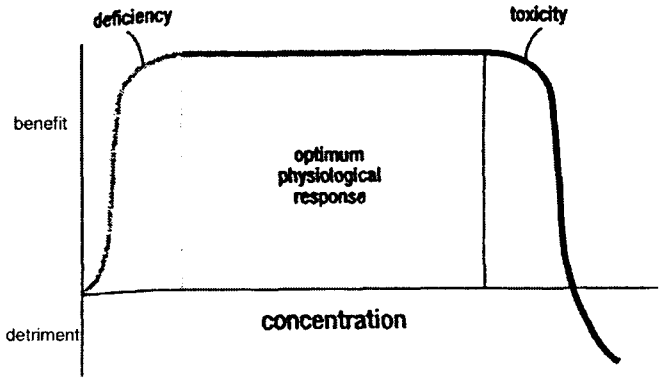

Figure 2. *Bertrand diagram indicating the relationship between benefit/detriment from an element and its concentration. Great variations are found in each region depending on the nature of the element.*

The area of optimum physiological response vary greatly according to the element. its speciation, oxidation state and the biochemistry of the specific compound in which it is found. Therefore, the areas of deficiency, toxicity and optimum physiological response can be dramatically varied by considering a combination of these variables, as well as design features of the potential ligand which may be altered to facilitate the delivery of that metal ion into the biological system [31]. Thus, the refinement of biological properties of metal complexes by well-tailored. multifunctional ligands offer exciting possibilities and play a substantial role in muting the potential toxicity of the metallodrug to deliver a positive impact in area of diagnosis and therapy [32].

Metal ions can be introduced into the biological system either for therapeutic or diagnostic aids. Alternatively, these metal ions can be removed from the biological system by the judicious use of metal binding molecules (termed as ligands). Ligands are most often but not limited to organic compounds that binds to

metal ions, thus modifying the physical and chemical properties of the ions. Ligands can modify the reactivity, lipophilicity, oral/systematic bioavailability of metal ions, stabilization of oxidation state, and substitutional inertness depending on the requirements for chemotherapy [33,34]. They ensure protection of tissues from toxic metal ion or in a contrasting strategy, enhance uptake of pharmacological beneficial metal ion [35]. It has been well documented in literature that carrier amine ligands of cisplatin analogues appear to modulate the antitumor properties of this class of drug [36,37]. The antitumor activity is usually lost or diminished if the primary or secondary amines on platinum are replaced by tertiary amines [38]. In addition, the carrier ligands may also affect bio-distribution and recognition of DNA adducts by repair enzymes, regulatory and DNA binding proteins. A notable class of amine ligands is 1,3-diamino-2-propanol as many amino alcohol derivatives have been extensively used as chemotherapeutic agents [39]. Besides this, a relatively large number of natural products contain amino alcohol functionality [40]. Keppler and Hartinger et al. [41] have demonstrated binding of 5'-GMP with platinum(II) cytotoxic complexes derived from amino alcohols. A judicious variation of ligand structure resulted in a series of platinum complexes bearing amino alcohol (Figure 3). These compounds were distinguished by the capability of eventually administered form to open intramolecular rings under the action of variable pH and chloride concentration giving rise to species more reactive towards 5'-GMP and possessing higher cytotoxicity. Another important feature of amino alcohol platinum(II) complexes is the ability of hydroxyl group as well as alcoholato oxygen atom in ring closed species, to form hydrogen bonds with nucleobases. This

hydrogen bonding is expected to play a crucial role in the binding of platinum compound to DNA [42].

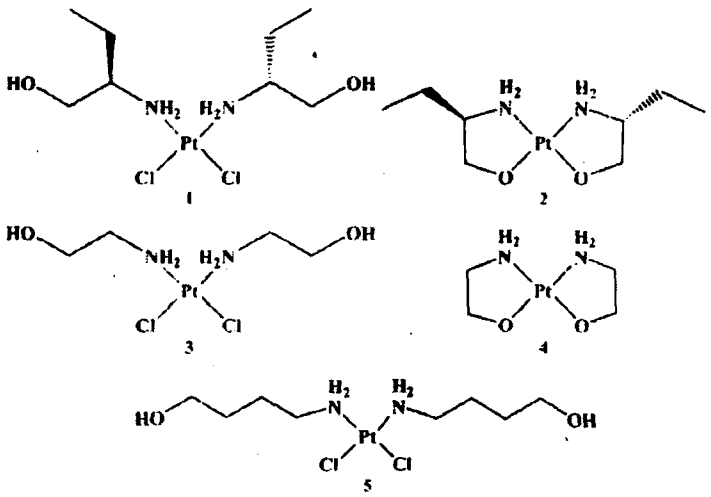

Figure 3. *Structural formulae of (SP-4-2)-bis-[(R)-(-)-2-aminobutanol-kN]-dichloroplatinum(II)* ***1****, (SP-4-2)-bis-[(R)-(-)-2-aminobutanolato-k²N,O]-platinum(II)* ***2****, (SP-4-2)-bis-[2-aminoethanol-kN)]-dichloroplatinum(II)* ***3****, (SP-4-2)-bis-[2-aminoethanolato-k²N,O]-platinum(II)****4****, and (SP-4-2)-bis-[4-aminobutanolato-k²N,O]-dichloroplatinum(II)* ***5.***

Bermejo et al. [43] have studied the versatility of potentially heptadentate ligand N,N-bis(3-hydroxysalicyldene)-1,3-diaminopropanol. The presence of four phenolic groups results in high nuclearity as it can simultaneously coordinate upto five metal centers in different ways resulting in complex structures. Nickel and copper centres in these polynuclear complexes possess distorted tetrahedral or square pyramidal geometry while zinc(II) was found to be hexacoordinated in the mononuclear complexes.

The condensation of primary amines with carbonyl compounds was first reported by Schiff and since then condensation products are referred to as Schiff bases [44]. The Schiff bases are widely studied because of increasing recognition of their role in biological systems [45]. The anti-microbial and anti-proliferative activities of Schiff

base copper(II) complexes [46] are not attributed to coordinated ligands alone but also to the physicochemical, structural and electronic properties that arise due to the coordination [47-49]. The effect of copper(II) Schiff base complexes of the type [Cu(dienXX)Y]Y with iodine or bromine {where (dienXX) = Schiff dibase of diethylenetriamine and Y=Cl, Br} on the single stranded, double stranded and pDNA was examined by DNA-binding spectroscopic studies and DNA electrophoretic mobility to study the structure-activity relationship [50]. Schiff base ligands derived from acetylacetone are widely employed in coordination chemistry because of their convenient tuning of steric and electronic properties [51-53]

Chohan et al. [51] have synthesized ligands (L_1-L_5) (Figure 4) obtained by the condensation reaction of amino acids (glycine, phenylalanine, alanine, valine or histidine) and acetylacetone for exploring metal-based bacteriostatic and carcinostatic pharmaceuticals with a high efficacy and low toxicity. All these ligands along with their metal complexes {cobalt(II), copper(II), nickel(II) and zinc(II)} were screened for their *in vitro* antibacterial activity against Gram-negative *(E. coli, S. flexenari, P. aeruginosa, and S. typhi)* and Gram-positive *(B. subtilis and S. aurens)* bacterial strains.

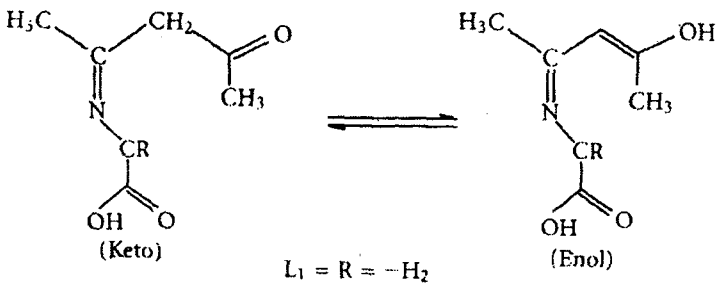

L_1 = R = $-H_2$
L_2 = R = $-HCH_2C_6H_5$
L_3 = R = $-HCH(CH_3)_2$
L_4 = R = $-HC_3H_3N_2$
L_5 = R = $-HCH_3$

Figure 4. *Proposed structure of the ligands (L_1-L_5).*

These compounds demonstrated not only good antibacterial and antifungal activity but also proved to be a new class of compound for metal-based drug therapies.

Increasing attention has also been devoted to Schiff base complexes of organotin(IV) moieties in view of their potential applications in medicinal chemistry and biotechnology [54-58]. Baul et al. [59] have reported series of new amino acetate functionalized Schiff base organotin(IV) complexes $[Ph_3SnLH]_n$ and $[Ph_2SnL]$. These organotin(IV) complexes were characterized by IR, NMR (^1H, ^{13}C, ^{119}Sn) spectroscopic techniques and were screened against A498, EVSA-T, H226, IGROV, M19 MEL, MCF7 and WIDR human tumor cell lines. Among the studied complexes $[Ph_3SnL^1H]_n$, $[Ph_3SnL^2H]_n$, $[Ph_3SnL^3]_n$, $[Ph_2SnL^2H]_n$, triphenyltin(IV) compound $[Ph_3SnL^3]_n$ exhibited a much higher ID_{50} values (35 ng/ml) compared to previously known drugs doxorubicin, cisplatin, 5-fluorouracil and etoposide and offers its promising candidature for further development as an anti-cancer agent.

M. Nath et al. [60] have synthesized and characterized organotin(IV)-amino acid Schiff bases derived from the condensation of 2-hydroxy-1-naphthaldehyde or acetylacetone with Gly, L-Ala, DL-Val, DL-4-aminobutyric acid, L-Met, L-Leu and PhGly with a general formula Bu_2SnL (L=dianion of tridentate Schiff base) (Figure 5). The central tin(IV) ions in all these complexes are pentacoordinated with a monodentate carboxylic group. An attempt was made to prove the structure of resulting complexes on the basis of elemental analysis, conductance measurement and electronic IR, multinuclear magnetic resonance (^1H, ^{13}C and ^{117}Sn) and ^{119}Sn Mössbauer spectral studies.

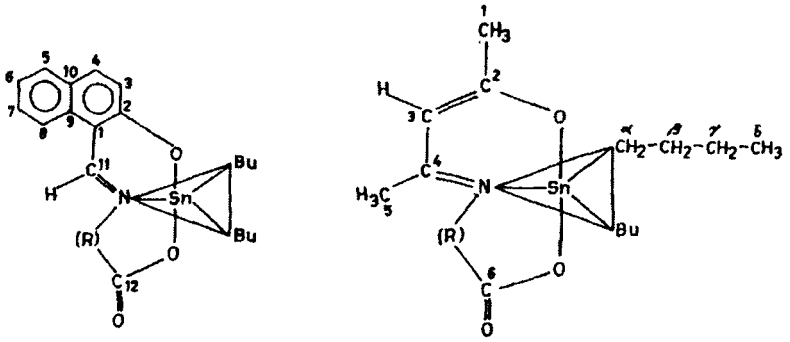

Figure 5. *Structures of Bu_2SnL with different Schiff base ligands.*

The *in vitro* cytotoxicity of the complexes against a panel of seven tumor cell lines, viz. MCF-7, EVSA-T, WiDr, IGROV, M19 MEL, A498 and H226 was found to be higher than those observed for cisplatin and carboplatin (Table 1).

	ID_{50} (ng ml^{-1}) against[a]:						
Complex	MCF-7	EVSA-T	WiDr	IGROV	MI9 MEL	A498	H226
Bu_2Sn-1(I)	75	35	480	75	90	170	190
Bu_2SnL-2(I)	20	17	114	27	71	62	160
Bu_2SnL-6(II)	60	120	420	130	70	130	200
Ph_2SnL-1(I)	170	70	490	120	530	230	350
Ph_2SnL-2(I)	600	150	1750	480	620	690	1100
Carboplatin[b]	10 500	4500	3500	2400	5500	18 000	25 000
Cisplatin[b]	1400	920	1550	230	780	1200	3160

Table 1. *ID_{50} values (in ng ml^{-1}) of selected diorganotin derivatives of Schiff base derived from amino-acids, and of some reference compounds.*

Benzimidazoles represent one of the largest groups of heterocyclic compounds and have attracted a great deal of interest over the decades due to their wide potential biological activities. Bis-benzimidazoles have potent activity against a number of microorganism including those that lead to AIDS-related infections [61], these compounds bind to DNA at AT-rich sequences and have been extensively studied as potential therapeutic agents owing to the fact that benzimidazole residue is a constituent of Vitamin B_{12} [62,63]. Benzimidazole sometimes called 1,3-dideazapurine and its derivatives can serve as model compounds for purine due to

their structural similarity [64,65]. Among the other biologically active ligands, benzimidazole has been found to play important roles in several DNA minor groove binding agents such as Hoechst 33258 and Hoechst 33342 [66,67].

Williams et al. [68] reported the synthesis and coordination chemistry of versatile chiral, tridentate facially coordinating 1,2-bis-(1H-benzimidazol-2-yl)-1,2-ethanediol ligands (Figure 6). The ligands were prepared by simple Phillips reaction [69-71] from tartaric acid with the appropriate 1,2-diaminobenzene. The copper(II) complexes exhibited 4+2 coordination with benzimidazole moiety occupying equatorial sites and alcohol functions weakly binding in the axial sites. In view of the fact that benzimidazole derivatives have displayed a wide range of biological activities including inhibition of DNA topoisomerase I, antitumor and antiparasitic activity [72,73], our research group has previously synthesised new chiral and achiral macrocyclic complexes [1,2-bis(1H-benzimidazol-2yl)-1-(1,8-dihydro-1,3,5,8,10,12-hexaazacyclotetradecane)-2-hydroxyethanolate]copper(II)perchlorate and [1,2-bis(1H-benzimidazol-2yl)-1-(1,8-dihydro-1,3,5,8,10,12-hexaazacyclotetradecane)-2-hydroxyethanolate]nickel(II) perchlorate exhibiting a pentacoordinated environment around the metal center [74] (Figure 6a). The comparative DNA-binding studies of the chiral complex [1,2-bis(1H-benzimidazol-2yl)-1-(1,8-dihydro-1,3,5,8,10,12-hexaazacyclotetradecane)-2-hydroxyethanolate]copper(II)perchlorate with achiral macrocycle (1,8-dihydro-1,3,5,8,10,12-hexazacyclotetradecane)copper(II) were performed by absorption, fluorescence spectral studies, circular dichroism, cyclic voltammetric and viscosity measurements. The results suggested a partial intercalation mode that is different from the parent achiral complex as revealed by the absorption titrations of the

complex with DNA (Figure 7). The binding constants K_b for the achiral and chiral complexes bound to DNA was found out to be $2.7x10^4$ M^{-1} and $6.6x10^4$ M^{-1}, respectively.

(a) (b)

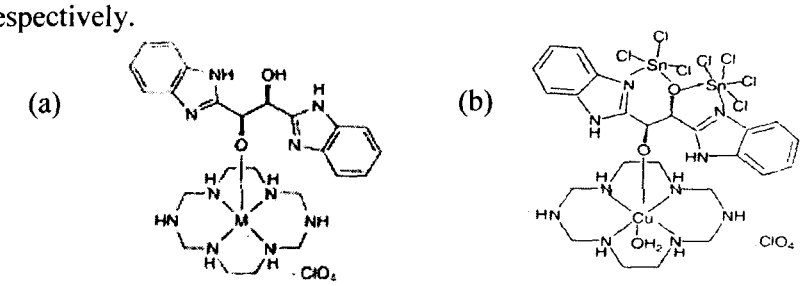

Figure 6. *Proposed structures of complexes (a) [1,2-bis(1H-benzimidazol-2yl)-1-(1,8-dihydro-1,3,5,8,10,12-hexaazacyclotetradecane)-2-hydroxyethanolate]copper(II)perchlorate (b) stannoxane capping macrocyclic complex.*

(a) (b)

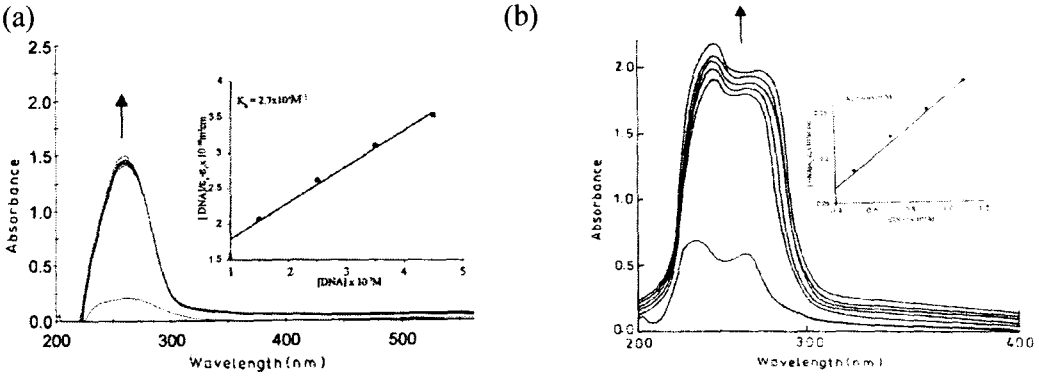

Figure 7. *Absorption spectral traces of complex (a) (1,8-dihydro-1,3,5,8,10,12-hexazacyclotetradecane)copper(II) (b) [1,2-bis(1H-benzimidazol-2-yl)-1-(1,8-dihydro-1,3,5,8,10,12-hexaazacyclotetradecane)-2-hydroxyethanolate]copper(II)perchlorate in tris-HCl buffer upon addition of CT DNA. Inset: Plots of [DNA]/$|\varepsilon_a-\varepsilon_f|$ vs. [Complex]=1.5 x 10^{-4} M.*

Furthermore, circular dichroic studies of the chiral complex have also been found to be consistent with the other spectral studies. The introduction of chirality has shown a pronounced effect on DNA binding event of macrocyclic metal complex which is witnessed by strong binding affinity of the benzimidazole modulated complex towards DNA.

In another attempt, comparative DNA binding studies of benzimidazole derived $\widehat{N}\widehat{N}O$ donor tridentate chiral dinuclear stannoxane complex (Figure 6b) and its modulated copper macrocyclic complex were carried out by various biophysical methods [75]. This stannoxane capping creates interesting differences in space, configuration and electronic structure. Chirality enhances extent of inhibition at the target site DNA in a stereoselective manner at the molecular level. It further tunes the reactivity and facilitates the modulation of the macrocycle by exhibiting unique electronic and kinetic effects.

Chromones (1-benzopyran-4-one) are ubiquitous in nature, especially in plants which were exploited since long as potential therapeutic agents due to the high anti-tumor activity and low toxicity. These natural products possess potential anticancer activity since they stimulate or inhibit a wide variety of enzyme systems as pharmacological agents [76,77]. Their biological and physiological activities also include antimycobacterial, antifungal, anticonvulsant, antimicrobial, mushroom tyrosinase inhibition activities [78,79]. Flavonoid-related chromone (Figure 8a) and its derivatives {Hormothamnione (Figure 8b) and 6-desmethoxyhormothamnione (Figure 8c)} are well known naturally occurring heterocyclic compounds with oxygen as heteroatom [80]. They possess antibacterial antifungal, anticancer, anti-HIV, spasmolytic and antiviral properties [81,82]. Flavonoids are effective metal ion chelators and play a key role in the initiation of free radical processes by acting on two antioxidant pathways: (1) direct reactions with free radicals, (2) chelating of metal ions involved in production of reactive oxygen pathways. Thus, experimental data indicate that the chelated compounds are more effective free radical scavengers than flavonoids alone [83].

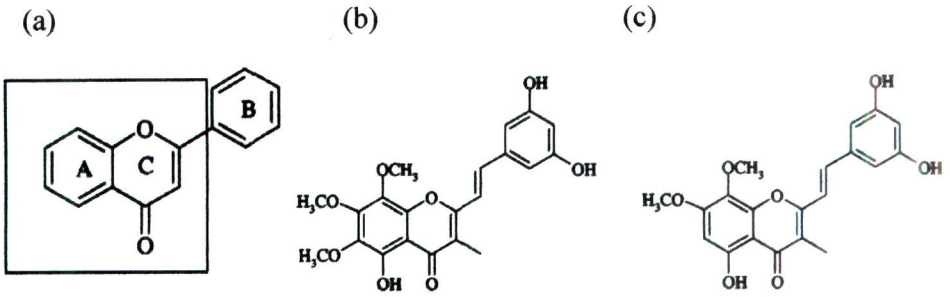

Figure 8. *Structures of (a) chromone (4H-benzopyran-4-one), (b) hormothamnione, (c) 6-desmethoxyhormothamnione.*

Recently E. Budzisz et al. [84] described some coumarin complexes with excellent cytotoxic activity obtained from the reaction of chromone derivatives. Starting from 2-methyl-4-oxo-chromone-3-carboxylic acid, new coumarin derivatives 3-[1-(alkylamino)-ethylidene]-chroman-2,4-dione were synthesized which displayed excellent cytotoxic activity against HL-60, NALM-6 cell lines. Another chromone derivative namely 2-methyl-4-oxo-4H-chromone-3-carboxylate also exhibited *in vitro* activity against human cancer cell lines A549, K562 and HeLa.

The DNA-binding properties of chromone complexes were also exploited by Yang et al. [85]. They have synthesized and characterized of novel glycine Schiff bases sodium salt, 6-hydroxychromone-3-methylidyneiminoacetate (LNa), derived from chromone and their complexes $[CuL{\cdot}(H_2O)_3]NO_3{\cdot}H_2O$ and $[NiL{\cdot}H_2O]NO_3{\cdot}2H_2O$ (Figure 9a-b).

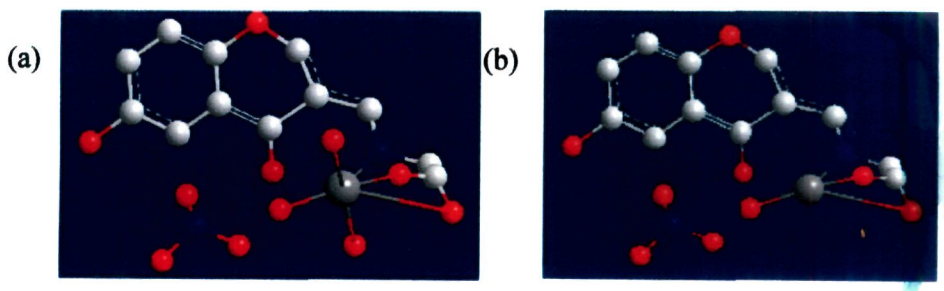

Figure 9. *Speculated structures of (a)* $[CuL{\cdot}(H_2O)_3]NO_3{\cdot}H_2O$ *(b)* $[NiL{\cdot}H_2O]NO_3{\cdot}2H_2O$.

Their DNA-binding properties have been elucidated by means of UV-visible spectroscopy, fluorescence spectroscopy, and viscosity measurement studies revealing an intercalative mode of interaction of these complexes. The interaction of $[CuL{\cdot}(H_2O)_3]NO_3{\cdot}H_2O$ and $[NiL{\cdot}H_2O]NO_3{\cdot}2H_2O$ with DNA was investigated by electronic absorption spectroscopy which revealed 50% hypochromism in the absorption band with a bathochromic shift of 3-10 nm for $[CuL{\cdot}(H_2O)_3]NO_3{\cdot}H_2O$ while the $[NiL{\cdot}H_2O]NO_3{\cdot}2H_2O$ exhibited 42% hypochromism with a bathochromic shift of 6 nm. These results were suggestive of either the electrostatic effect or intercalative association of the complexes with DNA (Figure 10).

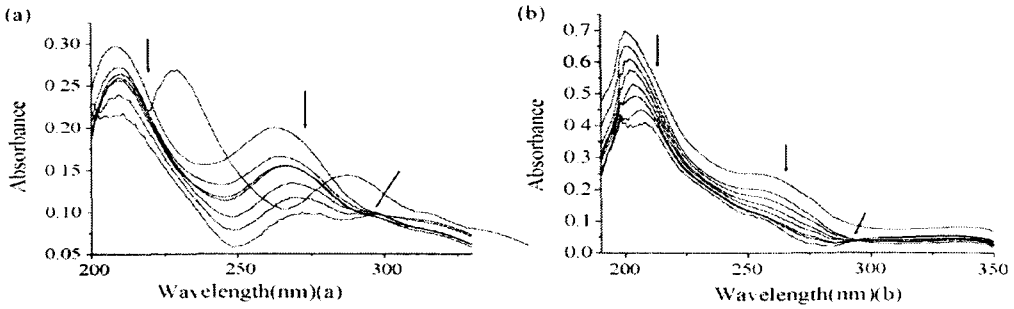

Figure 10. *(a) Electronic spectra of $[CuL{\cdot}(H_2O)_3]NO_3{\cdot}H_2O$ (10 μM) (b) Electronic spectra of $[NiL{\cdot}H_2O]NO_3{\cdot}2H_2O$ (10 μM) in presence of increasing amounts of DNA: [DNA] = 0–35 μM. The arrow indicates the absorbance changes upon increasing DNA concentration.*

Spectrofluorimetric titration of $[CuL{\cdot}(H_2O)_3]NO_3{\cdot}H_2O$ and $[NiL{\cdot}H_2O]NO_3{\cdot}2H_2O$ with DNA displayed an enhancement in the fluorescence intensity of the complexes which agrees well with those observed for intercalators [86]. The relative association constant of $[CuL{\cdot}(H_2O)_3]NO_3{\cdot}H_2O$ and $[NiL{\cdot}H_2O]NO_3{\cdot}2H_2O$ were 6.08×10^5 and 2.75×10^5 M^{-1} which suggest that the binding strength of $[CuL{\cdot}(H_2O)_3]NO_3{\cdot}H_2O$ was higher in magnitude than $[NiL{\cdot}H_2O]NO_3{\cdot}2H_2O$ complex (Figure 11a-b).

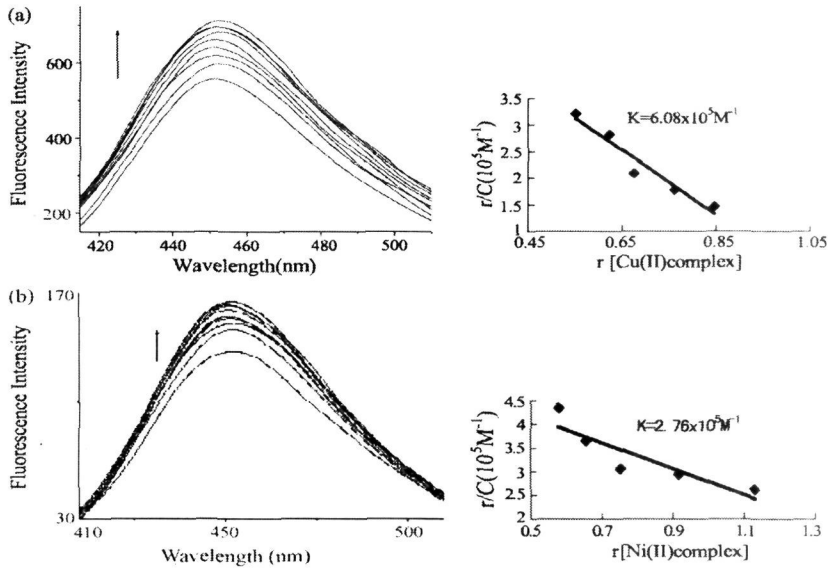

Figure 11. *The emission enhancement spectra of (a) $[CuL{\cdot}(H_2O)_3]NO_3{\cdot}H_2O$ (10 μM) (b) $[NiL{\cdot}(H_2O)_3]NO_3{\cdot}H_2O$ (10 μM) in the presence of increasing concentration of DNA from 0, 2.5, 5, 7.5, 10, 12.5, 15 and 17.5 μM.*

Recently, Yang et al. [87] have described the synthesis, characterization and DNA binding properties of novel fluorescent zinc(II) and nickel(II) complexes of (6-ethoxy chromone-3-carbaldehyde benzoyl hydrazone) ligand (Figure 12). The comparative interaction of the ligand (L) and $[ZnLNO_3]NO_3$ with DNA were carried out using UV-visible, fluorescence, circular dichroic methods and viscosity measurements. It was found that the zinc(II) complex strongly binds DNA presumably by an intercalative mode.

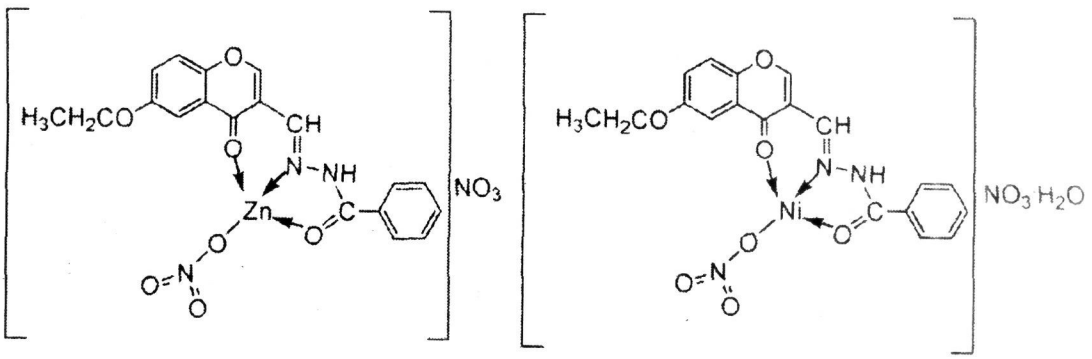

Figure 12. *Proposed structure of complexes (a) $[ZnLNO_3]NO_3$ complex and (b) $[NiLNO_3]NO_3.H_2O$ complex.*

Amongst various metal ions, Lewis acid metal centers such as copper(II), zinc(II) and tin(IV) are chemically well suited to influence fundamental biological processes at the cellular level owing to their high affinity for basic nitrogen and oxygen donor ligands and their capability to accommodate larger aromatic architectures capable of nucleic acid recognition. Their ability to directly hydrolyze phoshodiester linkages as well as redox chemistry of the metal center or generate reactive oxygen-derived species further accentuates their natural aptitude for participation in cellular functions involving nucleic acids. Because binding and cleavage of nucleic acid lies at the heart of cellular transcription and translation, these substrates are ultimate targets for therapeutic intervention and development of diagnostic probes of nucleic acid structures. Transition metals are compatible in the biological system in contrast to platinum based anticancer agents, which are non-specific, resulting in significant toxicity [88]. The oxidation state of metal ions dictate particular geometries, hence limiting appropriate binding for different ligand sets [89].

Among the first row transition metal ions, copper(II) complexes are attractive scaffold for metal based drug research as they possess biologically accessible redox potentials with relevant oxidation state +1 and +2. Due to the plasticity and participation of copper as an integral part of the active site of metalloproteins familiarize its coordination with the human body's functions. Copper was found to bind DNA by coordination to the electron-rich nucleobases with high affinity than any other divalent cation, thus, promoting DNA oxidation [90]. Copper(II) complexes selectively coordinate to the N7 position of guanine residue of DNA double helix [27,91,92] and are therefore, selective at the molecular target site. The

selectivity of copper ions to specific sites modifies the conformational structure of DNA, polynucleotides and biomembranes [93]. The binding is dependent on the size of the copper ions, charge, electron affinity and geometry of the formed adduct. Copper complexes which exhibit strong binding with DNA are also capable to induce a hydrolytic cleavage of DNA [94,95] therefore, a number of copper based synthetic nucleases have also been reported [96-100]. Among the copper complexes explored so far, the copper(II) complexes of 1,10-phenanthroline described by Sigman et al. [101] have attracted great attention due to their high artificial nucleolytic activity, as these complexes are able to break the DNA double helix in presence of H_2O_2 and reducing agents [102], have found application as foot printing agents of both proteins and DNA [103], probes of the dimensions of the minor groove of duplex structures [104], identifiers of transcription starting sites [105].

In the recent past, A. Kumbhar et al. [106] have described a series of crystalline mononuclear mixed ligand copper(II) malonate complexes [Cu(L)(maltol)] where L= 2,2′-bipyridine (bpy), 1,10-phenanthroline (phen), 1,10-phenanthroline-5,6-dione (phendione), dipyrido[3,2-a:2′,3′-c]phenazine (dppz), and 4b,5,7,7a-tetrahydro-4b,7a-epiminomethanoimino-6H-imidazo[4,5-f][1,10]-phenanthroline-6,13-dione (bpg) showing efficient DNA binding and cleavage activity (Figure 13). The coordinated bipy, phen, and dione complexes intercalate partially or display groove binding interactions with DNA while dppz complexes binds via intercalative interaction within DNA helix as revealed by various DNA-binding techniques such as absorption titrations, viscosity, thermal melting and fluorescence quenching and DNA cleavage studies (gel electrophoretic mobility assays). The cytotoxicity of the complexes against HeLa (cervical) cancer cell lines exhibited synergy between the

metal and the ligands resulting in significant enhancement in the cell death with IC_{50} of ~ 150-270 $\mu g/mL^{-1}$.

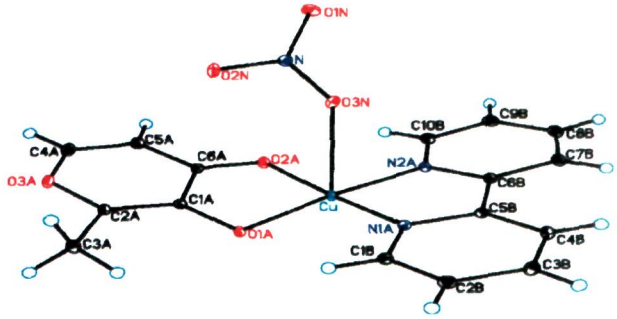

Figure 13. *ORTEP diagram of complex [Cu(bpy)(maltol)(NO_3)] showing the atom numbering scheme. Thermal ellipsoids are drawn at 50%probability.*

Divalent zinc(II) is an integral part of all biological systems and among the trace elements; zinc is second, only to iron, in abundance in human organisms. Zinc plays an important role in genetic stability and function [107,108]. Mechanistically, zinc has significant impact on DNA as a component of chromatin structure, DNA replication and transcription and DNA repair [109]. Lewis acidity affinity for hard oxygen ligands, substitutional lability together contributes towards the effective hydrolytic activity of zinc metal ions. Zinc enzymes efficiently catalyse the hydrolysis of nucleic acid under physiological condition in the living system. Structural changes induced by zinc(II) on DNA suggest that this cation can bind to both the nucleobase and the phosphate group [110]. A novel mononuclear zinc(II) complex **bis(3-methylpicolinato-κ^2,*N*,*O*)$_2$(1,10-phenanthroline-κ^2,*N*,*N*)-zinc(II)pentahydrate, [Zn(3-Me-pic)$_2$(phen)] prepared** by H.-L. Seng et al. [111] (Figure 14) has shown potential DNA-binding effects together with potent nucleolytic activity and inhibition of topoisomerase I. These octahedral [Zn(3-Me-pic)$_2$(phen)] complexes have been found to be able to differentiate different DNA

conformations (B-, A-, and Z- forms) to have a binding site selectivity (minor or major groove; mismatched nucleobase site) and nucleobase sequence recognition.

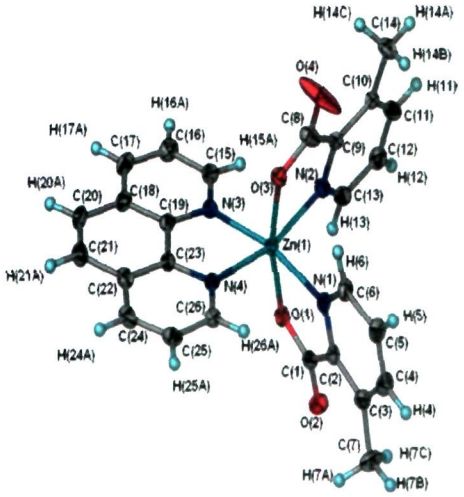

Figure 14. *Ortep plot of bis(3-methylpyridine-2carboxylato-κ^2,O,N)(1,10-phenathroline κ^2,N,N)zinc(II) pentahydrate (50% probability ellipsoids). Water molecules are not shown.*

Several other mononuclear zinc(II) complexes have also been exploited due to their potential anti-cancer activity. Recently, D. Kovala-Demertzi et al. [112] described the synthesis, crystal structure and spectral characterization of novel zinc(II) complexes namely bis(2-acetylpyridine-N4-1-(4-fluorophenyl)-piperazinyl thiosemicarbazonato)zinc(II) and bis(μ-acetato(2-acetylpyridine-N4-1-(4-fluorophenyl)-piperazinyl thiosemicarbazonato)zinc(II). The complexes were screened *in vitro* against four human cell lines namely HeLa (cervix adenocarcinoma cell line), K562 (chronic myelogenous leukaemia), MDA-MB-361 and MDA-MB-453 (breast cancer cell lines) showing potent cytotoxic activity and induction of apoptosis in cells resistant to cisplatin. The complex bis(2-acetylpyridine-N4-1-(4-fluorophenyl)-piperazinyl thiosemicarbazonato)zinc(II) is 305 and 59 times more active than cisplatin against MDA-MB-361 and MDA-MB-453 cell lines and 38 and 111 times more active than cisplatin against K562. Similarly, the cytotoxic activity of complex bis(μ-acetato(2-acetylpyridine-N4-1-

(4fluorophenyl)piperazinylthiosemicarbazonato)zinc(II) is 406 and 120 times more active than cisplatin against MDA-MB-361 and MDA-MB-453 and 60 and 298 times more active than cisplatin against HeLa and K562 cell lines. The above differences in the anti-proliferative activity of the zinc(II) complexes than the prevalent benchmark metallodrug cisplatin proves its clinical efficacy in the pharmaceutical regime and its significance in new metal based chemotherapeutic drug design [113].

In addition to transition metals, very important progress in field of medicinal organometallic chemistry has taken place during the past few years, allowing the design of novel, non-conventional, platinum compounds as well as innovative non-platinum metal-based antitumor agents. The antitumor potential of tin complexes have been established since 1929 [114] and among them organotin(IV) complexes were regarded as effective candidates in organometallic oncology due to their novel apoptosis inducing property. Promising success of different organotin derivatives which has shown acceptable *in vitro* and *in vivo* antiproliferative activity were developed as new lead chemotherapeutic agents [115,116]. Organotin chelated to oxygen/nitrogen donating ligands have been found to be active towards a number of tumour cells. During the period of 1980's and later on, M. Gielen [117] published a series of papers describing various biologically active organotin complexes which exhibited potent *in vitro* and *in vivo* cytotoxicities greater than the classical drug, cisplatin. In a recent review, P.J. Blower also described thirty interesting inorganic pharmaceuticals, four of which were tin complexes [118] which further atteunates the importance of these tin complexes. Pettinari et al. [119] developed a large number of organotin derivatives of beta-diketones and described their crystal and

molecular structures such as 1-(4-trifluoromethylphenyl)-3-methyl-4-R^1(C=O)-5-pyrazolone proligands LH (L^1 H; R^1 -C_6H_5:L^2H; R^1 -CH_3:L^3 H; R^1 -CF_3) and their interaction with R_3Sn(IV) acceptors (R-Me, Bu^n, Ph) (Figure 15). These fluorinated ligands reported were proved to be effective antitumor agents against several cell lines viz; MCF-7, EVSA-T, WiDr, IGROV, M19 MEL, A498. Various other tin(IV) complexes namely (4-acylpyrazolo-5-ato-dihalotin) derived from a variety of beta-diketone ligands were also explored by this group and their *in vitro* antitumor profiles were evaluated against all human melanoma cell lines.

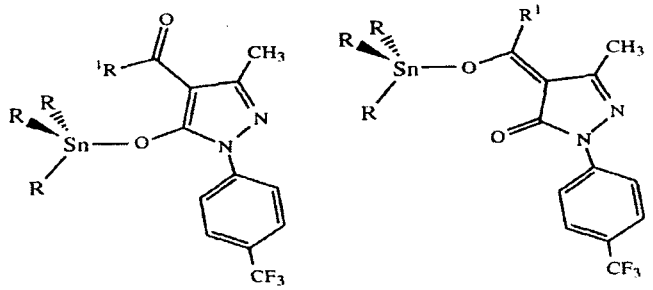

Figure 15. *Structures of tin complexes of 4-acyl-5-pyrazolone ligands developed by Pettinari group.*

Depending on the number of organic moieties, organotins are classified as mono, di, and tetraorganotin ($RSnX_3$, R_2SnX_2, R_3SnX, R_4Sn), where X is an anionic species (halide, oxide, hydroxide, carboxylate, or thiolate). Tin and organotin(IV) compounds containing electronegative atoms such as halogen atoms show Lewis acid character and the tin atom increases its coordination number from four or five, six or seven upon addition of neutral organic donor ligands [120,121]. The emergence of new experimental techniques (EXAFS, multinuclear ^1H, ^{13}C, ^{119}Sn NMR, ^{119}Sn Mössbauer, etc., spectroscopic techniques) provided useful information about the structure and stabilities of the complexes formed. L. Pellerito and L. Nagy [122] reviewed the literature on organotin(IV)$^{n+}$ complexes taking into account

the biological aspects of these complexes including the interactions of organotin(IV)$^{n+}$ with biologically active ligands viz. amino acids, peptides, carbohydrates, nucleic acids and DNA .

The binding ability of organotin compounds towards DNA largely depends upon both the nature and number of organic groups directly attached to the tin(IV) cation [123]. The phosphate group of DNA sugar back bone usually acts as an anchoring site. Nitrogen of DNA base binding is extremely effective, stabilizing the tin(IV) centre as an octahedral stable species. However, researches indicate that there is negligible interaction of tin complexes with nucleotide bases, but rather strong and irreversible binding to the vicinal phosphate groups of phosphoribose residues (Scheme 1) [124]. The presence of cyclic groups (aromatic or heterocyclic) in the tin-containing molecules was found to be important for anticancer activity as well [125-131].

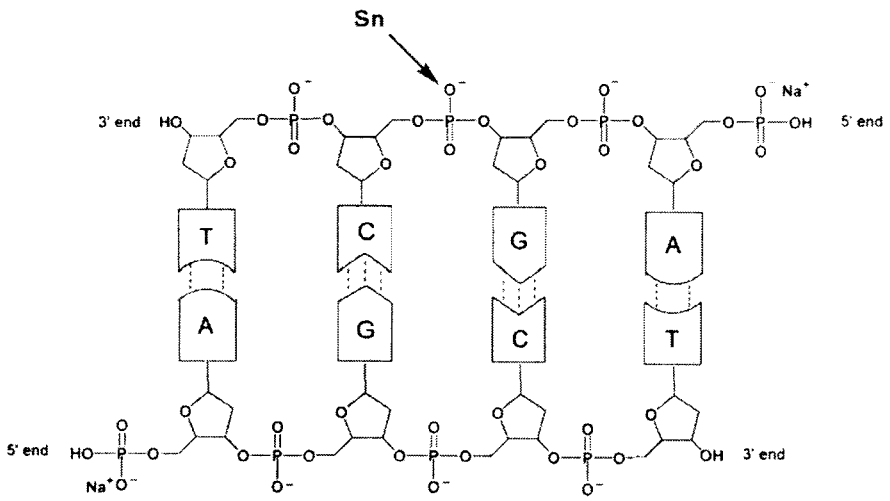

Scheme 1. *Irreversible binding to the peripheral phosphate groups of phosphoribose residues by tin(IV) metal ion.*

To evaluate the potential biomolecular recognition of the organotin(IV) complexes, various authors have investigated their interactions with model compounds of DNA

such as nucleotides. Barbieri et al. [132] have investigated coordination of $Me_2Sn(IV)^{2+}$ to 5′-GMP, 5′-ATP and 5′-[*d*(CGCGCG)$_2$] and to their sugar constituents (D-ribose and 2-deoxy-D-ribose) in aqueous solution by means of potentiometric titration and ^{1}H- and ^{31}P-NMR spectroscopic methods. The results indicated that the phosphate groups can provide suitable sites for metal ion coordination in acidic medium, while in the higher pH range the hydroxyl groups of the studied sugars or the sugar moieties of the two nucleotides play a role in the mechanistic process. Li et al. [133] investigated the interaction of Et_2SnCl_2(phen) with 5′-dGMP in aqueous medium, using [*trans*-$en_2Os(\eta\text{-}H_2)](CF_3SO_3)_2$, a versatile ^{1}H-NMR probe. Hadjiliadis et al. [134] have studied the interactions of purine nucleotides 5′-IMP and 5′-GMP with Et_2SnCl_2 using various techniques, including ^{1}H-, ^{13}C and ^{31}P-1D-NMR and Mössbauer spectroscopy. Other researchers studied the interactions of $Me_2Sn(IV)^{2+}$ with 5′-AMP, D-ribose-5-phosphate, D-glucose-6-phosphate and D-glucose-1-phosphate [135]. All these authors concluded that at low pH values (pH < 4) the organotin(IV) cations interact with pyrophosphate {O}. At intermediate pH values (pH = 4–9.5) no interaction takes place (depending on the concentration of metal ion and the ligand to metal ratio a precipitate is formed), while at pH > 9.5 the sugar O′-2 and O′-3 atoms are the preferred coordination sites. Additionally two oligomeric complexes were obtained, containing tin(IV) centers in trigonal-bipyramidal or octahedral geometry. From these investigations, it was concluded that the mechanism of antitumor action of organotin(IV) complexes (if the target is DNA) differs substantially from cisplatin as it forms stable adducts with the N7 of guanine residue of DNA whereas the activity of these organotin(IV)

complexes seems to come from their preferred binding to the phosphate backbone of DNA double helix.

The current synthetic trend in the pharmaceutical regime includes the development of multinuclear metal assemblies that provide better recognition for the drug target. Keeping with this trend, the novel heterobimetallic complexes of copper-tin scaffold were developed by our group [136]. Previous studies of copper(II) and copper(II)-tin(IV) complexes have shown interesting results against various cancerous cell lines (HeLa cells, T47D, HT29) [137,47]. These heterobimetallic complexes of copper(II)-tin(IV) ions enhance the chemotherapeutic action many-fold as they provide a dual mode of binding at the molecular target and also exhibit novelty due to preferential selectivity inside the cell (the tin(IV) ions interact with the phosphate backbone of DNA while the copper(II) ion show selectivity towards the N7 position of guanine nucleobase). The molecular design of novel chiral complex $[CuL_2Sn_2Cl_5]$ was very unique as it provided distinct recognition properties for biopolymer structure. The complex possesses two metal centers, a copper(II) and tin(IV) metal ion, which act in accord with each other to distort the DNA structure. Thus, the mechanism of antitumor action of tin(IV) complexes substantially differs from classical anticancer drugs (cisplatin) and modulatory activity of transition metal ions in presence of tin is a unique way to address resistance of the anticancer drugs. Preliminary DNA binding profile of the complexes exhibit an electrostatic mode of binding of the complex with DNA as revealed by the apparent hyperchromism in the absorption spectra of the complex (Figure 16b).

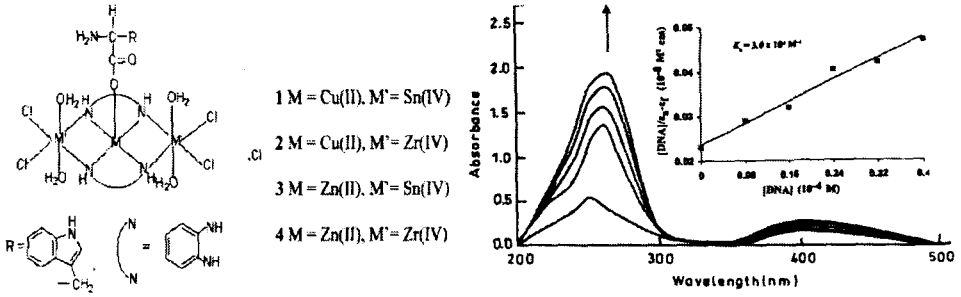

Figure 16. *(a) Chemical structure of heteronuclear tin(IV) modulated copper(II) trinuclear complexes. (b) Absorption spectral traces of complex* $[CuL_2Sn_2Cl_5]$ *)in Tris-HCl buffer upon addition of DNA. Inset: Plots of [DNA] /* ε_a-ε_f *vs [DNA] for the titration of CT-DNA with complexes* ■*, experimental data points; full lines, linear fitting of the data. [Complex]=0.16 x10*$^{-4}$ *M, [DNA]=0-0.40 x10*$^{-4}$ *M.*

It has been demonstrated that these complexes induce apoptosis via, mitochondrial pathway. *In vitro* antitumor activity of $[CuL_2Sn_2Cl_5]$ further justifies its potent antitumor effect, which is capable of inhibiting the growth of SY5Y by 60% at 8 μM and of PC-12 by 70% at 2 μM. In the case of the SY5Y neuroblastoma cell line, the complex exhibited significant antiproliferative activity indicative of apoptosis. The immunoblot analysis demonstrated that mitochondrion play a key role in governing the induction of apoptosis by $[CuL_2Sn_2Cl_5]$.

The combined interest to improve the DNA cleavage specificity of Cu(3-clip-Phen) complexes together with their ability to perform double strand breaks (DSB) and to circumvent drug resistance owing to the use of cisplatin has inspired Reedijk et al. [138] to synthesize heterodinuclear bifunctional molecules containing both active entities namely copper unit and platinum component from cisplatin (Figure 17). The inherently specific DNA binding characteristics of two seperate active metallic centers contribute towards a higher affinity of the complexes CuPt[N*1*{6-[3-Clip-Phen]-hexyl}-ethane-1,2-diamine]Cl_4 and CuPt[N*1*{10-[3-Clip-Phen]-decyl}-ethane-1,2-diamine]Cl_4 with DNA, binding selectively to their respective target sites.

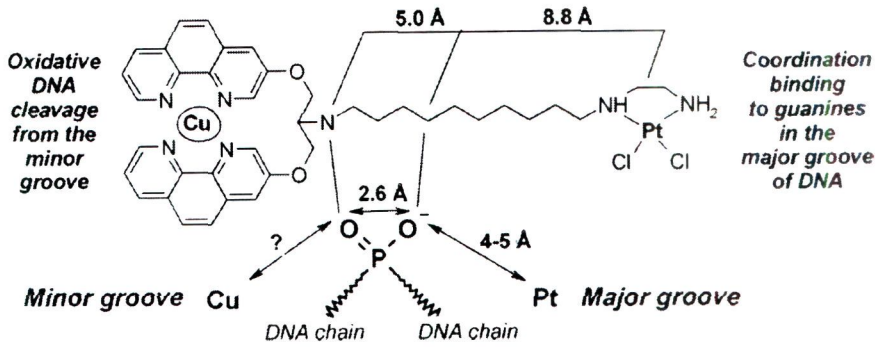

Figure 17. *Strategy adopted for the synthesis of heterodinuclear minor / major groove interacting complexes.*

Depending on their mutual degree of freedom, both molecule will or will not reach their preferential site of interaction (the nitrogen atom N7 of guanine in the major groove for the platinum component and and the minor groove for the copper unit) simultaneously.

Heterodinuclear complexes also exhibit cleavage activities and were able to perform direct double strand cuts in contrast to monometallic Cu(3-clip-Phen) alone which was capable of carrying out successive single strand cuts (Figure 18).

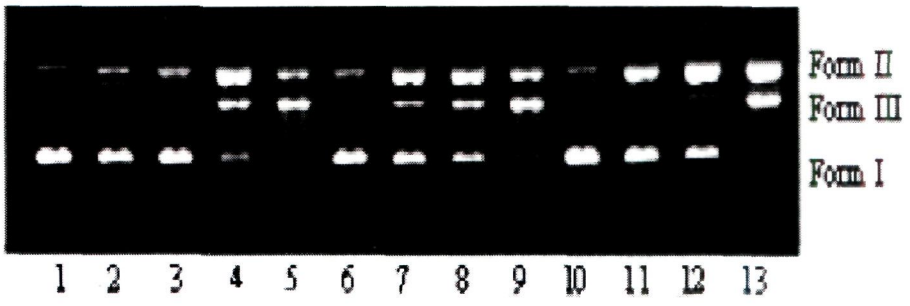

Figure 18. *Comparison of the oxidative cleavage of ΦX174 plasmid DNA performed by CuPt[N*1*-{6-[3-Clip-Phen]-hexyl}-ethane-1,2-diamine]Cl_4 (13), CuPt[N*1*-{10-[3-Clip-Phen]-decyl}-ethane-1,2-diamine]Cl_4 (14) and Cu(3-Clip-Phen) in the presence of 5 mM MPA. Lane 1: control DNA. Lane 2: 250 nM 13 without MPA. Lane 3: 100 nM 13. Lane 4: 150 nM 13. Lane 5: 250 nM 13. Lane 6: 250 nM 14 without MPA. Lane 7: 100 nM 14. Lane 8: 150 nM 14, Lane 9: 250 nM 14, Lane 10: 250 nM Cu(3-Clip-Phen) without MPA. Lane 11: 100 nM Cu(3-Clip-Phen). Lane 12: 150 nM Cu(3-Clip-Phen). Lane 13: 250 nM Cu(3-Clip-Phen).*

With the objective of lowering the systemic toxicity of metal-based drugs, successful modular synthesis of heterotrinuclear complexes has been carried out that combines the class of compounds with paltinum(II) centre, resembling cisplatin and two ruthenium (III) centres that resemble NAMI by bridging dinitrogen ligands [139]. Such design has been done to achieve both efficacy and selectivity of the drugs and studies pertaining to these complexes have demonstrated that these complexes are potent against both neoplastic tumors and metastatic cancer.

DNA biopolymer comprises of a polymorphic structure with a polyanionic nucleotide chains and sugar phosphate backbone [140]. It exists predominantly in a right handed B-form helical conformation although other conformations of DNA (A-form and Z-DNA) are also known (Figure 19). It plays an important role in the life processes since it contains all the genetic information necessary for cellular function.

Figure 19. *Different conformational variations of DNA (a) B-DNA (b) Z-DNA (c) A-DNA.*

The DNA molecules are much susceptible to damage by interacting with metal complexes under various physiological conditions. This damage may lead to various pathological changes in living organisms. Thus, the interaction of metal complexes with DNA was regarded deciding factor to ascertain the chemotherapeutic potential of these metal complexes. Based on these considerations, binding modes of

metallomolecules can be classified broadly into covalent binding and non-covalent interactions. Covalent binding involve the replacement of the labile ligand by nitrogenous base of DNA such as N7 of guanine. On the other hand, non-covalent interactions include intercalative, electrostatic and groove (surface) binding of the cationic metal complexes along the outside of the DNA helix (Figure 20). Intercalative interaction involves stacking of the planar fused aromatic cations in between the adjacent base pairs of DNA helix.

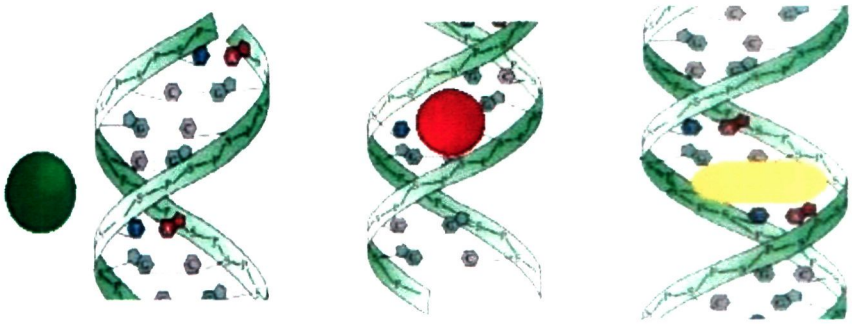

Figure 20. *Various interaction modes of small molecules with DNA (a) electrostatic (b) groove binding (c) intercalation.*

The other non-covalent interactions include the electrostatic and groove binding interactions. Molecules that bind in the minor grooves comprise arc shaped aromatic architectures with terminal base functions while the electrostatic mode of binding is governed by charge of the molecule, ligand hydrophobicity and total size of the ions. In the electrostatic mode of binding, complexes exhibit an effective binding with the phosphate backbone of DNA double helix. Apart from the damage of the secondary structure of DNA by these electrostatic interactions, the other consequences associated with the external binding of the cations to the DNA backbone is that separate DNA duplexes associate together to form aggregates or condensed structures.

The DNA-binding compounds such as BBR3464 (Figure 21) is covalent, but a significant non covalent component arises from the presence of the central platinum (tetramine) unit which interacts with DNA only through electrostatic and hydrogen bonding effects [141].

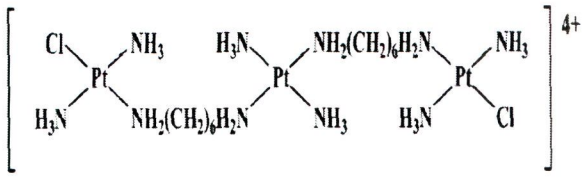

Figure 21. *Structure of BBR3464(1,0,1/t,t,t).*

The highly charged compound induces B→A and B→Z conformation changes in the canonical sequences of DNA. Non covalent concept is extended in this complex by use of dangling amines which increase the charge and charge dispersion along these linear cations, surprisingly results in significantly enhanced cellular accumulation, with a higher charge (8+) has about 5 times greater cellular uptake enhanced cytotoxity is observed across a panel of ovarian tumor cell lines despite the reversible nature of DNA binding. The ultimate goal of these approaches is to disrupt the vital cellular processes at the molecular level to trigger downstream events ultimately leading to cancer cell death.

The specific binding mode of metal complexes as well as consequent DNA structural changes can be analysed employing biophysical techniques such as UV-visible, fluorescence, NMR (^{1}H and ^{31}P NMR), circular dichroism, viscosity, gel electrophoresis. Each of these techniques has proven to be reliable for discerning the exact nature of DNA-metallomolecule interactions. The cooperative conformational and structural transitions induced by metal complexes were assessed primarily by UV-visible spectrometry revealed by absorption spectral perturbations of the

complexes upon addition of DNA. Recent report by U. Chaveerach et al. [142] described the synthesis and characterization of copper(II) complexes $[Cu(L^{1m})_2]Cl_2$ (L^{1m} = amidino-O-methylurea) and $[Cu(L^{2m})_2]Cl_2$ (L^{2m} = N-methylphenyl-amidino-O-methylurea) and their DNA binding studies. Upon addition of CT-DNA to the complexes $[Cu(L^{1m})_2]Cl_2$ and $[Cu(L^{2m})_2]Cl_2$, increase in the absorption intensity (hyperchromism) was obtained indicative of a partial or non-intercalative binding mode possibly by (i) hydrogen bonds of the amine group with the nucleobases of DNA (ii) electrostatic interactions among $[Cu(L^{1m/2m})_2]^{2+}$ cationic species and the negatively charged phosphate groups on the DNA backbone (iii) in case of complex $[Cu(L^{2m})_2]Cl_2$, an intercalative interactions by the aromatic species. The intrinsic binding constants (K_b) of complexes $[Cu(L^{1m})_2]Cl_2$ and $[Cu(L^{2m})_2]Cl_2$ were found out to be $5.67x10^4$ M^{-1} and $1.16x10^5$ M^{-1} respectively, lower than that of classical intercalator ethidium bromide ($1.40x10^6$ M^{-1}) suggesting a weak electrostatic association of these complexes with DNA (Figure 22a,b).

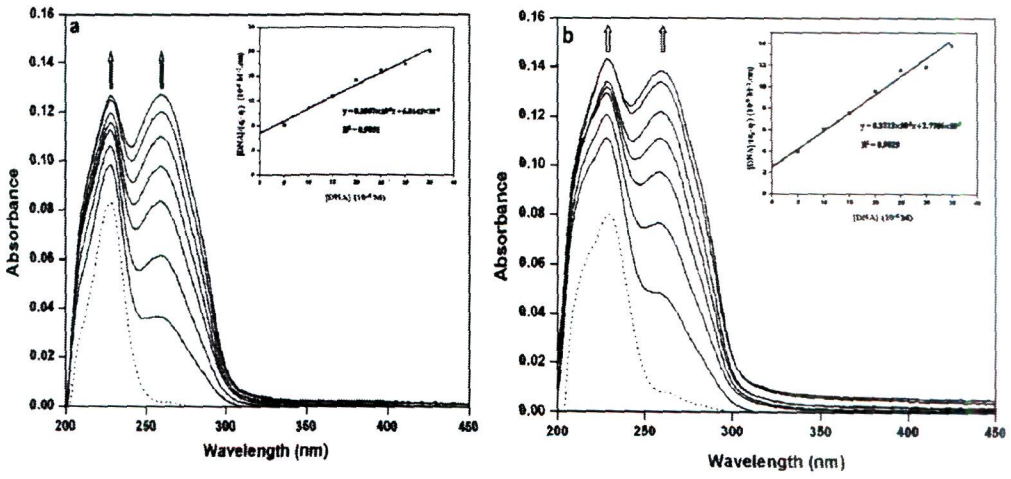

Figure 22. *Absorption titration spectra of complexes (a) $[Cu(L^{1m})_2]Cl_2$ and (b) $[Cu(L^{2m})_2]Cl_2$ in the absence (·····) and presence (—) of increasing amounts of DNA from 0 to 35 μM. [complex] = 25 μM. Arrows show the absorbance change with increasing DNA concentrations.*

Viscosity measurements were carried out on DNA by varying the concentration of copper(II) complexes in the [Complex]/[DNA] ratio (r) of 0.00-0.50 (Figure 23). The relative viscosity change of a classical intercalators ethidium bromide was compared with the synthesized complexes $[Cu(L^{1m})_2]Cl_2$ and $[Cu(L^{2m})_2]Cl_2$. Both the complexes exhibit considerable decrease in the relative viscosity (r=0.00-0.25) of DNA reducing its effective length by producing bends and kinks in the DNA strand. Secondly, when the value of r was increased from 0.25-0.40, a rapid increase in the DNA viscosity was observed attributed to an intercalative binding mode. Finally, the relative viscosity of DNA remains unchanged from 0.40-0.50 due to electrostatic interactions and saturation of the binding site. These results reveal that the complex $[Cu(L^{2m})_2]Cl_2$ exhibits greater binding propensity as compared to $[Cu(L^{1m})_2]Cl_2$.

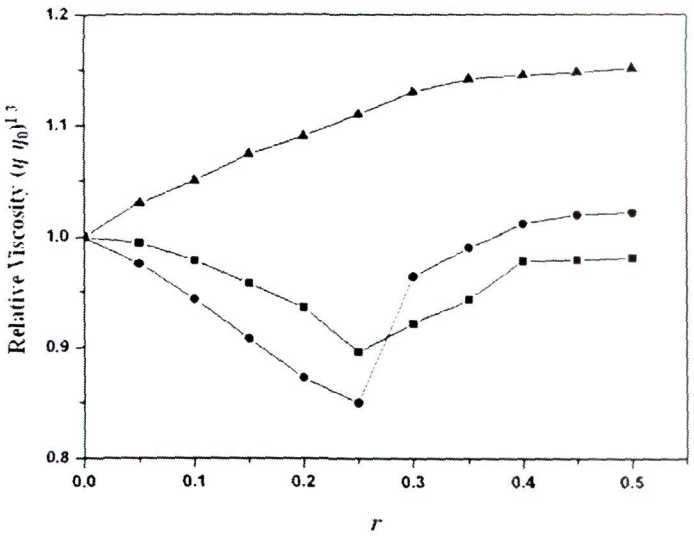

Figure 23. *Effect of increasing amount of ethidium bromide (▲) complex* $[Cu(L^{1m})_2]Cl_2$ *(■) and complex* $[Cu(L^{2m})_2]Cl_2$ *(●) on the relative viscosity of CT DNA vs. the [complex]/[DNA] (r) ratio with [DNA]= 50 μM.*

In addition to the above spectral studies carried out with CT-DNA, gel electrophoresis experiments using pBR322, plasmid DNA were also performed under physiological conditions to investigate the ability of the complexes to serve as metallonucleases. The naturally occurring supercoiled form (Form I), when nicked,

gives rise to an open circular relaxed form (Form II) and further cleaves to a linear form (Form III). When subjected to gel electrophoresis, Form I shows the fastest migration compared to Forms II and III. Form II migrates very slowly prior to its relaxed structure whereas Form III migrates somewhere between the positions of Form I and Form II. From the results, it was verified that at millimolar concentrations cleavage of plasmid DNA. (Figure 24a,b) (Lanes 2-6) represents the cleavage pattern observed for complexes $[Cu(L^{1m})_2]Cl_2$ and $[Cu(L^{2m})_2]Cl_2$ with increasing concentrations of the complex ranging from 50, 100, 200, 300, 400 μM. The results reveal that an increasing amount of the complex $[Cu(L^{1m})_2]Cl_2$ led to a gradual diminish of Form I with a subsequent increase in Form III by 16.55%.

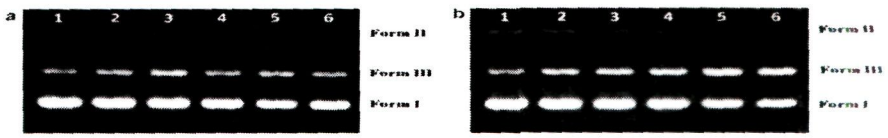

Figure 24. *Gel electrophoresis diagrams showing the cleavage of supercoiled pBR322 DNA (0.25 μg) by complexes (a) $[Cu(L^{1m})_2]Cl_2$ and (b) $[Cu(L^{2m})_2]Cl_2$ in 5 mM Tris–HCl/50 mM NaCl buffer at pH 7.0 and 37 °C with an incubation time of 24 h: Lane 1, DNA control; Lanes 2–6, DNA + [complex] (50, 100, 200, 300 and 400 μM, respectively). Forms I, II and III are supercoiled, nicked circular and linear DNA, respectively.*

While the complex $[Cu(L^{2m})_2]Cl_2$ also shows a similar result with a disappearance of Form I and gradual increase in the Form III by 17.75% suggestive of a stronger DNA cleavage activity for complex $[Cu(L^{2m})_2]Cl_2$ compared to complex $[Cu(L^{1m})_2]Cl_2$ which corroborates well with their DNA binding capabilities.

On incubation of complexes $[Cu(L^{1m})_2]Cl_2$ and $[Cu(L^{2m})_2]Cl_2$ (400 μM) with pBR322 DNA in the presence of hydrogen peroxide, the amount of Form III obtained was considerably greater than in the presence of complexes alone (Lanes 6,7 Figure 25a,b) showing that DNA degradation induced by the copper(II)

complexes via oxidative pathway was enhanced in the presence of hydrogen peroxide.

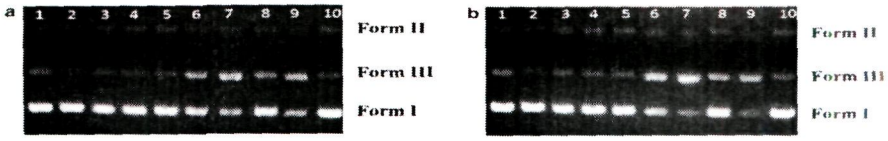

Figure 25. *Gel electrophoresis diagrams showing the cleavage of supercoiled pBR322 DNA (0.25 μg) by complexes (400 μM): (a) $[Cu(L^{1m})_2]Cl_2$ and (b) $[Cu(L^{2m})_2]Cl_2$, with addition of H_2O_2 (100 μM) with/without scavengers including DMSO (4 lL), t-BuOH (100 lM) and NaN_3 (100 lM) in 5 mM Tris–HCl/50 mM NaCl buffer at pH 7.0 and 37 °C with an incubation time of 24 h. Lane 1, DNA control; Lane 2, DNA + H_2O_2; Lanes 3–5, DNA + scavengers (DMSO, t-BuOH and NaN_3, respectively); Lane 6, DNA + complex; Lane 7, DNA + complex + H_2O_2; Lanes 8–10, DNA + complex + H_2O_2 + scavenger (DMSO, t-BuOH and NaN_3, respectively).*

In order to gain further insight of the DNA cleavage by these copper(II) complexes hydroxyl radical scavengers (DMSO and t-BuOH) and a singlet oxygen scavenger (NaN_3) were added into the samples under similar conditions (Lanes 8-10, Figure 25a,b). The results revealed that both the hydroxyl radical (Lane 8,9) and more dominant singlet oxygen species (Lane 10) were involved in the oxidative cleavage pathway.

Present Work

The development of metal-based chemotherapeutic drugs has gained much emphasis owing to their superior binding ability and specific recognition to the molecular target DNA. Heterobimetallic architecture utilizes a unique building block strategy which involves combination of two or more active metal centers exhibiting differential behaviour towards the cellular target DNA. Furthermore, the metal properties are fine-tuned by introducing appropriate ligands which are themselves active pharmacophores. Such combination agents behave as a single chemical entity capable to modulate multiple targets simultaneously acting in accord. possibly delivering superior efficacy against diseases in particular, for treating tumors. Literature supports that heterobimetallic complexes exhibit better cleavage activities as two or more metal centers involved were found to act synergistically in DNA cleavage in contrast to monometallic analogues.

In an attempt to identify new metal-based antitumor agents that show promise to overcome inherent resistance and exhibit fewer side effects, new heterobimetallic complexes $[C_6H_{24}N_4O_6CuSn_2Cl_4]Cl_2$ and $[C_6H_{24}N_4O_6ZnSn_2Cl_4]Cl_2$ derived from their monometallic analogues $[C_6H_{20}N_4O_2Cu]Cl_2$, $[C_6H_{20}N_4O_2Zn]Cl_2$, were designed and synthesized. These complexes were thoroughly characterized by spectroscopic (IR, ^1H, ^{13}C, ^{119}Sn NMR, EPR, UV-vis, ESI-MS) and analytical methods. Electronic absorption titrations, fluorescence and cyclic voltammetric studies in free complexes and in the presence of DNA supported that both the complexes bind to DNA by electrostatic interaction via phosphate backbone of the helix pertaining to the presence of Lewis acid metal binding sites- copper and tin centers. Cleaving activity of the complexes employing agarose gel electrophoresis with pBR322 plasmid DNA

was also carried out to examine their scission activity. These studies revealed that both the heterobimetallic complexes were efficient cleaving agents of pBR322 plasmid DNA.

Among the various factors governing the binding mode of complexes molecular shape, size and stereo chemical orientation of the molecule are regarded as most significant. Those complexes that best fit against the helical structure of DNA display the highest binding affinity for DNA. Thus, chirality plays a profound role in the different pharmacological effects exhibited by enantiomeric drug molecules revealing a preferential binding of one conformation over another, which is termed as enantioselectivity. The chiral discrimination of DNA has been crucial for the determination of the binding mode of the complexes with DNA. Keeping this in mind new chiral complexes(S)/(R)-[$C_{15}H_{21}NO_2Sn$] and (S)/(R)-[$C_{10}H_{16}NOSnCl$] were designed and synthesized with the aim to develop new chiral chemotherapeutic antitumor agents. The conformational difference arising due to the binding of S- and R-enantiomer of the organotin Schiff base complexes (S)/(R)-[$C_{15}H_{21}NO_2Sn$] and (S)/(R)-[$C_{10}H_{16}NOSnCl$]was ascertained by comparative DNA-binding studies of both forms of the complexes and ligands. Electronic absorption, fluorescence titrations and circular dichoric studies in the presence of CT-DNA supported that both the enantiomers bind to DNA by non-covalent mode of binding viz, electrostatic interaction via phosphate backbone of the helix, nevertheless, S-enantiomer is more potent and exhibits enhanced binding propensity for DNA as compared to R-enantiomer. Significantly promising *in vitro* cytotoxic activity of S-enantiomer of complexes demonstrates their high antitumor potential.

The ligand framework plays significant role in metal-based pharmaceuticals via, alteration in the biological properties by modifying reactivity or substitution inertness. Besides this, the introduction of chirality enhances the pharmacological behaviour of the metal complexes by adopting specific conformation and target selective binding with DNA. The organotin(IV) complexes $[C_{18}H_{19}N_4O_2SnCl]$, $[C_{28}H_{23}N_4O_2SnCl]$ and $[C_{52}H_{42}N_4O_2Sn_2]$ of biologically significant benzimidazole tridentate chiral ligand via, 1,2-Bis(1H-benzimidazole-2yl)-ethane-1,2-diol, were synthesized and their DNA-binding properties were elucidated by various biophysical techniques. The results of these techniques revealed a pronounced multifaceted binding for complex $[C_{28}H_{23}N_4O_2SnCl]$ owing to its different structural constraints in comparison to $[C_{18}H_{19}N_4O_2SnCl]$ and $[C_{52}H_{42}N_4O_2Sn_2]$ complexes. The varying DNA recognition of the complexes $[C_{18}H_{19}N_4O_2SnCl]$, $[C_{28}H_{23}N_4O_2SnCl]$ and $[C_{52}H_{42}N_4O_2Sn_2]$ was also elucidated on the basis of circular dichroism studies. Furthermore, specific mode of binding exhibited by the complexes as ascertained by nucleotide recognition of these complexes with 5′-GMP and 5′-TMP using electronic absorption and NMR techniques (^1H and ^{31}P NMR).

Another class of Schiff base ligand derived from condensation reaction of natural chromone derivative 2-amino-3-formylchromone and 2-amino-2-phenylethanol was synthesized and thoroughly characterized. The complexation of ligand 2-amino-3-((2-hydroxy-1-phenylethylimino)methyl)-4H-chromen-4-one with $Cu(NO_3)_2.3H_2O$ and $Zn(NO_3)_2.6H_2O$ was carried out to obtain desired complexes $[C_{36}H_{34}N_4O_7Cu](NO_3)_2$ and $[C_{36}H_{32}N_4O_6Zn](NO_3)_2$ in moderate yields. *In vitro* DNA binding and cleavage studies of both the complexes $[C_{36}H_{34}N_4O_7Cu](NO_3)_2$ and $[C_{36}H_{32}N_4O_6Zn](NO_3)_2$ were investigated to evaluate their comparative binding

extent with CT-DNA. The DNA binding studies reveal a clear preference of binding exhibited by copper(II) complex $[C_{36}H_{34}N_4O_7Cu](NO_3)_2$ with DNA in comparison to its $[C_{36}H_{32}N_4O_6Zn](NO_3)_2$ analogue. DNA cleavage studies with pBR322 plasmid DNA was carried out for $[C_{36}H_{34}N_4O_7Cu](NO_3)_2$complex owing to its high binding potential. The complex revealed an excellent DNA cleavage activity both in absence and presence of any external reducing or activating agents. The results of DNA binding and cleavage activity cumulatively show a groove binding pattern of complexes with CT-DNA.

CHAPTER II

Experimental

CHAPTER II

EXPERIMENTAL METHODS

The following techniques were employed

1. Materials

2. Characterization techniques

2.1 Infrared spectroscopy

2.2 Ultra-violet and visible spectroscopy

2.3 Nuclear magnetic resonance spectroscopy

2.4 Electron paramagnetic resonance spectroscopy

2.5 Mass spectroscopy

2.6 Molar conductance measurements

2.7 Polarimetry

3. DNA binding studies

3.1 Absorption spectral studies

3.2 Fluorescence spectral studies

3.3 Circular dichroic spectral studies

3.4 Cyclic voltammetry

3.5 Viscometry studies

3.6 Gel electrophoresis

4. *In vitro* antitumor studies

1.Materials

$CuCl_2.2H_2O$, $Cu(NO_3)_2.3H_2O$, $Zn(NO_3)_2.6H_2O$, acetylacetone and L-(+)-tartaric acid (E.Merck), 1,3-diamino-2-propanol, 2-amino-3-formylchromone (Aldrich), $ZnCl_2$ (anhydrous) (Rankem), $SnCl_4.5H_2O$ (Lancaster), (S)/(R)-2-amino-2-phenylethanol, dimethyltin(IV)dichloride, diphenyltin(IV)dichloride, triphenyltin(IV)chloride, Tris(hydroxymethyl)aminomethane or Tris-buffer (Sigma), 1,2-diamino benzene (Loba Chemie) were used as received. Disodium salt of calf thymus DNA (CT-DNA), guanosine 5′-monophosphate disodium salt (5′-GMP), thymine 5′-monophosphate disodium salt (5′-TMP), cytidine 5′-monophosphate, adenosine 5′-monophosphate (Sigma) and was stored at 4 °C. 6X loading dye (Fermental Life Science), agarose gel, ascorbic acid, sodium azide (NaN_3), DMSO, superoxide dismutase (SOD), methyl green, DAPI, mercaptopropionic acid (MPA) (Sigma-Aldrich) and Super coiled pBR322 DNA (Genei) were utilized as received. All reagent grade compounds were used without further purification.

2. Characterization techniques

Carbon, hydrogen and nitrogen contents were determined using Carlo Erba analyzer model 1108. Melting points were determined by electrothermal apparatus. TLC was performed on commercial aluminium sheets precoated with 0.20 mm layers of silica gel. The visualization of spots on TLC plates was effected by exposure to iodine.

2.1 Infrared spectroscopy

Fourier transform infrared spectra were recorded on Interspec 2020 FTIR spectrometer in KBr pellets from 4000-400 cm^{-1}. The infrared spectroscopy is a useful technique to characterize a compound. It results from transition between

vibrational and rotational energy levels. IR region of the electromagnetic spectrum covers a wide range of wavelength from 200-4000 cm^{-1}. It has been found that in IR absorption, some of the vibrational frequencies are associated with specific groups of atoms and remain same irrespective of the molecules in which the group is present. These are called characteristic frequencies and their constancy results from the constancy of bond force constants from molecule to molecule. The important observation that the IR spectrum of a complex molecule consists of characteristic group frequencies makes IR spectroscopy, unique and powerful tool in structural analysis.

2.2 Ultra-violet and visible spectroscopy

The electronic spectral studies of metal complexes provide useful information about the stereochemistry, oxidation state of the metal ion and in suitable circumstances, the nature of metal-ligand bond. Electronic spectra were recorded on a UV-1700 PharmaSpec UV-visible spectrophotometer in methanol and DMSO and methanol as solvent.

2.3 Nuclear magnetic resonance spectroscopy

The nuclei of certain isotopes possess a mechanical spin or angular momentum. The NMR spectroscopy is concerned with nuclei having nuclear spin quantum number I = 1/2, example of which include ^{1}H, ^{13}C, ^{31}P, ^{119}Sn and ^{19}F.

For a nucleus with I = 1/2, there are two values for the nuclear spin angular momentum quantum number $m_I = \pm 1/2$ which are degenerate in the absence of a magnetic field. However, in presence of the magnetic field, this degeneracy is destroyed such that the positive value of m_I corresponds to the lower energy state and negative value to higher energy state separated by ΔE.

In an NMR experiment, one applies strong homogeneous magnetic field causing the nuclei to presses. Radiation of energy comparable to ΔE is then imposed with radio frequency transmitter equal to precision or Larmor frequency and the two are said to be in resonance. The energy can be transferred from the source to the sample. The NMR signal is obtained when a nucleus is excited from low energy to high energy state.

^{1}H, ^{13}C and ^{119}Sn NMR spectra were obtained on a Bruker Avance DRX-400 spectrometer at 400 and 500 MHz, respectively operating at room temprature.

2.4 Electron paramagnetic resonance spectroscopy

Electron paramagnetic resonance (EPR) spectra of the Cu(II) complexes were obtained on a Varian E 112 EPR spectrometer using tetracyanoethylene (TCNE) as field marker. The spectra were recorded for solid and solutions of the complexes in appropriate solvents at room temperature (RT) as well as at liquid nitrogen temperature (LNT).

2.5 Mass spectroscopy

Mass spectrometry is one of the most accurate microanalytical technique which requires only a few nanomoles of the sample to obtain characteristic information regarding the molecular mass and to detect within a molecule the places at which it prefers to fragment from which the presence of recognizable group within the molecule can be deduced. Mass spectrometry is complementary to FT IR, NMR, UV-vis and EPR spectral techniques for structural identification of compounds.

Electrospray mass spectra were recorded on Micromass Quattro II triple quadrupol mass spectrometer.

2.6 Molar conductance measurements

The conductivity measurement is one of the simplest and easily available techniques used to study the nature of the complexes. It gives direct information regarding whether a given compound is ionic or covalent. For this purpose, the measurement of molar conductance (Λ_m), which is related to the conductance value in the following manner is made.

$$\Lambda_m = \frac{\text{cell constant x conductance}}{\text{concentration of solute expressed in mol cm}^{-3}}$$

Conventionally, solutions of 1.0×10^{-3} M strength are used for the conductance measurements. Molar conductance values of different types of electrolytes in a few solvents are given as, 1:1 electrolyte has a value of 80-115 ohm^{-1} cm^2 mol^{-1} in methanol, 65-90 Ω^{-1} cm^2 mol^{-1} in DMF, 78-80, 50-70 Ω^{-1} cm^2 mol^{-1} DMSO and 35-45 Ω^{-1} cm^2 mol^{-1} in ethanol [143]. Similarly a solution of 2:1 electrolyte has a value of 160-220 Ω^{-1} cm^2 mol^{-1} in methanol, 130-170 Ω^{-1} cm^2 mol^{-1} in DMF and 70-90 Ω^{-1} cm^2 mol^{-1} in ethanol.

Molar conductance was measured at room temperature on a Digisun electronic conductivity bridge.

2.7 Polarimetry

Optical isomerism manifests itself by the rotation that certain molecules impart to the plane of polarized light when in gaseous, liquid or molten state or in solution (Figure 29). This rotation is observed and measured by a rather simple instrument, known as polarimeter. The specific rotation [α] of a dissolved substance is given by the expression

$$[\alpha] = \frac{\alpha}{l \times c}$$

where α is the observed rotation in degrees

l is the path length of the sample in decimeters

c is the concentration in grams per milliliter

The dependence on wavelength and temperature is indicated by subscripts and superscripts respectively. Thus $[\alpha]_D^{25}$ means the specific rotation at 25 °C measured at the wavelength of the sodium D line.

Optical rotation is generally measured using light from a sodium-vapour lamp, which gives essentially monochromatic radiation (the yellow sodium D line is a doublet at 5890 and 5896 A°).

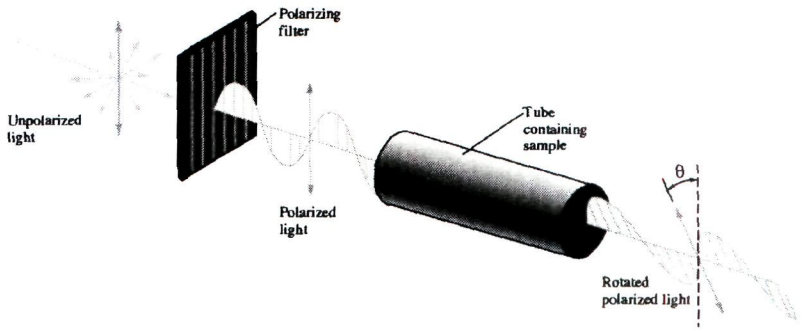

Figure 29. *Rotation of plane of polarized light by optically active compounds.*

A beam of light is polarized by passage through nicol prism (the polarizer),which consists of two calcite prisms cemented together so that only one of the two rays formed by double refraction is transmitted. The beam of polarized light passes through the solution and then through a second nicol prism. When no optically active material is placed between the prisms (0° rotation), the prisms are positioned at right angles so that no light is transmitted. When an optically active material is placed between the prisms, the analyzer must be turned in order to maintain the darkness in

the field of view. The optical rotation is the angle by which the analyzer is turned in order to reach darkness. It is very difficult to determine by eye the setting for complete darkness, because positions near the completely dark position are very dark. Therefore, many instruments are constructed such that the field of view is divided into two equal parts, and the analyzer is adjusted so as to equalize the light intensity in each half of the field.

Optical rotations of chiral ligands and complexes were determined on a Polarimeter Rudolf Autopol III.

3. DNA binding studies

All the experiments involving interaction of the complexes with CT-DNA were conducted in Tris buffer containing HCl (0.01 M) adjusted to pH 7.2 with hydrochloric acid. The CT-DNA was dissolved in Tris-HCl buffer and was dialyzed against the same buffer overnight. Solutions of CT-DNA gave ratios of UV absorbance at 260 and 280 nm above 1.8, indicating that the DNA was sufficiently free of protein [144]. DNA concentration per nucleotide was determined by absorption spectroscopy using the molar absorption coefficient 6600 $dm^3\ mol^{-1}\ cm^{-1}$ at 260 nm [145]. The stock solution was stored at 4 °C.

3.1 Absorption spectral studies

The intrinsic binding constant K_b of the complex to CT-DNA was determined from equation (1), through a plot of [DNA]/ ε_a-ε_f vs [DNA], where [DNA] represents the concentration of DNA, and ε_a, ε_f, and ε_b the apparent extinction coefficient (A_{obs} /[M]), the extinction coefficient for free metal complex (M), and the extinction

coefficient for the free metal complex (M) in the fully bound form, respectively. In plots of [DNA]/$|\varepsilon_a-\varepsilon_f|$ vs [DNA], K_b is given by the ratio of slope to intercept [146].

$$[DNA] / |\varepsilon_a-\varepsilon_f| = [DNA] / |\varepsilon_a-\varepsilon_f| + 1/ K_b |\varepsilon_a-\varepsilon_f| \quad (1)$$

Absorption spectral titration experiments were performed by maintaining a constant concentration of the complex and varying the nucleic acid/nucleotide concentration. This was achieved by diluting an appropriate amount of the metal complex solutions and DNA/5′-GMP and 5′-TMP stock solutions while maintaining the total volume constant. This results in a series of solutions with varying concentrations of DNA/5′-GMP and 5′-TMP but a constant concentration of the complex. The absorbance (A) was recorded after successive additions of DNA or 5′-GMP or 5′-TMP. While measuring the absorption spectra an equal amount of either CT-DNA or 5′-GMP or 5′-TMP was added to both the compound solution and the reference solution to eliminate the absorbance of the either CT-DNA or 5′-GMP or 5′-TMP itself.

3.2 Fluorescence spectral studies

The emission spectrum is obtained by setting the excitation monochromator at the maximum excitation wavelength and scanning with emission monochromator. Often an excitation spectrum is first made in order to confirm the identity of the substance and to select the optimum excitation wavelength. Further experiments were carried out to gain support for the mode of binding of complexes with CT DNA. Non-fluorescent or weakly fluorescent compounds can often be reacted with strong fluorophores enabling them to be determined quantitatively. On this basis molecular fluorophore EthBr was used which emits fluorescence in presence of CT DNA due to its strong intercalation. Quenching of the fluorescence of EthBr bound to DNA were measured with increasing amount of metal complexes as a second molecule

and Stern-Volmer quenching constant K was obtained from the following equation 2 [147].

$$I_0 / I = 1 + Kr \qquad (2)$$

where r is the ratio of total concentration of complex to that of DNA and I_0 and I are the fluorescence intensities of EthBr in the absence and presence of complex. Binding constant K of the metal complexes was also determined from equations 3 and 4 (Scatchard equations) by emission titration [148].

$$C_F = C_T (I / I_0 - P) (1-P) \qquad (3)$$

$$r / C_F = K (n-r) \qquad (4)$$

Where C_F is the free probe concentration, C_T is the total concentration of the probe added, I and I_0 are fluorescence intensities in presence and absence of CT DNA, respectively and P is the ratio of the observed fluorescence quantum yield of the bound probe to that of the free probe. The value P was obtained as the intercept by extrapolating from a plot of I/I_0 vs 1/ [DNA], r denotes ratio of C_B ($=C_T-C_F$) to the DNA concentration i.e., the bound probe concentration to the DNA concentration, K is the binding constant and C_F, is the free metal complex concentration and "n" is the binding site number. Emission intensity measurements were carried out using Hitachi F-2500 spectrofluorometer at room temperature.

3.3 Circular dichroic spectral studies

Circularly polarized light represents a wave in which the electrical component spirals around the direction of propagation of the ray, either clockwise or counterclockwise. Within the absorption band, the molar absorptivity for right and left handed

circularly polarized light is different, that is $(\varepsilon_d-\varepsilon_l) \neq 0$. This effect changes linearly polarized light into elliptically polarized light and is known as circular dichroism.

The amplitude of d component will be greater than the l component when l component of the substance absorbs left circularly polarized light, more strongly than d component which absorb the right circularly polarized light i.e. $\varepsilon_l > \varepsilon_d$ Furthermore, if $\varepsilon_d > \varepsilon_l$ then the d component will be retarded more than the l component (Figure 30).

The ellipticity, that is the angle whose tangent is ratio of minor axis of the ellipse OB to the major axis OA, is denoted by θ. The molecular ellipticity $[\theta]$ can be shown by the relationship [149].

$$[\theta] = 3305 (\varepsilon_l - \varepsilon_d)$$

Circular dichroism graphs are plots of $[\theta]$ against wavelength. Circular dichoric spectra were obtained on JASCO J-715/J-710 CD spectropolarimeter at 25 °C.

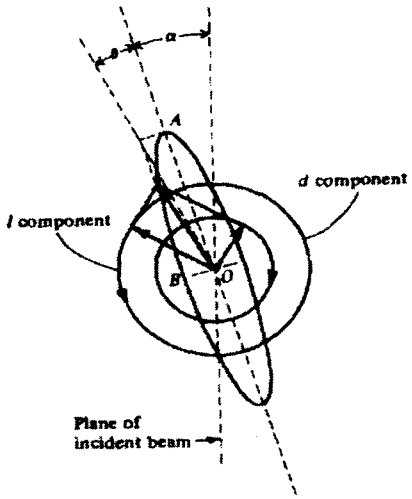

Figure 30. *Elliptically polarized light produced when $\eta_d > \eta_l$ and $\varepsilon_l > \varepsilon_d$.*

3.4 Cyclic voltammetry

Cyclic voltammetry involves the measurement of current-voltage curves under diffusion controlled, mass transfer conditions at a stationary electrode, utilizing

symmetrical triangular scan rates ranging from a few millivolts per second to hundred volts per second. The triangle returns at the same speed and permits the display of a complete polarogram with cathodic (reduction) and anodic (oxidation) waveforms one above the other. Two seconds or less is required to record a complete polarogram [150].

Consider the reaction

$$O + ne^- \longrightarrow R \qquad \text{(i)}$$

Assuming semi-infinite linear diffusion and a solution containing initially only species O. With the electron held at a potential E_I where no electrode reaction occurs. The potential is swept linearly at v v/sec so that the potential at any time is

$$E(t) = E_I - vt$$

$$\text{or} \quad E_{peak} = E^0 - 0.0285$$

The rate of electron transfer is so rapid at the electrode surface that species O and R immediately adjust to the ratio according to the Nernst equation, which is as follows,

$$C_o(0,t) = C_o^* - [nFA(\pi D_0)^{1/2}]^{-1} \int I(\pi)(t-\tau)^{-1/2}\, d\tau \qquad \text{(ii)}$$

$$I = nFAC_o^*(\pi D_0 \sigma)^{1/2} x\, (\sigma t) \qquad \text{(iii)}$$

Redox (electron-transfer) reactions of metal complexes can be investigated by cyclic voltammetry. An electrode is immersed in a solution of the complex and voltage is swept while current flow is monitored. No current flows until oxidation or reduction occurs. After the voltage is swept over a set range in one direction, the direction is reversed and swept back to the original potential. The cycle may be repeated as often

as desired. Figure 31(a-b). shows the cyclic voltammograms (CV) for a reversible one-electron redox reaction such as,

$$CpFe(CO)LMe \longrightarrow CpFe(CO)LMe^{+} + e^{-}$$

Sweeping the potential in an increasing direction oxidize the complex as the anodic current I_a flows; reversible reduction of $CpFe(CO)LMe^{+}$ generates cathodic current I_c on the reverse sweep. The magnitude of the current is proportional to the concentration of the species being oxidized or reduced.

The measured parameters of interest on these cyclic voltammograms are I_{pa}/I_{pc} the ratio of peak currents, E_{pa} - E_{pc} the separation of peak potentials and the formal electrode potential E^0. For a Nernstian wave with stable product, the ratio $I_{pa}/I_{pc} = 1$ regardless of scan rate, E^0 and diffusion coefficient, when I_{pa} is measured from the decaying current as a base line. The difference between E_{pa} and E_{pc} (ΔE_p) is a useful diagnostic test of a Nernstian reaction. Although ΔE_p is slightly a function of E^0. it is always close to 2.3RT/ nF.

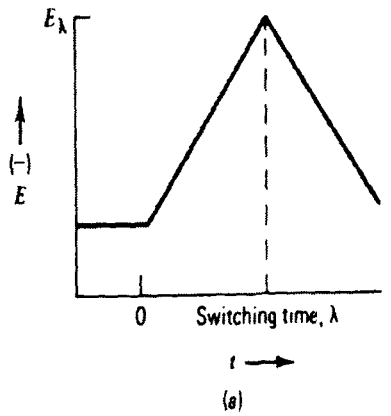

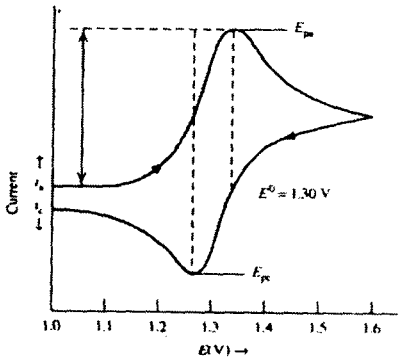

Figure 31. (a) *Cyclic potential sweep* (b) *Resulting cyclic voltammogram*

The technique yields information about reaction reversibilities and also offers a rapid means of analysis for suitable systems. The method is particularly valuable to study

interaction of metal ions to DNA as it provides a useful compliment to other methods of investigation, such as UV/vis spectroscopy. Cyclic voltammetric studies were accomplished on a CH Instrument Electrochemical analyzer using a three-electrode configuration comprised of a Pt wire as the auxiliary electrode, a platinum micro-cylinder as the working electrode and Ag/AgCl as the reference electrode. Supporting electrolyte for the experiments was 0.4 KNO_3. Electrochemical measurements were made under nitrogen atmosphere. All electrochemical data were collected at 298 K and are uncorrected for junction potentials.

Cyclic voltammetric measurements were carried out on a CH instrument electrochemical analyzer.

3.5 Viscometric studies

The hydrodynamic changes are the consequence of the change in length of the molecule, the diminished bending between layers and the diminished length-specific mass. Viscosity measurements were carried out using Ostwald's viscometer at 29±0.01 ^{0}C. Flow time was measured with a digital stopwatch. Each sample was measured three times and an average flow time was calculated. Data were presented as (η/η_0) versus binding ratio ([M]/[DNA]), [151] where η is a viscosity of DNA in the presence of complex and η_0 is the viscosity of DNA alone. Viscosity values were calculated from the observed flow time of DNA containing solution (t >100s) corrected for the flow time of buffer alone (t_0), $\eta = t - t_0$.

Viscosity measurements were carried out using Ostwald capillary viscometer maintained at 29±0.01 ^{0}C. Several time readings were obtained at each titration point. DNA binding and cleavage experiments were performed at 25 $^\circ$C.

3.6 Gel electrophoresis

Gel electrophoresis is a technique widely used for separation and analysis of charged biomolecules like nucleic acids [152]. Any charged biomolecule migrates when placed in an electric field. The ratio of migration of a molecule depends on its net charge, size, shape and the applied current. This can be represented as follows

$$V = E.q / f$$

Where V = velocity of migration of the molecule, E = electric field in volts/cm, q = net charge on the molecule, f = frictional coefficient which is function of mass and shape of molecule. The movement of a charged molecule in an electric field is often expressed in terms of electrophoretic mobility (μ), which is defined as the velocity per unit of electric field.

$$\mu = V/E = E.\ q/f.\ E$$

$$\mu = q/f$$

For molecules with similar conformation, 'f' varies with size but not with shape. Thus electrophoretic mobility (μ) of a molecule is directly proportional to the charge density (charge/mass ratio). Molecules with different charge/mass ratio migrate under the electric field at different rates and hence get separated. This is the basic principal for all the electrophoretic techniques. Depending upon the nature of support medium, electrophoresis is of different types such as paper, starch, polyacrylamide and agarose gel electrophoresis. We have opted agarose gel electrophoresis, because agarose gels are more porous as compared to polyacrylamide gels and are, therefore, used to fractionate large macromolecules such as DNA that cannot be readily penetrate into and move through other types of supporting materials. Agarose is a linear polymer of D-galactose and 3,6-anhydro-L-

galactose. When an electric field is applied across agarose gel, DNA molecules that are negatively charged at neutral pH, migrate towards oppositely charged electrode at rates determined by their molecular size and conformation. DNA molecules of the same size but with different conformation travel at different rates. The order of migration velocity in the increasing order of various forms of DNA is : supercoiled DNA> linearized DNA > open circular DNA.

4. *In vitro* antitumor studies

The cell lines used for *in vitro* antitumor screening activity were Hop62 (human lung), DWD (Human oral), K562 (Human leukemia), DU145 (Human prostrate) and MCF-7 (Human breast). These human malignant cell lines were procured and grown in RPMI-1640 medium supplemented with 10% Fetal Bovine Serum (FBS) and antibiotics to study growth pattern of these cells. The proliferation of the cells upon treatment with chemotherapy was determined using the Sulphorhodamine-B (SRB) semi automated assay [153]. Cells were seeded in 96 well plates at an appropriate cell density to give optical density in the linear range (from 0.5 to 1.8) and were incubated at 37 °C in CO_2 incubator for 24 h. Stock solutions of the complexes were prepared as 100mg/ml in DMSO and four dilutions i.e. 10µL, 20µL, 40µL, 80µL, in triplicates were tested, each well receiving 90µL of cell suspension and 10 µL of the drug solution. Appropriate positive control (Adriamycin) and vehicle controls were also run. The plates with cells were incubated in CO_2 incubator with 5% CO_2 for 24 h followed by drug addition. The plates were incubated further for 48 h. Termination of experiment was done by gently layering the cells with 50µL of chilled 30% TCA (in case of adherent cells) and 50 % TCA (in case of suspension cell lines) for cell fixation and kept at 4 °C for 1 h. Plates were stained with 50µL of

0.4% SRB for 20 min. The bound SRB was eluted by adding 100 μL 10 mM Tris (pH 10.5) to each of the wells. The absorbance was read at 540 nm with 690 nm as reference wave length. All experiments were repeated 3 times.

CHAPTER III

Comparative DNA binding studies of monometallic and heterobimetallic complexes possessing Cu-Sn_2/Zn-Sn_2 metallic cores: DNA cleavage activity of heterobimetallic complexes.

Synthesis of monometallic complexes

Synthesis of $[C_6H_{20}N_4O_2Cu]Cl_2$

This complex $[C_6H_{20}N_4O_2Cu]Cl_2$ was synthesized by adopting slight modification to the previously reported procedure [154]. To a methanolic solution of 1,3-diamino-2-propanol (1.80g, 20mmol), $CuCl_2.2H_2O$ (1.70g, 10mmol) in methanol (20 ml) was added dropwise in (2:1) molar ratio. The resulting blue solution thus obtained, was stirred for 12 h to obtain a dark blue crystalline solid product which was washed thoroughly with hexane and dried *in vacuo* (Scheme 2).

Yield 65%, m.p.= 276 ± 2 °C. Anal. (%) Calc. for $[C_6H_{20}N_4O_2Cu]Cl_2$: C, 22.90; H, 6.41; N, 17.80. Found: C, 22.92; H, 6.43; N, 17.80. IR ($\nu(cm^{-1})$): 3334 (O-H), 3292 (NH_2), 1400 (C-N), 1272 (C-O), 830 (H_2O), 537 (Cu-N), 462 (Cu-O). Molar conductance, $\wedge_M$ ($1x10^{-3}$ M, Methanol): 179 $\Omega^{-1}cm^2\ mol^{-1}$ (1:2 electrolyte). UV-vis. in Methanol [λ_{max} / nm]: 229, 308, 670.

Synthesis of $[C_6H_{20}N_4O_2Zn]Cl_2$

The complex $[C_6H_{20}N_4O_2Zn]Cl_2$ was synthesized with $ZnCl_2$ (anhydrous) (1.36g, 10mmol) by a similar procedure as described for $C_6H_{20}N_4O_2ZnCl_2$.

Yield 60%, m. p. = 60 ± 2 °C. Anal. (%) Calc. for $[C_6H_{20}N_4O_2Zn]Cl_2$: C, 22.77; H, 6.37; N, 17.70. Found: C, 22.73; H, 6.38; N, 17.71. IR ($\nu(cm^{-1})$): 3332 (O-H), 3233 (NH_2) , 1315 (C-N), 1170 (C-O), 849 (H_2O), 525 (Zn-N), 467 (Zn-O). Molar conductance, $\wedge_M$ ($1x10^{-3}$ M, Methanol): 194 $\Omega^{-1}cm^2\ mol^{-1}$ (1:2 electrolyte). UV-vis in Methanol [λ_{max} / nm]: 223, 245, 308.

^{1}H NMR (DMSO-d_6, ppm): 8.1 (OH), 5.2 (NH_2), 3.8 (CH), 3.5-2.0 (CH_2). ^{13}C NMR (DMSO-d_6, ppm): 66 (C-O), 45 (C-N).

Synthesis of heterobimetallic complexes

Synthesis of $[C_6H_{24}N_4O_6CuSn_2Cl_4]Cl_2$

To a methanolic solution of the complex $[C_6H_{20}N_4O_2Cu]Cl_2$ (1.57g, 5mmol), $SnCl_4$ (8ml in CCl_4, 10mmol) was added in (1:2) molar ratio. The blue coloured solution turned green which was further stirred for 1 h and allowed to stand at room temperature overnight. A yellow crystalline solid product was obtained. washed thoroughly with n-hexane and dried *in vacuo* (Scheme 3).

Yield 70%, m.p. = 220 ± 2 °C. Anal. (%) Calc. for $[C_6H_{24}N_4O_6CuSn_2Cl_4]Cl_2$: C, 9.46; H, 3.17; N, 7.35. Found: C, 9.46; H, 3.18; N, 7.36. IR (ν(cm^{-1})): 3337 (O-H), 3135 (N-H), 1592 δ(N-H), 1391 (C-N), 1275 (C-O), 842 (H_2O), 549 (Cu-N), 454 (Cu-O), 440 (Sn-N), 245 (Sn-Cl). Molar conductance, $\wedge_M$ ($1x10^{-3}$ M, Methanol): 173 $\Omega^{-1}cm^2mol^{-1}$ (1:2 electrolyte). UV-vis. in Methanol [λmax / nm]: 224, 270, 840.

Synthesis of $[C_6H_{24}N_4O_6ZnSn_2Cl_4]Cl_2$

To a methanolic solution of complex $[C_6H_{20}N_4O_2Zn]Cl_2$ (1.58g, 4mmol), $SnCl_4$ (8 mL in CCl_4, 10mmol) was added in (1:2) molar ratio. The white solid product thus, obtained on stirring, was filtered, washed with n-hexane and dried *in vacuo*.

Yield 65%, m.p.= 222 ± 2 °C Anal. (%) Calc. for $[C_6H_{24}N_4O_6ZnSn_2Cl_4]Cl_2$: C, 9.43; H, 3.17; N, 7.34. Found: C, 9.44; H, 3.16; N, 7.33. IR (ν(cm^{-1})): 3337 (O-H), 3190 (N-H), 1535 δ(N-H), 1300 (C-N), 1146 (C-O), 851 (H_2O), 556 (Zn -N), 480

(Zn-O), 443 (Sn-N), 235 (Sn-Cl). Molar conductance, $\wedge_M$ ($1x10^{-3}$ M, Methanol): 180 $\Omega^{-1}cm^2 mol^{-1}$ (1:2 electrolyte). UV-vis in Methanol [λmax / nm]: 224, 255.

^1H NMR (DMSO-d_6, ppm): 8.1 (-OH), 5.9 (-NH), 4.0 (CH), 3.5-2.8 (CH_2). ^{13}C NMR (DMSO-d_6, ppm): 68 (C-O), 45 (C-N). ^{119}Sn NMR (DMSO-d_6, ppm): -625, -668.

Results and discussion

Synthesis and characterization

Preparation of heterobimetallic complexes $[C_6H_{24}N_4O_6CuSn_2Cl_4]Cl_2$ and $[C_6H_{24}N_4O_6ZnSn_2Cl_4]Cl_2$ were carried out by the reaction of $[C_6H_{20}N_4O_2Cu]Cl_2$ and $[C_6H_{20}N_4O_2Zn]Cl_2$ with $SnCl_4$ in 1:2 metal-to-ligand stoichiometric ratio (Scheme 3). The complexes are highly hygroscopic and soluble in methanol and DMSO. Molar conductance values of complexes in methanol (173 and 180 Ω^{-1} cm^2 mol^{-1}) at 25 °C suggest their 1:2 electrolytic nature. The complexes $[C_6H_{20}N_4O_2Cu]Cl_2$, $[C_6H_{20}N_4O_2Zn]Cl_2$, $[C_6H_{24}N_4O_6CuSn_2Cl_4]Cl_2$, $[C_6H_{24}N_4O_6ZnSn_2Cl_4]Cl_2$ reveal octahedral coordination geometry for the central metal ions copper(II)/zinc(II) as well as the tin(IV) ions (in case of complexes $[C_6H_{24}N_4O_6CuSn_2Cl_4]Cl_2$ and $[C_6H_{24}N_4O_6ZnSn_2Cl_4]Cl_2$) as proposed by various spectroscopic studies. DNA binding studies were carried out with the complexes $[C_6H_{20}N_4O_2Cu]Cl_2$, $[C_6H_{20}N_4O_2Zn]Cl_2$, $[C_6H_{24}N_4O_6CuSn_2Cl_4]Cl_2$ and $[C_6H_{24}N_4O_6ZnSn_2Cl_4]Cl_2$. The interaction studies of these complexes reveal that complex $[C_6H_{24}N_4O_6ZnSn_2Cl_4]Cl_2$ binds to CT-DNA with highest affinity.

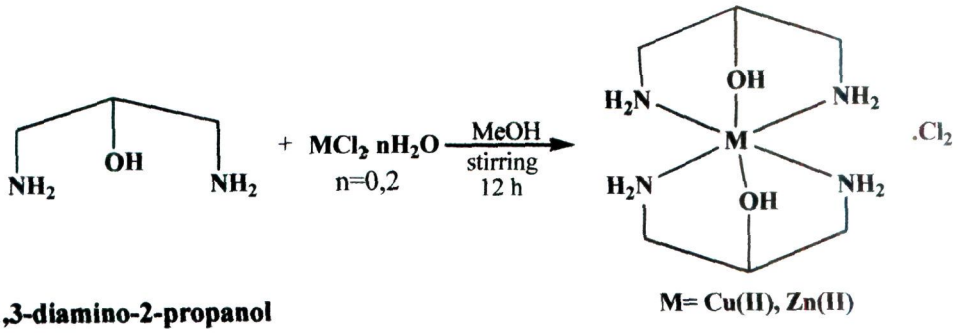

***Scheme** 2 Synthesis of monometallic complexes $[C_6H_{20}N_4O_2Cu]Cl_2$ and $[C_6H_{20}N_4O_2ZnCl_2$*

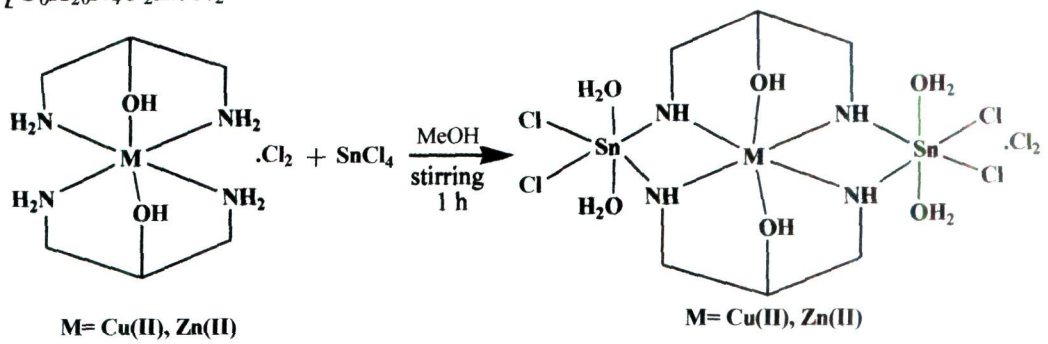

***Scheme** 3. Synthesis of heterobimetallic complexes $[C_6H_{24}N_4O_6CuSn_2Cl_4]Cl_2$ and $[C_6H_{24}N_4O_6ZnSn_2Cl_4]Cl_2$*

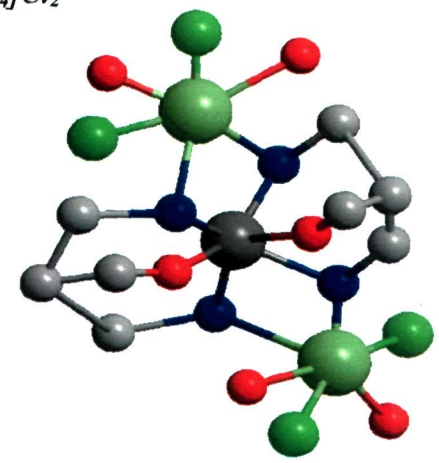

***Figure** 29. Cylindrical bonded three dimensional model of complexes (a) $[C_6H_{24}N_4O_6CuSn_2Cl_4]Cl_2$ and (b) $[C_6H_{24}N_4O_6ZnSn_2Cl_4]Cl_2$. Colour scheme: Copper(II) and Zinc(II) dark gray; Tin(IV) light green; Chloride fluorescent green; N dark blue; O red; C gray. Chloride ion and other H atoms and are omitted for clarity.*

IR spectral studies

The complexes $[C_6H_{20}N_4O_2Cu]Cl_2$ and $[C_6H_{20}N_4O_2Zn]Cl_2$ exhibit characteristic broad envelope at 3292 cm^{-1} attributed to $\nu(NH_2)$ coordinated to the copper(II)/zinc(II) centers [155]. The complexes $[C_6H_{24}N_4O_6CuSn_2Cl_4]Cl_2$ and $[C_6H_{24}N_4O_6ZnSn_2Cl_4]Cl_2$, exhibit bands in 3135-3190 cm^{-1} region and the 1592 cm^{-1} region attributed to ν(N-H) and δ(N-H), respectively suggesting that NH_2 groups of 1,3-diamino-2-propanol are coordinated to central metals copper(II)/zinc(II) and simultaneously to tin(IV) ion by the elimination of HCl molecules [156,155]. The ν(O-H) band of the free ligand at 3360 cm^{-1} [43] was shifted to lower wave numbers *ca.* 3334 cm^{-1} indicative of coordinated –OH group. Other medium intensity bands observed at 1300-1391 cm^{-1} and 1275-1146 cm^{-1} were assigned to ν(C-N) and ν(C-O) stretching vibration in the complexes[157,43]. The coordination of water molecules to the tin(IV) metal ion was supported by the appearance of non-ligand band in the region 845-858 cm^{-1} attributed to the rocking mode of water [158]. In far IR region, medium intensity Cu/Zn-N, Cu/Zn-O, Sn-N and Sn-Cl bands around ~525, ~ 480, ~ 441 and ~250 cm^{-1}, respectively revealing the complex formation [159-161] as proposed in Scheme 2.

Electronic spectra

The UV-visible absorption spectra of the monometallic complexes $[C_6H_{20}N_4O_2Cu]Cl_2$ and $[C_6H_{20}N_4O_2Zn]Cl_2$ in methanol were characterized by strong IL absorption bands centered at ~225-308 nm, respectively and a band in the visible region at 670 nm for complex $[C_6H_{20}N_4O_2Cu]Cl_2$ [162,163]. The heterobimetallic

complexes $[C_6H_{24}N_4O_6CuSn_2Cl_4]Cl_2$ and $[C_6H_{24}N_4O_6ZnSn_2Cl_4]Cl_2$ display sharp absorption maxima in the UV region at ~224-270 nm while complex $[C_6H_{24}N_4O_6CuSn_2Cl_4]Cl_2$ exhibited a broad and intense d-d absorption maximum at 840 nm in the visible region. This spectral feature is typical of copper(II) complexes in an octahedral coordination environment [164].

EPR spectrum

The solid state X-band EPR spectrum of the polycrystalline copper(II) complex was recorded in DMSO at LNT (25 °C) with a magnetic field strength of 3000 G. The EPR spectrum of $[C_6H_{24}N_4O_6CuSn_2Cl_4]Cl_2$ revealed a set of four well resolved peaks both in low field and high field region with an axial symmetry with $g_{\parallel} >> g_{\perp} > 2.0023$ pattern indicating that the unpaired electron is localized in $d(x^2-y^2)$ orbital (spectroscopic state $^2B_{1g}$) of a copper(II) center [165,166] with $g_{\parallel} = 2.36$, $g_{\perp} = 2.09$ [167] (Figure 30).

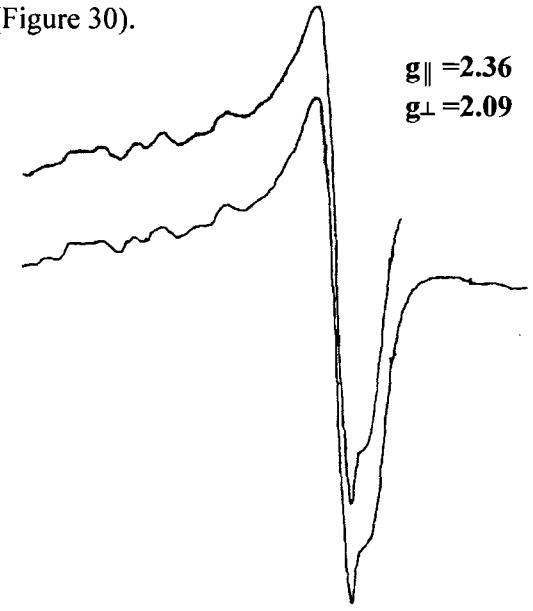

Figure 30. *X-band EPR spectrum of complex $[C_6H_{24}N_4O_6CuSn_2Cl_4]Cl_2$ at LNT with $g_{\parallel}$ =2.36 and $g_{\perp}$ =2.09.*

These values were consistent with an octahedral geometry of copper with d^9 (Cu^{+2}) configuration *i.e.* $(eg)^4$ $(a_1g)^2$ $(b_2g)^2$ $(b_1g)^1$ [168], occupied by an unpaired electron. The exchange interaction parameter G = 4.07, suggesting absence of exchange coupling between the copper centers.

NMR spectra

The monometallic and heterobimetallic complexes $[C_6H_{20}N_4O_2Zn]Cl_2$ and $[C_6H_{24}N_4O_6ZnSn_2Cl_4]Cl_2$ were characterized by ^1H, ^{13}C and ^{119}Sn NMR spectra recorded in DMSO-d_6 solution. The complex $[C_6H_{20}N_4O_2Zn]Cl_2$ exhibited the characteristic signal of NH_2 group of bis-[1,3-diamino-2-propanol] at ~5.2 ppm [155]. The free -OH group of bis-[1,3-diamino-2-propanol] also appeared in the same region while the coordinated -OH group to the zinc(II) center appears at 8.1 ppm, therefore it becomes quite amenable that the -OH group of bis-[1,3-diamino-2-propanol] is coordinated to the zinc(II) center in complex $[C_6H_{20}N_4O_2Zn]Cl_2$ [169]. The ^1H NMR spectrum of complex $[C_6H_{24}N_4O_6ZnSn_2Cl_4]Cl_2$ reveals a sharp resonance at ~5.9 ppm attributed to -NH proton of bis-[1,3-diamino-2-propanol] coordinated simultaneously to the zinc(II) ion and to tin(IV) metal ion through deprotonation. Other resonances of the complex $[C_6H_{24}N_4O_6ZnSn_2Cl_4]Cl_2$ appeared at 2.8-3.5 ppm and 4.0 ppm for methylene proton and -CH proton adjacent to the OH group, respectively [170,155].

The ^{13}C NMR spectrum of complexes $[C_6H_{20}N_4O_2Zn]Cl_2$ and $[C_6H_{24}N_4O_6ZnSn_2Cl_4]Cl_2$ recorded two signals at ~68 ppm and ~45 ppm attributed to -CHOH and $-CH_2N$ carbon atom, respectively [171,172].

^{119}Sn NMR spectra of complex $[C_6H_{24}N_4O_6ZnSn_2Cl_4]Cl_2$ displayed two signals at -625 and -668 ppm, due to the presence of two tin(IV) metal centers (Figure 31)

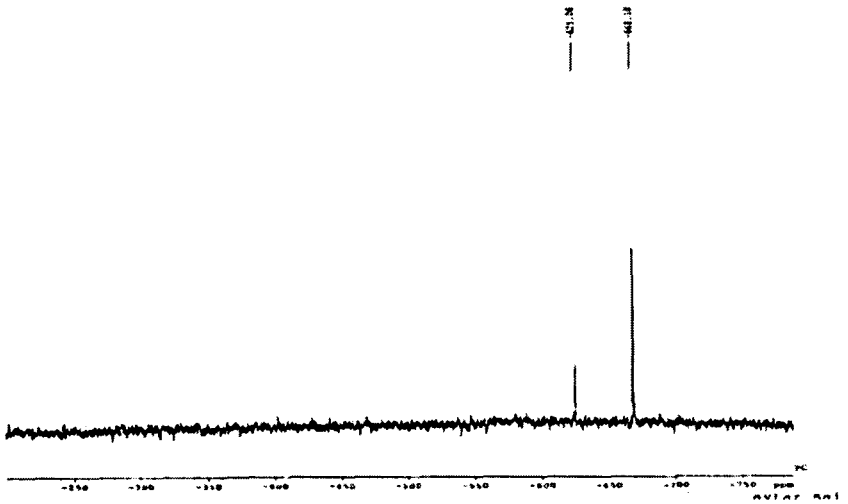

Figure 31. *^{119}Sn NMR spectrum of complex $[C_6H_{24}N_4O_6ZnSn_2Cl_4]Cl_2$*

These chemical shift values are consistent with those reported for complexes with the hexacoordinated tin(IV) metal atom [173].

DNA binding studies

UV-visible absorption studies

The interaction of complexes $[C_6H_{20}N_4O_2Cu]Cl_2$, $[C_6H_{20}N_4O_2Zn]Cl_2$, $[C_6H_{24}N_4O_6CuSn_2Cl_4]Cl_2$, $[C_6H_{24}N_4O_6ZnSn_2Cl_4]Cl_2$ with DNA were investigated by UV absorption titrations. Fixed amount of the complexes $[C_6H_{20}N_4O_2Cu]Cl_2$, $[C_6H_{20}N_4O_2Zn]Cl_2$, $[C_6H_{24}N_4O_6CuSn_2Cl_4]Cl_2$ and $[C_6H_{24}N_4O_6ZnSn_2Cl_4]Cl_2$ were titrated with increasing amount of CT-DNA (0-0.33x10^{-4} M) resulting in an overall hyperchromism at the intraligand absorption bands at 224-308 nm of the complexes (Figure 32a,b). Hyperchromicity and hypochromicity is the spectral feature of DNA concerning its double helix structure [174]. "Hyperchromic effect" reflects the corresponding changes of DNA in its conformation and structure after the complexes

are bound to CT-DNA. Hypochromism results from contraction of DNA in the helix axis while hyperchromism results from the damage of DNA double helix structure. A strong "hyperchromic effect" [175] with a moderate red shift of 1-4 nm was observed for heterobimetallic complexes $[C_6H_{24}N_4O_6CuSn_2Cl_4]Cl_2$ and $[C_6H_{24}N_4O_6ZnSn_2Cl_4]Cl_2$ in comparison to monometallic complexes, implying their higher DNA binding propensity. The propensity for DNA binding enhances in $[C_6H_{24}N_4O_6CuSn_2Cl_4]Cl_2$ and $[C_6H_{24}N_4O_6ZnSn_2Cl_4]Cl_2$ by the introduction of tin(IV) cations in the monometallic core; tin ions have a hard Lewis acid nature and thus, neutralize the dinegative charge of the phosphate sugar backbone of the DNA double helix [176]. In the complexes $[C_6H_{24}N_4O_6CuSn_2Cl_4]Cl_2$ and $[C_6H_{24}N_4O_6ZnSn_2Cl_4]Cl_2$, heterobimetallic core possesses two tin(IV) ions and one copper(II)/zinc(II) ions; tin(IV) ions are accessible at two ends to a pair of DNA double helix in end-to-end fashion as illustrated by Mc Millan et al [177] to form a bridge-like structure which minimizes the Coulombic repulsions between the negatively charged duplexes (Figure 33). Such trinuclear complexes exhibit electrostatic binding, involving inner sphere complex formation via, negative charge of the phosphate oxygen with the positive charge of complex [178]. Furthermore, no significant changes were observed at ligand field bands of complexes monometallic and heterobimetallic complexes as the coordination environment around the transition metal ion is coordinatively saturated (octahedral); however, we cannot rule out the possibility of covalent binding of the transition metal ions {copper(II) and zinc(II)} via, N7 and N3 atom of nucleobase of DNA helix which is their inherent characteristic trait [27].

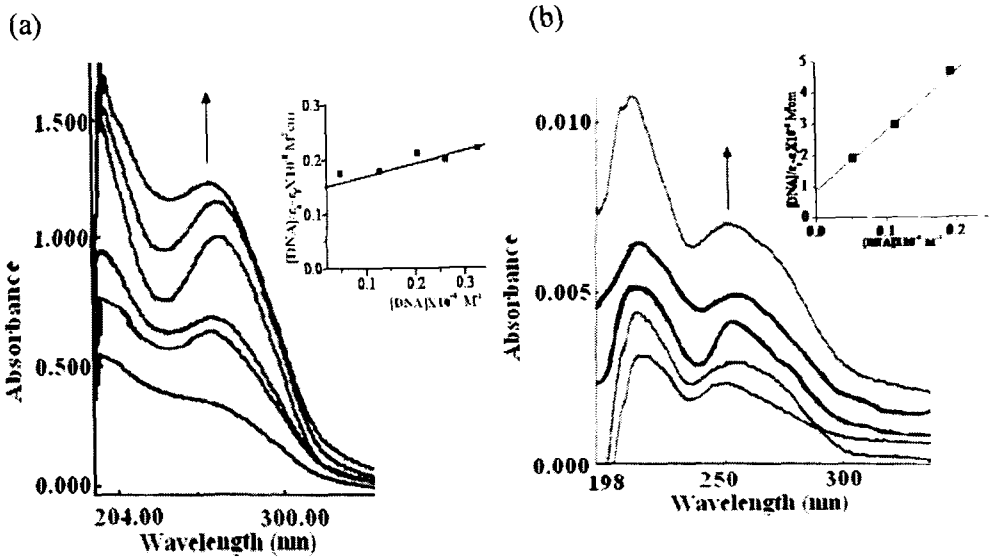

Figure 32. *Absorption spectra of (a) complex $[C_6H_{24}N_4O_6CuSn_2Cl_4]Cl_2$ (b) complex and $[C_6H_{24}N_4O_6ZnSn_2Cl_4]Cl_2$ in Tris-HCl buffer (pH= 7.2) in the absence and presence of increasing amount of CT-DNA. Inset: Plots of [DNA]/(ε_a-ε_f) vs [DNA] for the titration of CT-DNA with complexes. Arrow indicate the increase in the absorbance upon increasing CT-DNA concentration. Plots of [CT-DNA]/ (ε_a – ε_f) vs. [CT-DNA].*

The spectral "hyperchromic effect" arises mainly due to the presence of enhanced positive charge of cations copper(II)/zinc(II) and tin(IV) which bind to DNA via, non-covalent interaction presumably through strong electrostatic attraction to the phosphate group of the DNA backbone and thereby causing a contraction and overall damage to the secondary structure of CT-DNA [179].

To evaluate the binding affinity of the mono and heterobimetallic complexes with DNA, the intrinsic binding constant were determined by observing the changes of absorbance with varying concentration of CT-DNA. To quantify the extent of DNA binding the intrinsic binding constant K_b of complexes were determined (Table 2) which follows the order $[C_6H_{24}N_4O_6ZnSn_2Cl_4]Cl_2$>$[C_6H_{24}N_4O_6CuSn_2Cl_4]Cl_2$ >$[C_6H_{20}N_4O_2Zn]Cl_2$ > $[C_6H_{20}N_4O_2Cu]Cl_2$.

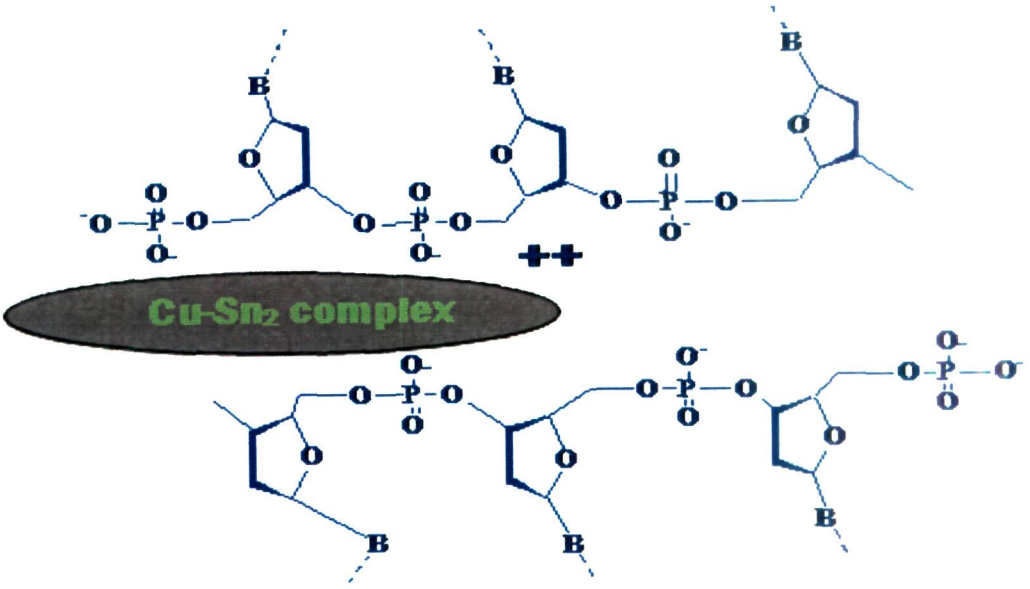

Figure 33. *A schematic representation of a pair of B-form DNA duplexes bridged by Cu-Sn_2 complex $[C_6H_{24}N_4O_6CuSn_2Cl_4]Cl_2$ at the sugar phosphate backbone.*

Thus, we can deduce from the intrinsic binding value that the complex $[C_6H_{24}N_4O_6ZnSn_2Cl_4]Cl_2$ bind more avidly to CT-DNA in comparison to complex $[C_6H_{24}N_4O_6CuSn_2Cl_4]Cl_2$ as the divalent zinc(II) complexes are known to distinctively recognize the thymine base in double stranded DNA by cleavage of the A-T base pairs and making the DNA exposed at the A-T region for nuclease activity, thereby altering the local structure of the A-T regions of DNA duplex [180].

Table 2. *The binding constant (K_b) values of complexes with the CT-DNA.*

Complexes	K_b (M^{-1})	Monitored at (nm)	% Hyperchromism	Red shift (nm)
$[C_6H_{20}N_4O_2Cu]Cl_2$	$1.42\pm0.02\times10^4$	308	20	02
$[C_6H_{20}N_4O_2Zn]Cl_2$	$1.67\pm0.02\times10^4$	308	39	03
$[C_6H_{24}N_4O_6CuSn_2Cl_4]Cl_2$	$4.75\pm0.01\times10^4$	225	20	04
$[C_6H_{24}N_4O_6ZnSn_2Cl_4]Cl_2$	$2.01\pm0.02\times10^5$	254	42	04

Interaction with 5'-GMP and 5'-TMP

The principles that govern the site-selective recognition of nucleic acid fragments such as 5'-GMP and 5'-TMP by the complexes $[C_6H_{24}N_4O_6CuSn_2Cl_4]Cl_2$ and $[C_6H_{24}N_4O_6ZnSn_2Cl_4]Cl_2$ include inherent specificity of binding of the copper(II) and zinc(II) ions towards N7 of guanine as well as N3 of thymine base, respectively. In order to elucidate this preferential selectivity, the interaction of complexes with low molecular building blocks of large DNA molecules viz; guanosine 5'-monophosphate (5'-GMP) and thymidine 5'-monophosphate and (5'-TMP) were investigated using electronic absorption spectroscopy. Addition of 5'-GMP to the complexes $[C_6H_{24}N_4O_6CuSn_2Cl_4]Cl_2$ and $[C_6H_{24}N_4O_6ZnSn_2Cl_4]Cl_2$ results in sharp increase in absorbance, 'hyperchromism' of the intraligand transitions with a red shift of 2-3 nm (Figure 34a,b). This observation provides an authentic proof for binding of complex to 5'-GMP through electrostatic interaction via, phosphate backbone of the DNA helix. It was observed copper(II) complex displays higher binding for 5'-GMP as compared to 5'-TMP validated by a larger K_b values of heterobimetallic copper(II) complex with 5'-GMP in contrast to its zinc(II) analogue suggestive of strong binding preference of the complex with 5'-GMP. The intrinsic binding constant K_b values for $[C_6H_{24}N_4O_6CuSn_2Cl_4]Cl_2$ and $[C_6H_{24}N_4O_6ZnSn_2Cl_4]Cl_2$ were compared to quantify the extent of binding of copper(II) and zinc(II) complexes which were found out to be $6.66x10^4$, $1.75 x10^4$, respectively indicative of higher preference of copper complex to the 5'-GMP in comparison to zinc complex $[C_6H_{24}N_4O_6ZnSn_2Cl_4]Cl_2$. This observation is in accord

with the literature revealing that the copper(II) ions exhibit substantially large selectivity for N7 of guanine residue [27,181].

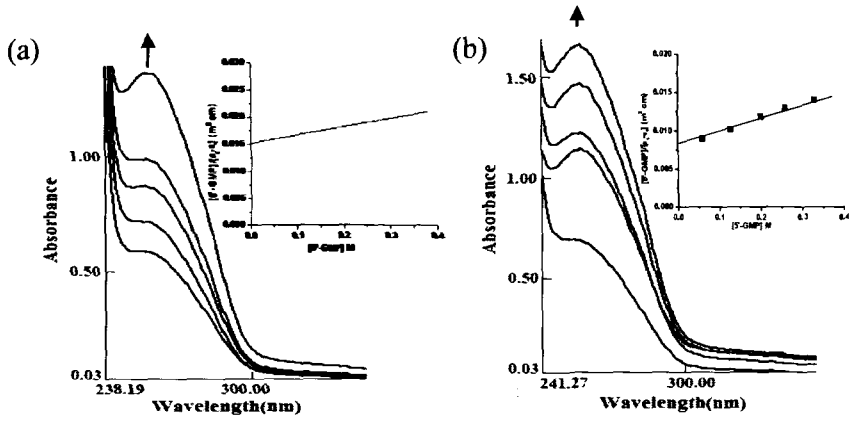

Figure 34. *Absorption spectral traces of (a) Complex $[C_6H_{24}N_4O_6CuSn_2Cl_4]Cl_2$ and (b) Complex $[C_6H_{24}N_4O_6ZnSn_2Cl_4]Cl_2$ in DMSO upon addition of 5'-GMP. Inset: Plots of [5'-GMP]/(ε_a-ε_f) vs [5'-GMP] for the titration of 5'-GMP with complexes. [Complex]=1.0 x 10^{-4} M, [5'-GMP]=0-0.33 x10^{-4} M.*

Furthermore, interaction studies of $[C_6H_{24}N_4O_6CuSn_2Cl_4]Cl_2$ and $[C_6H_{24}N_4O_6ZnSn_2Cl_4]Cl_2$ with 5'-TMP were carried under similar conditions (Figure 35a,b). The K_b binding constant follows the order $[C_6H_{24}N_4O_6ZnSn_2Cl_4]Cl_2$> $[C_6H_{24}N_4O_6CuSn_2Cl_4]Cl_2$.

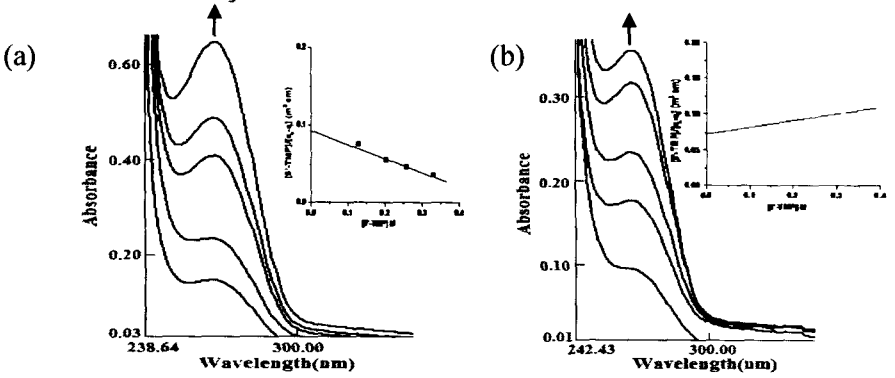

Figure 35. *Absorption spectral traces of (a) Complex $[C_6H_{24}N_4O_6CuSn_2Cl_4]Cl_2$ and (b) Complex $[C_6H_{24}N_4O_6ZnSn_2Cl_4]Cl_2$ in DMSO upon addition of 5'-TMP. Inset: Plots of [5'-TMP]/(ε_a-ε_f) vs [5'-TMP] for the titration of 5'-TMP with complexes. [Complex]=1.0 x 10^{-4} M, [5'-TMP]=0-0.33 x10^{-4} M.*

The zinc(II) complex $[C_6H_{24}N_4O_6ZnSn_2Cl_4]Cl_2$ displays a much higher K_b value for 5′-TMP compared to copper(II) complex exhibiting preference of zinc for thymine in contrast to guanine [180]. The oxo groups at the C2 and C3 position of the thymine lowers the energy of the lone pair orbital at N3 of thymine base resulting in stronger molecular orbital interaction of complex with thymine in comparison to guanine.

Table 3. *The binding constant (K_b) values of complexes $[C_6H_{24}N_4O_6CuSn_2Cl_4]Cl_2$ and $[C_6H_{24}N_4O_6ZnSn_2Cl_4]Cl_2$ with the 5′-GMP and 5′-TMP*

Complex	5′-GMP ($x10^4$)	5′-TMP ($x10^4$)	Monitored at (nm)	% Hyper--chromism	Red Shift (nm)
$[C_6H_{24}N_4O_6CuSn_2Cl_4]Cl_2$	6.66	3.74	256	22	02
$[C_6H_{24}N_4O_6ZnSn_2Cl_4]Cl_2$	1.75	6.21	259	38	03

Fluorescence studies

In the absence of CT-DNA, complexes $[C_6H_{24}N_4O_6CuSn_2Cl_4]Cl_2$ and $[C_6H_{24}N_4O_6ZnSn_2Cl_4]Cl_2$ emit weak luminescence in Tris-HCl buffer at room temperature, with a fluorescence maximum appearing at 520 nm and 524 nm, respectively, when excited at 260 nm. Upon addition of increasing concentration of CT-DNA over a range $0\text{-}0.16x10^{-4}$ M, to the fixed amount of complex ($1.0x10^{-3}$ M) the emission intensity of $[C_6H_{24}N_4O_6CuSn_2Cl_4]Cl_2$ and $[C_6H_{24}N_4O_6ZnSn_2Cl_4]Cl_2$ increases appreciably as illustrated in the Figure 36(a-b), respectively. The enhancement of the emission intensity is largely due to the change in the environment of the metal complex and related to the extent to which the complex gets into a hydrophobic environment inside the CT-DNA. Since, it is found that complexes with increased ligand hydrophobicities show greater increase in emission

intensities upon binding to polyelectrolytes via, DNA, therefore, such an increase in emission intensities is attributed to electrostatic association. Thus, we infer that the complexes are less deeply accommodated inside the hydrophobic pockets inside the DNA which is indicative of electrostatic mode of binding of the complex to the CT-DNA. The relative fluorescence intensity plotted as a function of DNA concentration (in terms of ([DNA]/[M])), (Figure 36a,b) shows larger increase in the emission intensity of complex $[C_6H_{24}N_4O_6ZnSn_2Cl_4]Cl_2$ than the complex $[C_6H_{24}N_4O_6CuSn_2Cl_4]Cl_2$. This implies that complex $[C_6H_{24}N_4O_6ZnSn_2Cl_4]Cl_2$ is bound to the DNA more strongly by means of surface binding with the duplex (Table 4).

Table 4. *Emission properties of complexes $[C_6H_{24}N_4O_6CuSn_2Cl_4]Cl_2$ and $[C_6H_{24}N_4O_6ZnSn_2Cl_4]Cl_2$ bound to CT DNA.*

Complex	Emission	Excitation	Monitored At	$K(M^{-1})$
$[C_6H_{24}N_4O_6CuSn_2Cl_4]Cl_2$	220	260	520	$6.00x10^{2}$
$[C_6H_{24}N_4O_6ZnSn_2Cl_4]Cl_2$	220	262	524	$8.50x10^{3}$

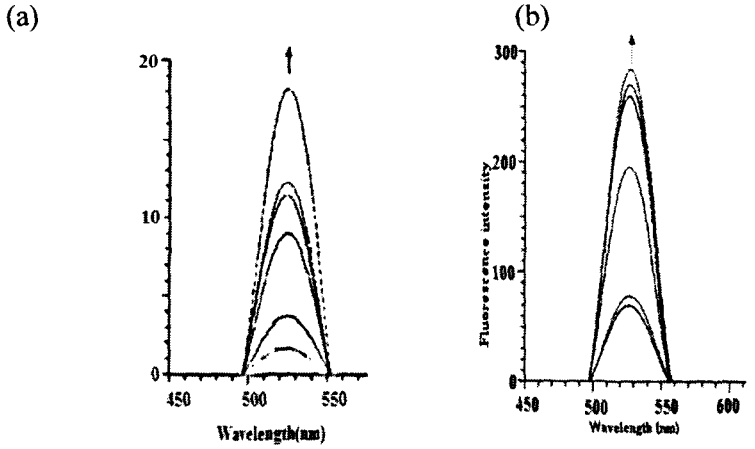

Figure 36. *Emission spectra of (a) complex $[C_6H_{24}N_4O_6CuSn_2Cl_4]Cl_2$ (b)complex $[C_6H_{24}N_4O_6ZnSn_2Cl_4]Cl_2$ in Tris-HCl buffer (pH 7.2) in the absence and presence of CT-DNA. Arrow indicates the change in the intensity upon increasing DNA concentration.*

To demonstrate the interaction strength of the complexes $[C_6H_{24}N_4O_6CuSn_2Cl_4]Cl_2$ and $[C_6H_{24}N_4O_6ZnSn_2Cl_4]Cl_2$ with CT-DNA, steady state emission quenching experiments using $[Fe(CN)_6]^{4-}$ as quencher were also performed [182,183]. The propensity to CT-DNA for the complexes follows the order: $[C_6H_{24}N_4O_6ZnSn_2Cl_4]Cl_2$ > $[C_6H_{24}N_4O_6CuSn_2Cl_4]Cl_2$ as evidenced by the binding constant K_{sv} values given in the Table 5.

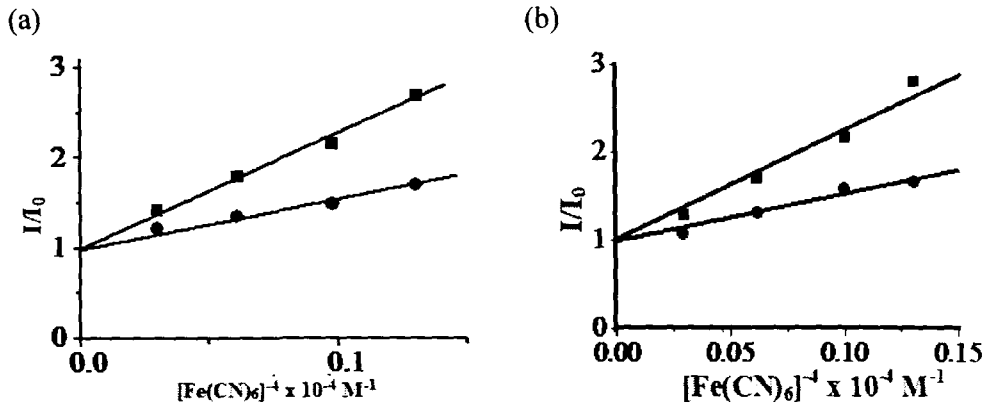

Figure 37. Emission quenching curves of (a) complex $[C_6H_{24}N_4O_6CuSn_2Cl_4]Cl_2$ in the absence of CT-DNA (■) and in the presence of CT-DNA (●) and (b) complex $[C_6H_{24}N_4O_6ZnSn_2Cl_4]Cl_2$ in the in the absence of CT-DNA (■) and in the presence of CT-DNA(●).[M] = 1.0 x 10^{-3} M.

In the absence of CT-DNA, emission intensity of complex $[C_6H_{24}N_4O_6CuSn_2Cl_4]Cl_2$ and $[C_6H_{24}N_4O_6ZnSn_2Cl_4]Cl_2$ were efficiently quenched by $[Fe(CN)_6]^{4-}$ as shown in Figure 37(a,b). The greater decrease of the K_{sv} value for $[C_6H_{24}N_4O_6ZnSn_2Cl_4]Cl_2$ as compared to $[C_6H_{24}N_4O_6CuSn_2Cl_4]Cl_2$ indicates higher DNA binding ability of $[C_6H_{24}N_4O_6ZnSn_2Cl_4]Cl_2$. These results are consistent with the electronic absorption titration (Table 5).

Table 5. *Emission quenching of CT-DNA bound $[Fe(CN)_6]^{4-}$ by complexes $[C_6H_{24}N_4O_6CuSn_2Cl_4]Cl_2$ and $[C_6H_{24}N_4O_6ZnSn_2Cl_4]Cl_2$.*

Complex	Emission	Excitation	Monitored at	K_{sv1} ($x10^4$)	K_{sv2} ($x10^4$)
$[C_6H_{24}N_4O_6CuSn_2Cl_4]Cl_2$	462	260	432	10.66	2.60
$[C_6H_{24}N_4O_6ZnSn_2Cl_4]Cl_2$	460	262	440	15.00	4.00

Effect of ionic strength

Monitoring the changes of ionic strength is an efficient method for distinguishing the binding modes between small molecules and DNA. Due to a competition for phosphate anion, the addition of cation weakens the surface binding interactions viz; the electrostatic and hydrogen binding between the DNA and molecules [184,185].

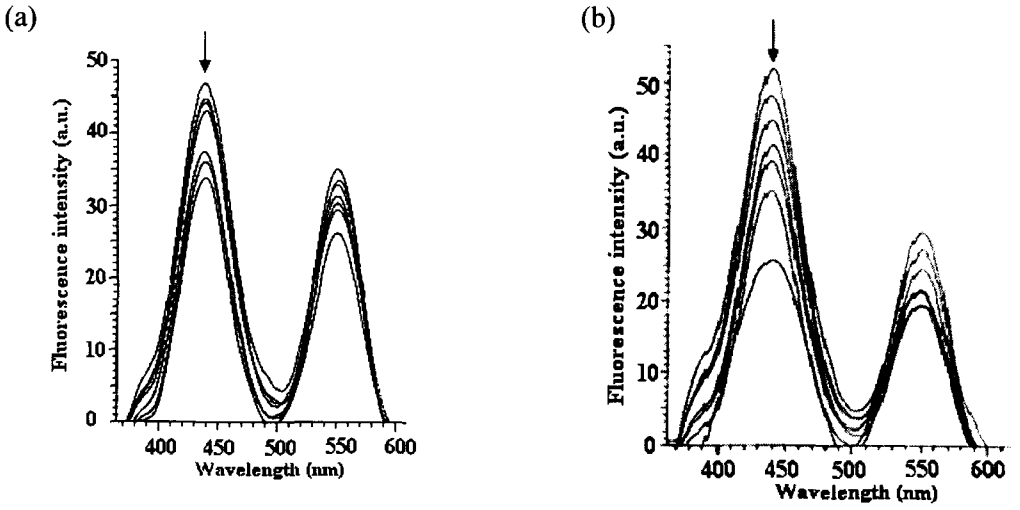

Figure 38. *Effect of different concentration of NaCl on the fluorescence spectra of (a) complex $[C_6H_{24}N_4O_6CuSn_2Cl_4]Cl_2$ (b) complex $[C_6H_{24}N_4O_6ZnSn_2Cl_4]Cl_2$ (1.0×10^{-3} M) with CT-DNA (1.0×10^{-4} M). Arrow indicate the gradual decrease of emission intensity as a function of NaCl concentration.*

The effect of ionic strength on complex-DNA binding of $[C_6H_{24}N_4O_6CuSn_2Cl_4]Cl_2$ and $[C_6H_{24}N_4O_6ZnSn_2Cl_4]Cl_2$ was studied and spectral changes were presented in Figure 38(a,b), which reveals a strong dependence of fluorescence intensity on ionic

strength. The fluorescence of zinc(II) complex-CT-DNA system displayed a distinct quenching with the increasing concentration of NaCl from 0.06-0.40x10^{-4} M. However, moderate fluorescence quenching was observed for copper(II) complex-DNA system. The results indicate that the interaction between complexes and CT-DNA is predominantly electrostatic via; DNA phosphate backbone. Furthermore, zinc(II) complex displays stronger electrostatic interaction in comparison to the copper(II) complex. This is concomitant with our other DNA binding assays.

Cyclic voltammetric studies

Cyclic voltammetry is a useful technique for studying the interaction of metal complexes with DNA and understanding the nature of DNA binding [186]. The cyclic voltammetric responses of complex $[C_6H_{24}N_4O_6CuSn_2Cl_4]Cl_2$ in absence and presence of CT-DNA are shown in Figure 39.

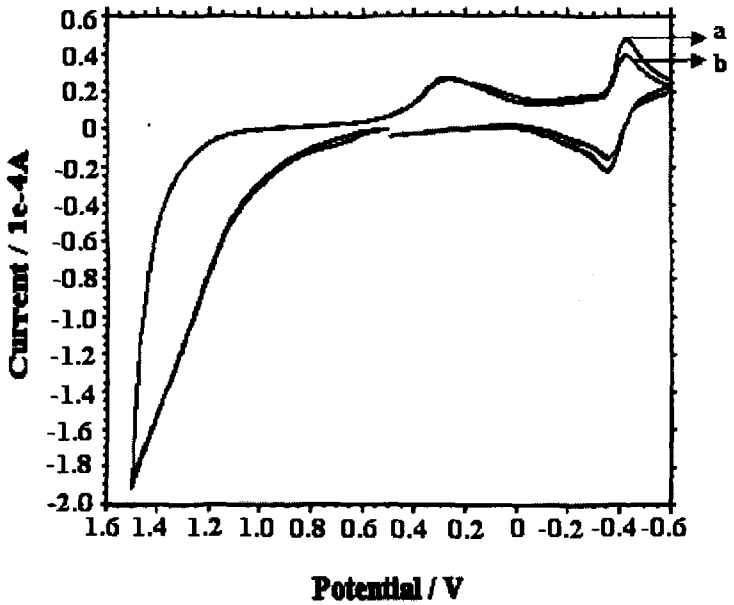

Figure 39. *Cyclic voltammogram (95:5 MeOH/H_2O) of complex $[C_6H_{24}N_4O_6CuSn_2Cl_4]Cl_2$ in the (a) absence and (b) presence of CT-DNA. [M]= 1.0 x10^{-3}M, [DNA] =1.0 x10^{-4} M.*

The redox properties of complex $[C_6H_{24}N_4O_6CuSn_2Cl_4]Cl_2$ were explored by cyclic voltammetry in MeOH/H_2O 95:5 at 0.2 $Vsec^{-1}$ in presence and in the absence of CT-DNA over a potential range of 0.5-(-0.6 V). The complex $[C_6H_{24}N_4O_6CuSn_2Cl_4]Cl_2$ contains a bimetallic core of copper(II) and tin(IV) ions. While the copper(II) ions are redox active, tin(IV) metal ions are inaccessible to the surface of the electrode. In the absence of DNA, complex $[C_6H_{24}N_4O_6CuSn_2Cl_4]Cl_2$ displays a one electron quasi-reversible electrochemical wave for Cu(II)/Cu(I) couple at a cathodic peak potential E_{pc}= -0.429 V and the corresponding anodic wave E_{pa} = -0.359 V. The formal electrode potential $E_{1/2}$ taken as an average of E_{pa} and E_{pc} was found to be -0.388V. On addition of CT-DNA to the complex $[C_6H_{24}N_4O_6CuSn_2Cl_4]Cl_2$, significant reduction in the cathodic (E_{pc}= -0.410 V) and anodic (E_{pa}= -0.348 V) peak currents were observed due to slow diffusion of an equilibrium mixture of the free and DNA bound complexes to the electrode surface [187].

In addition, the $E_{1/2}$ potential shifts to a slightly more negative value $E_{1/2}$ = -0.394 V upon addition of CT-DNA to the complex suggesting that the complex binds strongly by electrostatic association to CT-DNA [188] which corroborates well with the results of absorption titration studies with CT-DNA. To elucidate the binding mechanism involving the copper(II) or copper(I) forms of complex to DNA, the net shift in $E_{1/2}$ can be used to estimate the ratio of equilibrium constants by the following equation (Scheme 4).

$$E^{0}{}_{b}{}' - E^{0}{}_{f}{}' = 0.059 \log (K_{1+}/K_{2+})$$

The ratio of binding constants of +1 and +2 species was (1.01) suggesting that both Cu(II) and Cu(I) forms interact with CT-DNA to the same extent.

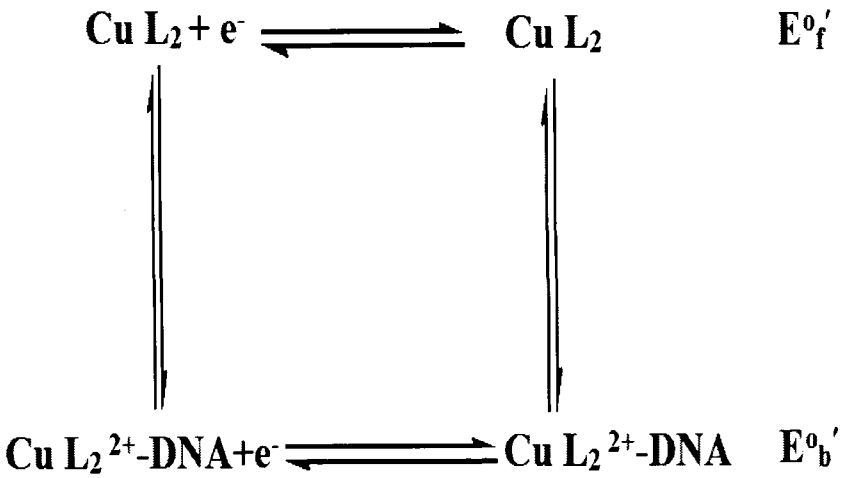

Scheme 4. *Cyclic voltammetric behaviour of heterobimetallic copper(II)-tin(IV) complex* $[C_6H_{24}N_4O_6CuSn_2Cl_4]Cl_2$ *bound to CT-DNA.*

Viscosity studies

The interaction of the metal complexes $[C_6H_{24}N_4O_6CuSn_2Cl_4]Cl_2$ and $[C_6H_{24}N_4O_6ZnSn_2Cl_4]Cl_2$ with CT-DNA was further explored by the relative specific viscosity of DNA after the addition of varying concentration of complexes $[C_6H_{24}N_4O_6CuSn_2Cl_4]Cl_2$ and $[C_6H_{24}N_4O_6ZnSn_2Cl_4]Cl_2$ (Figure 40). In the absence of crystallographic structural data, viscosity measurements are regarded as most critical test of a DNA binding model in solution [58].

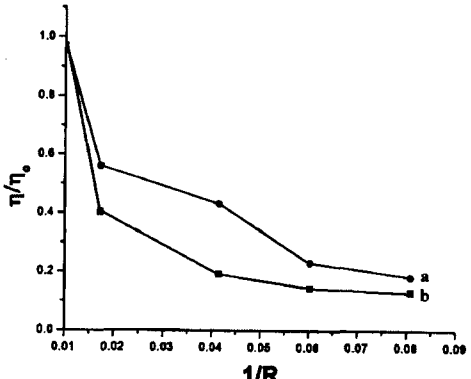

Figure 40. *Effect of increasing amount of complex (a)* $[C_6H_{24}N_4O_6CuSn_2Cl_4]Cl_2$ *(●) and (b)*$[C_6H_{24}N_4O_6ZnSn_2Cl_4]Cl_2$ *(■) on the relative viscosities* (η/η_o) *of CT-DNA in tris-HCl buffer (pH 7.2).*

A classical intercalation tends to increase the length of the DNA helix, due to the accommodation of the ligand in between the base pairs of CT-DNA resulting in an increase in the CT-DNA viscosity [189]. Partial or non-classical intercalation reduces the effective CT-DNA length as they produce kinks in the DNA helix, which results a decrease in viscosity [190]. Figure 40 shows the relative changes in the viscosity upon addition of complexes $[C_6H_{24}N_4O_6CuSn_2Cl_4]Cl_2$ and $[C_6H_{24}N_4O_6ZnSn_2Cl_4]Cl_2$. The relative specific viscosity decreases suggesting that the complexes could bend and kink the DNA helix, reducing its effective length and consequently its viscosity. The decrease for complex $[C_6H_{24}N_4O_6ZnSn_2Cl_4]Cl_2$ is much greater than the complex $[C_6H_{24}N_4O_6CuSn_2Cl_4]Cl_2$ which imply that complex $[C_6H_{24}N_4O_6ZnSn_2Cl_4]Cl_2$ binds to CT- DNA strongly by simple electrostatic binding.

DNA cleavage activity

The DNA cleavage activity of the complex $[C_6H_{24}N_4O_6CuSn_2Cl_4]Cl_2$ and $[C_6H_{24}N_4O_6ZnSn_2Cl_4]Cl_2$ was assessed by agarose gel electrophoresis with supercoiled (SC) pBR322 DNA as substrate. A concentration dependant DNA cleavage was observed as shown in Figure 41(a,b). The activity of complexes $[C_6H_{24}N_4O_6CuSn_2Cl_4]Cl_2$ and $[C_6H_{24}N_4O_6ZnSn_2Cl_4]Cl_2$ was assessed by the conversion of DNA from Form I to Form II and Form III. When pBR322 plasmid DNA undergoes electrophoresis, there is fast migration to the supercoiled (Form I). If one strand is cleaved, the supercoiled form will relax to produce slower-moving nicked circular (Form II). If both strands are cleaved, a linear form (Form III) will be

generated which migrates in between [191]. With increase in concentration of the complexes more intense Form II was observed (shown in Lane 2-6, Figure 41) with the simultaneous reduction of Form I, whereas no conversion to Form III was observed. The reduction in the intensity of Form I and appearance of more intense Form II of pBR322 DNA on the gel shows that both the complexes $[C_6H_{24}N_4O_6CuSn_2Cl_4]Cl_2$ and $[C_6H_{24}N_4O_6ZnSn_2Cl_4]Cl_2$ are involved in an efficient double strand DNA cleavage pathway.

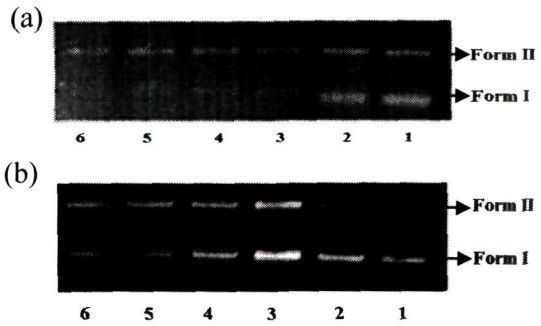

Figure 41. *Agarose gel electrophoresis patterns for the cleavage of pBR322 plasmid DNA as a function of increasing concentration of (a) complex* $[C_6H_{24}N_4O_6CuSn_2Cl_4]Cl_2$*; Lane 1: DNA control, Lane 2: DNA + 50μM of* $[C_6H_{24}N_4O_6CuSn_2Cl_4]Cl_2$*, Lane 3: DNA + 100μM of* $[C_6H_{24}N_4O_6CuSn_2Cl_4]Cl_2$*, Lane 4: DNA + 150μM of* $[C_6H_{24}N_4O_6CuSn_2Cl_4]Cl_2$*, Lane 5: DNA + 200μM of* $[C_6H_{24}N_4O_6CuSn_2Cl_4]Cl_2$ *Lane 6: DNA + 250μM of* $[C_6H_{24}N_4O_6CuSn_2Cl_4]Cl_2$*. (b) complex* $[C_6H_{24}N_4O_6ZnSn_2Cl_4]Cl_2$*; Lane 1: DNA control, Lane 2: DNA + 50μM of* $[C_6H_{24}N_4O_6ZnSn_2Cl_4]Cl_2$*, Lane 3: DNA + 100μM of* $[C_6H_{24}N_4O_6ZnSn_2Cl_4]Cl_2$ *Lane 4: DNA + 150μM of* $[C_6H_{24}N_4O_6ZnSn_2Cl_4]Cl_2$*, Lane 5: DNA + 200μM of* $[C_6H_{24}N_4O_6ZnSn_2Cl_4]Cl_2$*, Lane 6: DNA+250μM of* $[C_6H_{24}N_4O_6CuSn_2Cl_4]Cl_2$.

The nuclease activity of complex $[C_6H_{24}N_4O_6ZnSn_2Cl_4]Cl_2$ markedly depends on different activators [192,193]. Thus, activators such as ascorbate (Asc), 3-mercaptopropionic acid (MPA), and glutathione (GSH) (Lanes 2-4, Figure 42) were also used to investigate the DNA cleavage activity of complex $[C_6H_{24}N_4O_6ZnSn_2Cl_4]Cl_2$ at a concentration of 100μM. The activity followed the

order MPA > Asc > GSH, therefore, it appears that nuclease activity is significantly enhanced in presence of MPA.

Minor groove binding agent DAPI [194], and major groove binding agent methyl green [195] (Lane 5 and 6, Figure 42) were used to examine the potential interacting site of complex $[C_6H_{24}N_4O_6ZnSn_2Cl_4]Cl_2$ with supercoiled plasmid DNA. The cleavage patterns, demonstrated that in presence of both DAPI and methyl green DNA cleavage activity is not affected significantly, suggesting that neither major nor minor groove are involved in the complex-DNA interactions.

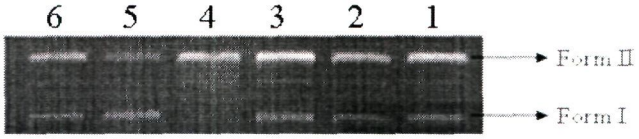

Figure 42. *Gel electrophoresis of pBR322 by complex $[C_6H_{24}N_4O_6ZnSn_2Cl_4]Cl_2$ (100 μM) in the presence of different activators Lane 1: DNA contol, Lane 2: DNA + complex $[C_6H_{24}N_4O_6ZnSn_2Cl_4]Cl_2$ (100 μM) + Ascorbic acid, Lane 3: DNA + complex $[C_6H_{24}N_4O_6ZnSn_2Cl_4]Cl_2$ (100 μM) + GSH, Lane 4: DNA + complex $[C_6H_{24}N_4O_6ZnSn_2Cl_4]Cl_2$ (100μM) + MPA, Lane 5: DNA + complex $[C_6H_{24}N_4O_6ZnSn_2Cl_4]Cl_2$ (100 μM) + DAPI, Lane 6: DNA+ complex $[C_6H_{24}N_4O_6ZnSn_2Cl_4]Cl_2$ (100 μM) + methyl green.*

In these circumstances, complexes may interact directly with the exterior phosphate of DNA through electrostatic attraction. Such interactions would enhance the local concentrations of complexes around DNA [91] and consequently enhance DNA cleavage activity. The pattern of cleavage is in accord with the proposed electrostatic binding mode of complexes $[C_6H_{24}N_4O_6CuSn_2Cl_4]Cl_2$ and $[C_6H_{24}N_4O_6ZnSn_2Cl_4]Cl_2$ to CT-DNA.

Conclusions

In this work, we have described the synthesis and characterization of heterobimetallic complexes $[C_6H_{20}N_4O_2Cu]Cl_2$, $[C_6H_{20}N_4O_2Zn]Cl_2$, $[C_6H_{24}N_4O_6CuSn_2Cl_4]Cl_2$ and $[C_6H_{24}N_4O_6ZnSn_2Cl_4]Cl_2$ which can be explored as potential cancer chemotherapeutic agents. *In vitro* DNA binding studies of these complexes $[C_6H_{20}N_4O_2Cu]Cl_2$, $[C_6H_{20}N_4O_2Zn]Cl_2$, $[C_6H_{24}N_4O_6CuSn_2Cl_4]Cl_2$ and $[C_6H_{24}N_4O_6ZnSn_2Cl_4]Cl_2$ were carried out by using various biophysical and spectroscopic techniques. These complexes are unique as they possess two different metal ions (transition and non-transition, copper(II)/zinc(II) and tin(IV) respectively) which act synergistically at molecular level but with a different binding mode. The interaction studies revealed that the complexes bind to the phosphate sugar backbone of the DNA double helix via, electrostatic interaction, in addition to the coordinate covalent binding favored by the transition metal ions to N7 or N3 site of the nucleobases which was elucidated by the absorption titration of the complexes with nucleotides 5'-GMP and 5'-TMP. The results revealed that the complex $[C_6H_{24}N_4O_6ZnSn_2Cl_4]Cl_2$ exhibits highest propensity for DNA which is attributed to the presence of the hydrolytically active zinc metal ion together with tin(IV) metal ion as compared to complex $[C_6H_{24}N_4O_6CuSn_2Cl_4]Cl_2$. Both the complexes $[C_6H_{24}N_4O_6CuSn_2Cl_4]Cl_2$ and $[C_6H_{24}N_4O_6ZnSn_2Cl_4]Cl_2$ exhibited an effective DNA cleavage activity at physiologically relevant conditions.

CHAPTER IV

In vitro DNA binding studies of chiral [4-(2-hydroxy-1-phenylethylimino)pent-2-ol]dimethyltin(IV) and 2-(chlorodimethylstannyloxy)-1-phenylethanamine: Antitumor activity of their S-enantiomer against human tumor cell lines.

Synthesis of Ligand

Synthesis of (S) and (R)-[$C_{13}H_{17}NO_2$]

The Schiff base ligand was prepared by adopting the reported procedure [196]. To a methanolic solution (20 mL) of acetylacetone (1.03 ml) was added a stirred solution of (S)-2-amino-2-phenylethanol (1.37g, 10mmol) in 1:1 molar ratio. The reaction mixture was refluxed for 4-8 h with continuous stirring during which the color of the solution tuned to yellow-orange. The completion of the reaction was monitored by TLC. After the completion of the reaction, it was cooled on an ice bath affording a solid product. The ligand thus, obtained was washed with hexane and dried *in vacuo* (Scheme 5).

The corresponding Schiff base ligand (R)-[$C_{13}H_{17}NO_2$] was synthesized according to the above procedure described for (S)-[$C_{13}H_{17}NO_2$] by using (R)-2-amino-2-phenylethanol.

(S-enantiomer): Yield 65%, m.p.= 110 ± 2 °C Anal. (%) Calc. for [$C_{13}H_{17}NO_2$]: C, 71.21; H, 7.81; N, 6.39: Found: C, 71.24; H, 7.80; N, 6.38. $[\alpha]^{25}_D$ = +37. ESI-MS (m/z) 220 [$C_{13}H_{17}NO_2$+H].

(R-enantiomer): Yield 60%. m.p. 115 ± 2 °C. Anal. (%) Calc. for [$C_{13}H_{17}NO_2$]: C, 71.21; H, 7.81; N, 6.39: Found: C, 71.22; H, 7.79; N, 6.38. $[\alpha]^{25}_D$ = -39. ESI-MS (m/z) 219 $[C_{13}H_{17}NO_2]^+$.

Both enantiomers exhibited identical IR, UV-vis spectra

Selected IR data in KBr (ν/cm^{-1}): 3204-3028 (OH); 2837 (CH_2); 1551 (C=N); 797 (Ar). UV-vis in Methanol [λ_{max}/nm]: 228, 266, 315.

(S)-[$C_{13}H_{17}NO_2$], ^{1}H NMR (DMSO-d_6, ppm): 2.3 (-OH, Aliphatic); 3.6 (-CH_2): 3.7 (Chiral CH); 1.9 (N=C-CH_3); 3.9 (-CH_2); 4.9 (=CH); 7.1-7.3 (Aromatic-H). ^{13}C NMR (DMSO-d_6, ppm): 193.6 (C=N); 19.0 (-C=C-CH_3); 28.8 (-C=N-CH_3): 95.5 (=C-), 162.7 (O-C=); 126.0-128.0 (Ar-C); 68.0 (-CH_2OH); 65.7 (Chiral C).

(R)-[$C_{13}H_{17}NO_2$], ^{1}H NMR (DMSO-d_6, ppm): 2.5 (-OH, Aliphatic); 3.5 (-CH_2): 3.7 (Chiral CH); 1.5 (N=C-CH_3); 4.0 (-CH_2); 4.5 (=CH); 7.3-7.7 (Aromatic-H). ^{13}C NMR (DMSO-d_6, ppm): 196.6 (C=N); 17.0-19.0 (-C=C-CH_3); 24.8 (-C=N-CH_3); 97.4 (=C-), 163.7 (O-C=); 128.0-133.0 (Ar-C); 69.5 (-CH_2OH); 64.9 (Chiral C).

Synthesis of Complexes

Synthesis of (S) and (R)-[$C_{15}H_{21}NO_2Sn$]

To a methanolic solution (20 ml) of the Schiff base ligand (S)-[$C_{13}H_{17}NO_2$] (1.07g, 4.90mmol), two drops of triethylamine was added and the resulting yellow solution was allowed to stir for 3-4 h. To this solution, 20 ml methanolic solution of dimethyltin(IV)dichloride (1.07g, 4.90mmol) was added dropwise in equivalent molar ratio. The final product obtained was washed with n-hexane and dried *in vacuo*.

The corresponding (R)-[$C_{15}H_{21}NO_2Sn$] complex was synthesized in accordance with the procedure described for (S)-[$C_{15}H_{21}NO_2Sn$] by using ligand (R)- [$C_{13}H_{17}NO_2$] (Scheme 6).

(S-enantiomer): Yield 57%. m.p. 138 ± 2 °C. Anal. (%) Calc. for [$C_{15}H_{21}NO_2Sn$]: C, 49.22; H, 5.78; N, 3.83. Found: C, 49.23; H, 5.75; N, 3.80. $[\alpha]^{25}_D$ = +12. ESI-MS (m/z): 367 $[C_{15}H_{21}NO_2Sn+H]^+$. ^{119}Sn NMR (DMSO-d_6, ppm): -179.

(R-enantiomer): Yield 55%. m.p. 139 ± 2 °C. Anal. (%) Calc. for [$C_{15}H_{21}NO_2Sn$]: C, 49.22; H, 5.78; N, 3.83. Found: C, 49.24; H, 5.75; N, 3.82. $[\alpha]^{25}_D$ = -14. ESI-MS (m/z): 368 $[C_{15}H_{21}NO_2Sn+2H]^+$. ^{119}Sn NMR (DMSO-$d_6$, ppm): -200.

Both enantiomeric metal complexes exhibited identical molar conductance, IR, UV-vis spectra.

Molar conductance, $\wedge_M$ ($1.0x10^{-3}$ M, Methanol): 29 $\Omega^{-1}cm^2$ mol^{-1} (non-electrolyte). Selected IR data (ν/cm^{-1}): 2568 (-CH_2); 1525 (-C=N); 771 (Ar); 569 (Sn-O); 424 (Sn-N); 549 (Sn-C). UV-vis in Methanol [λ_{max}/nm]: 211, 258, 299.

(S)-[$C_{15}H_{21}NO_2Sn$], ^{1}H NMR (DMSO-d_6, ppm): 0.6-1.0 (Sn-CH_3); 3.6 (-CH_2); 3.7 (Chiral CH); 1.8 (N=C-CH_3); 4.9 (=CH); 7.3-7.1 (Aromatic-H). ^{13}C NMR (DMSO-d_6, ppm): 193.5 (C=N); 19.0 (C=C-CH_3); 28.8 (C=N-CH_3); 95.5 (=C-), 162.7 (-O-C=); 126.0-128.0 (Ar-C); 65.6 (-CH_2OH); 63.3 (Chiral C); 10.0-14.0 (Sn-CH_3).

(R)-[$C_{15}H_{21}NO_2Sn$], ^{1}H NMR (DMSO-d_6, ppm): 0.9-1.0 (Sn-CH_3); 3.2 (-CH_2); 3.8 (Chiral CH); 1.3 (N=C-CH_3); 4.9 (=CH); 7.3-7.4 (Aromatic-H). ^{13}C NMR (DMSO-d_6, ppm): 196.2 (C=N); 20.0 (C=C-CH_3); 25.8 (C=N-CH_3); 97.3 (=C-), 162.7 (-O-C=); 126.0-127.9 (Ar-C); 67.6 (-CH_2OH); 63.2 (Chiral C); 11.2-13.0 (Sn-CH_3).

Synthesis of (S) and (R)-[$C_{10}H_{16}NOSnCl$]

To a stirring solution of (S)-2-amino-2-phenylethanol (1.37g, 10.00mmol) in methanol, the solution of dimethyltin(IV)dichloride (2.19g, 10.00mmol) was added in 1:1 molar ratio. After 3-4 h a white amorphous compound was isolated, which was washed with n-hexane and dried *in vacuo* (Scheme 7).

The corresponding (R)-[$C_{10}H_{16}NOSnCl$] complex was also synthesized according to the above procedure by using (R)-2-amino-2-phenylethanol.

(S-enantiomer): Yield 72%. m.p. 240 ± 2 °C. Anal. (%) Calc. for [$C_{10}H_{16}NOSnCl$]: C, 37.49; H, 5.03; N, 4.37. Found: C, 37.47; H, 5.01; N, 4.39. $[\alpha]^{25}_{D}$ = +23. ESI-MS (m/z): 336 $[C_{10}H_{16}NOSn+0.5CH_3OH]^+$. ^{119}Sn NMR (DMSO-$d_6$, ppm): -161.

(R-enantiomer): Yield 78%. m.p. 231 ± 2 °C. Anal. (%) Calc. for [$C_{10}H_{16}NOSnCl$]: C, 37.49; H, 5.03; N, 4.37. Found: C, 37.46; H, 5.02; N, 4.35. $[\alpha]^{25}_{D}$ = -20. ESI-MS (m/z): 336 $[C_{10}H_{16}NOSnCl+0.5CH_3OH]$. ^{119}Sn NMR (DMSO-$d_6$, ppm): -166.

Both enantiomeric metal complexes exhibited identical molar conductance, IR, UV-vis spectra.

Molar Conductance, $\wedge_M$ ($1.0x10^{-3}$ M, Methanol): 87 $\Omega^{-1}cm^2$ mol^{-1} (non-electrolyte). Selected IR data (ν/cm^{-1}): 3007 (NH_2); 2362 (CH_2); 704 (Ar); 575 (Sn-C); 549 (Sn-O); 466 (Sn-N); 279 (Sn-Cl). UV-vis in Methanol [λ_{max}/nm]: 222, 252.

(S)-[$C_{10}H_{16}NOSnCl$], ^{1}H NMR of (DMSO-d_6, ppm): 0.6-1.1 (Sn-CH_3); 3.6 (-CH_2); 4.1 (Chiral CH); 7.3-7.4 (Aromatic-H). ^{13}C NMR (DMSO-d_6, ppm): 127.0-132.0 (Ar-C); 66.0 (-CH_2OH); 64.1 (Chiral C); 10.0-14.0 (Sn-CH_3).

(R)-[$C_{10}H_{16}NOSnCl$], ^{1}H NMR of (DMSO-d_6, ppm): 0.8-1.2 (Sn-CH_3); 3.8 (-CH_2); 4.2 (Chiral CH); 7.3-7.7 (Aromatic-H). ^{13}C NMR (DMSO-d_6, ppm): 128.0-135.0 (Ar-C); 68.0 (-CH_2OH); 65.0 (Chiral C); 10.0-13.2 (Sn-CH_3).

Results and Discussion

Synthesis and characterization

The *in situ* condensation reaction of chiral 2-amino-2-phenylethanol and acetyl acetone in 1:1 molar ratio resulted in a light yellow Schiff base ligands

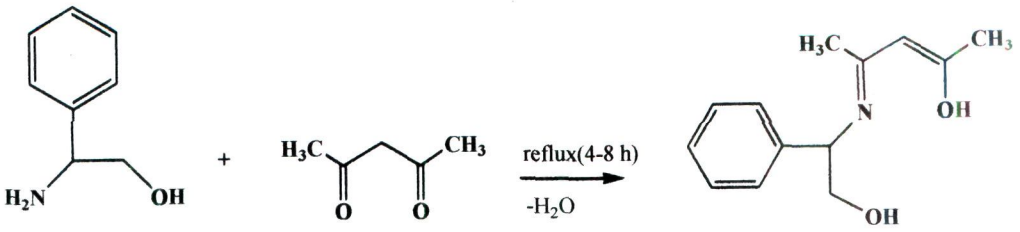

2-amino-2-phenylethanol **Acetylacetone** **Schiff base ligands**

(S)/(R)-[$C_{13}H_{17}NO_2$]

Scheme 5. *Synthesis of chiral ligands (S)/(R)-[$C_{13}H_{17}NO_2$].*

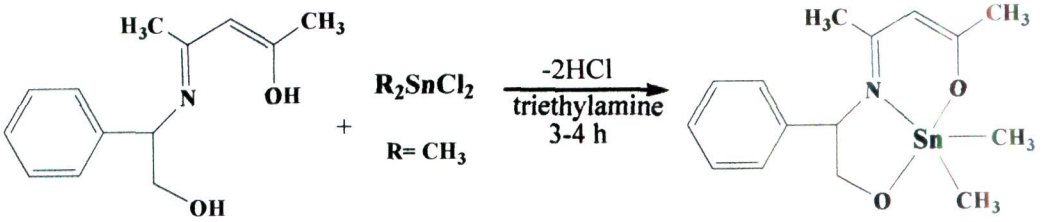

Schiff base ligands **dimethyltin(IV)dichloride** **Complex (S)/(R)-[$C_{15}H_{21}NO_2Sn$]**

(S)/(R)-[$C_{13}H_{17}NO_2$]

Scheme 6. *Synthesis of dimethyltin(IV) complexes derived from ligands (S)/(R)-$C_{13}H_{17}NO_2$.*

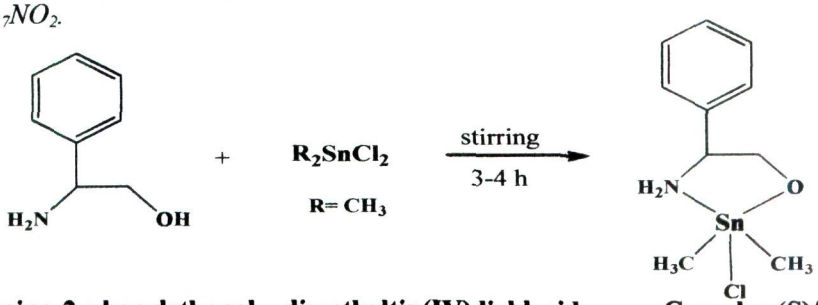

2-amino-2-phenylethanol **dimethyltin(IV)dichloride** **Complex (S)/(R)-[$C_{10}H_{16}NOSnCl$]**

Scheme 7. *Synthesis of dimethyltin(IV) complexes of (S)/(R)-$C_{10}H_{16}NOSnCl$.*

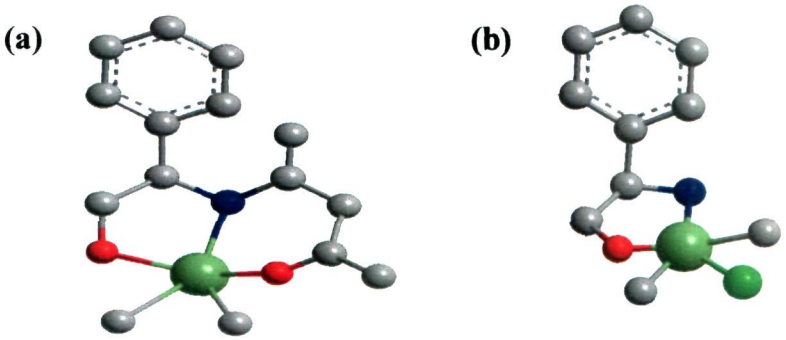

Figure 43. *Cylindrical bonded three dimensional model of complexes (a) (S)/(R)-$C_{15}H_{21}NO_2Sn$ and (b) (S)/(R)-$C_{10}H_{16}NOSnCl$ Color scheme: Tin(IV) light green; Chloride, fluorescent green; N dark blue; O red; C gray. The H atoms and are omitted for clarity.*

(S)-[$C_{13}H_{17}NO_2$] and (R)-[$C_{13}H_{17}NO_2$] respectively, by the slight modification of above mentioned procedure (Scheme 5). The ligands on complexation with dimethyltin(IV)dichloride behave as a dibasic tridentate $\overset{-}{O}\ N\ \overset{-}{O}$ donor ligand corresponding to enol tautomer of acetyl acetone [197]. Since the ligand exist in enol tautomeric form, an electron shift from the -OH group enhances the negative charge on the azomethine nitrogen atom so the transamination reaction of the carbonyl group is prohibited which would prevent the formation of the ligands in 1:2 stoichiometric ratio. The complexes (S)-[$C_{10}H_{16}NOSnCl$] and (R)-[$C_{10}H_{16}NOSnCl$] were prepared by mixing equimolar ratio of both enantiomeric form of 2-amino-2-phenylethanol with dimethyltin dichloride, (Scheme 7). These complexes were characterized by spectral studies using IR, ^{1}H NMR, ^{13}C NMR, ^{119}Sn NMR, ESI-MS and elemental analysis.

IR spectral studies

The formation of the complexes (S)-[$C_{15}H_{21}NO_2Sn$], (R)-[$C_{15}H_{21}NO_2Sn$], (S)-[$C_{10}H_{16}NOSnCl$] and (R)-[$C_{10}H_{16}NOSnCl$] has been ascertained by the comparison of the IR spectra of the ligands with complexes. The spectra of the ligand (S)/(R)-[$C_{13}H_{17}NO_2$] revealed a broad envelope at 3028-3204 cm^{-1} region assigned to intramolecular hydrogen bonded -OH group which was found absent in complexes (S)/(R)-[$C_{15}H_{21}NO_2Sn$] indicating the deprotonation of the hydroxyl group upon coordination to the metal ions. The bands corresponding to azomethine group υ(-C=N) at 1551-1568 cm^{-1}, in the spectra of the free ligand (S)- and (R)-[$C_{13}H_{17}NO_2$] respectively [198] has been considerably shifted to lower frequencies ~1518 cm^{-1} and 1525 cm^{-1} in the complexes (S)/(R)-[$C_{15}H_{21}NO_2Sn$] indicating the

involvement of azomethine nitrogen in the coordination with tin(IV) metal ion which is further supported by the appearance of new bands in their spectra at 424-432 cm^{-1} assigned to υ(Sn-N) stretching vibrations [60]. The absence of ketonic group vibrations υ(C=O) at 1700 cm^{-1} in the IR spectra of ligands reveal that the ligands exist predominantly in enolic form rather than ketonic form. Further evidence for the complexation is provided by the appearance of bands at 549-557 cm^{-1} and 565-593 cm^{-1} for υ(Sn-O) and υ(Sn-C) stretching frequencies for (S)/(R)-[$C_{15}H_{21}NO_2Sn$], respectively [199,200].

On the other hand, ligand 2-amino-2-phenylethanol reveals a band at 3335-3276 cm^{-1} region assigned to υ(OH) and υ(NH_2) stretching vibrations. A considerable lowering observed in the NH_2 frequency at 3007-3002 cm^{-1} together with a subsequent disappearance of –OH frequency is indicative of the coordination through -NH_2 and -OH groups for the formation of (S)/(R)-[$C_{10}H_{16}NOSnCl$]. The coordination of dimethyltin(IV)dichloride with the ligand to yield (S)/(R)-[$C_{10}H_{16}NOSnCl$] was revealed by the presence of medium intensity bands υ(Sn-C), υ(Sn-N), υ(Sn-O) and υ(Sn-Cl) bands 569-575 cm^{-1}, 461-466 cm^{-1} and 549-550 cm^{-1} and 279-295 cm^{-1}, respectively in the IR region [60, 201,202]

Electronic spectra

The ligands (S)/(R)-[$C_{13}H_{17}NO_2$] display broad bands around 312-315 nm range attributed to $n\rightarrow\pi^*$ transition of the azomethine group and band appearing at 228-230 nm with a shoulder at 266-269 nm assigned to intraligand $\pi\rightarrow\pi^*$ transition [203]. In the spectra of the complexes (S)/(R)-[$C_{15}H_{21}NO_2Sn$], the bands of the azomethine chromophore were shifted to lower frequencies (299 nm) indicating the

coordination of imine nitrogen atom to the tin(IV) metal ion. Other bands associated with complexes (S)/(R)-[$C_{15}H_{21}NO_2Sn$] at 258 and 211 nm were attributed to intraligand transitions.

The complexes (S)/(R)-[$C_{10}H_{16}NOSnCl$] reveal a band in 210-258 nm region attributed to IL transitions.

NMR spectra

The ligands (S)/(R)-[$C_{13}H_{17}NO_2$] and complexes (S)/(R)-[$C_{15}H_{21}NO_2Sn$] show approximately same peaks except that in the ^1H NMR spectra of the complex additional signals due to methyl protons attached to the tin metal ion were observed at 0.6-0.9 ppm, respectively [204]. The other characteristic signatures for (S)-[$C_{10}H_{16}NOSnCl$] corresponding to ArH, CH-N and CH_2-OH protons appear at 7.3-7.4, 4.7-3.7, 3.1-3.6 ppm, respectively, as compared to ligand [205].

The position of the azomethine carbon at 193.6-196.6 ppm of the ligands (S)/(R)-[$C_{13}H_{17}NO_2$] [205], respectively, is slightly shifted downfield in complexes (S)/(R)-[$C_{15}H_{21}NO_2Sn$] indicating the coordination of azomethine nitrogen with the tin metal ion. Additional resonances observed in the ^{13}C NMR spectra of the complexes (S)-[$C_{15}H_{21}NO_2Sn$] at 126-128, 162, 95, 28, 19 ppm were attributed to ArC, O-C=, -C=, CH_3-C=O, CH_3-C=N carbons, respectively [206]. The ^{13}C NMR spectra of complex (S)-[$C_{10}H_{16}NOSnCl$] reveals various other resonances attributed to -CH_2-O, CH-N, ArC and CH_3-Sn carbons at 66, 38-40, 128 and 10-14 ppm, respectively, of the coordinated 2-amino-2-phenylethanol [207].

The ^{119}Sn NMR spectra displays peaks in the range of -179 ppm for complex (S)-[$C_{15}H_{21}NO_2Sn$] and in range -161 ppm for complex (S)-[$C_{10}H_{16}NOSnCl$], respectively (Figure 44a,b).

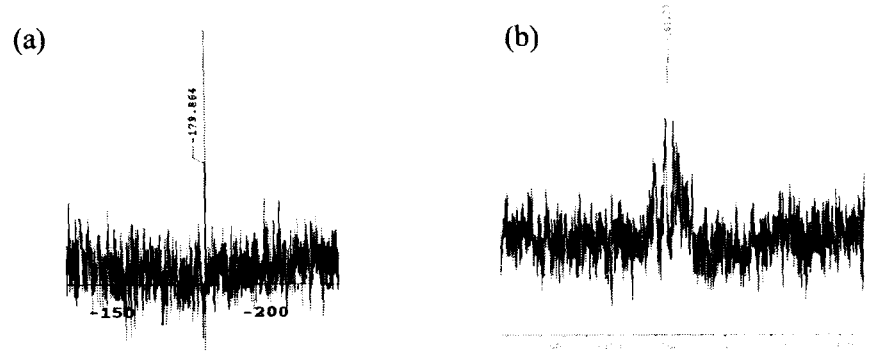

Figure 44. *^{119}Sn NMR spectra of complexes (a) (S)-$C_{15}H_{21}NO_2Sn$ and (b) (S)-$C_{10}H_{16}NOSnCl$.*

These chemical shift values obtained are typical of a five coordinated environment around tin metal ion [208].

DNA binding studies

UV-visible absorption studies

The comparative DNA binding ability of chiral ligands (S)/(R)-[$C_{13}H_{17}NO_2$], complexes (S)/(R)-[$C_{15}H_{21}NO_2Sn$], (S)/(R)-[$C_{10}H_{16}NOSnCl$] and cisplatin drug were evaluated using metal complex-DNA interactions. Figure 45(a-f) illustrates the respective absorption spectral changes of the (S)-[$C_{13}H_{17}NO_2$] and its complexes in absence and the presence of CT-DNA. Upon addition of incremental amount of CT-DNA (0-0.40x10^{-4} M) to a fixed concentration of complex/ligand (0.06x10^{-4} M) an increase in the absorbance of the intraligand bands was observed. This increase in the absorbance is attributed to the "hyperchromic effect". Cations can cause the hypochromism of DNA by predominant binding to the phosphate group of CT-DNA

backbone and make contraction in the helix axis of CT-DNA while destruction or complete structural damage of the DNA double helix is caused by the hyperchromism [209,174]. In the complexes (S)/(R)-[$C_{15}H_{21}NO_2Sn$] and (S)/(R)-[$C_{10}H_{16}NOSnCl$] and ligands (S)/(R)-[$C_{13}H_{17}NO_2$], hyperchromism was followed by concomitant red shift of 2-4 nm which arises due to the preferential binding of the predissociated tin(IV) to nucleotides via; phosphate group of DNA. This preferential binding of tin(IV) arises as the tin(IV) cations in the complexes, in an unsaturated geometry (TBP), exhibit tendency to expand their coordination number by the addition of solvent molecules or further by the coordination to the nucleotides, the geometry changes to octahedral [210]. Moreover, the affinity of tin(IV) with dinegative phosphate group is very strong because of its hard Lewis acidic property which is also evidenced by the intrinsic binding constant K_b values.

Ligands (S)/(R)-[$C_{13}H_{17}NO_2$] also differ significantly in their DNA binding ability which is attributed to the enantiomeric selectivity of CT-DNA. The K_b values of ligand (S)-[$C_{13}H_{17}NO_2$] (S-enantiomer) reveal multifold higher preferential binding to the DNA in comparison to (R)-[$C_{13}H_{17}NO_2$] (R-enantiomer). The complexes (S)-[$C_{15}H_{21}NO_2Sn$] and (S)-[$C_{11}H_{19}NOSnCl$] show greater propensity for DNA as compared to free ligands due to the presence of tin(IV) metal center which is attributed to its strong tendency for phosphate binding as observed from Table 6.

Table 6. *The binding constant (K_b) values of ligand (S)/(R)-[$C_{13}H_{17}NO_2$] and complexes (S)/(R)-[$C_{15}H_{21}NO_2Sn$] and (S)/(R)-[$C_{10}H_{16}NOSnCl$] with CT-DNA (mean standard deviation ± 0.15)*

Complex	K_b (M^{-1})	Monitored at (nm)	% Hyperchromism	Red Shift (nm)
(S)-[$C_{13}H_{17}NO_2$]	$1.27x10^4$	220	25	02
(R)-[$C_{13}H_{17}NO_2$]	$1.10x10^4$	220	17	02
(S)-[$C_{15}H_{21}NO_2Sn$]	$4.20x10^4$	226	42	04
(R)-[$C_{15}H_{21}NO_2Sn$]	$1.42x10^4$	226	35	03
(S)-[$C_{10}H_{16}NOSnCl$]	$3.96x10^4$	224	46	04
(R)-[$C_{10}H_{16}NOSnCl$]	$1.27x10^4$	224	21	02
Cisplatin	$3.20x10^4$	248	17	02

Furthermore, it has also been observed that, S-enantiomer of both [$C_{15}H_{21}NO_2Sn$] and [$C_{10}H_{16}NOSnCl$] complexes exhibits pronounced propensity for DNA binding in comparison to R-enantiomer. As DNA itself is a chiral molecule, the fact that optical isomers of the complexes differ in their biological effects is a priori not surprising. DNA-complex interactions are usually dependent on chirality and conformation of the isomers involving two pole complimentary recognition hypotheses to right handed domain of B-form of DNA. Complexes (S)/(R)-[$C_{15}H_{21}NO_2Sn$] and (S)/(R)-[$C_{10}H_{16}NOSnCl$] show structural dissimilarity due to the presence of Schiff base ligand in (S)/(R)-[$C_{15}H_{21}NO_2Sn$] which actually mutes the toxicity as well as tunes the metal to enforce stereoselective binding to the DNA leading to a spectacular propensity for DNA binding for the complex (S)-[$C_{15}H_{21}NO_2Sn$]. These K_b values were compared to the cisplatin which revealed that the K_b value of cisplatin

($3.20x10^4 \pm 0.15\ M^{-1}$) was slightly lower in comparison to K_b values of the complexes (S)-[$C_{15}H_{21}NO_2Sn$] and (S)-[$C_{10}H_{16}NOSnCl$].

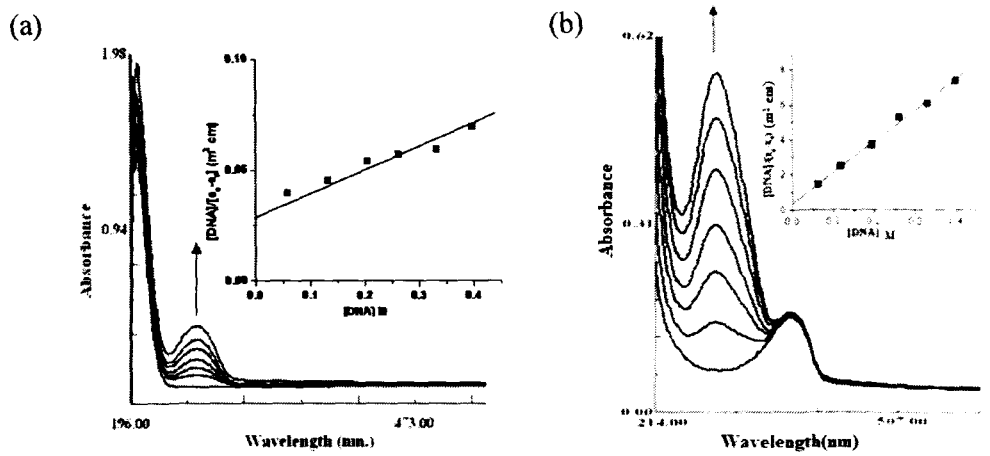

Cisplatin (Figure 45a) and classical metal based cisplatin drug show covalent binding with DNA via; 1,2-intrastrand crosslinks between adjacent N7 atoms of guanine nucleobase (GpG) and adenine (ApG) and secondary interaction with phosphate backbone [211].

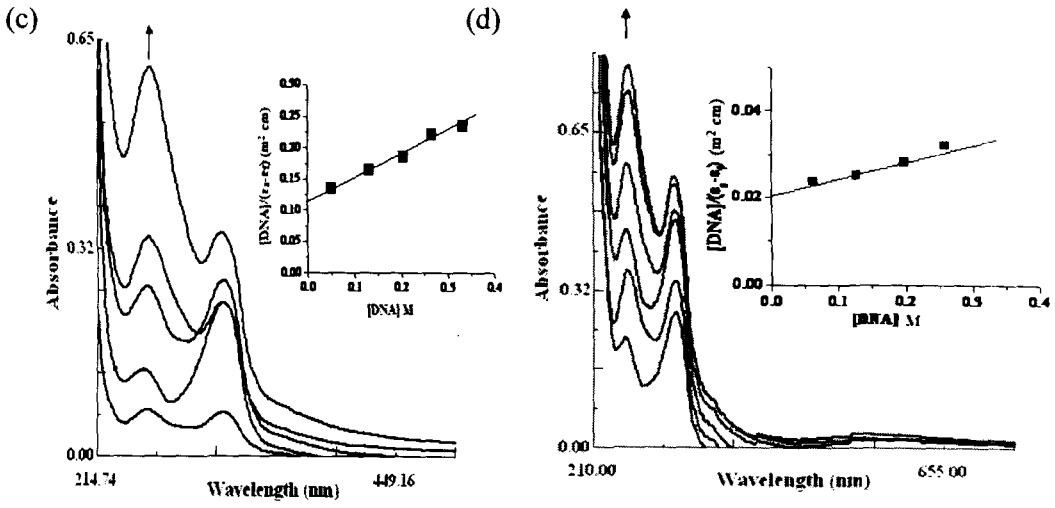

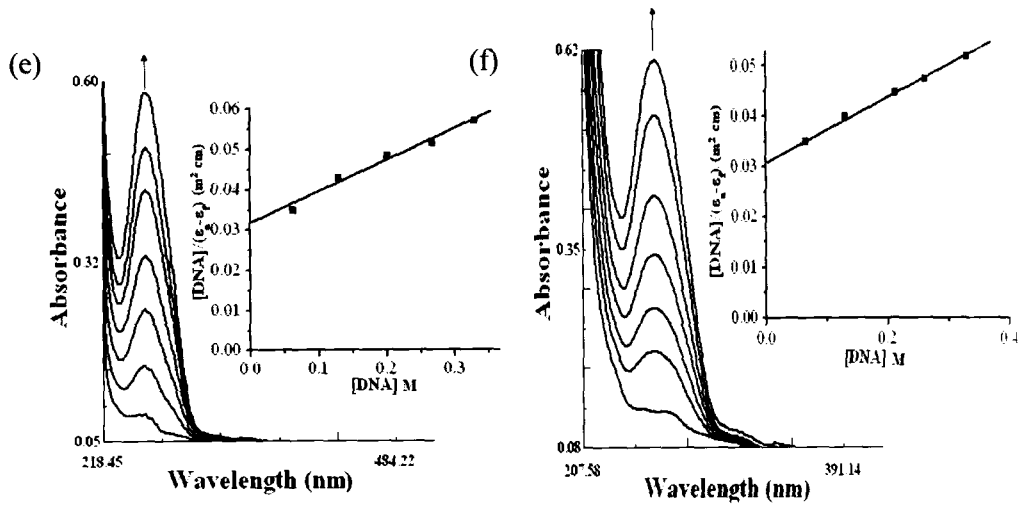

Figure 43. *Absorption spectra of (a) cisplatin (b) (S)-$C_{13}H_{17}NO_2$ (c) (S)-$C_{15}H_{21}NO_2Sn$ (d) (R)-$C_{15}H_{21}NO_2Sn$ (e) (S)-$C_{10}H_{16}NOSnCl$ (f) (R)-$C_{10}H_{16}NOSnCl$ in Tris-HCl buffer (pH= 7.2) in the absence and presence of increasing amount of CT-DNA. Inset: Plots of [DNA]/(ε_a-ε_f) vs [DNA] for the titration of CT-DNA with complexes. Arrow indicate the increase in the intensity upon increasing DNA concentration.[Complex]=1.0x10^{-4} M, [DNA]=1.0x10^{-4} M*

On the contrary, organotin prefer phosphate binding to the oxygen atom of sugar phosphate backbone and the nitrogen involved in the CT-DNA base binding is extremely effective, often resulting in the stabilization of the tin(IV) center as a stable octahedral species [212]. Therefore, the above results indicate that all the studied complexes bind predominantly to the phosphate group, neutralizing the negative charge of the CT-DNA and causing contraction and conformational changes in the DNA by an electrostatic interaction.

Interaction with 5′-GMP by absorption spectroscopy

In order to elucidate the mechanism of binding phenomenon with CT-DNA at the molecular level, interaction of the complexes with nucleotides is notably important. We have undertaken the UV-visible absorption titrations of complex (S)-[$C_{15}H_{21}NO_2Sn$] and (S)-[$C_{10}H_{16}NOSnCl$] with 5′-GMP owing to the fact that (S)

enantiomer of complexes (S)-[$C_{15}H_{21}NO_2Sn$] and (S)-[$C_{10}H_{16}NOSnCl$] exhibited greater K_b value in comparison to other complexes studied (Figure 46a,b).

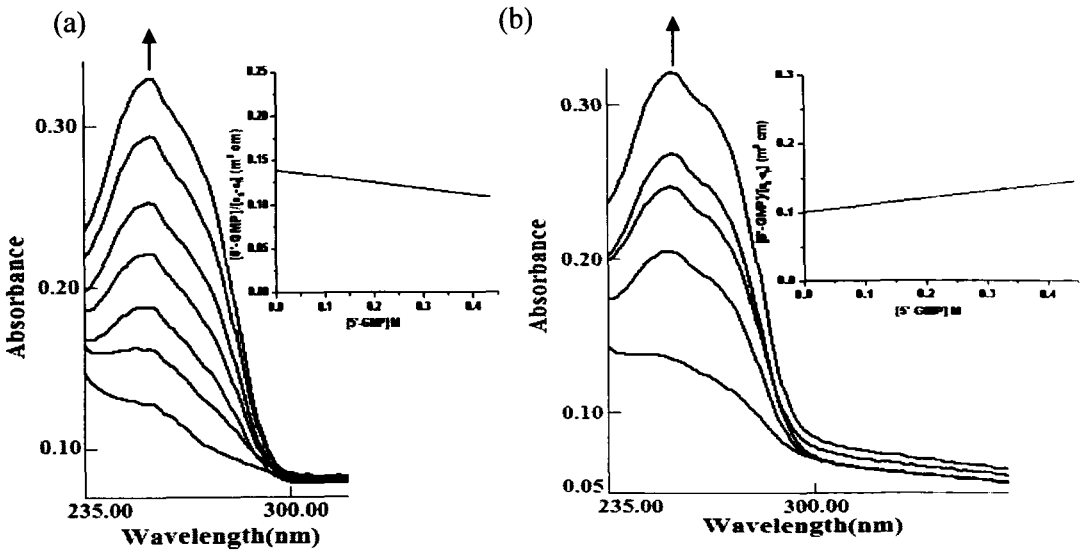

Figure 46. *Absorption spectra of (a) (S)-[$C_{15}H_{21}NO_2Sn$] in Tris-HCl buffer (pH= 7.2) in the absence and presence of increasing amount of 5'-GMP. Inset: Plots of [5'-GMP]/(ε_a-ε_f) vs [5'-GMP] for the titration of 5'-GMP with complexes. Arrow indicate the increase in the intensity upon increasing DNA concentration.*

On addition of increasing amount of 5'-GMP to the (S)-[$C_{15}H_{21}NO_2Sn$] and (S)-[$C_{10}H_{16}NOSnCl$], a sharp increase in the absorption intensity "hyperchromism" with slight shift of 2-3 nm was observed in the spectra of both the complexes indicative of electrostatic binding involving damage to the secondary structure of CT-DNA through phosphate backbone interaction. However, the higher intrinsic K_b value of for the complex (S)-[$C_{15}H_{21}NO_2Sn$] accounts for its higher binding with CT-DNA in comparison to the other complex (S)-[$C_{10}H_{16}NOSnCl$] (Table 7).

***Table** 7. The comparative binding constant (K_b) values of complexes (S)-[$C_{15}H_{21}NO_2Sn$] and (S)-[$C_{10}H_{16}NOSnCl$] with the 5'-GMP (mean standard deviation of ± 0.025).*

Complex	5'-GMP ($x10^4$)	Monitored at (nm)	% Hyperchromism (nm)	Red Shift
(S)-[$C_{15}H_{21}NO_2Sn$]	1.40	247	36	02
(S)-[$C_{10}H_{16}NOSnCl$]	1.02	246	38	03

^1H and ^{31}P NMR interaction with 5'-GMP

The more conclusive evidence for the interaction of (S)-[$C_{15}H_{21}NO_2Sn$] with 5'-GMP was further obtained by ^1H and ^{31}P NMR spectroscopy, being the most sensitive and reliable technique. The ^1H NMR of 5'-GMP in D_2O solvent records the proton resonance of guanine H8 at 8.1 ppm and ribose H1'-H5' at 3.8-5.8 ppm, respectively [213]. The resonance of 2-NH_2 was obscured due to the exchange of proton with deuterium solvent. On interaction of (S)-[$C_{15}H_{21}NO_2Sn$] with 5'-GMP, G-H8 signal did not display significant shift (8.1 ppm in free 5'-GMP to 7.96 ppm in 5'-GMP bound complex) which shows non-involvement of N7 position of guanine in coordination (Figure 47a,b). However, the resonances of ribose were perturbed to a substantial extent revealing their binding to the tin(IV) complex through O_2' and O_3' atoms of the sugar moiety of 5'-GMP. This type of binding behaviour is suggestive of electrostatic binding mode of the complexes while covalent coordination is ruled out as evidenced also by the UV-vis. titration of complexes with 5'-GMP and CT-DNA itself.

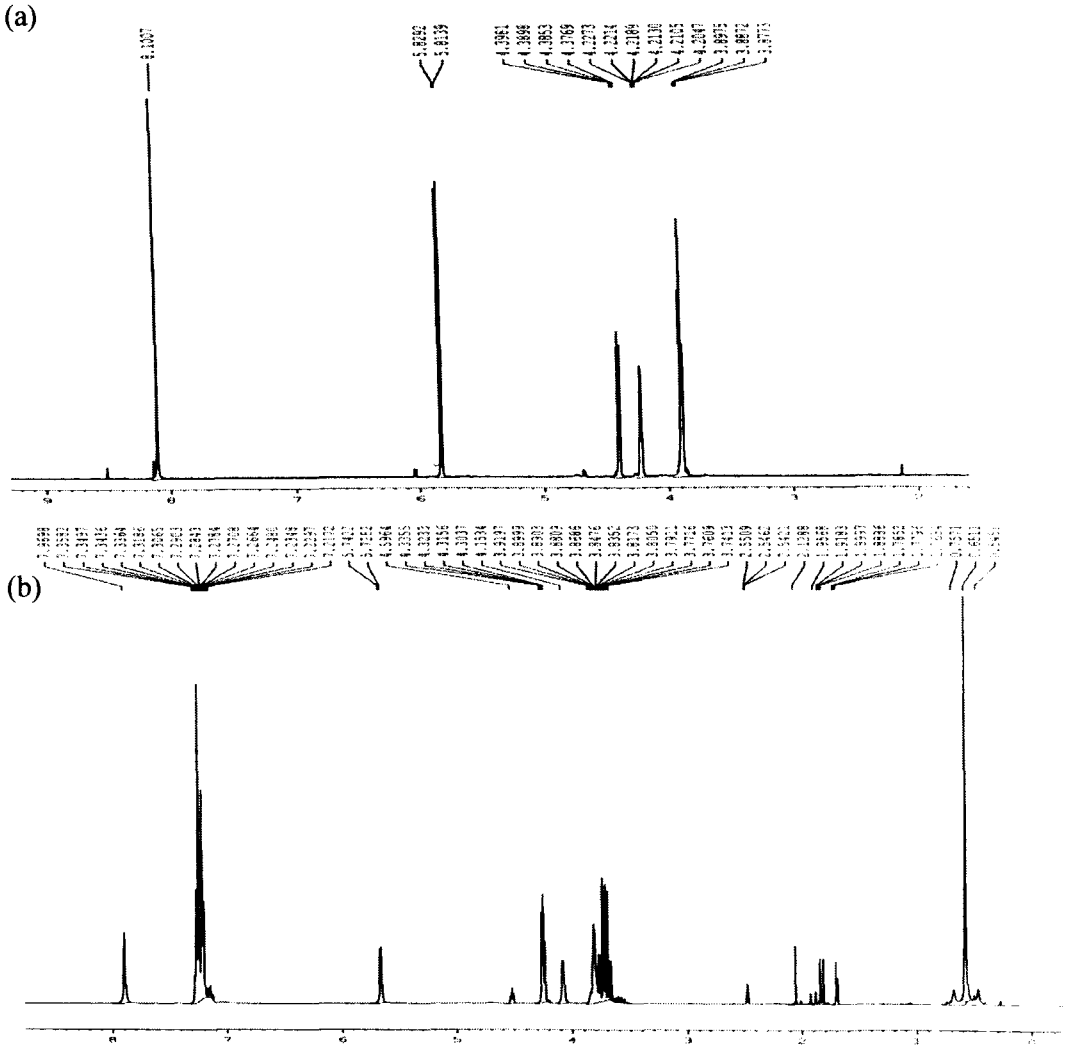

Figure 47. *^{1}H NMR spectra of (a) 5'-GMP alone and (b) the reaction of complex (S)-[$C_{16}H_{24}NO_2Sn$] (2.5 mmol) with 5'-GMP (5 mmol) at 25 °C.*

^{31}P NMR spectrum of 5'-GMP records a signal at 3.73 ppm which undergoes a large upfield shift to 1.20 ppm (Figure 48). Such large upfield chemical shift in ^{31}P signal provides a strong evidence for the selective binding of complex to the phosphate oxygen of 5'-GMP and validates the electrostatic interaction [214].

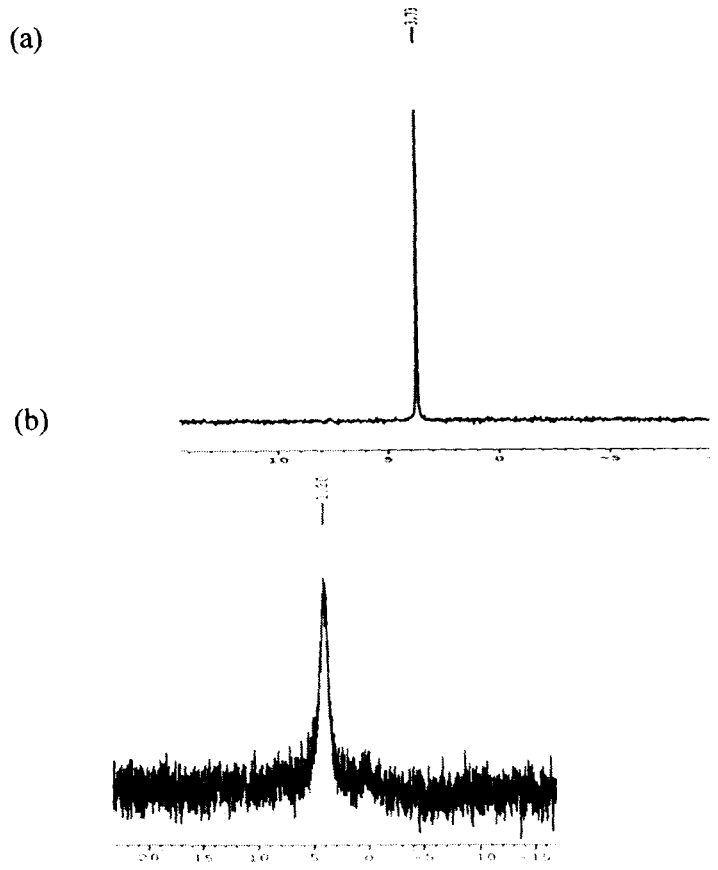

Figure 48. *^{31}P NMR spectra of (a) 5'-GMP and (b) the reaction of complex (S)-[$C_{15}H_{21}NO_2Sn$] (2.5 mmol) with 5'-GMP (5 mmol) at 25 °C.*

Fluorescence studies

To further elucidate the mode of binding of optically active complexes (S)/(R)-[$C_{15}H_{21}NO_2Sn$] and (S)/(R)-[$C_{10}H_{16}NOSnCl$] with CT-DNA, fluorescence spectral methods were employed by following the changes in the emission intensity of the complexes. In absence of CT-DNA, complexes (S)/(R)-[$C_{15}H_{21}NO_2Sn$] and (S)/(R)-[$C_{10}H_{16}NOSnCl$] emit luminescence around 260-500 nm in Tris-HCl buffer pH 7.2 when excited at 260 nm. Fixed volumes ($1.0x10^{-4}$ M) of the studied complexes were titrated, respectively with increasing concentration of DNA in the range from

(0-0.40x10^{-4} M). As seen from the Figure 49(a,b), the intensity of emission increases appreciably in the presence of DNA.

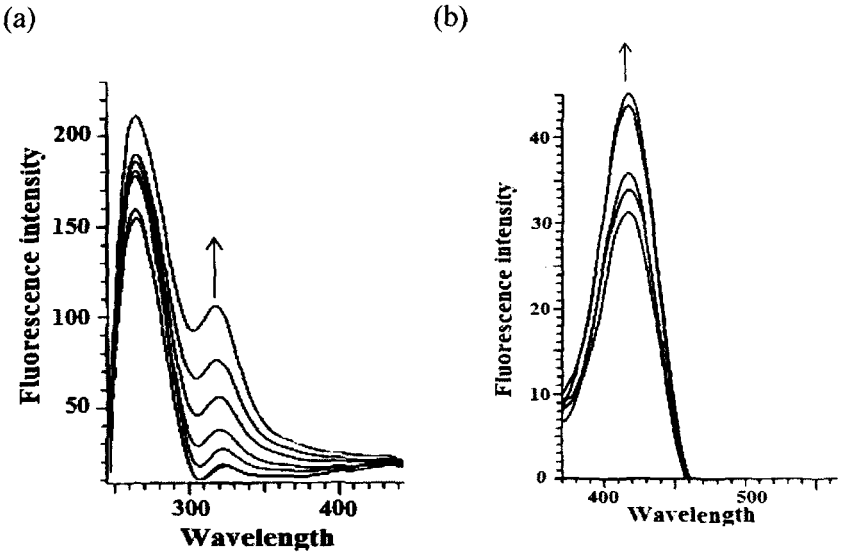

Figure 49. *Emission spectra of (a) (S)-[$C_{15}H_{21}NO_2Sn$] (b) (S)-[$C_{10}H_{16}NOSnCl$] in Tris-HCl buffer (pH 7.2) in the absence and presence of CT-DNA. Arrow indicate the change in the intensity upon increasing DNA concentration.*

The observed enhancement could be due to relatively non-polar environment of the bound metal complex in the presence of DNA, such that the complexes were less deeply inserted inside the hydrophobic pockets or grooves of CT-DNA [215]. Cationic complexes usually bind to DNA non-covalently as the cationic core of the complexes exerts a strong electrostatic attraction to the anionic phosphate backbone of DNA thus precluding substantial overlap with the base pairs leading to higher emission intensity indicative of electrostatic binding of the probe to the DNA. The binding constant K of the complexes follows the order: (S)-[$C_{15}H_{21}NO_2Sn$] > (S)-[$C_{10}H_{16}NOSnCl$] > (R)-[$C_{15}H_{21}NO_2Sn$] > (R)-[$C_{10}H_{16}NOSnCl$] as given in Table 8.

Table 8. *Emission properties of complexes (S)/(R)-[$C_{15}H_{21}NO_2Sn$] and (S)/(R)-[$C_{10}H_{16}NOSnCl$] bound to CT DNA (mean standard deviation ±0.09).*

Complex	Emission (nm)	Excitation (nm)	Monitored at (nm)	K(M^{-1})
(S)-[$C_{15}H_{21}NO_2Sn$]	230	450	315	$2.90x10^7$
(R)-[$C_{15}H_{21}NO_2Sn$]	230	450	315	$1.10x10^6$
(S)-[$C_{10}H_{16}NOSnCl$]	235	520	430	$1.83x10^6$
(R)-[$C_{10}H_{16}NOSnCl$]	235	520	430	$6.70x10^5$

A variety of molecular interactions can result in quenching phenomena including excited state reactions, molecular rearrangement, energy transfer, ground state complex formation, and collisional quenching. Quenching normally refers to non-radiative energy transfer from the excited species to the other molecules.

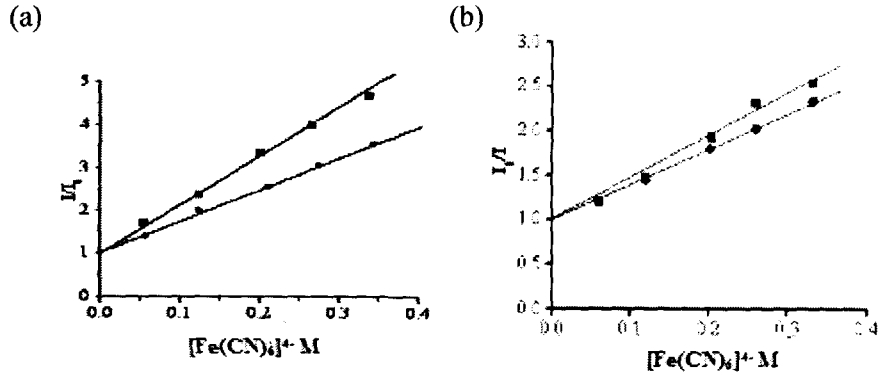

Figure 50. *Emission quenching curves of (a) (S)-[$C_{15}H_{21}NO_2Sn$] (b) (S)-[$C_{10}H_{16}NOSnCl$] in absence of CT-DNA (■) and in the presence of CT-DNA (●). [Complex] = $1.0x10^{-3}$ M.*

The fluorescence quenching studies using $K_4[Fe(CN)_6]$ as an anionic quencher were performed to further probe the binding characteristic of both chiral complexes (S)/(R)-[$C_{15}H_{21}NO_2Sn$] and (S)/(R)-[$C_{10}H_{16}NOSnCl$]. Figure 50(a,b) shows a typical Stern-Volmer plot of F_0/F versus $[Fe(CN)_6]^{4-}$ for the complexes (S)-[$C_{15}H_{21}NO_2Sn$]

and (S)-[$C_{10}H_{16}NOSnCl$]. In the absence of DNA, the positively charged complexes (S)-[$C_{15}H_{21}NO_2Sn$] and (S)-[$C_{10}H_{16}NOSnCl$] were efficiently quenched by $[Fe(CN)_6]^{4-}$ ion resulting in linear Stern-Volmer plot with a slope of $10.71x10^4$ and $8.57x10^4$ M^{-1}, respectively. In presence of DNA, the slope was remarkably decreased to $3.50x10^4$ and $6.42x10^4$ M^{-1}, respectively. Similarly, the slope of linear Stern-Volmer plot for the complexes (R)-[$C_{15}H_{21}NO_2Sn$] and (R)-[$C_{10}H_{16}NOSnCl$] were also quenched from $7.14x10^4$ and $4.85x10^4$ M^{-1} in the absence of DNA to $5.0x10^4$ and $3.71x10^4$ M^{-1} in presence of CT-DNA, respectively (Table 9).

Table 9. *Emission quenching of CT-DNA bound $[Fe(CN)_6]^{4-}$ by complexes (S)/(R)-[$C_{15}H_{21}NO_2Sn$] and (S)/(R)-[$C_{10}H_{16}NOSnCl$]*

Complex	Emission (nm)	Excitation (nm)	Monitored at (nm)	K_{sv1} ($x10^4$)	K_{sv2} ($x10^4$)
(S)-[$C_{15}H_{21}NO_2Sn$]	462	260	432	10.71	3.50
(R)-[$C_{15}H_{21}NO_2Sn$]	462	240	430	7.14	5.00
(S)-[$C_{10}H_{16}NOSnCl$]	460	260	440	8.57	6.42
(R)-[$C_{10}H_{16}NOSnCl$]	460	262	440	4.85	3.71

A greater decrease in the K_{sv} value for complexes (S)-[$C_{15}H_{21}NO_2Sn$] and (S)-[$C_{10}H_{16}NOSnCl$] than (R)-[$C_{15}H_{21}NO_2Sn$] and (R)-[$C_{10}H_{16}NOSnCl$] corresponds to a stronger binding of these complexes with DNA double helix [216]. Therefore, the above results are consistent with our UV-visible titration observations that both the S-enantiomeric forms of the complexes [$C_{15}H_{21}NO_2Sn$] and [$C_{10}H_{16}NOSnCl$] bind to the DNA more avidly as compared to R-enantiomeric form. Such type of quenching behavior is regarded as non-competitive quenching pertaining to electrostatic binding of the complexes with DNA.

Effect of ionic strength

In order to ascertain the probable binding mode between the molecule and DNA, fluorescence titrations were carried out under the conditions of increasing ionic strength (0-0.40x10^{-4} M) through added amounts of NaCl. It was observed that the fluorescence intensity of the studied (S)- as well as (R)- enantiomer of complexes was appreciably quenched with increasing ionic strength. However, the (S)-enantiomer of complexes shows a higher change in emission intensity upon increasing concentration of NaCl. A cation such as Na^+ can bind to phosphate group of the DNA by electrostatic forces to form a cation atmosphere around DNA. This cationic atmosphere shields the DNA and inhibits the binding of the positively charged molecules to the DNA phosphate backbone. This invokes a competitive interaction for the phosphate anions and subsequent addition of the cations weakens the surface binding interactions and hydrogen bonding between DNA and molecule.

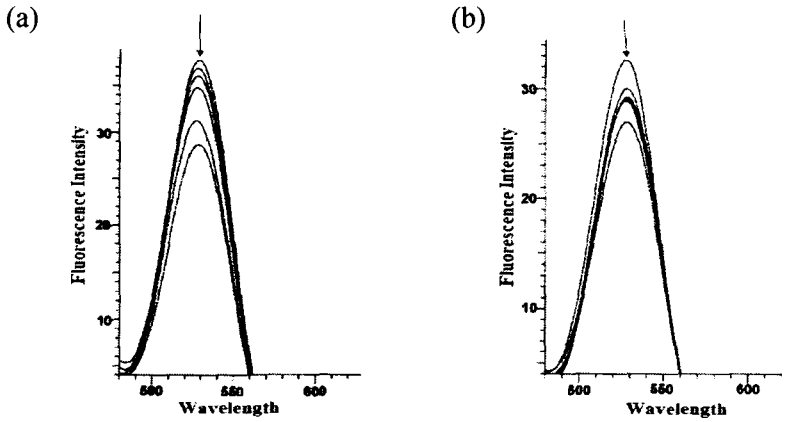

Figure 51. *Effect of different concentration of NaCl on the fluorescence spectra of complex (a) (S)-[$C_{15}H_{21}NO_2Sn$] (b) (S)-[$C_{10}H_{16}NOSnCl$]. [Complex]=1.0 x10^{-4} M, [DNA]=1.0x10^{-4} M. Arrow indicate the gradual decrease of emission intensity as a function of NaCl concentration.*

Therefore, the results implicate that the complexes (S)/(R)-[$C_{15}H_{21}NO_2Sn$] and (S)/(R)-[$C_{10}H_{16}NOSnCl$] preferably bind to the DNA phosphate backbone by electrostatic interactions [184,185]. In addition, it could be seen from Figure 51(a,b), that the effect of salt concentration on the fluorescence intensity of (S)-[$C_{15}H_{21}NO_2Sn$]-DNA system was far greater than the other complex (S)-[$C_{10}H_{16}NOSnCl$] so the complex (S)-[$C_{15}H_{21}NO_2Sn$] has a greater propensity for DNA binding.

Effect of phosphate group

As a means of further exploring the selective binding site of complexes (S)/(R)-[$C_{15}H_{21}NO_2Sn$] and (S)/(R)-[$C_{10}H_{16}NOSnCl$] with DNA, fluorescence titrations were performed in presence of increasing amount of K_2HPO_4 (Figure 50a,b). It was observed from the Figure 52(a,b) that fluorescence intensity of the complexes increases when K_2HPO_4 is added to the system. These results demonstrate a competitive binding behavior between the phosphate group of K_2HPO_4 and DNA for complexes studied.

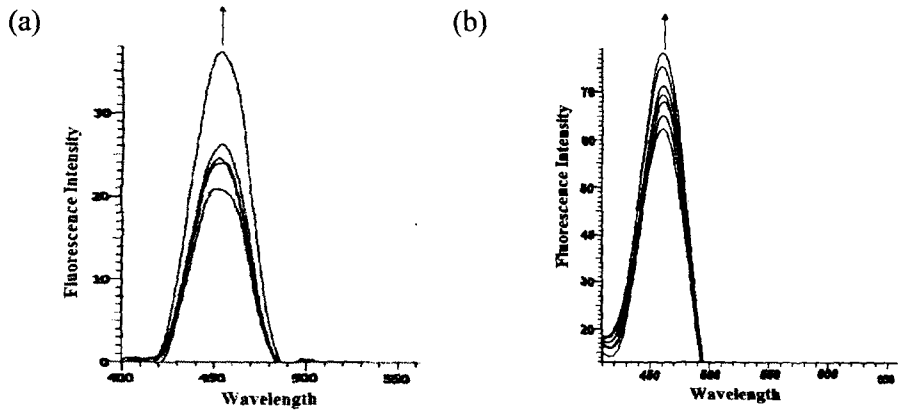

Figure 52. *Effect of increasing concentration of K_2HPO_4 on the fluorescence intensity of complex (a) (S)-[$C_{15}H_{21}NO_2Sn$] (b) (S)-[$C_{10}H_{16}NOSnCl$]. [Complex]=1.0x10^{-3} M, DNA=1.0x10^{-4} M.*

Thus, the phosphate group of K_2HPO_4 weakens the interaction between the complexes and CT-DNA, this observation provides supportive evidence for electrostatic interaction of the complexes (S)/(R)-[$C_{15}H_{21}NO_2Sn$] and (S)/(R)-[$C_{10}H_{16}NOSnCl$] which bind selectively to the phosphate group of DNA double helix [217]. Furthermore, there is a strong evidence in literature for tin(IV)-phosphate binding which was validated by binding studies of tin(IV) complexes with nucleotide employing ^{1}H and ^{31}P NMR techniques as illustrated above [174]. It was observed that the complex (S)-[$C_{15}H_{21}NO_2Sn$] binds with relatively higher affinity towards CT-DNA in contrast to (R)-[$C_{15}H_{21}NO_2Sn$] and (S)/(R)-[$C_{10}H_{16}NOSnCl$] complexes due to the effect of phosphate group.

Circular dichroic studies

Circular dichroic spectral studies have been performed to diagnose the changes in DNA morphology during complex-DNA interactions. The CT-DNA exhibits two consecutive bands, a positive band at 275 nm due to base stacking and a negative band at 245 nm due to helicity in the UV region [218]. The changes in CD signals of DNA observed on interaction of both enantiomers (R)/(S)-[$C_{15}H_{21}NO_2Sn$] and (S)/(R)-[$C_{10}H_{16}NOSnCl$] complexes are depicted in Figure 53(a-d). On addition of complex (S)-[$C_{15}H_{21}NO_2Sn$] to CT-DNA there is a pronounced red shift in both the positive and negative bands attributed to the helicity and base stacking of DNA and the absorbtion intensities show decrease in intensity in both the enantiomers to the extent there is inversion in the base stacking CD signal at 275 nm.

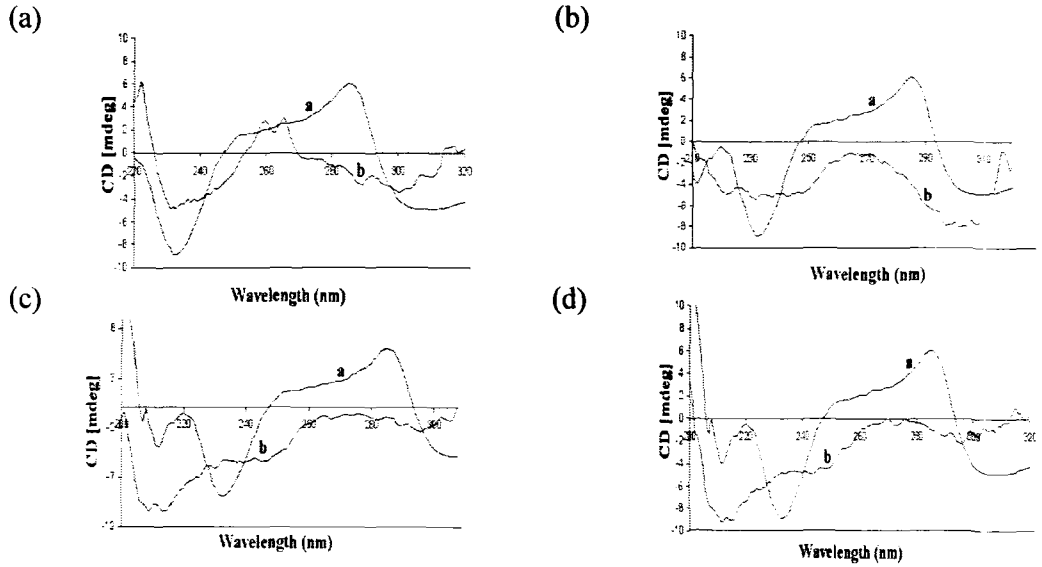

Figure 53. *CD spectra of CT-DNA in the absence (a) and presence (b) of complexes (1 μM) in plot. (a) DNA in the presence of (R)-[$C_{15}H_{21}NO_2Sn$] (b) DNA in the presence of (S)-[$C_{15}H_{21}NO_2Sn$] (c) DNA in the presence of (R)-[$C_{10}H_{16}NOSnCl$] (d) DNA in the presence of (S)-[$C_{10}H_{16}NOSnCl$].*

However, in case of (S)- enantiomeric form there is more predominant perturbations in comparison to (R)-enantiomeric form indicative of preferential enantiomeric binding of the complexes. These observations have been ascribed to conformational changes [219] induced by B→A transition of DNA. Furthermore, both the enantiomers of (R)/(S)-[$C_{10}H_{16}NOSnCl$] reveal identical CD changes of equal magnitude but opposite signs resulting from structural perturbations. (S)-enantiomeric form of complex [$C_{15}H_{21}NO_2Sn$] displays a greater affinity than both the enantiomers (R)/(S)- of complex [$C_{10}H_{16}NOSnCl$].

Viscosity studies

To clarify further the mode of interaction between the complexes (S)/(R)-[$C_{15}H_{21}NO_2Sn$] and (S)/(R)-[$C_{10}H_{16}NOSnCl$] and DNA, viscosity measurements

were performed and the results were presented as (η/η_0) versus binding ratio, where η is the viscosity of DNA in the presence of complex and η_0 is the viscosity of DNA alone.

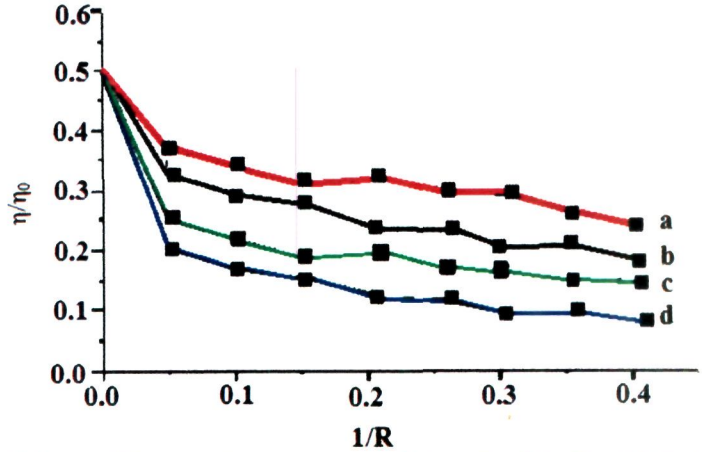

Figure 52. *Effect of increasing amount of (a) (R)-[$C_{10}H_{16}NOSnCl$](red) (b) (R)-[$C_{15}H_{21}NO_2Sn$](black) (c) (S)-[$C_{10}H_{16}NOSnCl$](green) (d) (S)-[$C_{15}H_{21}NO_2Sn$] (blue)on the relative viscosities (η/η_o) of CT-DNA in Tris-HCl buffer (pH 7.2).*

Figure 52 shows the relative viscosity of DNA ($0.06x10^{-4}$ M) in the presence of increasing concentration of complexes (S)/(R)-[$C_{15}H_{21}NO_2Sn$] and (S)/(R)-[$C_{10}H_{16}NOSnCl$] from ($0\text{-}0.40x10^{-4}$ M). In case of complex (S)/(R)-[$C_{15}H_{21}NO_2Sn$], the relative viscosity decreases steadily upon addition of varying concentration of complexes. A similar behaviour was also observed for complex (S)/(R)-[$C_{10}H_{16}NOSnCl$]. The decrease in the viscosity of the two complexes reveal an electrostatic non classical mode of binding of complexes with DNA [190]. However, decrease observed for complex (S)-[$C_{15}H_{21}NO_2Sn$] and (S)-[$C_{10}H_{16}NOSnCl$] is more pronounced than complex (R)-[$C_{15}H_{21}NO_2Sn$] and (R)-[$C_{10}H_{16}NOSnCl$] which supports a more strong electrostatic binding of complexes (S)-[$C_{15}H_{21}NO_2Sn$] and (S)-[$C_{10}H_{16}NOSnCl$] with CT-DNA compared to complexes (R)-[$C_{15}H_{21}NO_2Sn$] and (R)-[$C_{10}H_{16}NOSnCl$].

DNA cleavage activity

Gel electrophoretic pattern of complexes (S)-[$C_{15}H_{21}NO_2Sn$] and (S)-[$C_{10}H_{16}NOSnCl$] were obtained due to their high binding ability with DNA as evidenced by UV, fluorescence and viscosity studies. Initially in the untreated pBR322 plasmid DNA (Lane 1) two bands corresponding to Form I and Form II were observed. When the supercoiled pBR322 plasmid DNA were treated with both the complexes (S)-[$C_{15}H_{21}NO_2Sn$] and (S)-[$C_{10}H_{16}NOSnCl$] supercoiled (Form I) was cleaved to nicked circular DNA (Form II) (Lane 2 and 4, Figure 55), respectively. With increasing concentration of the complex from 50-200 μM apparently very little transformation of the plasmid DNA from Form I to Form II was observed (Lanes 3 and 5, Figure 55).

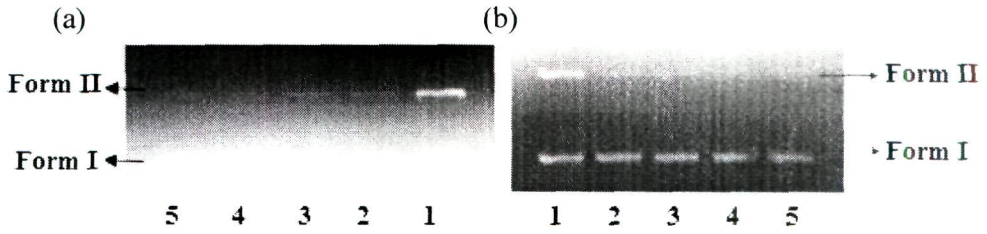

Figure 55. *Agarose gel electrophoresis patterns for the cleavage of pBR322 plasmid DNA as a function of increasing concentration of (a) complex (S)-[$C_{15}H_{21}NO_2Sn$] (b) complex (S)-[$C_{10}H_{16}NOSnCl$]. (a) DNA control (Lane 1); DNA + 50μM (S)-[$C_{15}H_{21}NO_2Sn$] (Lane 2); DNA + 100μM (S)-[$C_{15}H_{21}NO_2Sn$]. (Lane 3); DNA + 150μM (S)-[$C_{15}H_{21}NO_2Sn$] (Lane 4; DNA + 200μM (S)-[$C_{15}H_{21}NO_2Sn$] (Lane 5).(b) DNA control (Lane 1); DNA + 50μM (S)-[$C_{10}H_{16}NOSnCl$]. (Lane 2); DNA + 100μM (S)-[$C_{10}H_{16}NOSnCl$] (Lane 3); DNA + 150μM (S)-[$C_{10}H_{16}NOSnCl$] (Lane 4); DNA + 200μM (S)-[$C_{10}H_{16}NOSnCl$] (Lane 5).*

These small changes in the intensity of Form I and Form II with an increase in the concentration of the complexes is due to the unwinding of the supercoiled Form I to Form II owing to cleavage of DNA phosphodiester backbone. Thus, the complex

(S)-[$C_{15}H_{21}NO_2Sn$] and (S)-[$C_{10}H_{16}NOSnCl$] does not cleave the plasmid DNA efficiently [220]. These results are consistent with the observations of other spectroscopic studies. Thus, we can conclude that the activity of these complexes against various tumor cell lines seems not to come from the complete destruction of DNA caused by the complexes but from the high affinity of these complexes towards DNA.

In vitro antitumor activity

In vitro antitumor activity of complexes (S)-[$C_{15}H_{21}NO_2Sn$] and (S)-[$C_{10}H_{16}NOSnCl$] has been evaluated in terms of GI50, TGI and LC50 values against five different human carcinoma cell lines of different histological origin: Hop62 (Human lung), DWD (Human oral), K562 (Human leukemia), DU145 (Human prostrate) and MCF-7 (Human breast). The *in vitro* antitumor screening of these complexes (S)-[$C_{15}H_{21}NO_2Sn$] and (S)-[$C_{10}H_{16}NOSnCl$] was evaluated as a consequence of their high binding affinity towards CT-DNA by applying microculture sulforhodamine B test (SRB) [153]. The initial cytotoxic screening data (Table 10) shows that the complex (S)-[$C_{15}H_{21}NO_2Sn$] act as a potential selective anticancer agent with a pronounced GI50 values <10 μg/mL specifically towards Hop62, K562 and DWD tumor cell lines while complex (S)-[$C_{10}H_{16}NOSnCl$] exhibited efficient *in vitro* activity towards Hop62, DWD, MCF-7 and DU145 tumor cell lines.

Table 10. *Cytotoxicity against different tumor cells in terms of GI_{50} value.*

Where GI_{50} = ***Growth inhibition of 50 % (GI_{50})*** *calculated from [(Ti-Tz)/ (C-Tz) x 100 = 50, drug concentration resulting in a 50% reduction in the net protein increase.*

Complexes	**Hop62**	**DU145**	**DWD**	**MCF7**	**K562**
(S)-[$C_{15}H_{21}NO_2Sn$]	<10	30.8	15.5	23.3	<10
(S)-[$C_{10}H_{16}NOSnCl$]	<10	15.0	<10	<10	>80

$GI_{50} \leq 10$ is considered to demonstrate activity.

Conclusions

The newly synthesized modulated organotin complexes derived from (R)- and (S)-enantiomers of [4-(2-hydroxy-1-phenylethylimino)pent-2-ol] and 2-amino-2-phenylethanol [$C_{15}H_{21}NO_2Sn$] and [$C_{10}H_{16}NOSnCl$], respectively were synthesized with the aim to examine the effect of chirality on the DNA binding ability of two enantiomeric forms (enantiomeric selectivity). Many properties of metal complexes such as size, charge, shape, and chirality could influence the binding mode and modification extent to DNA. *In vitro* complex-DNA interaction studies (UV-vis., fluorescence, ^{1}H and ^{31}P NMR, circular dichroism, viscosity measurements and gel electrophoresis) reveal that complexes (S)/(R)-[$C_{15}H_{21}NO_2Sn$] and (S)/(R)-[$C_{10}H_{16}NOSnCl$] bind to DNA via, electrostatic interaction mode preferentially involving phosphodiester backbone. However, (S)-enantiomers bind more strongly in comparison to (R)-enantiomeric analogues. (S)-[$C_{15}H_{21}NO_2Sn$] and (S)-[$C_{10}H_{16}NOSnCl$] exhibit higher K_b values for DNA binding as compared to cisplatin drug as well which is used for clinical treatment in cancer chemotherapy. Higher binding propensity of (S)-$C_{15}H_{21}NO_2Sn$ could be attributed to *(i)* Availability of coordination sites at tin, tin(IV) is five-coordinate with trigonal bipyramidal geometry. *(ii)* Tin(IV) being a strong Lewis acid exhibits strong affinity preferentially towards the anionic phosphate backbone of DNA helix.

(S)-enantiomer of [$C_{15}H_{21}NO_2Sn$] possess good cytotoxic activity against Hop62 (human lung), K562 (human leukemia), DWD (human oral) with pronounced GI50 values <10 μg/mL and warrants further vigorous *in vivo* investigations.

CHAPTER V

In vitro binding studies of organotin(IV) complexes of 1,2-bis-(2-1H-benzimidazol-2-yl)-1,2-ethanediol with CT-DNA and nucleotides (5′-GMP and 5′-TMP): Effect of the ancillary ligand on the binding propensity.

Synthesis of ligand

$[C_{16}H_{14}N_4O_2]$

Ligand was prepared were prepared by reaction of 1,2-diamino benzene (4.6g, 40mmol) and L-tartaric acid (3.0g, 20mmol), following the method described earlier [68].

1,2-diaminobenzene (4.32g, 40mmol) and L (+)-tartaric acid (3.00g, 20mmol) were dissolved in 50 ml of 4M hydrochloric acid. The solution was refluxed for 24 h. After cooling a brown compound (the chloride salt of the protonated ligand) crystallized from the dark brown solution. The crystals were filtered and re-dissolved in 150 ml water and 150 ml ethanol. After adding active carbon, the solution was heated to reflux for 2 h. The colorless solution was neutralized with concentrated ammonia and white precipitate was filtered.

Yield 65%. m.p. 270 ± 2 °C. Anal. (%) Calc. for $[C_{16}H_{14}N_4O_2]$: C, 65.30; H, 4.79; N, 19.04: Found: C, 65.32; H, 4.81; N, 19.01. $[\alpha]^{25}_D$ = +110. ESI-MS (m/z) 295 $[C_{16}H_{14}N_4O_2]$.

Selected IR data on KBr pellet (ν/cm^{-1}): 3322 (OH); 1623 (C=N); 1227 (C–O); 740 (Ar). UV-vis in Methanol [λ_{max}/nm]: 206, 247, 278. ^{1}H NMR (DMSO-d_6, ppm): 5.49-5.67 (-CH); 6.41(-OH); 7.10-7.52 (Aromatic-H). ^{13}C NMR (DMSO-d_6, ppm): 155 (C=N); 115-121 (Ar-C); 71 (C-O).

Synthesis of complexes

$[C_{18}H_{19}N_4O_2SnCl]$

To a stirring solution of dimethyltin(IV)dichloride (1.07g, 5mmol) in methanol (20 mL) was added to the ligand $[C_{16}H_{14}N_4O_2]$ (1.47g, 5mmol). The reaction mixture

was refluxed at 80 °C with constant stirring on the rotamantle for 4 h and then allowed to stand at room temperature overnight (25 °C). Slow evaporation of the resulting mixture afforded white amorphous complex. The above complex was washed with hexane and dried *in vacuo* over anhydrous $CaCl_2$ (Scheme 8).

Yield 56%. m.p. 210 ± 2 °C. Anal. (%) Calc. for [$C_{18}H_{19}N_4O_2SnCl$]: C, 45.27; H, 4.01; N, 11.73: Found: C, 45.30; H, 4.1; N, 11.76. $[\alpha]^{25}_D$ = +193. ESI-MS (m/z) 478 [$C_{18}H_{19}N_4O_2Sn$]. Molar Conductance, $\wedge_M$ (1 x 10^{-3} M, Methanol): 59 $\Omega^{-1}cm^2$ mol^{-1} (non-electrolyte).

Selected IR data (ν/cm^{-1}): 3220 (OH); 3042 (NH); 1625 (C=N); 1222 (C–O); 759 (Ar); 557 (Sn-C); 470 (Sn-N); 435 (Sn-O); 256 (Sn-Cl). UV-vis in Methanol [λ_{max}/nm]: 210, 245, 275. ^{1}H NMR (DMSO-d_6, ppm): 5.9 (-CH); 6.4 (-OH); 7.1-7.8 (Aromatic-H). ^{13}C NMR (DMSO-d_6, ppm): 154 (C=N); 114-128 (Ar-C); 70 (C-O); 10-12 (-CH_3). ^{119}Sn NMR (DMSO-d_6, ppm): -189.

[$C_{28}H_{23}N_4O_2SnCl$]

The complex [$C_{28}H_{23}N_4O_2SnCl$] was prepared with diphenyltin(IV)dichloride (1.71g, 5mmol) and ligand [$C_{16}H_{14}N_4O_2$] (1.47g, 5mmol) according to the procedure described above for complex [$C_{18}H_{19}N_4O_2SnCl$].

Yield 64%. m.p. 215 ± 2 °C. Anal. (%) Calc. for [$C_{28}H_{23}N_4O_2SnCl$]: C, 55.89; H, 3.85; N, 9.31: Found: C, 55.85; H, 3.86; N, 9.34. $[\alpha]^{25}_D$ = +120. ESI-MS (m/z) 604 [$C_{28}H_{23}N_4O_2SnCl$+2H]. Molar Conductance, $\wedge_M$ (1 x 10^{-3} M, Methanol): 34 $\Omega^{-1}cm^2$ mol^{-1} (non-electrolyte).

Selected IR data (ν/cm^{-1}): 3208 (OH); 3046 (NH); 1625 (C=N); 1226 (C–O); 747 (Ar); 588 (Sn-C); 472 (Sn-N); 435 (Sn-O); 263 (Sn-Cl). UV-vis in Methanol [λ_{max}/nm]: 207, 244, 274. ^{1}H NMR (DMSO-d_6, ppm): 5.5-5.4 (-CH); 6.6 (-OH); 7.1-7.9 (Aromatic-H). ^{13}C NMR (DMSO-d_6, ppm): 154 (C=N); 114-136 (Ar-C); 69 (C-O). ^{119}Sn NMR (DMSO-d_6, ppm): -586.

[$C_{52}H_{42}N_4O_2Sn_2$]

The complex [$C_{52}H_{42}N_4O_2Sn_2$] was prepared with triphenyltin(IV)chloride (1.92g, 5 mmol) and ligand [$C_{16}H_{14}N_4O_2$] (1.47g, 5mmol) according to the procedure described above for complex [$C_{18}H_{19}N_4O_2SnCl$].

Yield 69%. m.p. < 300 °C (decompose). Anal. (%) Calc. for [$C_{52}H_{42}N_4O_2Sn_2$]: C, 62.94; H, 4.27; N, 5.65: Found: C, 62.86; H, 4.22; N, 5.66. $[\alpha]^{25}_{D}$ = +90. ESI-MS (m/z) 1009 [$C_{52}H_{42}N_4O_2Sn_2$+0.5CH_3OH]. Molar Conductance, $\wedge_M$ (1 x 10^{-3} M, Methanol): 37 $\Omega^{-1}cm^2mol^{-1}$ (non-electrolyte).

Selected IR data (ν/cm^{-1}): 1621 (C=N); 3062 (NH); 1222 (C–O); 735 (Ar); 561 (Sn-C); 452 (Sn-N); 446 (Sn-O). UV-vis in Methanol [λ_{max}/nm]: 207, 245, 275. ^{1}H NMR (DMSO-d_6, ppm): 5.5-5.8 (-CH); 7.1-7.9 (Aromatic-H). ^{13}C NMR (DMSO-d_6, ppm): 155 (C=N); 114-136 (Ar-C); 70 (C-O). ^{119}Sn NMR (DMSO-d_6, ppm): -222.

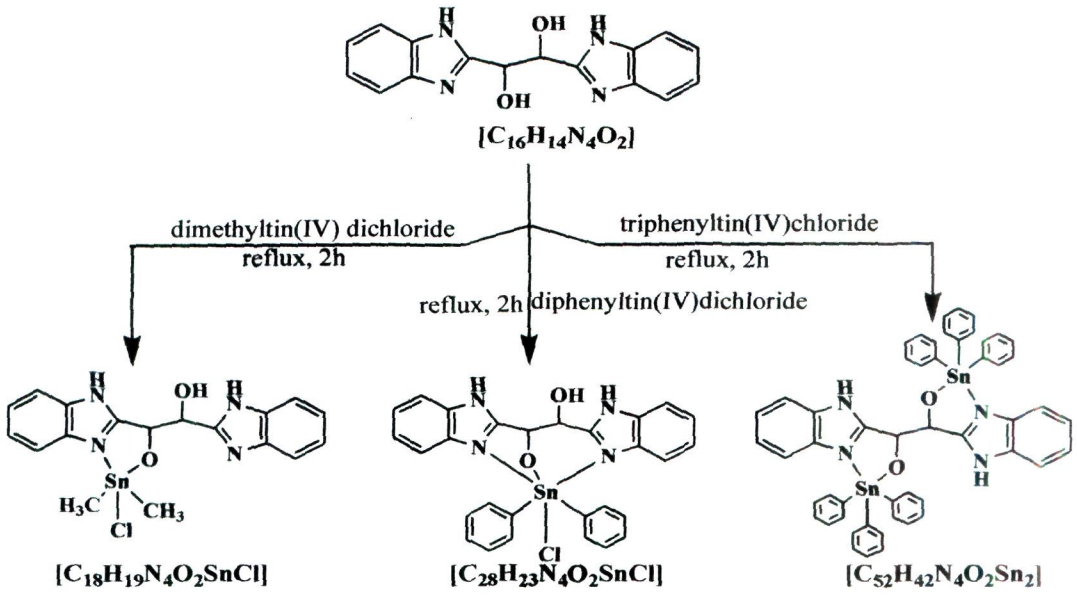

Scheme 8. *Schematic representation of the formation of complexes* $[C_{18}H_{19}N_4O_2SnCl]$, $[C_{28}H_{23}N_4O_2SnCl]$ *and* $[C_{52}H_{42}N_4O_2Sn_2]$

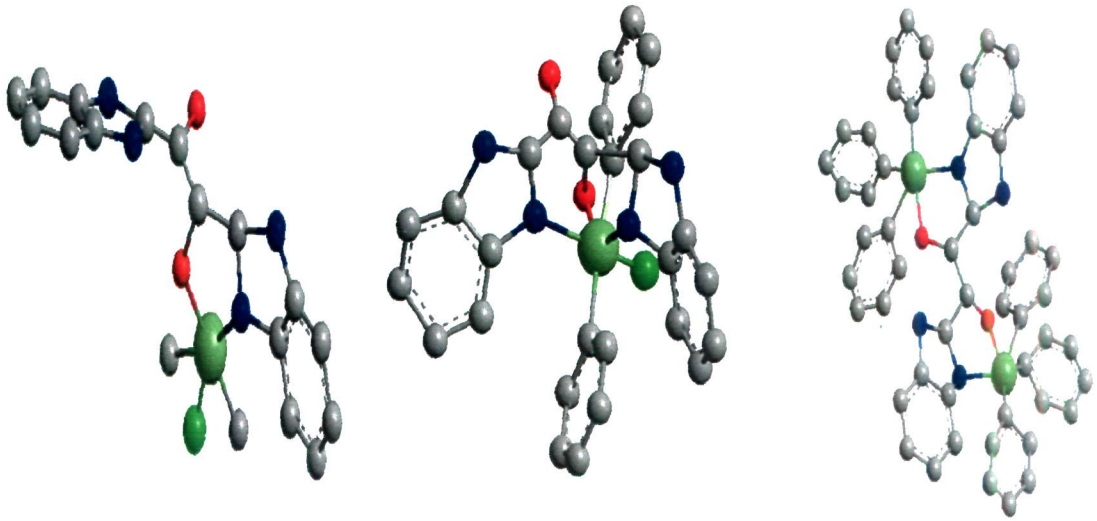

Figure 56. *Cylindrical bonded three dimensional model of complexes (a)* $[C_{18}H_{19}N_4O_2SnCl]$ *(b)* $[C_{28}H_{23}N_4O_2SnCl]$ *(c)* $[C_{52}H_{42}N_4O_2Sn_2]$. *Color scheme: Tin(IV) light green; Chloride, fluorescent green; N dark blue; O red; C gray. The H atoms and are omitted for clarity*

Results and Discussion

Synthesis and characterization

The synthesis of the ligand was a straightforward Phillips condensation reaction and the new organotin(IV) complexes $[C_{18}H_{19}N_4O_2SnCl]$, $[C_{28}H_{23}N_4O_2SnCl]$ and $[C_{52}H_{42}N_4O_2Sn_2]$ were prepared by the coordination of ligands to the central metal ion via nitrogen and oxygen donor atom. Nitrogen atoms participate through the coordinate linkages, while oxygen atom is involved in coordination under release of HCl in 1:1 stoichiometric ratio (Scheme 8). These complexes were stable at room temperature and soluble in various organic solvents such as methanol, ethanol and DMSO. Molar conductance values of complexes in methanol were recorded as 59, 34 and 37 Ω^{-1} cm^2 mol^{-1} for the complexes $[C_{18}H_{19}N_4O_2SnCl]$, $[C_{28}H_{23}N_4O_2SnCl]$ and $[C_{52}H_{42}N_4O_2Sn_2]$ suggesting their non-electrolytic nature. The geometry of the around the tin metal ion was ascertained by ^{119}Sn NMR spectra which revealed a pentacoordinated geometry for $[C_{18}H_{19}N_4O_2SnCl]$, $[C_{52}H_{42}N_4O_2Sn_2]$ and hexacoordinated environment for $[C_{28}H_{23}N_4O_2SnCl]$ complexes, respectively.

IR spectral studies

The IR spectra of the ligands undergo several modifications upon coordination to the metal atoms. In the IR spectra of the ligands the -OH and NH frequencies are present as a broad envelope in the region from 3450-3199 cm^{-1} due to intermolecular hydrogen bonding NH and OH groups [221,75] which display minor changes on complexation. However, a medium or relatively weak band at 1623 cm^{-1} with a small shoulder at 1536 cm^{-1} corresponding to ν(C=N) in the IR spectra of the ligands [222]

were considerably shifted by 2-3 cm^{-1} and becoming larger and sharper indicating the involvement of the nitrogen atom in complexation with tin(IV) metal ion in all the complexes $[C_{18}H_{19}N_4O_2SnCl]$, $[C_{28}H_{23}N_4O_2SnCl]$ and $[C_{52}H_{42}N_4O_2Sn_2]$. Other frequencies in complexes corresponding to ν(Sn-C), ν(Sn-N), ν(Sn-O), and ν(Sn-Cl) appear at 557-588, 435-446, 517-546 and 279-256 cm^{-1}, respectively [223-225].

Electronic spectra

The absorption spectra of the complexes $[C_{18}H_{19}N_4O_2SnCl]$, $[C_{28}H_{23}N_4O_2SnCl]$ and $[C_{52}H_{42}N_4O_2Sn_2]$ were recorded in methanol at room temperature. The spectra of the complexes $[C_{18}H_{19}N_4O_2SnCl]$, $[C_{28}H_{23}N_4O_2SnCl]$ and $[C_{52}H_{42}N_4O_2Sn_2]$ reveal bands at 207-210, 245, and 275 nm attributed to IL transitions of the ligands.

NMR spectra

The conclusions drawn from the ^1H NMR spectrum of free ligand were extrapolated to the complexes $[C_{18}H_{19}N_4O_2SnCl]$, $[C_{28}H_{23}N_4O_2SnCl]$ and $[C_{52}H_{42}N_4O_2Sn_2]$ owing to the data similarity. In complex $[C_{18}H_{19}N_4O_2SnCl]$, the characteristic satellite peak of the methyl groups attached to the tin is observed at 0.7-1.9 ppm [226]. While in complexes $[C_{28}H_{23}N_4O_2SnCl]$ and $[C_{52}H_{42}N_4O_2Sn_2]$, the presence of Sn-Ph protons at 7.8 and 7.9 ppm [227] shows the formation of the complexes. The ^1H NMR spectra of all the complexes reveals a resonance for the CH proton attached to the hydroxyl group at 5.9-5.8 ppm which is shifted downfield compared to the free ligand at 5.4 ppm [68] showing the involvement of adjacent hydroxyl group in complexation with tin metal ion. However, the most striking difference in the ^1H NMR of complex $[C_{52}H_{42}N_4O_2Sn_2]$ with the other complexes $[C_{18}H_{19}N_4O_2SnCl]$ and

[$C_{28}H_{23}N_4O_2SnCl$] is the disappearance of the hydroxyl protons of ligand at 6.4 ppm concomitant with the formation of complex in 1:2 stoichiometric ratio [68]. The aromatic protons of the ligand appear as a multiplet in the range of 7.1-7.5 ppm. In addition, due to rapid exchange between the two nitrogen atoms of imidazole ring the NH protons of the ligand were not observed in the NMR spectra. This observation was in accordance with the earlier reports [228,229].

The ^{13}C NMR spectra of the ligand exhibit signals corresponding to C=N, C-O at 155 and 68-70 ppm, respectively [68] which were shifted in the downfield in the complexes. In addition, the complex [$C_{18}H_{19}N_4O_2SnCl$] displays the methyl carbons attached to the tin metal ion (Sn-CH_3) at 10-14 ppm; the other complexes [$C_{28}H_{23}N_4O_2SnCl$] and [$C_{52}H_{42}N_4O_2Sn_2$] exhibit only one set of NMR signals for both the phenyl groups (Sn–Ph) and for the ligands from 127-136 ppm, which provide evidence for the magnetic equivalence of both the phenyl groups of the ligands and the complexes on the NMR time scale [230,231].

In order to provide further evidence to establish the structure of the complexes in solution [232], we recorded ^{119}Sn NMR spectra (Figure 57a-c). The complexes [$C_{18}H_{19}N_4O_2SnCl$] and [$C_{52}H_{42}N_4O_2Sn_2$] displays chemical shifts values of -186 and -222 ppm while complex [$C_{28}H_{23}N_4O_2SnCl$] exhibit a signal at -586 ppm which lie in the range delimited for five and six coordinated organotin(IV) complexes, respectively [233, 234].

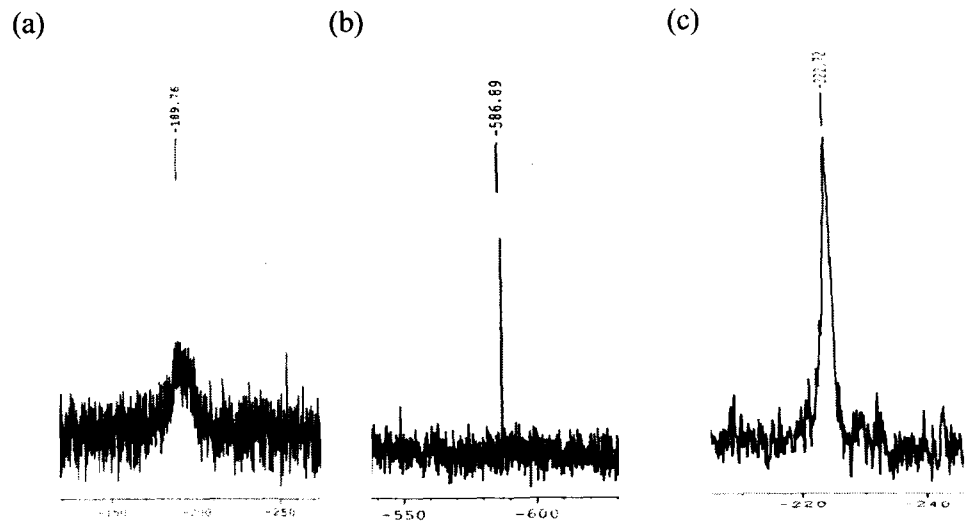

Figure 57. *^{119}Sn NMR spectra of complexes (a) $[C_{18}H_{19}N_4O_2SnCl]$ (b) $C_{28}H_{23}N_4O_2SnCl$ (c) $C_{52}H_{42}N_4O_2Sn_2$.*

DNA binding studies

UV-visible absorption studies

The absorption spectra of complexes in presence and in the absence of CT-DNA are shown in Figure 58(a-c). In absence of CT-DNA, all the complexes exhibit similar absorption spectra with the peaks centered at 245 and 275 nm corresponding to n-π* and at 207-210 nm for π-π* IL transitions owing to the presence of benzimidazole ligand scaffold (Figure 58a-c). In presence of incremental amount of CT-DNA, a significant "hyperchromic" effect with a strong bathochromic shift was observed for all studied complexes. Complex $[C_{28}H_{23}N_4O_2SnCl]$ displays a substantial bathochromic shift of ca. 4-5 nm which supports a higher degree of binding for this complex towards CT-DNA [235]. Thus, from these spectral changes, we deduce that the complexes bind to the CT-DNA by a strong electrostatic interaction mode as a

result of a high affinity of cationic tin(IV) to the polyanionic phosphate backbone and lack of base specificity in DNA binding. Literature reveals [174,209] strong Lewis acid tin(IV) ions neutralize the negative charge of the CT-DNA thereby, causing contraction and conformational changes in the CT-DNA via, an electrostatic interaction with the phosphate backbone of DNA double helix. The spectral features reveal that the complex [$C_{28}H_{23}N_4O_2SnCl$] has much higher affinity towards CT-DNA among the other complexes which could be attributed to the presence of labile groups of varying steric demand and hydrophobicity thereby facilitating multifaceted binding modes. The hydrophobic phenyl groups leads to more intimate binding and possibly promoting partial insertion of the complex [$C_{28}H_{23}N_4O_2SnCl$] into the DNA helix. In addition, hydrolysis of labile chloride atoms in the complex [$C_{28}H_{23}N_4O_2SnCl$] [236] and hard Lewis acidic property of tin(IV) together contribute to the vicinal electrostatic binding of complex with the polyanionic phosphate backbone of CT-DNA [237]. Furthermore, the presence of -OH group in the ligand being out of the planar phenyl rings, as validated by the crystal structure of the ligand [68] forms hydrogen bonds with DNA. Although complete intercalation between a set of adjacent base pairs is sterically prohibited, but some type of partial intercalation can be envisioned for complex [$C_{28}H_{23}N_4O_2SnCl$]. Similarly, complex [$C_{18}H_{19}N_4O_2SnCl$] also exhibit an electrostatic binding mode pertaining to presence of tin(IV) central metal ion which substantiate preferential binding to the DNA phosphate backbone; the discerning binding exhibited by complex [$C_{18}H_{19}N_4O_2SnCl$] compared to complex [$C_{28}H_{23}N_4O_2SnCl$] is due to the absence of phenyl group in the complex.

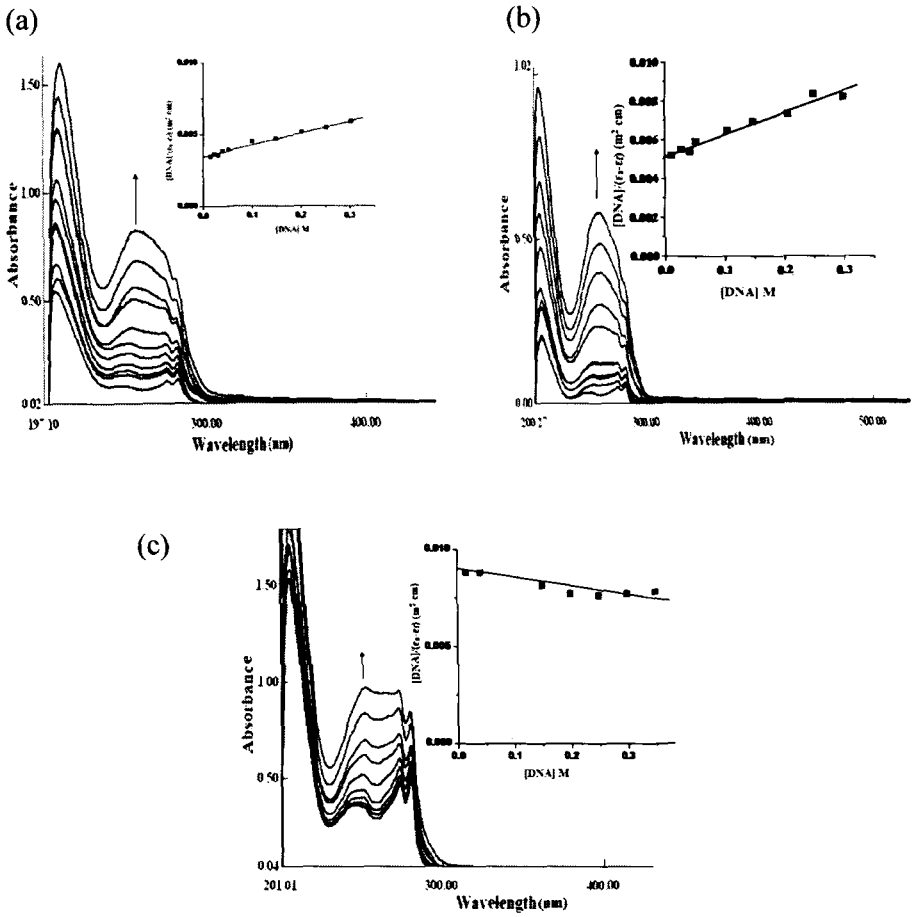

Figure 58. *Absorption spectra of complexes (a) $[C_{18}H_{19}N_4O_2SnCl]$ (b) $[C_{28}H_{23}N_4O_2SnCl]$ (c) $[C_{52}H_{42}N_4O_2Sn_2]$ in the (b-j) presence of increasing amount of CT-DNA. Inset: Plots of $[DNA]/(\varepsilon_a-\varepsilon_f)$ vs [DNA] for the titration of CT-DNA with complexes. [Complex]= 1.3x10^{-4} M, [CT-DNA]= 1.2x10^{-4} M.*

The complex $[C_{52}H_{42}N_4O_2Sn_2]$ has steric constraints caused by the bulky phenyl groups of the triphenyltin(IV) moiety which accounts for its lower binding propensity with DNA. Thus, the comparative binding strength of the complexes with CT-DNA were in the order $[C_{28}H_{23}N_4O_2SnCl]$>$[C_{18}H_{19}N_4O_2SnCl]$>$[C_{52}H_{42}N_4O_2Sn_2]$ as given in Table 11 below.

Table 11. *The binding constant (K_b) values of complexes [$C_{18}H_{19}N_4O_2SnCl$], [$C_{28}H_{23}N_4O_2SnCl$] and [$C_{52}H_{42}N_4O_2Sn_2$] with the CT-DNA*

Complex	K_b (M^{-1})	% Hyperchromism	Red Shift (nm)
[$C_{18}H_{19}N_4O_2SnCl$]	$2.16x10^4$ (± 0.04)	32	06
[$C_{28}H_{23}N_4O_2SnCl$]	$3.47x10^4$ (± 0.04)	45	05
[$C_{52}H_{42}N_4O_2Sn_2$]	$4.60x10^3$ (± 0.04)	20	05

Interaction with 5′-GMP and 5′-TMP by absorption spectroscopy

To avoid the macrostructural effects of larger nucleic acid which might obscure the fundamental biomolecular selectivity of these complexes, absorption titration with small nucleic acid fragments such as mononucleotides (5′-GMP and 5′-TMP) were performed under physiological conditions. Nucleotides contain three characteristic ligating regions capable of metal binding ie. (a) heterocyclic ring N atoms and nucleobase functionalities of purine and pyrimidine (b) phosphate O atoms (c) hydroxyl oxygen atoms of ribose sugar moiety. Earlier work of Gellert et al. [238] demonstrated X-ray structural studies showing predominant binding of thirty binary and ternary mononucleotide-transition metal complexes by first two modes through exocyclic nitrogen atom of purine rings (N1 and N7 atom) and N3 of the pyrimidine and oxygen atom of the phosphate group present in the nucleotides. Later, extensive work on the interaction of organotin(IV) complexes DNA and nucleotides was also carried out by Yang et al to elucidate the probable mode of binding of the tin(IV) complexes [209,174]

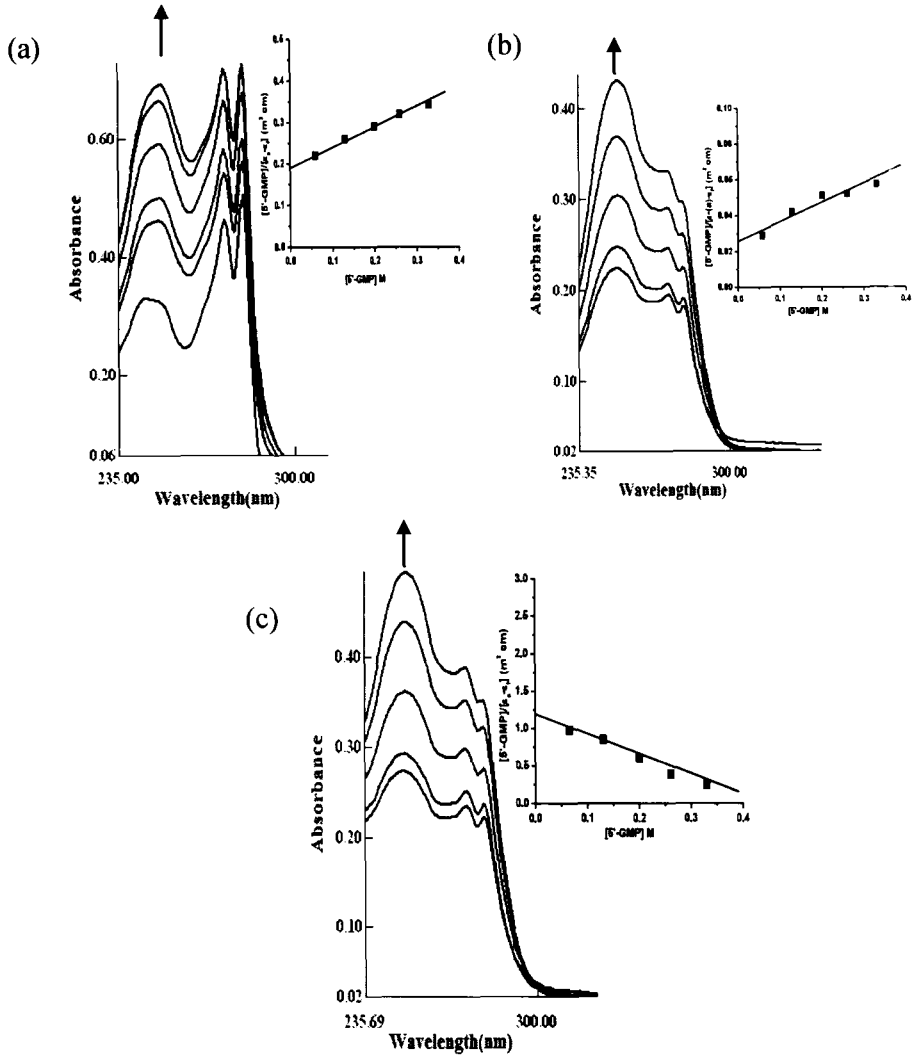

Figure 59. *Absorption spectral traces of complexes* (a) *[$C_{18}H_{19}N_4O_2SnCl$] (b) [$C_{28}H_{23}N_4O_2SnCl$] (c) [$C_{52}H_{42}N_4O_2Sn_2$] upon addition of 5'-GMP. [Complex]=1.3 x 10^{-4} M, [5'-GMP]=0-0.50x10^{-4} M. Inset: Plots of [5'-GMP]/ ε_a-ε_f vs [5'-GMP] for the titration of 5'-GMP with complexes. [complex] 1.3 x 10^{-4} M, [5'-GMP]=0-0.33x10^{-4} M*

The gradual addition of 5′-GMP/5′-TMP from (0-0.50x10^{-4}M) to the metal complexes leads to significant "hyperchromic effect" and strong perturbations in absorption peak of complexes (Figure 59,60).

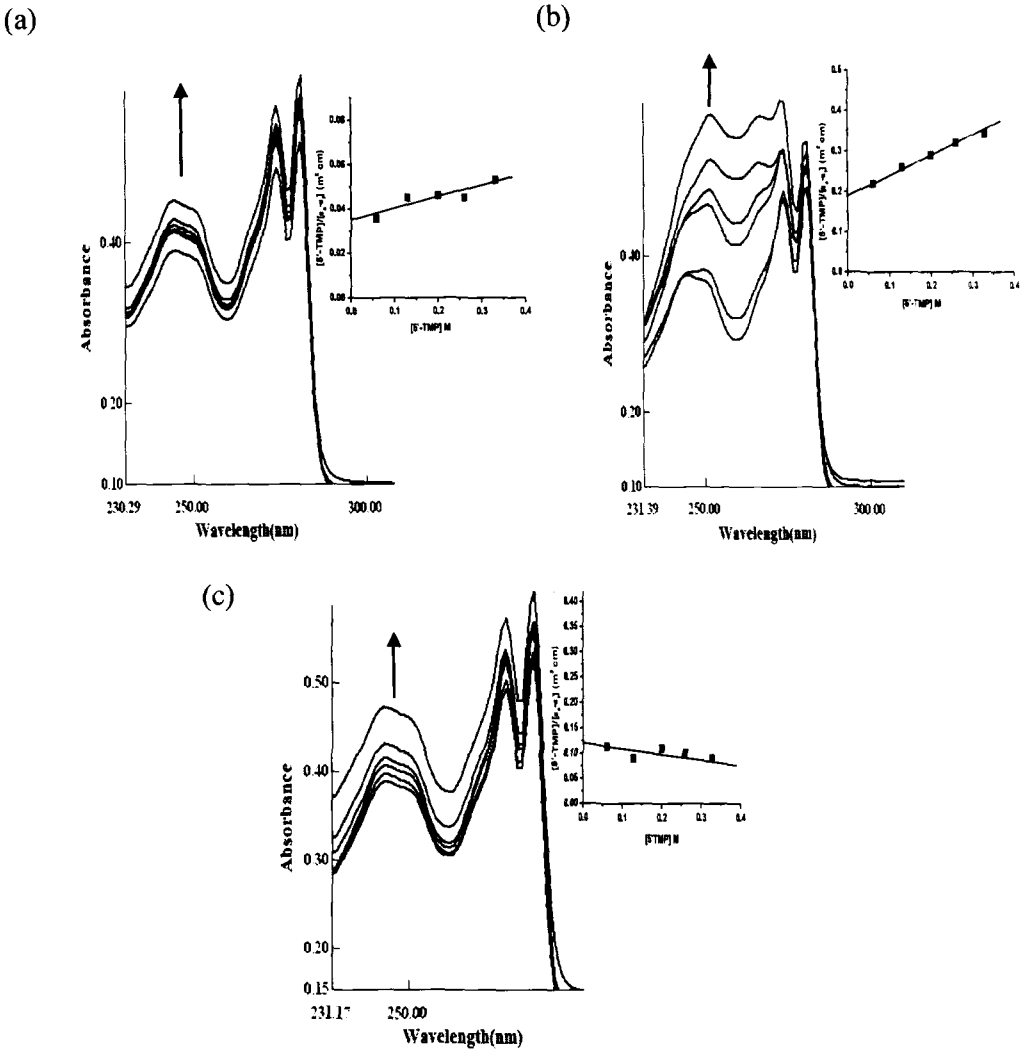

Figure 60. *Absorption spectral traces of complexes* (a) *$[C_{18}H_{19}N_4O_2SnCl]$ (b) $[C_{28}H_{23}N_4O_2SnCl]$ (c) $[C_{52}H_{42}N_4O_2Sn_2]$ upon addition of 5'-TMP. [Complex] = 1.3 x 10^{-4} M, [5'-TMP]=0-0.33x10^{-4}. Inset: Plots of [5'-TMP]/$|\varepsilon_a-\varepsilon_f|$ vs [5'-TMP] for the titration of 5'-TMP with complexes. [Complex] 1.3 x 10^{-4} M, [5'-TMP] 0-0.50x10^{-4} M*

As evident from above absorption titration, both the electrostatic binding as well as steric effects play an eminent role in the determining the binding potential of these analogous complexes with DNA, so the binding of the complexes $[C_{18}H_{19}N_4O_2SnCl]$, $[C_{28}H_{23}N_4O_2SnCl]$ and $[C_{52}H_{42}N_4O_2Sn_2]$ towards nucleotides is also governed by these interactions. The "hyperchromic effect" in the absorption

spectra of the complexes indicates an electrostatic outside binding of the complexes with nucleotides owing to the presence of tin(IV) moiety which exerts predominate phosphate binding of the complexes with nucleotide.

Moreover, as observed from the binding constant data given in Table 12, the interaction of complexes $[C_{18}H_{19}N_4O_2SnCl]$, $[C_{28}H_{23}N_4O_2SnCl]$ and $[C_{52}H_{42}N_4O_2Sn_2]$ with 5′-GMP produces more pronounced changes in the absorption spectra as compared to 5′-TMP showing a clear preference of binding of the complexes with 5′-GMP compared to 5′-TMP (Figure 59,60).

Table 12. *The comparative binding constant (K_b) values of complexes $[C_{18}H_{19}N_4O_2SnCl]$, $[C_{28}H_{23}N_4O_2SnCl]$, $[C_{52}H_{42}N_4O_2Sn_2]$ with the 5′-GMP and 5′-TMP (mean standard deviation of ± 0.07).*

Complex	5′-GMP ($x10^4$)	5′-TMP ($x10^4$)	Monitored at (nm)	% Hyperchromism
$[C_{18}H_{19}N_4O_2SnCl]$	3.03	0.40	246	36
$[C_{28}H_{23}N_4O_2SnCl]$	4.80	1.51	246	48
$[C_{52}H_{42}N_4O_2Sn_2]$	0.28	0.16	246	23

^1H and ^{31}P NMR interaction with 5′-GMP

To further understand the selectivity of the complex $[C_{28}H_{23}N_4O_2SnCl]$ owing to its stronger binding with the CT-DNA and to the strong perturbations induced in the absorption spectra when treated with nucleotide 5′-GMP, we have carried out ^1H and ^{31}P NMR interaction of the complex with 5′-GMP. The ^1H NMR spectrum of the 5′-GMP after addition of the complex $[C_{28}H_{23}N_4O_2SnCl]$ shows no significant chemical shift differences as depicted in Figure 61.

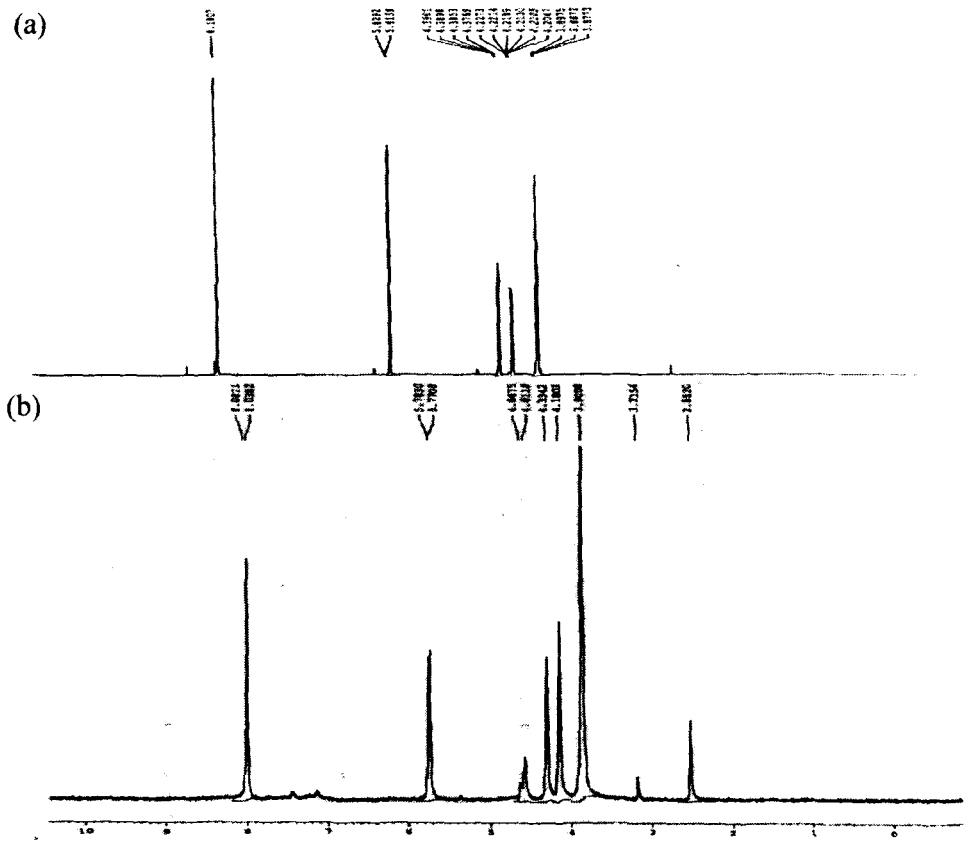

Figure 61. *^1H NMR spectra of (a) 5'-GMP alone and (b) the reaction of complex $[C_{28}H_{23}N_4O_2SnCl]$ (2.5 mmol) with 5'-GMP (5 mmol) at 25 °C.*

The absence of such shift of H8 signal suggests non-involvement of the nucleobase in complex binding thus, precluding the base specific interactions with the complex. Slight shift of free ribose protons of 5'-GMP after interaction with complex $[C_{28}H_{23}N_4O_2SnCl]$ from 5.8-3.8 ppm to 5.7-3.9 ppm indicate the binding of the tin(IV) complex through O_2' and O_3' atoms of the sugar moiety owing to its high affinity for the backbone binding. Thus, the ^1H NMR studies indicates an electrostatic binding mode of complex $[C_{28}H_{23}N_4O_2SnCl]$ with 5'-GMP.

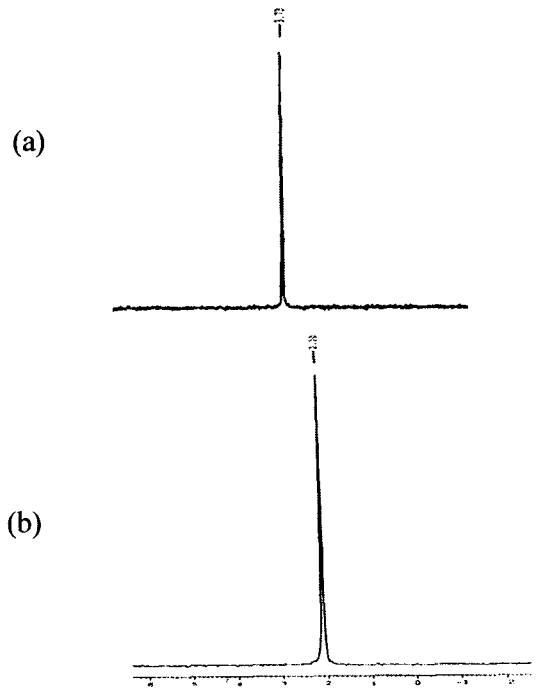

Figure 62. *^{31}P NMR spectra of (a) 5'-GMP and (b) the reaction of complex [$C_{28}H_{23}N_4O_2SnCl$] (2.5 mmol) with 5'-GMP (5 mmol) at 25^0C.*

Additional evidence for the selective and specific binding of tin(IV) complex with the phosphate group of 5'-GMP was provided by ^{31}P NMR (Figure 62). There is significant upfield shift of the ^{31}P signal of free 5'-GMP from 3.73 to 2.10 ppm which corresponds to a strong binding exhibited by the complex [$C_{28}H_{23}N_4O_2SnCl$] to the phosphate group of the mononucleotide [214]. These observations provide a definitive affirmation of phosphate selectivity of complex with biomolecules (CT-DNA and 5'-GMP).

Fluorescence studies

In the absence of DNA, complex [$C_{18}H_{19}N_4O_2SnCl$], [$C_{28}H_{23}N_4O_2SnCl$] and [$C_{52}H_{42}N_4O_2Sn_2$] emit weak luminescence in Tris-HCl buffer at ambient temperature, with a fluorescence maximum centered at 710 nm when excited with a

wavelength of 354 nm as depicted in Figure 63. Upon increasing DNA from 0–$0.50x10^{-4}$ M, the enhancement in the emission intensity was observed. This observed enhancement in the emission intensity results from shielding effect of these complexes as a consequence of their unspecific binding to the low affinity outer sphere of DNA polyanionic phosphate backbone. However, another possibility envisioned for such an increase is the effective shielding of these outer sphere complexes to the metal complexes intercalated inside the DNA pockets [239]. Generally there is interplay between electrostatic and hydrophobic interactions: even in systems in which intercalation is evident. The degree to which hydrophobic interactions predominate over electrostatic is likely to be dictated by structural, geometric, and charge considerations for the binding molecule. Since, the complex $[C_{28}H_{23}N_4O_2SnCl]$ displays structural variability as compared to $[C_{18}H_{19}N_4O_2SnCl]$ and $[C_{52}H_{42}N_4O_2Sn_2]$, the partial-intercalative hydrophobic interaction along with electrostatic binding predominates for the complex. The propensity to CT-DNA of the complexes follows the order $[C_{28}H_{23}N_4O_2SnCl]$ > $[C_{18}H_{19}N_4O_2SnCl]$ > $[C_{52}H_{42}N_4O_2Sn_2]$. The binding constant K values gave similar trend of the DNA binding propensity as observed in case of absorption spectral studies (Table 13).

Table 13. *Emission properties of complexes $[C_{18}H_{19}N_4O_2SnCl]$, $[C_{28}H_{23}N_4O_2SnCl]$, $[C_{52}H_{42}N_4O_2Sn_2]$ bound to CT-DNA (mean average deviation of ± 0.02).*

Complex	Emission (nm)	Excitation (nm)	Monitored At (nm)	$K(M^{-1})$
$[C_{18}H_{19}N_4O_2SnCl]$	442	354	710	$2.0x10^4$
$[C_{28}H_{23}N_4O_2SnCl]$	446	354	710	$4.3x10^4$
$[C_{52}H_{42}N_4O_2Sn_2]$	442	354	710	$1.4x10^4$

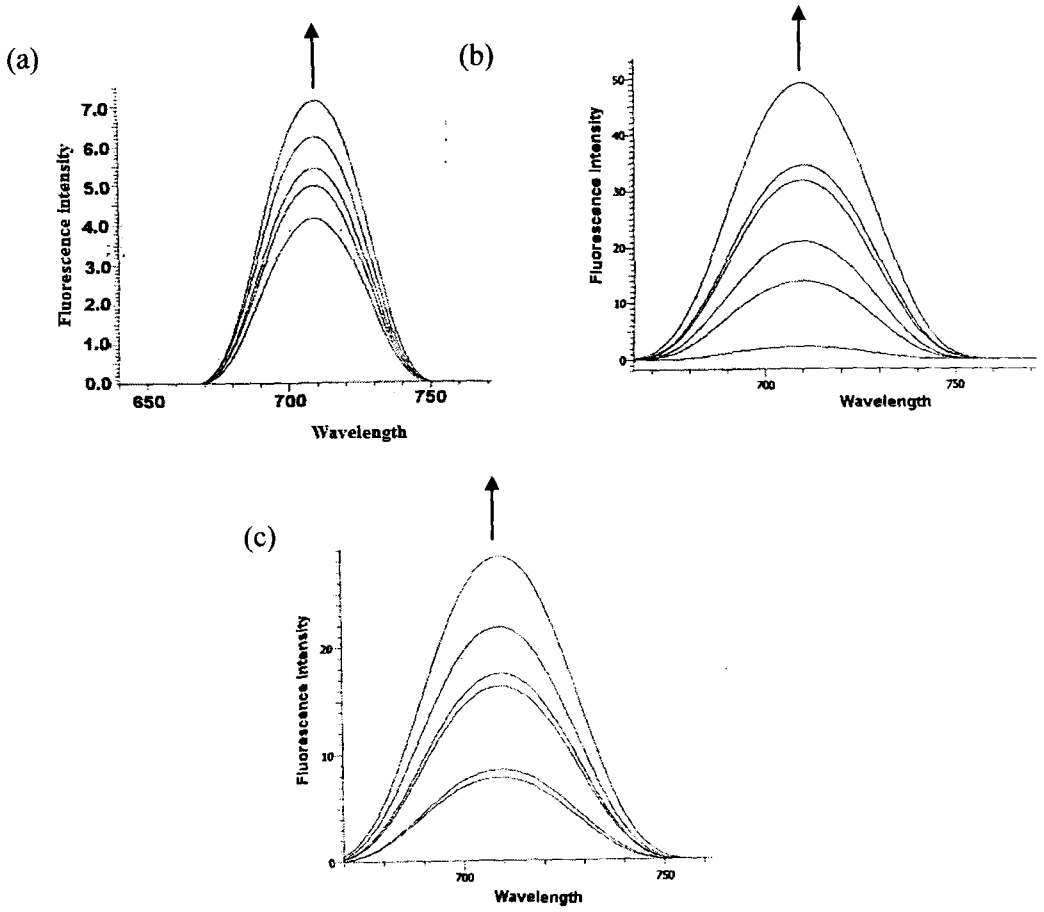

Figure 63. *Emission spectra of complexes* (a) *[$C_{18}H_{19}N_4O_2SnCl$] (b) [$C_{28}H_{23}N_4O_2SnCl$] (c) [$C_{52}H_{42}N_4O_2Sn_2$] in Tris–HCl buffer (pH = 7.2) in the absence and presence of CT-DNA. [Complex]=1.3x10^{-4} M, [DNA] = 0–0.50x10^{-4} M. Arrows indicate the change in emission intensity upon increasing the DNA concentration.*

Steady-state emission quenching experiments were performed by using anionic quencher which has been found to be able to distinguish between the binding modes of the complex with DNA [240,241]. Upon addition increasing CT-DNA, the quenching of the fluorescence intensity was observed for the complexes [$C_{18}H_{19}N_4O_2SnCl$], [$C_{28}H_{23}N_4O_2SnCl$] and [$C_{52}H_{42}N_4O_2Sn_2$].

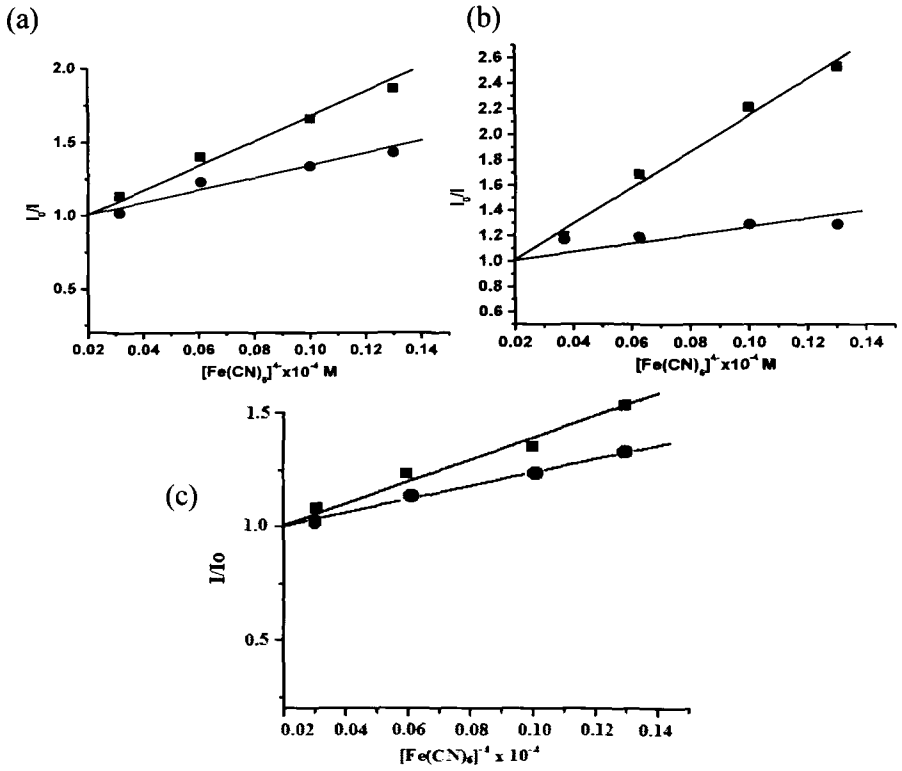

Figure 64. *Emission quenching curves of (a) $[C_{18}H_{19}N_4O_2SnCl]$ (b) $[C_{28}H_{23}N_4O_2SnCl]$ (c) $[C_{52}H_{42}N_4O_2Sn_2]$ in the absence of CT-DNA (■) and in the presence of CT-DNA (●). [Complex] = 1.3 x 10^{-4} M.*

It is speculated that intercalated chromophores are less accessible to quenching by quencher due to electrostatic repulsion between the highly negatively charged DNA and anionic quencher [242] whereas compounds which are bound at the DNA surface (groove binding or electrostatic binding) are more accessible and therefore, the emission from these molecules can be quenched more efficiently. The fluorescence-quenching plots of DNA-bound quencher by complexes $[C_{18}H_{19}N_4O_2SnCl]$, $[C_{28}H_{23}N_4O_2SnCl]$ and $[C_{52}H_{42}N_4O_2Sn_2]$ are shown in Figure 64 which illustrate that quenching phenomena of DNA bound $[Fe(CN)_6]^{4-}$ by complexes $[C_{18}H_{19}N_4O_2SnCl]$, $[C_{28}H_{23}N_4O_2SnCl]$ and $[C_{52}H_{42}N_4O_2Sn_2]$ are in good agreement

with the linear Stern–Volmer equation.However, in presence of DNA the slope of the plot of was remarkably decreased as shown in Table 14. These results corroborate well with the observations of absorption titrations indicating that the complex $[C_{28}H_{23}N_4O_2SnCl]$ bind with higher affinity towards DNA as compared to other complexes $[C_{18}H_{19}N_4O_2SnCl]$ and $[C_{52}H_{42}N_4O_2Sn_2]$ (Figure 64) predominantly via, electrostatic interactions. (Table 14).

Table 14. *Emission quenching of CT-DNA bound* $[Fe(CN)_6]^{4-}$ *by complexes* $[C_{18}H_{19}N_4O_2SnCl]$, $[C_{28}H_{23}N_4O_2SnCl]$ *and* $[C_{52}H_{42}N_4O_2Sn_2]$*(mean average deviation of* ± 0.02*).*

Complex	Emission (nm)	Excitation (nm)	Monitored at (nm)	K_{sv1}	K_{sv2}
$[C_{18}H_{19}N_4O_2SnCl]$	442	354	710	$2.57x10^4$	$1.28x10^4$
$[C_{28}H_{23}N_4O_2SnCl]$	446	354	710	$1.00x10^4$	$5.70x10^4$
$[C_{52}H_{42}N_4O_2Sn_2]$	442	354	710	$3.14x10^4$	$1.42x10^4$

Effect of ionic strength

In order to validate the probable binding mode between the molecule and DNA, fluorescence titrations were carried out under the conditions of increasing ionic strength ($0\text{-}0.50x10^{-4}$ M) through added amounts of NaCl. As shown in Figure 65, the fluorescence intensity of the studied complexes was appreciably quenched with increasing ionic strength [184,185]. This change in CT-DNA is in favour of the electrostatic binding between complexes $[C_{18}H_{19}N_4O_2SnCl]$, $[C_{28}H_{23}N_4O_2SnCl]$, $[C_{52}H_{42}N_4O_2Sn_2]$ and CT-DNA. As evident from Figure 65(a-c), the effect of salt concentration on complex $[C_{28}H_{23}N_4O_2SnCl]$-DNA system was more pronounced in case of $[C_{28}H_{23}N_4O_2SnCl]$ than the other complexes $[C_{18}H_{19}N_4O_2SnCl]$ and

$[C_{52}H_{42}N_4O_2Sn_2]$ so, the complex $[C_{28}H_{23}N_4O_2SnCl]$ reveals a greater potency for DNA binding.

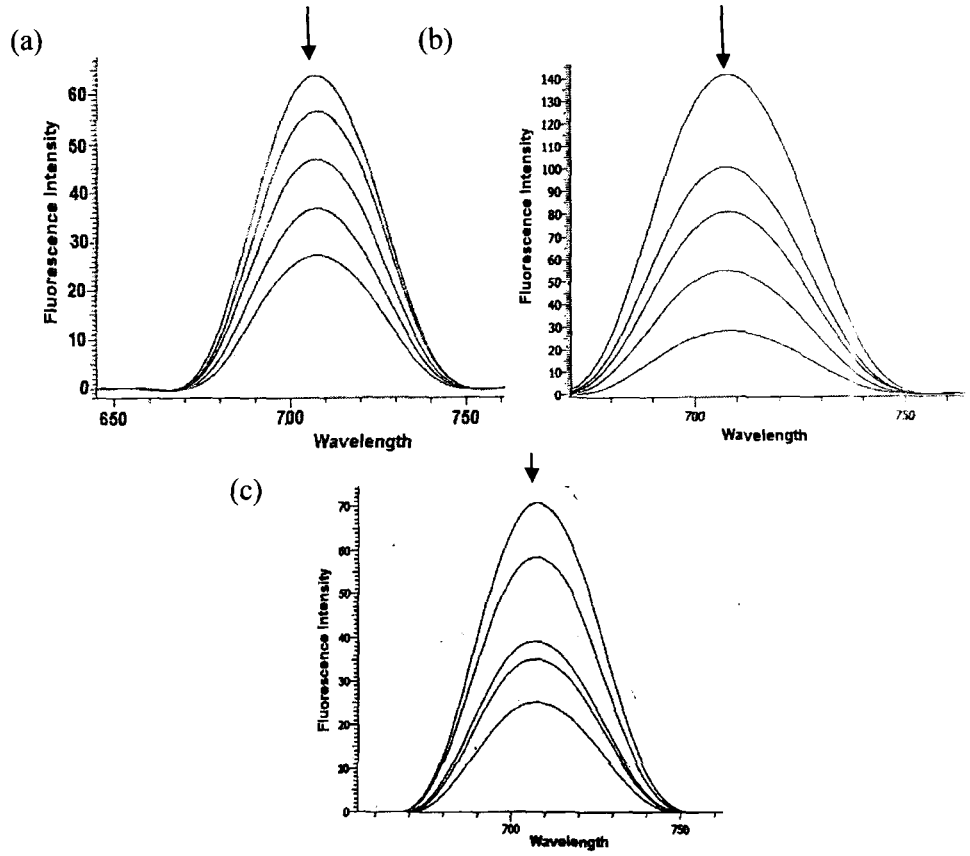

Figure 65. *Effect of different concentration of NaCl on the fluorescence spectra of (a) complexes $[C_{18}H_{19}N_4O_2SnCl]$ (b) $[C_{28}H_{23}N_4O_2SnCl]$ (c) $[C_{52}H_{42}N_4O_2Sn_2]$ where [Complex]=1.3x10^{-4} M with [DNA]=1.0x10^{-4} M. Arrow indicate the gradual decrease of emission intensity as a function of NaCl concentration.*

Effect of phosphate group

It could be seen from the Figure 66(a-c) that fluorescence intensity of all the complexes increases with increase in the K_2HPO_4 concentration. This observation provides supportive evidence for electrostatic interaction of the complexes binding preferentially to the phosphate group of DNA double helix.

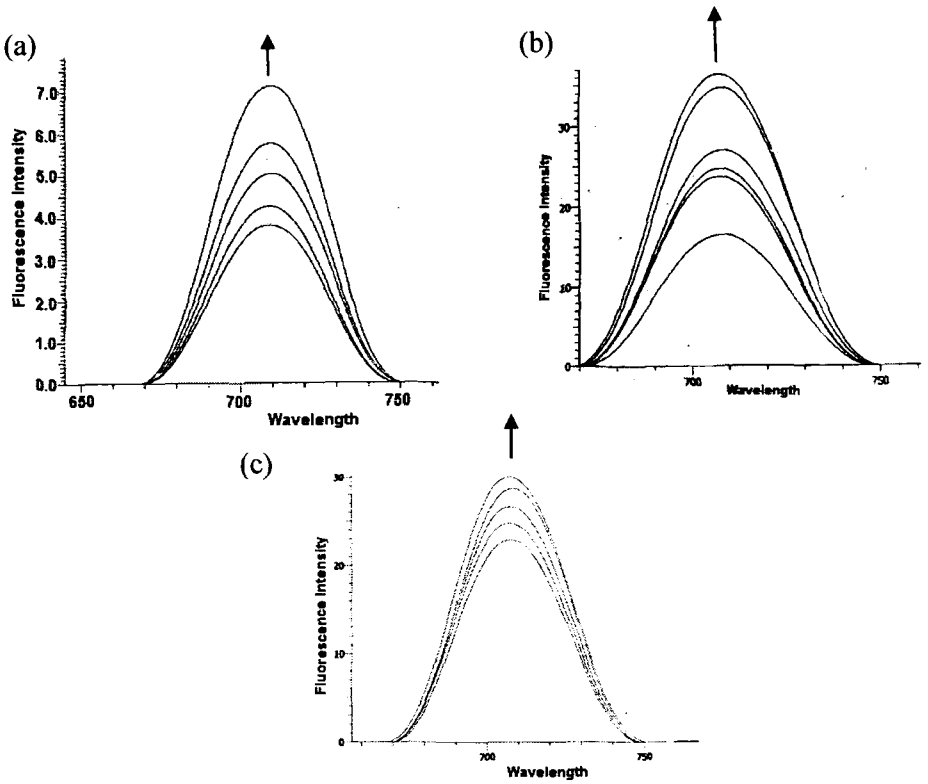

Figure 66. *Effect of increasing concentration of K_2HPO_4 on the fluorescence intensity of the complexes (a) $[C_{18}H_{19}N_4O_2SnCl]$ (b) $[C_{28}H_{23}N_4O_2SnCl]$ (c) $[C_{52}H_{42}N_4O_2Sn_2]$. [Complex]=1.0x10^{-4} M with [CT-DNA]=1.20x10^{-4} M. Arrow indicate the gradual decrease of emission intensity as a function of K_2HPO_4 concentration.*

The spectra depicts that the interaction of complex $[C_{28}H_{23}N_4O_2SnCl]$ is relatively strong than complexes $[C_{18}H_{19}N_4O_2SnCl]$ and $[C_{52}H_{42}N_4O_2Sn_2]$ which is consistent with the absorption spectral studies.

Circular dichroic studies

The circular dichroism pattern observed for CT-DNA provide further and definitive confirmation of the probable mode of CT-DNA binding of complexes $[C_{18}H_{19}N_4O_2SnCl]$, $[C_{28}H_{23}N_4O_2SnCl]$ and $[C_{52}H_{42}N_4O_2Sn_2]$ which is depicted by the perturbation induced in the DNA morphology upon the binding of complexes to CT-DNA (Figure 67a-c). The two bands of CT-DNA are a net result of exciton

coupling interaction of bases which depend on the skewed orientation on the CT-DNA backbone [243]. On incubation of the complexes with CT-DNA. moderate changes in both the positive and negative bands of CT-DNA were observed as shown in Figure 67(a-c).

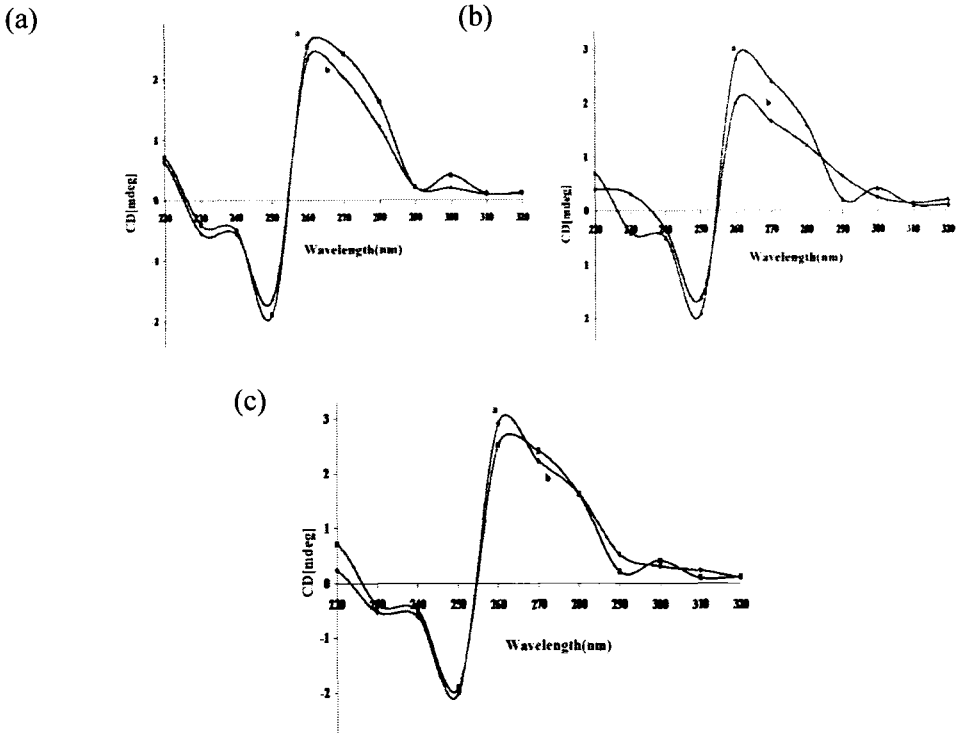

Figure 67. *CD spectra of (a) CT-DNA alone (b) CT-DNA in presence of metal complexes* $[C_{18}H_{19}N_4O_2SnCl]$, $[C_{28}H_{23}N_4O_2SnCl]$, $[C_{52}H_{42}N_4O_2Sn_2]$, *respectively, in Tris-HCl buffer at 25* ^0C. *[Complex] =* $1.0x10^{-4}$ *M, [DNA]=*$1.20x10^{-4}M$

The multifaceted binding mode observed for complex $[C_{28}H_{23}N_4O_2SnCl]$ promotes its higher binding towards the DNA such that effective screening of the negative charge on the N7 base site as well as phosphate oxygen, simultaneously along the phosphate backbone is observed which support a transconformational change [244] of the DNA double helical conformation. It has been speculated that the electrostatic components of interactions are effective in bringing about such transconformational

changes. Further transformation of the DNA structure proceeds by removal of labile groups attached in the complexes which removes the water from the base sites and grooves of DNA helix resulting in effective binding of the complex to DNA. The CD spectrum of DNA shows a significant decrease in intensity of positive band upon addition of the complex [$C_{28}H_{23}N_4O_2SnCl$] which reveal a right handed conformational change of the DNA double helix possibly due to its partial intercalative binding of the complex. In contrast, the complexes [$C_{18}H_{19}N_4O_2SnCl$] and [$C_{52}H_{42}N_4O_2Sn_2$] {Figure 67(a and c)} exhibit less pronounced CD spectral changes in the positive ellipticity band. However, on addition of the complexes, no appreciable change in the negative helicity band of CT-DNA was observed for all the complexes. The observation is in accordance with the above spectroscopic studies revealing avid binding of complex [$C_{28}H_{23}N_4O_2SnCl$] as compared to complexes [$C_{18}H_{19}N_4O_2SnCl$] and [$C_{52}H_{42}N_4O_2Sn_2$].

Viscosity studies

The relative viscosity of CT-DNA ($1.20x10^{-4}$ M) in presence of varying amounts of complexes [$C_{18}H_{19}N_4O_2SnCl$], [$C_{28}H_{23}N_4O_2SnCl$] and [$C_{52}H_{42}N_4O_2Sn_2$] in the [complex]/[DNA] (r) ratio of 0.00–0.40 with an interval of 0.1 are shown in Figure 68(a-c). Complex [$C_{28}H_{23}N_4O_2SnCl$] interacts with the CT-DNA more strongly and deeply than other complexes [$C_{18}H_{19}N_4O_2SnCl$] and [$C_{52}H_{42}N_4O_2Sn_2$], leading to the greater decrease in viscosity of the DNA with an increasing value of r = 0.00-0.20 followed by a substantial increase in the viscosity of the CT-DNA from r=0.20-0.40.

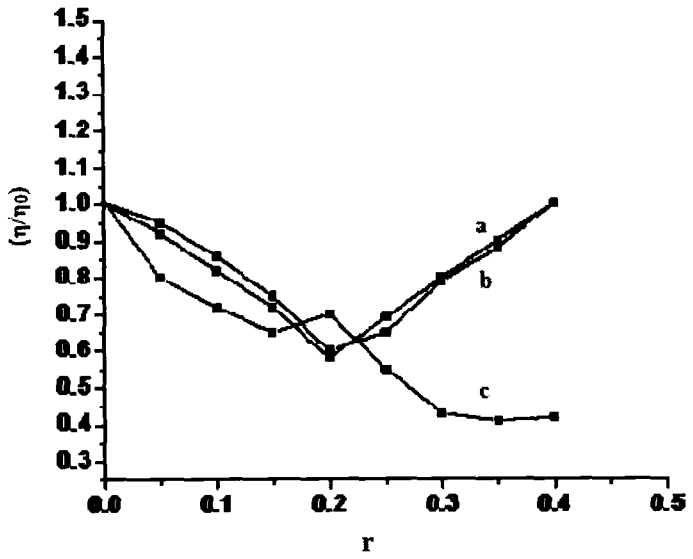

Figure 68. *Effect of increasing amount of complexes (a) $[C_{28}H_{23}N_4O_2SnCl]$ (b) $[C_{18}H_{19}N_4O_2SnCl]$ (c) $[C_{52}H_{42}N_4O_2Sn_2]$ on the relative viscosity of CT-DNA [DNA]=1.20x10^{-4} M, [Complex]=1.0x10^{-4} M*

Firstly, the initial decrease in the relative viscosity of CT-DNA indicate non-intercalative interaction presumably electrostatic interactions of the complexes with DNA which would produce bends or kinks in the DNA strand and hence, diminish its effective length along with its viscosity. Secondly, when the r ratios were increased from 0.20 to 0.40, rapidly increasing viscosity was observed which indicates the partial intercalative binding mode of the complexes and supports an electrostatic binding mode together with some partial intercalative interactions for the complexes $[C_{28}H_{23}N_4O_2SnCl]$ and $[C_{18}H_{19}N_4O_2SnCl]$ [142]. However, the higher reduction at r = 0.00–0.20 and the higher enhancement at r = 0.20–0.40 in the DNA viscosity for complex $[C_{28}H_{23}N_4O_2SnCl]$ compared to $[C_{18}H_{19}N_4O_2SnCl]$ recommends that former complex reveals a greater DNA binding potential than the

latter. However, in contrast to this observation, there is a gradual decrease in the viscosity of DNA on addition of complex [$C_{52}H_{42}N_4O_2Sn_2$] supporting only an electrostatic association of the complex towards CT-DNA. These results obtained from viscosity studies are consistent with those obtained from above spectroscopic studies.

Conclusions

In this report, we have attempted to unravel the binding behaviour of the complexes $[C_{18}H_{19}N_4O_2SnCl]$, $[C_{28}H_{23}N_4O_2SnCl]$ and $[C_{52}H_{42}N_4O_2Sn_2]$ with CT-DNA by employing various spectroscopic and biophysical methods. The results suggest a multifaceted mode of binding of the complexes $[C_{18}H_{19}N_4O_2SnCl]$, $[C_{28}H_{23}N_4O_2SnCl]$ with CT-DNA i.e. electrostatic binding mode in addition to partial intercalative interactions owing to the presence of planar architectures within the molecule as evidenced by absorption titrations and fluorescence studies. The complex $[C_{28}H_{23}N_4O_2SnCl]$ ($K_b=3.47x10^4 \pm 0.04\ M^{-1}$) binds to CT-DNA more strongly than complexes $[C_{18}H_{19}N_4O_2SnCl]$ ($K_b=2.16x10^4 \pm 0.04\ M^{-1}$) and $[C_{52}H_{42}N_4O_2Sn_2]$ ($K_b=4.60x10^3 \pm 0.04\ M^{-1}$). Further studies of the complexes $[C_{18}H_{19}N_4O_2SnCl]$, $[C_{28}H_{23}N_4O_2SnCl]$ and $[C_{52}H_{42}N_4O_2Sn_2]$ with mononucleotides 5′-GMP and 5′-TMP by employing UV-visible absorption titrations as well as ^1H and ^{31}P NMR lends a strong affirmation of electrostatic interaction of complexes with biomolecules. The CD spectra reveal higher perturbations in DNA helical conformation for complex $[C_{28}H_{23}N_4O_2SnCl]$ as compared to other complexes $[C_{18}H_{19}N_4O_2SnCl]$ and $[C_{52}H_{42}N_4O_2Sn_2]$ suggestive of its higher binding affinity with DNA leading to strong conformational changes in the double helical structure of CT-DNA. The above DNA binding results were in agreement with viscometric studies which supports to two probable mode of association of the complexes $[C_{18}H_{19}N_4O_2SnCl]$ and $[C_{28}H_{23}N_4O_2SnCl]$ with DNA viz; electrostatic together with some partial intercalative interactions. While the complex $[C_{52}H_{42}N_4O_2Sn_2]$ only binds via an electrostatic interaction with DNA.

CHAPTER VI

Synthesis of new chiral heterocyclic Schiff base modulated Cu(II)/Zn(II) complexes: their comparative binding studies with CT-DNA and mononucleotides (5′-GMP, 5′-TMP, 5′-AMP, 5′-CMP) and cleavage activity.

Synthesis of Ligand

$[C_{18}H_{16}N_2O_3]$

To a methanolic solution of 2-amino-3-formylchromone (1.89g, 10mmol), a solution of (R)-2-amino-2-phenylethanol (1.37g, 10mmol) was added dropwise with continuous stirring. After refluxing the above solution for 2 h on rotamantle (80 °C), the solution was allowed to stand at room temperature overnight. until a yellow precipitate was separated out after the slow evaporation of the solvent. The precipitate, thus obtained, was then washed thoroughly with hexane and diethyl ether and dried *in vacuo* (Scheme 9).

Yield 78%. m.p. 142 ± 2 °C. Anal. (%) Calc. for $[C_{18}H_{16}N_2O_3]$: C, 70.12; H, 5.23; N, 9.09: Found: C, 70.15; H, 5.22; N, 9.08. $[\alpha]^{25}_D$ = -110. ESI-MS (m/z) 309 $[C_{18}H_{16}N_2O_3+H]^+$.

Selected IR data on KBr pellet (ν/cm^{-1}): 1611 ν(C=N); 1654 ν(C=O); 757 ν(Ar). UV-vis. in Methanol [λ_{max}/nm]: 206, 247, 267, 310. ^{1}H NMR (DMSO-d_6, ppm): 8.8 (-CH=N); 2.5(OH); 7.2-7.6 (aromatic-H); 4.3(chiral-CH); 3.3-3.7 (CH_2-O). ^{13}C NMR (DMSO-d_6, ppm): 174 (C=O), 164 (C=N); 116-132 (Ar-C); 76 (C-O); 67 (C-N).

Synthesis of complexes

$[C_{36}H_{34}N_4O_7Cu](NO_3)_2$

The complex $[C_{36}H_{34}N_4O_7Cu](NO_3)_2$ was prepared in a moderate yield from the reaction of $Cu(NO_3)_2.3H_2O$ with the prepared ligand in 1:2 molar ratio. The ligand $[C_{18}H_{16}N_2O_3]$ (0.61g, 2mmol) dissolved in methanol was added slowly to a

methanolic solution of $Cu(NO_3)_2.3H_2O$ (0.24g, 1mmol) with continuous stirring which was followed by change in the colour of solution to intense green. After stirring for 24 h at room temperature, a green precipitate obtained was separated out. This precipitate was then washed with hexane and dried *in vacuo* (Scheme 10).

Yield 69%. m.p. 279 ± 2 °C. Anal. (%) Calc. for $[C_{36}H_{34}N_6O_{13}Cu]$: C, 52.59; H, 4.13; N, 10.22: Found: C, 52.58; H, 4.12; N, 10.23. $[\alpha]^{25}_D$ = -110. Molar conductance, $\wedge_M$ (1 x 10^{-3} M, Methanol): 210 $\Omega^{-1}cm^2 mol^{-1}$ (1:2 electrolyte).

Selected IR data on KBr pellet (ν/cm^{-1}): 1559 (C=N); 1384 (NO_3); 579 (Cu-O); 452 (Cu-N). UV-vis in Methanol [λ_{max}/nm]: 246, 302, 419, 564. ESI-MS (m/z) 698 $[C_{36}H_{32}N_4O_7Cu]^+$.

$[C_{36}H_{32}N_4O_6Zn](NO_3)_2$

The complex $[C_{36}H_{32}N_4O_6Zn](NO_3)_2$ was synthesized by employing same procedure as described above for $[C_{36}H_{34}N_4O_7Cu](NO_3)_2$ with ligand $[C_{18}H_{16}N_2O_3]$ (0.61g, 2mmol) and $Zn(NO_3)_2.6H_2O$ (0.29g, 1mmol).

Yield 72%. m.p. < 300 °C (decompose). Anal. (%) Calc. for $[C_{36}H_{32}N_6O_{12}Zn]$: C, 53.64; H, 4.00; N, 10.43: Found: C, 53.65; H, 4.01; N, 10.46. $[\alpha]^{25}_D$ = -47. Molar conductance, $\wedge_M$ (1 x 10^{-3} M, methanol): 189 $\Omega^{-1}cm^2 mol^{-1}$ (1:2 electrolyte).

Selected IR data on KBr pellet (ν/cm^{-1}): 1579 (C=N); 1388, (NO_3); 555 (Zn-O); 420 (Zn-N). UV-vis in Methanol [λ_{max} / nm]: 245, 302, 420. ^1H NMR (DMSO-d_6, ppm): 8.29(-CH=N); 2.58(-OH); 7.54-7.81 (aromatic-H); 3.86(chiral-CH); 3.20-3.30(CH_2-O). ^{13}C NMR (DMSO-d_6, ppm): 175 (C=O), 168 (C=N); 115-133 (Ar-C); 72 (C-O); 67(C-N). ESI-MS (m/z) 682 $[C_{36}H_{32}N_4O_6Zn]^+$.

Scheme 9.

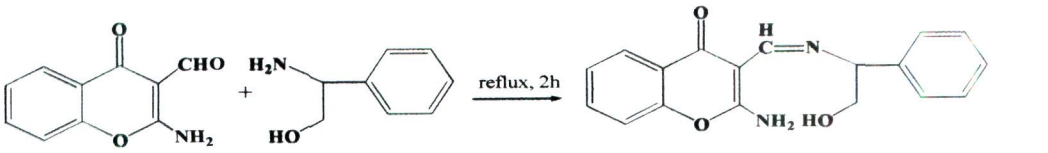

2-amino-3-formylchromone + **(R)-2-amino-2-phenylethanol** → **2-amino-3-((2-hydroxy-1-phenylethylimino)methyl)-4*H*-chromen-4-one**

Ligand $[C_{18}H_{16}N_2O_3]$

Scheme 10.

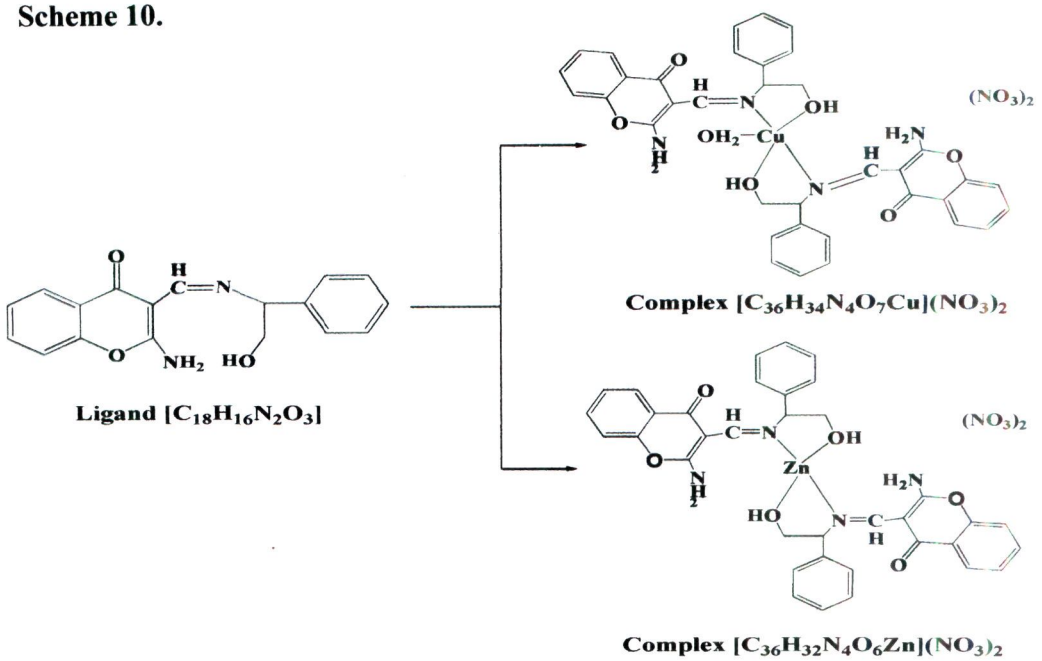

Ligand $[C_{18}H_{16}N_2O_3]$

Complex $[C_{36}H_{34}N_4O_7Cu](NO_3)_2$

Complex $[C_{36}H_{32}N_4O_6Zn](NO_3)_2$

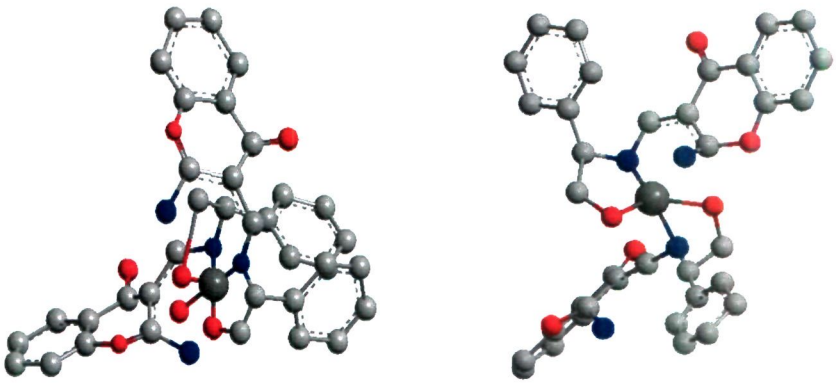

Figure 69. *Cylindrical bonded three dimensional model of complexes (a)$[C_{36}H_{34}N_6O_{13}Cu](NO_3)_2$ (b)$[C_{36}H_{32}N_4O_{12}Zn](NO_3)_2$. Color scheme: copper(II) dark gray; N dark blue; O red; C gray. The H atoms and are omitted for clarity*

Results and discussion

Synthesis and characterization

The ligands were derived from the condensation reaction of 2-amino-3-formylchromone with (R)-2-amino-2-phenylethanol in 1:1 stoichiometric ratio. The subsequent complexation of the ligand $[C_{18}H_{16}N_2O_3]$ with metal salts $Cu(NO_3)_2.3H_2O$ and $Zn(NO_3)_2.6H_2O$ in 2:1 molar ratio achieved the desired complex in moderate yields as depicted in Scheme 9. The structural characteristics of both ligand $[C_{18}H_{16}N_2O_3]$ and complexes $[C_{36}H_{34}N_6O_7Cu](NO_3)_2$. $[C_{36}H_{32}N_4O_6Zn](NO_3)_2$ were elucidated by employing elemental analysis, UV-vis., IR, EPR, ^1H NMR and ^{13}C NMR spectral studies. Both the complexes are air stable and readily soluble in common organic solvents such as methanol, ethanol, DMSO, DMF, THF. The molar conductivity of the complexes in methanol was in the range 210-189 $\Omega^{-1}cm^2\,mol^{-1}$, which is in conformity for 1:2 electrolytic nature.

IR spectral studies

The comparative IR spectra of the ligand $[C_{18}H_{16}N_2O_3]$ and complexes $[C_{36}H_{34}N_4O_7Cu](NO_3)_2$ and $[C_{36}H_{32}N_4O_6Zn](NO_3)_2$ give intricate details about the binding behaviour of the ligand with metal ions. In free ligand a strong ν(C=N) band at 1611 cm^{-1} gives strong indication of the formation of the Schiff base [245]. However, a relative decrease of ν(C=N) frequency to 1559-1579 cm^{-1} supports the coordination of imine nitrogen atom with metal ion in complexes. Besides, a ν(OH) band at 3420 cm^{-1} was also observed in copper(II) complex $[C_{36}H_{34}N_4O_7Cu](NO_3)_2$ owing to the presence of coordinated water molecule [246]. The presence of nitrate

group in complexes $[C_{36}H_{34}N_4O_7Cu](NO_3)_2$ and $[C_{36}H_{32}N_4O_6Zn](NO_3)_2$ was ascertained by the existence of characteristic $\nu(NO_3)$ frequency at 1384-1388 cm^{-1} [247]. Additional support for the formation of the complexes was provided by the existence of medium intensity bands in the region 579-555 cm^{-1} and 452-420 cm^{-1} assigned to ν(M-O) and ν(M-N) ,respectively [248,249].

Electronic spectra

For complexes $[C_{36}H_{34}N_4O_7Cu](NO_3)_2$ and $[C_{36}H_{32}N_4O_6Zn](NO_3)_2$, three absorption bands with varied intensity were observed in the high energy UV region at ~246 and ~303 nm corresponding to IL transitions of the ligand. While a band centered at 420 nm was observed in both the complexes $[C_{36}H_{34}N_4O_7Cu](NO_3)_2$ and $[C_{36}H_{32}N_4O_6Zn](NO_3)_2$ ascribed to ligand to metal charge transfer (LMCT) [250]. Besides, a broad band was also observed in case of $[C_{36}H_{34}N_4O_7Cu](NO_3)_2$ complex at 564 nm, corresponding to the d–d transition band consistent with a square pyramidal geometry of copper(II) ion [251] assigned to d_{xz}, $d_{yz} \leftarrow d_{(x^2-y^2)}$ and $d_{z^2} \leftarrow d_{(x^2-y^2)}$ transitions [252,253] as evidenced further by EPR studies.

EPR spectrum

The solid state X-band EPR spectrum of the polycrystalline copper(II) complex $[C_{36}H_{34}N_4O_7Cu](NO_3)_2$ was recorded in DMSO at LNT with a magnetic field strength of 3000 G. The EPR spectrum of complex $[C_{36}H_{34}N_4O_7Cu](NO_3)_2$ revealed an isotropic spectrum with a broad signal indicating that the copper ion display a distorted square pyramidal geometry with g_{iso} value of ~2.08 [254]. Thus, an unpaired electron of paramagnetic $3d^9$ copper(II) ion occupy $d(x^2-y^2)$ orbital in (B_1g)

ground state configuration with an elongated square based pyramidal geometry (Figure 70).

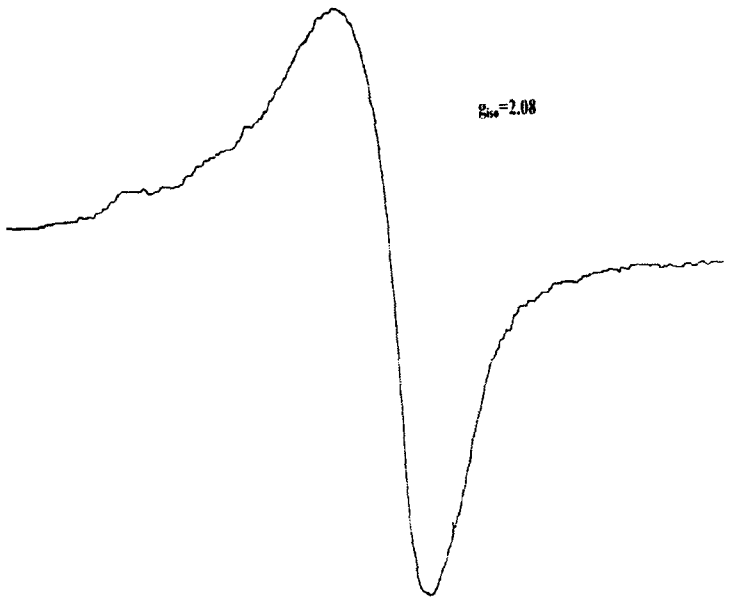

Figure 70. *X-band EPR spectrum of complex* $[C_{36}H_{34}N_6O_7Cu](NO_3)_2$ *at LNT with* g_{iso} *=2.08.*

NMR spectra

The ^1H and ^{13}C NMR spectra of the ligand $[C_{18}H_{16}N_2O_3]$ and its complex $[C_{36}H_{32}N_4O_6Zn](NO_3)_2$ exhibits well resolved signals and exhibit significant differences in their chemical shifts. The ^1H NMR spectrum of the ligand exhibited signal at 8.84 ppm for –CH=N which has been shifted to 8.29 ppm in the zinc(II) complex indicating the involvement of azomethine group in complexation [245]. The persistence of NH_2 protons and OH protons at 9.2 ppm and 2.56 ppm respectively, in both the NMR spectra of the ligand and complex suggest the non-coordination of these groups in the complex [255].

The 13C NMR of the ligand [$C_{18}H_{16}N_2O_3$], display resonance signals at 164 ppm corresponding to C=N group [256]. A slight shift observed in C=N resonance supports its involvement in complexation with the metal ions. However, due to non-involvement of other groups in complexation, their resonances remain unaltered compared to the free ligand.

DNA binding studies

UV-visible absorption studies

The comparative DNA binding profiles of classical cisplatin drug, ligand [$C_{18}H_{16}N_2O_3$] and complexes [$C_{36}H_{34}N_4O_7Cu$]$(NO_3)_2$ and [$C_{36}H_{32}N_4O_6Zn$]$(NO_3)_2$ were elucidated to gain evidence for the probable binding mode of the complexes and ligand. The absorption spectra of ligand and complexes, in presence and in the absence of CT-DNA are shown in Figure 71(a-d). Upon addition of increasing amount of CT-DNA from 0-0.33x10^{-4} M, a significant "hyperchromic" effect in the intraligand bands at 246-303 nm was observed accompanied by a moderate red shift of 2-3 nm, indicative of stabilization of the DNA helix. These spectral characteristic suggest that the complexes and ligand bind either to the external contact (electrostatic binding) or to the major and minor grooves of DNA. Moreover, this "hyperchromic effect" can be explained on the basis of two phenomena. Firstly, the large surface area of the ligand as well as presence of planar aromatic chromophore facilitates a strong binding interaction of the complexes with CT-DNA thereby, providing ample opportunity for the complex to bind with the CT-DNA via, partial insertion of the aromatic moiety in between the stacking base pair. The binding interaction between the cationic complex and CT-DNA leads to diffusion-limited

ion-pair formation at higher concentration of the complex such that the complex is fitted along the contour of DNA double helix in an induced-fit fashion. Thus, the complexes preferably bind to the DNA helix via, groove binding interactions.

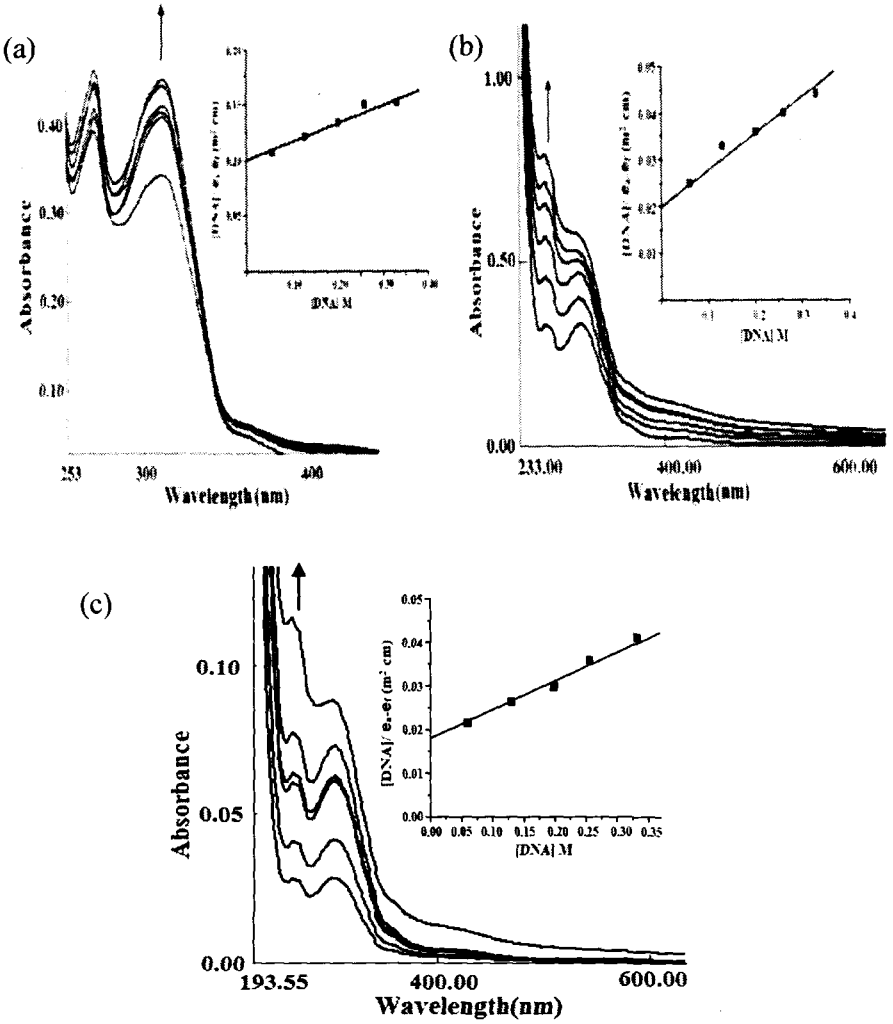

Figure 71. *Absorption spectral traces of (a) Ligand $[C_{18}H_{16}N_2O_3]$ (b) complex $[C_{36}H_{34}N_4O_7Cu](NO_3)_2$ (c) complex $[C_{36}H_{32}N_4O_6Zn](NO_3)_2$ in DMSO upon addition of CT-DNA at 25 °C. Inset: Plots of [DNA]/ ε_a-ε_f vs [DNA] for the titration of CT-DNA with complexes. [Complex]=0.10x10^{-4} M, [DNA]=0-0.33 x 10^{-4} M*

This groove binding results in structural reorganization of CT-DNA which entails partial unwinding or damage of the double helix at the exterior phosphate backbone leading to the formation of a cavity to accommodate the complex. Consequently,

uptake occurs with partial melting of the double helix and generation of an appropriate binding pocket [257,258].

Secondly, the presence of transition metal ions in complexes also accounts for the higher binding extent of the complexes with CT-DNA in comparison to free ligand. The complexes could uncoil the helical structure of DNA and expose the embedded base pairs to the helix exterior ultimately leading to an effective binding with transition metal ions {copper(II) and zinc(II)}. It has been reported earlier that a square-planar copper(II) meso-tetra(N-methyl-4-pyridyl)porphyrin, containing four positively charged pyridyl rings, binds to DNA via, normal intercalation [259]. However, the five-coordinated copper(II) complex, $Cu(IDB)Cl_2$ (IDB = 1,5-bis(2-benzimidazolyl)diethylamine), with the aromatic moiety extending from the metal center does not bind to DNA by insertion; instead, the DNA base nitrogen atoms substitute for the two Cl ions and then coordinate to the cupric ion in the complex [260] which reveals the significance of coordination geometry around the metal ion in CT-DNA binding. However, the presence of labile water molecule in complex $[C_{36}H_{34}N_4O_7Cu](NO_3)_2$ also provide a greater binding extent of this complex to CT-DNA relative to the $[C_{36}H_{32}N_4O_6Zn](NO_3)_2$ which were efficiently replaced by nucleophile on DNA, usually a nitrogenous base such as guanine N7, leading to some covalent interactions with DNA [261]. Such covalent interactions were, however, prevented due to strong steric hindrance caused by large size of the molecule, yet, the partial insertion of the ligand phenyl group can be envisioned. Our results illustrate that complexes may bind to DNA primarily via electrostatic interactions, preferably groove binding. Further validation of the DNA-binding

mode of the complexes was provided by viscosity measurements which was concomitant with the above explanation.

To study quantitatively, the binding ability of complexes with CT-DNA, the intrinsic binding constant K_b values determined as given in Table 15. The binding constant K_b values follows the order $[C_{36}H_{34}N_4O_7Cu](NO_3)_2$ > $[C_{36}H_{32}N_4O_6Zn](NO_3)_2$ > $[C_{18}H_{16}N_2O_3]$ > cisplatin. From the results of the binding constants, it was concluded that the studied complexes reveal a higher binding affinity for DNA double helix compared to cisplatin ($3.20\pm0.15x10^4$ M^{-1}). This relative difference in the K_b values might be the result of different binding mode of the complexes and cisplatin. Cisplatin binds to the CT-DNA via, base specific interactions forming 1,2-intrastrand crosslinks between adjacent N7 atoms of guanine (GpG) and adenine nucleobase (ApG) and secondary interaction with phosphate backbone [211] which obscure the DNA helix to a much larger extent (Figure 43a). Moreover, the K_b values of the complexes were slightly higher than that of classical minor groove binder 4',6-diamino-2-phenylindole (DAPI-DNA, $8.90x10^3$ M^{-1} in 2 mM Tris-0.2 mM EDTA containing 30 mM NaCl buffer, pH 8) [262].

Table 15. *The binding constant (K_b) values of cisplatin, ligand and complexes with CT-DNA*

Complex	K_b (M^{-1})	Monitored at λ (nm)	% Hyperchromism	Red Shift (nm)
Cisplatin	$3.20\pm0.15x10^4$	248	17	02
$[C_{18}H_{16}N_2O_3]$	$1.37\pm0.02x10^4$	310	54	02
$[C_{36}H_{34}N_4O_7Cu](NO_3)_2$	$3.55\pm0.02x10^4$	264	75	03
$[C_{36}H_{32}N_4O_6Zn](NO_3)_2$	$2.33\pm0.02x10^4$	303	65	02

Interaction with 5′-GMP, 5′-TMP, 5′-AMP and 5′-CMP by absorption spectroscopy

The site-selective recognition of nucleic acid fragments such as 5′-GMP, 5′-TMP, 5′-AMP and 5′-CMP by complexes was monitored owing to the base specific interaction of the transition metal ions. Nucleotide-metal interactions [263,264] have been reported to occur nitrogen atom of the purine and pyrimidine rings as well as oxygen atom of the phosphate group present on the nucleotide. These base specific interaction of the complexes $[C_{36}H_{34}N_4O_7Cu](NO_3)_2$ and $[C_{36}H_{32}N_4O_6Zn](NO_3)_2$ include a higher affinity of the copper(II) complexes to bind with N7 of guanine and zinc(II) complex with N3 of thymidine.

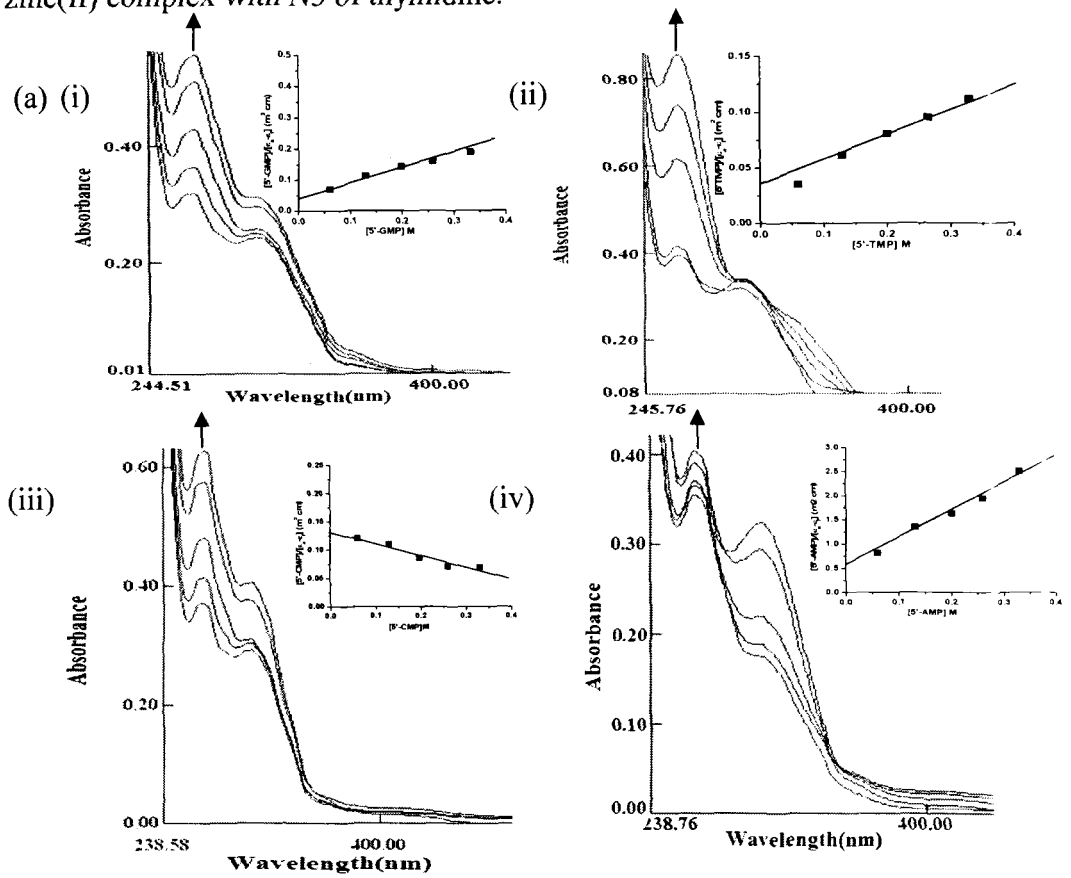

Figure 72. Absorption spectral traces of (a) complex $[C_{36}H_{34}N_4O_7Cu](NO_3)_2$ in DMSO upon addition of (i) 5′-GMP (ii) 5′-TMP (iii) 5′-CMP (iv) 5′-AMP. [Complex]=1.0 x 10^{-4} M, [Nucleotide]=0-0.33 x10^{-4} M.

On addition of increasing amounts of mononucleotides (5'-GMP, 5'-TMP, 5'-AMP and 5'-CMP) to the complexes $[C_{36}H_{34}N_4O_7Cu](NO_3)_2$ and $[C_{36}H_{32}N_4O_6Zn](NO_3)_2$ there is a sharp increase "hyperchromic" effect in the absorption bands at 246-302 nm (Figure 72a,b).

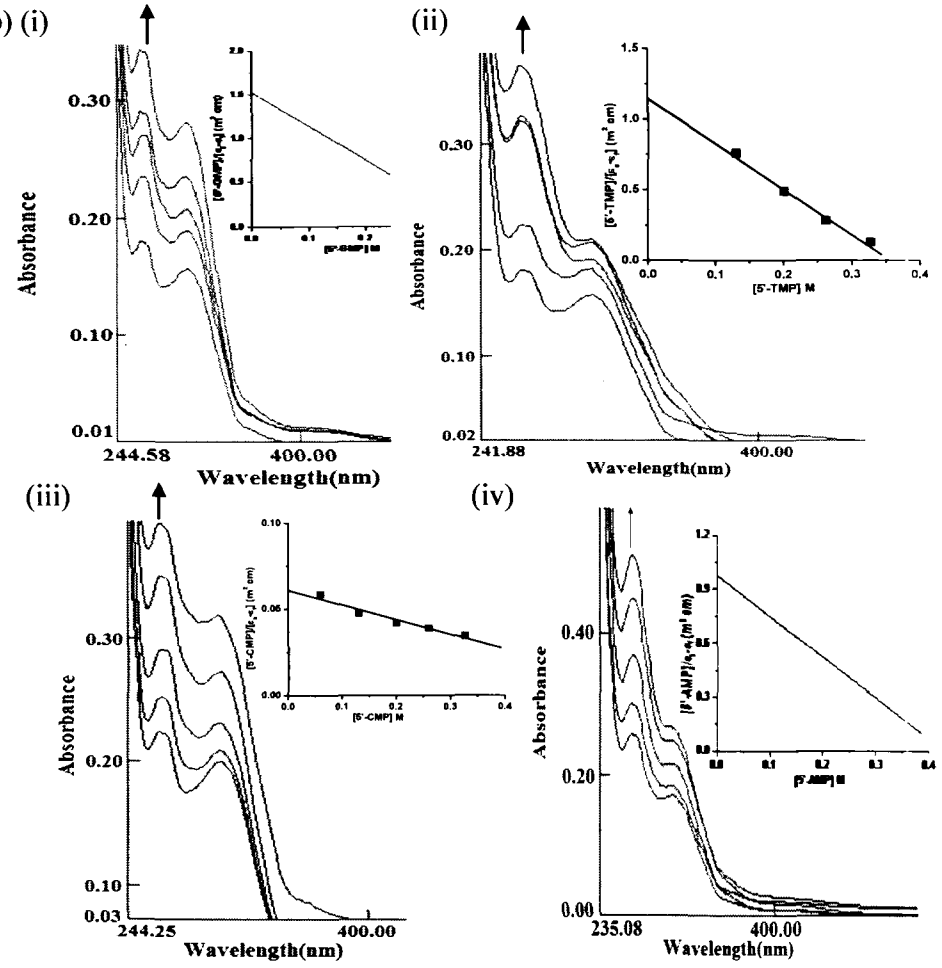

***Figure** 72. Absorption spectral traces of (a) Complex $[C_{36}H_{32}N_4O_6Zn](NO_3)_2$ in DMSO upon addition of (i) 5'-GMP (ii) 5'-TMP (iii) 5'-CMP (iv) 5'-AMP. [Complex]=1.0 x 10^{-4} M, [Nucleotide]=0-0.33 x10^{-4} M.*

Even though no substantial change in the position of the intraligand band was observed by the addition of increasing amount of mononucleotide (0-0.33x10^{-4} M),

marked increase in the absorption intensity of the complexes authenticate binding of the complexes to different nucleotides through electrostatic surface binding interactions via, phosphate backbone of the DNA double helix. The purine and pyrimidine bases of CT-DNA become exposed because of the unwinding of the DNA helix promoting an effective binding to these base pairs with the transition metal complexes. To compare quantitatively, the affinity of the complexes to mononucleotides (5′-GMP, 5′-TMP, 5′-AMP and 5′-CMP), the intrinsic binding constants were also determined. The binding constants obtained for the complexes $[C_{36}H_{34}N_4O_7Cu](NO_3)_2$ and $[C_{36}H_{32}N_4O_6Zn](NO_3)_2$ have been given in Table 16.

Table 16. *The comparative binding constant (K_b) values of complexes with the 5′-GMP and 5′-TMP (mean standard deviation of ± 0.07).*

Complex	5′-GMP ($x10^4$)	5′-TMP ($x10^4$)	5′-AMP ($x10^4$)	5′-CMP ($x10^4$)	Monitored at (nm)	Red Shift (nm)
$[C_{36}H_{34}N_4O_7Cu](NO_3)_2$	22.0	1.20	8.50	1.22	303	04
$[C_{36}H_{32}N_4O_6Zn](NO_3)_2$	1.41	3.50	2.55	0.28	303	02

The trend of mononucleotide interaction with $[C_{36}H_{34}N_4O_7Cu](NO_3)_2$ as validated by K_b values was 5′-GMP > 5′-TMP > 5′-CMP > 5′-AMP while for $[C_{36}H_{32}N_4O_6Zn](NO_3)_2$ complex, 5′-TMP > 5′-GMP > 5′-CMP > 5′-AMP trend was observed. The stronger coordination of complex $[C_{36}H_{34}N_4O_7Cu](NO_3)_2$ to 5′-GMP compared to the $[C_{36}H_{32}N_4O_6Zn](NO_3)_2$ supports a preferential binding of the complex to the N7 nitrogen of 5′-GMP occurring due to thermodynamic and kinetic stability of guanine residue [265]. However, the presence of two electron withdrawing oxo groups at the C2 and C3 position of the thymine lowers the energy

of the lone pair orbital at N3 of thymine base facilitating a stronger molecular orbital interaction of complex $[C_{36}H_{32}N_4O_6Zn](NO_3)_2$ with thymine residue compared to guanine residue.

^{1}H and ^{31}P NMR interaction with 5′-GMP and 5′-TMP

Interaction studies of complex $[C_{36}H_{32}N_4O_6Zn](NO_3)_2$ with nucleotides 5′-GMP and 5′-TMP provide additional support for the mode of binding of these complexes with biomolecules and exhibited preferential selectivity of the zinc(II) complex for 5′-TMP . Figure 73(a,b), illustrates comparative ^{1}H NMR spectra for free 5′-GMP and after addition of complex $[C_{36}H_{32}N_4O_6Zn](NO_3)_2$. A mixture of complex-5′-GMP shows insignificant shifts of the all the resonances of the nucleobase compared to the free nucleotide, suggestive of an electrostatic association of the complex with 5′-GMP probably through the phosphate groups along the groove of DNA double helix. This observation agrees well with observations of UV-visible studies as electrostatic bonding has essentially no effect on the chemical shifts values [266]. The other resonances of the free 5′-GMP undergo a slight shift of sugar hydroxyl protons from 5.82-3.87 ppm to 5.78-3.83 ppm revealing binding of the ribose ring protons with complex $[C_{36}H_{32}N_4O_6Zn](NO_3)_2$.

To validate the binding preference of the zinc(II) complex with 5′-TMP. the interaction pattern of the complex-5′-TMP with ^{1}H NMR was also studied (Figure 74a,b).

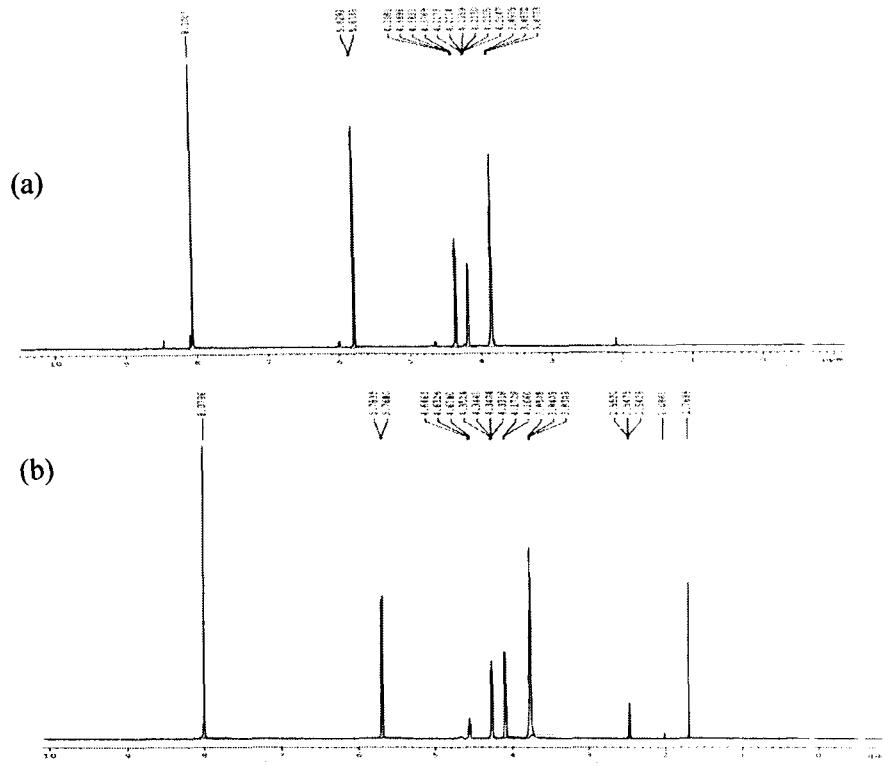

Figure 73. *^{1}H NMR spectra of (a) 5'-GMP alone and (b) the reaction of complex $[C_{36}H_{32}N_4O_6Zn](NO_3)_2$ (2.5 mmol) with 5'-GMP (5 mmol) at 25°C*

The ^{1}H NMR spectrum of free 5'-TMP (5 mM in D_2O), before the addition of complex reveals signals at 7.6, 6.2, 4.2, 1.7 ppm for N3 proton, C6 and CH_3 of thymine group, respectively. After the addition of complex $[C_{36}H_{32}N_4O_6Zn](NO_3)_2$, there is chemical slight shift of N3 from 7.65 ppm to 7.68 ppm suggestive of some interaction of complex with 5'-TMP.

The ^{31}P NMR signal of free of 5'-TMP appeared at 2.39 ppm which was shifted upfield to 3.17 ppm in presence of complex $[C_{36}H_{32}N_4O_6Zn](NO_3)_2$ (Figure 75), however, in case of 5'-GMP, no such pronounced shift in the ^{31}P NMR signal was observed after the addition of the complex to 5'-GMP (in free 5'-GMP at 3.73 ppm, in complex bound-5'-GMP at 3.76 ppm) (Figure 76). This accounts for the presence of higher binding exhibited by the zinc(II) complex for 5'-TMP as compared to 5'-GMP phosphate group.

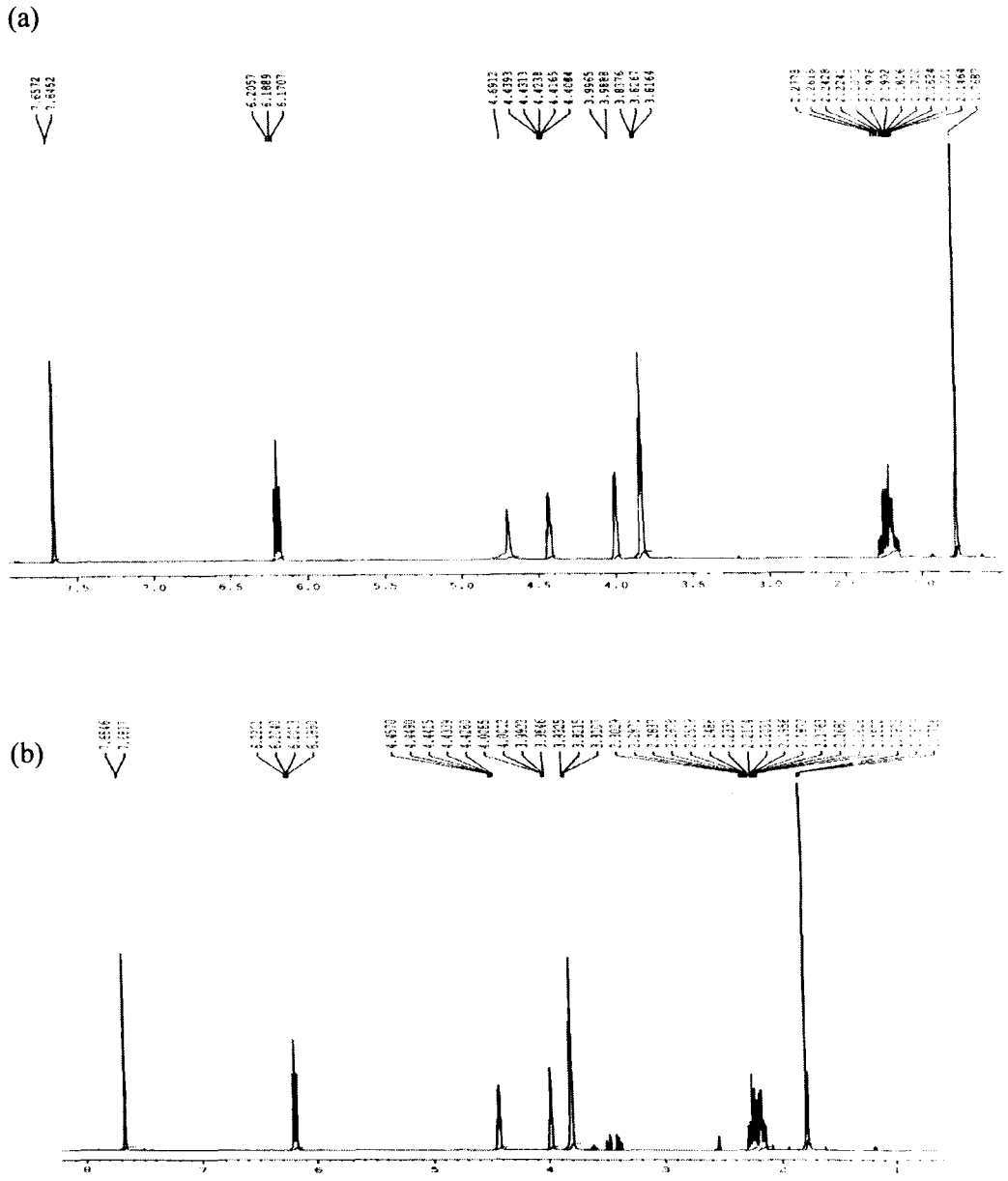

Figure 74. *^{1}H NMR spectra of (a) 5'-TMP alone and (b) the reaction of complex $[C_{36}H_{32}N_4O_6Zn](NO_3)_2$ (2.5 mmol) with 5'-TMP (5 mmol) at 25^{0}C*

These pronounced changes in ^{31}P chemical shift values arise due to the changes in O-P-O bond angles after its coordination with the complex $[C_{36}H_{32}N_4O_6Zn](NO_3)_2$ revealing a strong coordination of the complex with phosphate groups of nucleotide. The present observation is in agreement with preferential selectivity of the complex

$[C_{36}H_{32}N_4O_6Zn](NO_3)_2$ towards 5'-TMP revealing an electrostatic binding mode of this complex with the nucleotide.

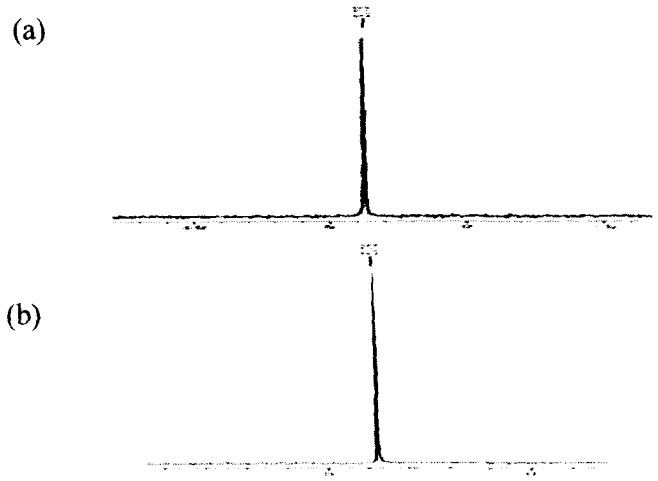

Figure 75. *^{31}P NMR spectra of (a) free 5'-GMP (5 mmol) (b) complex $[C_{36}H_{32}N_4O_6Zn](NO_3)_2$ (2.5 mmol) with 5'-GMP at 25 °C*

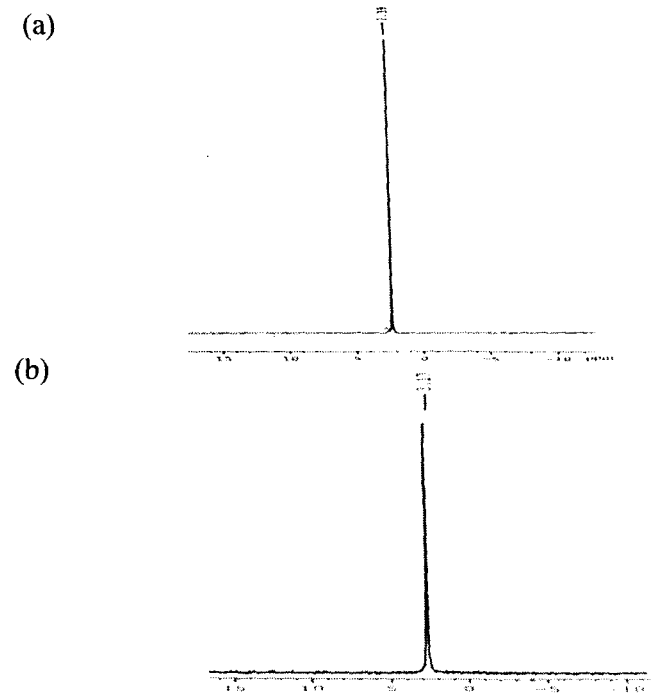

Figure 76. *^{31}P NMR spectra of (a) free 5'-TMP (5 mmol) (b) complex $[C_{36}H_{32}N_4O_6Zn](NO_3)_2$ (2.5 mmol) with 5'-TMP at 25 °C.*

Fluorescence studies

The emission spectra of the complexes $[C_{36}H_{34}N_4O_7Cu](NO_3)_2$ and $[C_{36}H_{32}N_4O_6Zn](NO_3)_2$ in the absence and presence of increasing amounts of CT-DNA are depicted in Figure 77(a,b). In the absence of CT-DNA, both the complexes emit weak luminescence in Tris-HCl buffer at ambient temperatures with a maxima appearing at 480 nm when excited at 260 nm. However, the subsequent addition of CT-DNA from 0-0.33x10^{-4} M causes a gradual enhancement in the fluorescence intensity of the complexes with no apparent change in the shape and position of the emission bands. This implies that the complexes strongly interact with CT-DNA probably due to the inaccessibility of the solvent water molecules to reach the hydrophobic environment inside the DNA helix, and the mobility of the complexes is restricted at the binding site ultimately leading to decrease in vibrational mode of relaxation. However, this enhancement is much less as compared to classical intercalators [267,268]. The binding constant K values of the complexes were given in Table 17 shows a higher binding propensity of complex $[C_{36}H_{34}N_4O_7Cu](NO_3)_2$ in contrast to complex $[C_{36}H_{32}N_4O_6Zn](NO_3)_2$ concomitant with the absorption studies. The extent of DNA binding is evaluated by competitive fluorescence displacement assay of DNA-bound ethidium bromide. The studies involve the addition of complex with CT-DNA pretreated with EthBr and then the measurements of the intensities of EthBr emission. The emission spectra of EB-DNA in the absence and presence of complexes are presented in Figure 78. Though the emission intensity of ethidium bromide in buffer medium is quenched by solvent

molecules, it is enhanced by its strong stacking interaction in between the adjacent DNA base pairs [185].

***Table** 17. Emission properties of complexes $[C_{36}H_{34}N_4O_7Cu](NO_3)_2$ and $[C_{36}H_{32}N_4O_6Zn](NO_3)_2$ bound to CT-DNA.*

Complex	Emission (nm)	Excitation (nm)	Monitored At	K(M^{-1})
$[C_{36}H_{34}N_4O_7Cu](NO_3)_2$	330	260	380	$7.48x10^5$
$[C_{36}H_{32}N_4O_6Zn](NO_3)_2$	330	260	430	$9.83x10^4$

The addition of increasing amount of the complexes $[C_{36}H_{34}N_4O_7Cu](NO_3)_2$ and $[C_{36}H_{32}N_4O_6Zn](NO_3)_2$ to DNA pretreated with ethidium bromide ([DNA]/[EthBr]=1) resulting in apparent quenching of the emission intensity, indicative of the competitive displacement of the bound ethidium bromide from the CT-DNA by the complexes. The extent of quenching of the fluorescence of ethidium bromide bound to DNA would reflect the extent of DNA binding of $[C_{36}H_{34}N_4O_7Cu](NO_3)_2$ and $[C_{36}H_{32}N_4O_6Zn](NO_3)_2$.

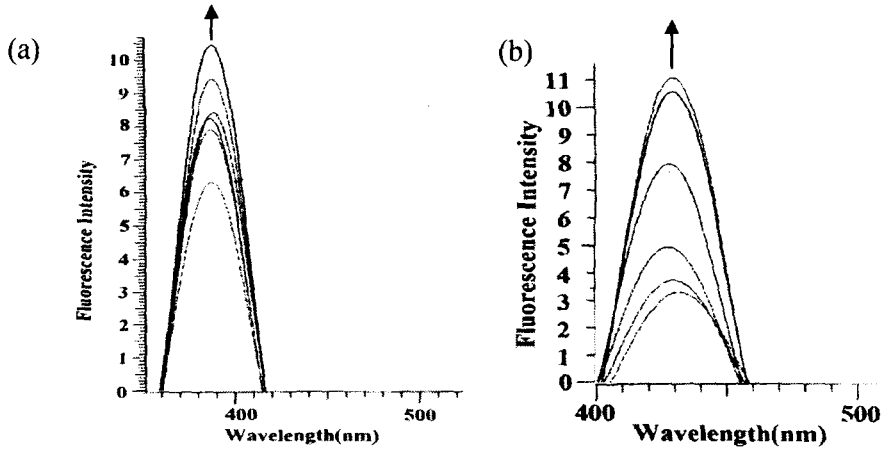

***Figure** 77. Emission spectra of (a) complex $[C_{36}H_{34}N_4O_7Cu](NO_3)_2$ and (b) complex $[C_{36}H_{32}N_4O_6Zn](NO_3)_2$ in Tris-HCl buffer the absence and presence of CT-DNA. Arrow shows the intensity change upon increasing CT-DNA concentration*

Ethidium bromide, itself is a known intercalator, so a direct as well as an indirect displacement could occur. The direct competitive replacement would arise when the complex prefers to bind (though not necessarily by intercalation) at the same site as fluorescent dye. The dynamic equilibria and the concentration differences between the EthBr and complex would effectively exclude the dye from the binding site. It appears that the DNA helix simultaneously accommodates both the complex and ethidium bromide in the grooves, as validated by viscosity measurements, so an indirect displacement could take place, when the complex induces structural modifications in DNA from B→A conformation via, untwisting of DNA base pairs, revealed by CD results due to its groove binding statistics thus, affecting the binding affinity for ethidium bromide by destabilising the excited state of bound ethidium bromide and facilitating an efficient displacement of bound ethidium bromide from CT-DNA.

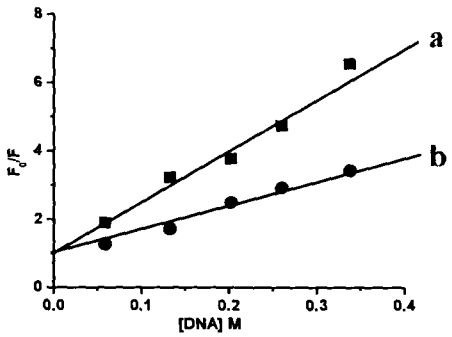

Figure 78. *Stern-Volmer plot of fluorescence titration data of DNA-EthBr system (λ_{ex}=525 nm, λ_{em}=520-680 nm) in presence of increasing concentration of complexes (a) $[C_{36}H_{32}N_4O_6Zn](NO_3)_2$ (■) (b) complex $[C_{36}H_{34}N_4O_7Cu](NO_3)_2$ (●) from 0-0.33x10^{-4} M. Quenching constant K_{sv}= 6.71x10^4 and 1.89x10^4 M^{-1}*

The fluorescence quenching curves of EB-DNA by the complexes is given in Figure 73. The quenching plots obey a linear Stern-Volmer equation with K_{sv} value of

$6.71x10^4$ and $1.89x10^4$ M^{-1} for complexes $[C_{36}H_{34}N_4O_7Cu](NO_3)_2$ and $[C_{36}H_{32}N_4O_6Zn](NO_3)_2$, respectively.

Table 18. *Emission quenching of CT-DNA bound EthBr by complexes* $[C_{36}H_{34}N_6O_{13}Cu](NO_3)_2$ *and* $[C_{36}H_{32}N_4O_{12}Zn](NO_3)_2$.

Complex	Emission	Excitation	Monitored at	K_{sv}
$[C_{36}H_{34}N_4O_7Cu](NO_3)_2$	520	525	580	$6.71x10^4$
$[C_{36}H_{32}N_4O_6Zn](NO_3)_2$	520	525	580	$1.89x10^4$

The high K_{sv} value for copper relative to zinc complex show that copper complex exhibit much higher binding affinity with CT-DNA compared to zinc complex (Table 18). Thus, the ability to hinder the DNA induced emission decreases in the order $[C_{36}H_{34}N_4O_7Cu](NO_3)_2 > [C_{36}H_{32}N_4O_6Zn](NO_3)_2$; which is consistent with the decrease in the binding constant of the complexes as illustrated above.

Viscosity studies

The changes in the relative viscosity of CT-DNA in presence of increasing amount of the complexes $[C_{36}H_{34}N_4O_7Cu](NO_3)_2$ and $[C_{36}H_{32}N_4O_6Zn](NO_3)_2$ and EthBr (a classical intercalators) are presented in Figure 79. Ethidium bromide (EthBr), a known DNA classical intercalator, increases the relative specific viscosity of DNA double helix due to lengthening of helix axis owing to its intercalative binding mode. In presence of increasing amount of ethidium bromide (EB) and complexes $[C_{36}H_{34}N_4O_7Cu](NO_3)_2$, $[C_{36}H_{32}N_4O_6Zn](NO_3)_2$, the relative viscosity of CT-DNA increases steadily [269]. However, this increase is rather less as compared to classical intercalators EthBr. The increasing degree of viscosity follows the order EB > $[C_{36}H_{34}N_4O_7Cu](NO_3)_2$ > $[C_{36}H_{32}N_4O_6Zn](NO_3)_2$. On the basis of viscosity results,

at first glance, the increase in the viscosity of CT-DNA appears to result from the intercalative interactions but the increase is quiet less than that for potential intercalator viz; EthBr with the same concentration ranges of CT-DNA.

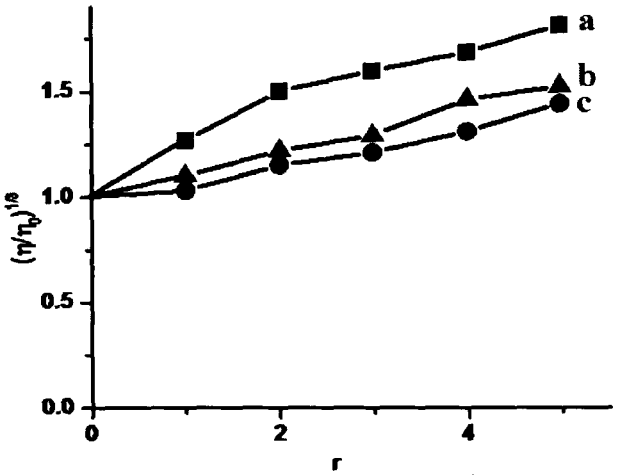

Figure 79. *Effect of addition of (a) EthBr and complexes (b) $[C_{36}H_{34}N_4O_7Cu](NO_3)_2$, (c) $[C_{36}H_{32}N_4O_6Zn](NO_3)_2$ on the relative viscosity of CT-DNA. [DNA]=1.45x10^{-4} M, r ([Complex]/[DNA]) = 1-5, respectively.*

Thus, we conclude that, although the complexes exhibit affinity for the intercalative site on DNA but the binding affinity to a lower extent than EthBr. These results indicate that the complexes bring conformational changes in a manner, probably due to the steric matching of the DNA grooves and the complexes $[C_{36}H_{34}N_4O_7Cu](NO_3)_2$, $[C_{36}H_{32}N_4O_6Zn](NO_3)_2$ resulting in some partial intercalation of the complexes within the hydrophobic DNA pockets through the aromatic rings. This aggregation of the complexes into the groove of DNA helix inducing partial intercalative interactions causes an extension of the DNA helix with concomitant increase in its viscosity. Thus, the above results cumulatively indicate that the complexes $[C_{36}H_{34}N_4O_7Cu](NO_3)_2$ and $[C_{36}H_{32}N_4O_6Zn](NO_3)_2$ bind to CT-DNA in the groove regions [270]. Moreover, the increase in viscosity observed for

$[C_{36}H_{34}N_4O_7Cu](NO_3)_2$ complex (Figure 79b) is more pronounced as compared to $[C_{36}H_{32}N_4O_6Zn](NO_3)_2$ complex (Figure 79c), indicating that $[C_{36}H_{34}N_4O_7Cu](NO_3)_2$ complex bind more avidly with CT-DNA than $[C_{36}H_{32}N_4O_6Zn](NO_3)_2$ complex .

Circular dichroic studies

The CD spectra of CT-DNA on addition complexes $[C_{36}H_{34}N_4O_7Cu](NO_3)_2$ and $[C_{36}H_{32}N_4O_6Zn](NO_3)_2$ depicted in Figure 80, exhibit significant perturbations both in negative and positive bands. The complex $[C_{36}H_{34}N_4O_7Cu](NO_3)_2$ exhibit increase in both the positive and negative bands with respect to unbound CT-DNA which was attributed to partial insertion of planar aromatic chromophores in between the DNA base pairs causing stabilization of base stacking consequently, leading to conformational transition of B-form of DNA into more A-like conformation. However, complex $[C_{36}H_{32}N_4O_6Zn](NO_3)_2$ displays small change in the positive band with respect to DNA accompanied by a large increase in the negative band as exhibited by complex $[C_{36}H_{34}N_4O_7Cu](NO_3)_2$. This corroborates well with the hypothesis in literature that simple groove binding and electrostatic interaction of the complexes with DNA shows less or no perturbation on the base stacking and helicity bands while intercalator enhances the intensities of both the bands [271]. These results supports groove binding nature of the complexes $[C_{36}H_{34}N_4O_7Cu](NO_3)_2$ and $[C_{36}H_{32}N_4O_6Zn](NO_3)_2$ probably due to some partial intercalative interactions which modifies the CT-DNA morphology during drug-DNA interactions. It is conceivable that the bigger size of the complex is critical for promoting B→A conformational

transitions. The nucleobases in the deep major groove of DNA double helix were preferably accessible to the multivalent positively charged transition metal complexes. These positively charged transition metal complexes neutralize the two closely associated negatively charged sugar phosphate backbone along the major groove in A-DNA and results in B→A conformational transitions.

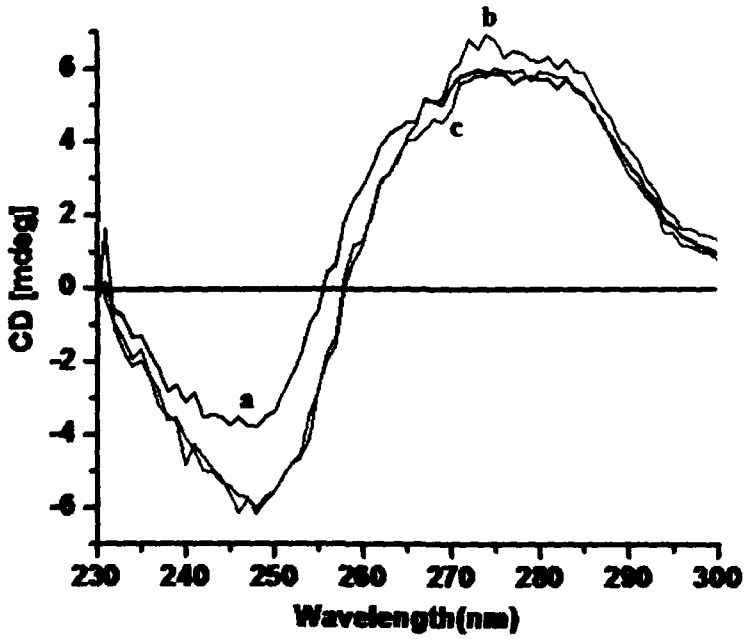

Figure 80. *Circular dichroism spectra of CT-DNA in the (a) absence and presence of complex (b) $[C_{36}H_{34}N_4O_7Cu](NO_3)_2$ (blue line) (c) $[C_{36}H_{32}N_4O_6Zn](NO_3)_2$ (red line) in Tris-HCl buffer at 25 °C. [Complex]= $1x10^{-4}$ M and [DNA]=$1.45x10^{-4}$ M.*

Gel electrophoresis

Since the complex $[C_{36}H_{34}N_4O_7Cu](NO_3)_2$ shows maximum binding propensity with CT-DNA, therefore, the cleavage activity has been evaluated for complex $[C_{36}H_{34}N_4O_7Cu](NO_3)_2$. It has been well established in literature that copper(II)

complexes are selective for the cleavage of DNA either through oxidative or hydrolytic mechanism.

The nuclease activity of complex $[C_{36}H_{34}N_4O_7Cu](NO_3)_2$ have been studied using supercoiled pBR322 DNA as a substrate (Figure 81). To ascertain the DNA cleavage ability of complex, supercoiled pBR322 DNA was incubated with different concentration of complex in aqueous buffer solution (5mM Tris-HCl/40 mM NaCl, pH 7.42) without addition of any reductant.

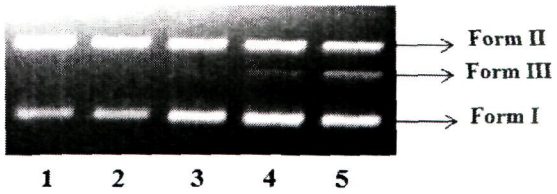

Figure 81. *The cleavage patterns of the agarose gel electrophoresis for pBR322 plasmid DNA (300ng) by* $[C_{36}H_{34}N_4O_7Cu](NO_3)_2$*; Lane 1: DNA control; Lane 2: 10 μM complex + DNA; Lane 3: 20 μM complex + DNA; Lane 4: 30 μM complex + DNA; Lane 5: 40 μM complex + DNA.*

As observed from the Figure, that there is a gradual decrease in the amount of Form I with a simultaneous increase in Form II (Lanes 2 and 3) on increasing the concentration of the complex. A notable cleavage feature observed for this complex is the appearance of Form III before the disappearance of Form I (Lanes 3 and 4). This phenomenon indicates that the complex is capable of performing direct strand scission, as a consequence, this complex is better suited for therapeutic applications particularly, in cancer chemotherapeutics, while many complexes are only able to cleave single strand successively [272].

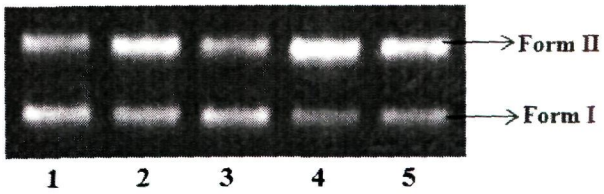

Figure 82. *Agarose gel electrophoresis pattern for the cleavage pattern of pBR322 plasmid DNA (300ng) by complex* $[C_{36}H_{34}N_4O_7Cu](NO_3)_2$ *(20 μM) in presence of different activating agent at 312 K after incubation for 30 min. Lane 1, DNA control; Lane 2, DNA +* $[C_{36}H_{34}N_4O_7Cu](NO_3)_2$ *+ GSH (40 μM); Lane 3, DNA +* $[C_{36}H_{34}N_4O_7Cu](NO_3)_2$ *+ Asc (40 μM); Lane 4, DNA +* $[C_{36}H_{34}N_4O_7Cu](NO_3)_2$ *+ MPA (40 μM); Lane 5, DNA +* $[C_{36}H_{34}N_4O_7Cu](NO_3)_2$ *+* H_2O_2 *(40 μM)*

In the presence of activators viz; glutathione (GSH), ascorbic acid (Asc), hydrogen peroxide (H_2O_2) and mercaptopropionic acid (MPA), the complex $[C_{36}H_{34}N_4O_7Cu](NO_3)_2$ showed significant increase in the cleavage of the DNA and follows the order H_2O_2 > MPA > GSH > Asc (Figure 82).

The mechanistic pathway for the cleavage of plasmid DNA followed by complex was investigated by gel electrophoresis in the presence of various radical scavengers such as NaN_3, DMSO, tert-butyl alcohol, NaN_3 (Figure 83, Lane 2-5). The DNA cleavage of the plasmid was inhibited in the presence of NaN_3 suggesting that $^1O_2$ is likely to be the reactive species responsible for the nuclease activity (Lane 2). When hydroxyl radical scavenger, DMSO and tert-butyl alcohol were added to the reaction mixture, they were found to diminish the nuclease activity which was indicative of the involvement of $OH^{\bullet}$ radicals in the cleavage process (Lane 3 and 4). Similarly, in the presence of SOD, the cleavage was repressed which indicate that $O_2^{\bullet-}$ might be an inhibitor in the cleavage process and reducing the amount of $O_2^{\bullet-}$ can improve the cleavage effect (Lane 5). Thus, the results suggested the oxidative pathway of the complex to cleave the DNA.

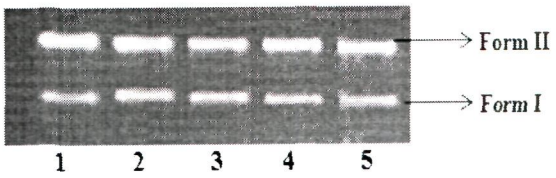

Figure 83. *Agarose gel electrophoresis pattern for the cleavage of pBR322 plasmid DNA (300ng) by complex* $[C_{36}H_{34}N_4O_7Cu](NO_3)_2$ *(20 μM) in presence of standard radical scavengers at 310 K after incubation for 30 min. Lane 1, DNA control; Lane 2, DNA +* $[C_{36}H_{34}N_4O_7Cu](NO_3)_2$ *+* NaN_3 *(40 μM); Lane 3, DNA +* $[C_{36}H_{34}N_4O_7Cu](NO_3)_2$ *+ DMSO (40 μM); Lane 4, DNA +* $[C_{36}H_{34}N_4O_7Cu](NO_3)_2$ *+ tert-butyl alcohol (40 μM); Lane 5, DNA +* $[C_{36}H_{34}N_4O_7Cu](NO_3)_2$ *+ Superoxide dismutase (15 Units).*

When supercoiled pBR322 DNA was treated with DAPI, the cleavage reaction mediated by complex was not quenched (Figure 84, Lane 2). This clearly suggests that the complex prefers to bind to DNA major groove. Further support to this observation was provided by complete inhibition of the cleavage by the complex in presence of methyl green, a major groove binding agent (Figure 84, Lane 3).

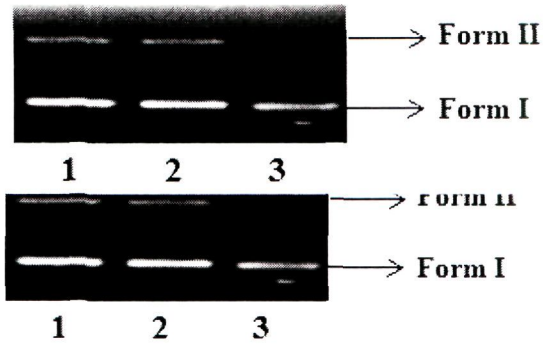

Figure 84. *Agarose gel electrophoresis pattern for the clevage of pBR322 plasmid DNA (300ng) by complex* $[C_{36}H_{34}N_4O_7Cu](NO_3)_2$ *(20 μM) in the presence of DNA minor binding agent DAPI and major binding agent methyl green at 310 K after incubation for 30 min. Lane 1, DNA control; Lane 2, DNA +* $[C_{36}H_{34}N_4O_7Cu](NO_3)_2$ *+ DAPI (8 μM); Lane 3, DNA +* $[C_{36}H_{34}N_4O_7Cu](NO_3)_2$ *+ Methyl green (2.5 μL of a 0.01mg/ml solution)*

Conclusions

Two new transition metal complexes $[C_{36}H_{34}N_4O_7Cu](NO_3)_2$ and $[C_{36}H_{32}N_4O_6Zn](NO_3)_2$ have been synthesized and characterized. The comparative binding propensities of the two complexes with CT-DNA were also investigated by absorption, emission, circular dichroism and viscosity measurements. Experimental results indicate that the two complexes bind to CT-DNA by electrostatic groove binding mechanism. As observed for gel electrophoretic mobility assay, the complex $[C_{36}H_{34}N_4O_7Cu](NO_3)_2$ displays efficient cleavage activity of plasmid pBR322 DNA converting the Form I to Form II and ultimately to leading to the formation of linearized Form III with increasing concentrations of the complex. Singlet oxygen ($^1O_2$) and hydroxyl radicals ($^{\bullet}OH$) is likely to be the reactive species responsible for the nuclease activity of plasmid DNA. Additionally, the most notable evidence for the groove binding of the complexes was provided by gel electrophoresis of plasmid DNA in presence of groove recognition agents DAPI and methyl green suggesting a major groove selectivity of the complex.

References

References

[1] K.S. Tomi, *Chem. Biol. Drug Des.*, (2006), **67**, 196.

[2] B.R. Stockwell, *Nature,* (2004), **432**, 846.

[3] P.J. Sadler, Inorganic Chemistry and Drug Design, *Adv. Inorg. Chem.*, (1991), **36**, 1.

[4] C.F. Shaw III, *Chem. Rev.,* (1999), **99**, 2589.

[5] H.E. Howard-Lock, C.J.L. Lock, Comprehensive Coordination Chemistry, Ed. G. Wilkinson, R.D. Gillard, J.A. McCleverty, Pergamon, New York, (1987).

[6] B. Rosenberg, L. VanCamp, J.E. Trosko, V.H. Mansour, *Nature,* (1969), **222,** 385.

[7] B. Rosenberg, L. VanCamp, E.B. Grimley, A.I. Thompson, *J. Biol. Chem.*, (1967), **242,** 1347.

[8] E. Wong, C.M. Giandomenico, *Chem. Rev.,* (1999), **99,** 2451.

[9] E.R. Jamieson, S.J. Lippard, *Chem. Rev.,* (1999), **99,** 2467.

[10] (a) C.X. Zhang, S.J. Lippard, *Curr. Opin. Chem. Biol.,* (2003), **7,** 481; (b) P.J. Dyson, G. Sava, *Dalton Trans.,* (2006), 1929.

[11] G. Damia, M.D'Incalci, *Eur. J. Cancer,* (2009), **45,** 2768.

[12] R.J.P. Williams, J.J.R. Fraústo da Silva, Biological Chemistry of the Elements, Oxford University Press, Oxford, U.K., (2001)

[13] I. Bertini, A. Sigel, H. Sigel, Handbook on Metalloproteins, Marcel Dekker, New York, (2001).

[14] T.W. Hambley, *Dalton Trans.,* (2007), 4929.

[15] J. Luis, *Chem. Soc. Rev.,* (2004), **23**, 445.

[16] E.N. Jacobsen, W. Zhang, M.N. Guler, *J. Am. Chem. Soc.,* (1991), **113**, 6703.

[17] (a) O. Kahn, Molecular Magnetism, VCH: New York, (1993); (b) D. Gatteschi, R. Sessoli, T. Villain, J. Molecular Nanomagnets: Oxford University Press; New York (2006).

[18] A.E. Friedman, J.C. Chambron, J.P. Sauvage, N.J. Turro, J.K. Barton, *J. Am. Chem. Soc.*, (1990), **112**, 4960.

[19] J.-M. Lehn, Supramolecular Chemistry: Concepts and Perspectives, VCH, Weinheim, Germany, (1995).

[20] M. Fujita, M. Tominaga, A. Hori, B. Therrien, *Acc. Chem. Res.*, (2005), **38**, 369.

[21] I. Bertini, H.B. Gray, E.I. Stiefel, J.S. Valentine, Biological Inorganic Chemistry: Structure and Reactivity, University Science Books, Sausalito, CA, (2007).

[22] S.J. Lippard, J.M. Berg, Principles of Bioinorganic Chemistry, University Science Books, Mill Valley, CA, (1994).

[23] H. Li, X.Y. Le, D.W. Pang, H. Deng, Z.H. Xu, Z.H. Lin, *J. Inorg. Biochem.*, (2005), **99**, 2240.

[24] D.S. Sigman, D.R. Graham, V. D'Aurora, A.M. Stern, *J. Biol. Chem.*, (1979), **254**, 12265.

[25] D.S. Sigman, A. Mazumder, D.M. Perrin, *Chem. Rev.*, (1993), **93**, 2295.

[26] M.W. Göbel, *Angew. Chem. Int. Ed. Engl.*, (1994), **33**, 1141.

[27] T. Ito, S. Thyagarajan, K.D. Karlin, S.E. Rokita, *Chem. Commun.*, (2005), 4812.

[28] V. Uma, M. Kanthimathi, T. Weyhermuller, B.U. Nair, *J. Inorg. Biochem.* (2005), **99**, 2299.

[29] J.S. Lewis, R. Laforest, T.L. Buettner, S.K. Song, Y. Fujibayashi, J.M. Connett, M.J. Welch, *Proc. Nat. Acad. Sci., USA*, (2001), **98**, 1206.

[30] G. Bernard, *8th Int. Conf. Appl. Chem.*, (1912), **28**, 30.

[31] C. Orvig, M. J. Abrams, *Chem. Rev.,* (1999), **99,** 2201.

[32] T. Storr, K.H. Thompson, C. Orvig, *Chem. Soc. Rev.,* (2006), **35,** 534.

[33] K.H. Thompson, C. Orvig, *Dalton Trans,* (2006), 761.

[34] L. Xu, J. Pierreroy, B.O. Patrick, and C. Orvig, *Inorg. Chem.,* (2001). **40**, 2005.

[35] K.H. Thompson, C. Orvig, *Science,* (2003), **300,** 936.

[36] S.E. Sherman, S.J. Lippard, *Chem. Rev.,* (1987), **87**, 1153.

[37] W.I. Sundquist, S.J. Lippard., *Coord. Chem. Rev.*, (1990), **100**, 293.

[38] J. Malina, C. Hofr, L. Maresca, G. Natile, V. Brabec, *Biophys. J.*, (2000), **78**, 2008.

[39] S.-Z. Seifried, C.G. Hartinger, K. Meelich, M. Galanski, B.K. Keppler, H. Zorbas, *Biochemistry,* (2006), **45**, 14817.

[40] C. Clarkson, C.C. Musonda, K. Chibale, W.E. Campbell, P. Smith, *Bioorg. Med. Chem.,* (2003), **11**, 4417.

[41] P. Schluga, C.G. Hartinger, M. Galanski, K. Meelich, A.R. Timerbaev, B.K. Keppler, *The Analyst,* (2005), **130**, 1383.

[42] A. Küng, M. Galanski, C. Baumgartner, B.K. Keppler, *Inorg. Chim Acta.*, (2002), **339**, 9.

[43] J. Sanmartin, M.R. Bermejo, A.M. Garia-Diebe, M. Maneiro, C. Lage, A.J. Costa-Filho, *Polyhedron,* (2000), **19,** 185.

[44] H. Schiff, *Ann. Chem. Pharm.,* (1964), **131**, 118.

[45] E. Ritter, P. Przybylski, B. Brzinski, F. Bartl, *Curr. Org. Chem.,* (2009), **13**, 241.

[46] C.A. Bolos, G.St. Nikolov, L. Ekateriniadou, A. Kortsaris, D.A. Kyriakidis, *Metal Based Drugs,* (1998), **5**, 323.

[47] A. Th.Chaviara, P.J. Cox, K.H. Repana, R.M. Papi, K.T. Papazisis. D. Zambouli, A.H. Kortsaris, D.A. Kyriakidis, C.A. Bolos, *J. Inorg. Biochem.*, (2004), **98**, 1271.

[48] A. Th.Chaviara, P.J. Cox, K.H. Repana, A.A. Pantazaki, K.T. Papazisis. A.H. Kortsaris, D.A. Kyriakidis, G.St. Nikolov, C.A. Bolos, *J. Inorg. Biochem.*, (2005), **99**, 467.

[49] J.R.J. Sorenson, *Prog. Med. Chem.*, (1989), **26**, 437.

[50] A.T. Chaviara, E.E. Kioseoglou, A.A. Pantazaki, A.C. Tsipis, P.A. Karipidis, D.A. Kyriakidis, C.A. Bolos, *J. Inorg. Biochem.*, (2009), **102**, 1749.

[51] Z.H. Chohan, M. Arif, M.A. Akhtar, C.T. Supuran, *Bioinorg. Chem. Appl.*, (2006), **2006**, 83131.

[52] K.C. Joshi, V.K. Pathak, *Coord. Chem. Rev.*, (1977), **22**, 37.

[53] N. Raman, R. Jayamurugan, R.U. Rani, T. Baskaran, L. Mitu, *J. Coord. Chem.*, (2010), **63**, 1629.

[54] R.H. Holm, G.L. Eichorn Ed., Inorganic Biochemistry, Elsevier, Amsterdam. (1974).

[55] L. Albanus, N.E. Bjorklund, B. Gustafsson, M. Johsson, *Acta Pharmacol. Toxicol. Suppl.*, (1975), **36,** 93.

[56] C. Pettinari, F. Marchetti, R. Pettinari, D. Martini, A. Drozlov, S. Troyanov, *Inorg. Chim. Acta,* (2001), **325,** 103.

[57] N. Kobakhidze, N. Farfan, M. Romero, J.M. M.-Stivalet, M.G. B.-Lopez, H.G.-Ortega, O. Dominguez, R. Santillan, F.S. -Bartez, I.G. -Mora, *J. Organomet. Chem.*, (2010), **695**, 1189.

[58] W. Rehman, M.K. Baloch, A. Badshah, *Eur. J. Med. Chem.*, (2008), **43**, 2380.

[59] T.S. Basu Baul, S. Basu, D. deVos, A. Linden, *Invest. New Drugs*, (2009), **5**, 419.

[60] M. Nath, R. Yadav, M. Gielen, H. Dalil, D. deVos, G. Eng, *Appl. Organomet. Chem.*, (1997), **11**, 727.

[61] C.A. Bell, C.C. Dykstra, N.A. Naimen, M. Cory, T.A. Fairley, R.R. Tidwell, *Antimicrob. Agents Chemother.*, (1993), **37**, 2668.

[62] D.J, Shalitzky, J.T. Marakovits, K.A. Maegley, A. Ekker, X.-H. Yu, Z. Hostomsky, S.E. Webber, B.W. Eastman, R. Almassy, J. Li, N.J. Curtin, D.R. Newell, A.H. Calvert, R.J. Griffin, B.T. Golding, *J. Med. Chem.*, (2003), **46**. 210.

[63] (a) J.P. Lalezari, J.A. Aberg, L.H. Wang, M.B. Wire, R. Miner, W. Snowden, C.L. Talarico, S. Shaw, M.A. Jacobson, W.L. Drew, *Antimicrob. Agents Chemother.*, (2002), **46**, 2969; (b) J. Valdez, R. Cedillo, A.H. Camos, L. Yepez, F.H. Luis, G.N. Vazquez, A. Tapia, R. Cortes, M. Hernandez, R. Castillo, *Bioorg. Med. Chem. Lett.*, (2002), **12**, 2221.

[64] F. Seela, T. Wenzel, *Helv. Chim. Acta,* (1995), **78**, 833.

[65] M.J.S. Moreno, A.F. Botello, R.B.G. Coca, R. Griesser, J. Ochocki, A. Kotynski, J.N. Gutierrez, V. Moreno, H. Sigel, *Inorg. Chem.*, (2004), **43**, 1311.

[66] C. Bailly, G. Chessari, C. Carrasco, A. Joubert, J. Mann, W.D. Wilson, S. Niedle, *Nucleic Acids Res.*, (2003), **31,** 1514.

[67] C.E. B.-Smith, M.S. Searle, *Nucleic Acids Res.*, (1999), **27**, 1619.

[68] K. Isele, V. Broughton, C.J. Matthews, A.F. Williams, G. Bernardinelli, P. Franz, S. Decurtins, *Dalton Trans.*, (2002), 3899.

[69] M.A. Phillips, *J. Chem. Soc.*, (1928), 172.

[70] L.L.-Y. Wang, M.M. Joullié, *J. Am. Chem. Soc.*, (1957), **97**, 5706.

[71] K.H. Taffs, L.V. Prosser, S.B. Wington, M.M. Joullié, *J. Org. Chem.*, (1961), **26**, 462.

[72] J.S. Kim, Q. Sun, B. Gatto, C. Yu, A. Liu, L.F. Liu, E.J. LaVoie, *Bioorg. Med. Chem.*, (1996), **4,** 621.

[73] A.R. Ruchelman, S.K. Singh, A. Liu, N. Zhou, L.F. Liu, E.J. LaVoie, *Lett. Drug Design and Discovery,* (2004), **1**, 198.

[74] M. Chauhan, F. Arjmand, *Chem. Biodiv.,* (2006), **3**, 660.

[75] M. Chauhan, F. Arjmand, *J. Organomet. Chem.,* (2007), **692**, 5156.

[76] P.J. Houghton, *Stud. Nat. Prod. Chem.*, (2000), **21,** 123.

[77] J. Ungwitayatorn, W. Samee, J. Pimthon, *J. Mol. Str.,* (2004), **689**, 99.

[78] G. Singh, R. Singh, N.K. Girdhar, M.P.S. Ishar, *Tetrahedron,* (2002), **58,** 2471.

[79] L.Z. Piao, H.R. Park, Y.K. Park, S.K. Lee, J.H. Park, M.K. Park, *Chem. Pharm. Bull.,* (2002), **50**, 309.

[80] A.M.S. Silva, D.C.G.A. Pinto, J.A.S. Cavaleiro, A. Levai, T. Patonay, *ARKIVOC, Part 7,* (2004), **106,** 123.

[81] D.O. Bennardi, G.P. Romanelli, J.L. Jios, J.C. Autino, G.T. Baronetti, H.J. Thomas, *ARKIVOC,* (2008), **(xi),** 123.

[82] M. Recanatini, A. Bisi, A. Cavalli, F. Belluti, S. Gobbi, A. Rampa, P. Valenti, M. Palzer, A. Palusczak, R.W. Hartmann, *J. Med. Chem.,* (2001), **44**, 672.

[83] R.F.V. deSouza, W.F. deGiovani, *Redox Rep.,* (2004), **23**, 38.

[84] M. Grazul, E. Budzisz, *Coord. Chem. Rev.,* (2009), **253**, 2588.

[85] D.-D. Qin, Z.-Y. Yang, B.-D. Wang, *Spectrochim. Acta, Part A*, (2007), **68**, 912.

[86] S. Satyanarayana, J.C. Dabrowiak, J.B. Chaires, *Biochemistry,* (1992), **31**, 9319.

[87] J. Wang, Z-Y. Yang, X.-Y. Yi, B.-D. Wang, *J. Photochem. Photobiol. A: Chem.,* (2009), **201**, 183.

[88] K. -Maier, *Eur. J. Clin. Pharmacol.,* (1994), **47**, 1.

[89] Z. Guo, P.J. Sadler, *Angew. Chem. Int. Ed..,* (1999), **38**, 1512.

[90] M.J. Burkitt, *Methods Enzymol.,* (1994), **234**, 66.

[91] K.J. Humphreys, K.D. Karlin, S.E. Rokita, *J. Am. Chem. Soc.,* (2002), **124**, 8055.

[92] C. Marzano, M. Pellei, F. Tisato, C. Santini, *Anti-Cancer Agents in Med. Chem.,* (2009), **9,** 185.

[93] T.F. Kagawa, B.H. Geierstanger, A.H.J. Wang, P.S. Ho, *J. Biol. Chem.,* (1991), **266**, 20175.

[94] B.K. Santra, P.A.N. Reddy, G. Neelakanta, S. Mahadevan, M. Nethaji, A.R. Chakravarty, *J. Inorg. Biochem.,* (2002), **89**, 191.

[95] S.Y, Tsang, S.C. Tam, I. Bremner, M.J. Burkitt, *Biochem. J.* (1996), **317**, 13.

[96] F.B. Amrani, L. Perello, J. Borras, L. Torres, *Metal Based Drugs,* (2000), 7, 365.

[97] A. Bencini, E. Berni, A. Bianchi, C. Giorgi, B. Valtancoli, D.K. Chand. H.J. Schenieder, *Dalton Trans.,* (2003), 793.

[98] M. Laine, F. Richards, E. Tarnaud, C.B. -Charreton, C.V. -Beaur, *J. Biol. Inorg. Chem.,* (2004), **9**, 550.

[99] J. Bernadou, G. Pratviel, F. Bennis, M. Girardet, B. Meunier, *Biochemistry.* (1989), **28,** 7268.

[100] F.B. Tamboura, M. Gaye, A.S. Sall, A.H. Barry, T. Jouini, *Inorg. Chem. Commun.,* (2002), **5,** 235.

[101] D.S. Sigman, T.W. Bruice, A. Mazumder , C.L. Sutton, *Acc. Chem. Res.,* (1993), **26,** 98.

[102] S.A. Ross, M. Pitie, B. Meunier, *Eur. J. Inorg. Chem.,* (1999), 557.

[103]M.D. Kuwabara, C. Yoon, T.E. Goyne, T. Thederahn, D.S. Sigman, *Biochemistry,* (1986), **25**, 7401.

[104] J.A. Cowan, *Curr. Opin. Chem. Biol.,* (2001), **5,** 634.

[105] T.B. Thederahn, A. Spassky, M. D. Kuwabara, D.S. Sigman, *Biochem. Biophys. Res. Commun.,* (1990), **168**, 756.

[106] A. Barve, A. Kumbhar, M. Bhat, B. Joshi, R. Butcher, U. Sonawane, R. Joshi. *Inorg. Chem.,* (2009), **48**, 9120.

[107] J.E. Coleman, *Curr. Opin. Chem. Biol.,* (1998), **2**, 222.

[108] K .H. Falchuk, *Mol. Cell Biochem.,* (1998), **188**, 41.

[109] J.-H. Li, J.-T. Wang, L.-Y. Zhang, Z.-N. Chen, Z.-W. mao, L.-N. Ji, *Inorg. Chim. Acta,* (2009), **362**, 1918.

[110] S.K. Miller, D.G. Vanderveer, L.G. Marzilli, *J. Am. Chem. Soc.,* (1985), **107**, 1048.

[111] H.-L. Seng, S.-T. Von, K.-W. Tan, M.J.M.S.-W. Ng, R.N.Z.R.A. Rahman, I. Caracelli, C.-H. Ng, *Biometals*, (2010), **23,** 99.

[112] T.P. Stanojkovic, D. K. -Demertzi, A. Primikyri, I.G. -Santos, A. Castineiras, Z. Juranic, M.A. Demertzi, *J. Inorg. Biochem.,* (2010), **104**, 467.

[113] S. Mueller, M. Schittenhelm, F. Honecker, E. Malenke, K. Lauber, S. Wesselborg, J.T. Hartmann, C. Bokemeyer, F. Mayer, *Int. J. Oncol.,* (2006), **29**, 471.

[114] W.A. Collier, *Z. Hyg. Infektionskr,* (1929), **110**, 169.

[115] A.J. Crowe, *Drugs, Fut.,* (1987), **12**, 1255.

[116] M. Gielen, Ed.: Tin Based Antitumor drugs, Springer-Verlag, Berlin, (1990).

[117] M. Gielen, *Appl. Organomet. Chem.,* (2002), **16,** 481 and references therein.

[118] P.J. Blower, *Annu. Rep. Prog, Chem., Sect. A,* (2004), **100,** 633.

[119] F. Marchetti, C. Pettinari, A. Cingolani, L. Brocanelli, M. Rossi, F. Caruso, *J. Organomet. Chem.,* (2002), **645**, 134.

[120] F. Huber, R. Schmiedgen, M. Schurmann, R. Barbieri, G. Ruisi, A. Silvestri, *Appl. Organomet. Chem.,* (1997), **11**, 869.

[121] C. Ma, J. Zhang, R. Zhang, *Can. J. Chem.,* (2003), **81**, 1070.

[122] L. Pellerito, L. Nagy, *Coord. Chem. Rev.,* (2002) **224**, 111.

[123] X. Song, A. Zapata, G. Eng, *J. Organomet. Chem.,* (2006), **691**, 1756.

[124] (a) Q. Li, R-L. Liu, J.-J. Huang, P. Yang, *Gaodeng Xuexiao Huaxue Xuebao,* (2000), **21**, 513; (b) J.S. Casas, E.E.Castellano, M.D. Couce, J.Ellena, A. Sanchez, J. L.Sanchez, J. Sordo, C.Taboada, *Inorg. Chem.*, (2004), **43**, 1957.

[125] M.Gielen, M. El Khloufi, M. Biesemans, R.Willem, *Appl. Organomet. Chem.*, (1993), 7, 119.

[126] M. Gielen, M. Biesemans, A. El Khloufi, J. Meunier-Piret, F. Kayser, R.J. Willem, *Fluorine Chem.*, (1992), **64**, 279.

[127] C. C. Camacho, D. De Vos, R. Mahieu, M. Gielen, M. Kemmer, M. Bieseman, R. Willem, *Main Group Met. Chem.,* (2000), **23**, 381.

[128] C. Syng.-Ai, B. T. S. Basu, A. Chatterjee, *Mutat. Res.*, (2002), **513**, 49.

[129] C. Syng.-Ai, B. Basu, S. Tushar, A. Chatterjee, *J. Environm. Path. Toxic. Oncol.*, (2001), **20**, 333.

[130] H. Dai, H. Wang, S. Yue, X. Yang, H. Pan, X. Chen. D. S. Xuebao, *Ziran Kexueban.*, (1998), **2**, 43.

[131] M. Hanif, M. Hussain, S. Ali, M.H. Bhatti, M.S. Ahmed, B. Mirza, H.S. Evans, *Polyhedron*, (2010), **29**, 613.

[132] R. Barbieri, A. Silvestri, A.M. Giuliani, V.S. Piro, G. Madonia, *Dalton Trans.* (1992), 585.

[133] Q. Li, P. Yang, H. Wang, T. Bakas, A.S. -Diaz, C. Charalambopoulos, J. Tsangaris, N. Hadjiliadis, *J. Inorg. Biochem.*, (1996), **64,** 181.

[134] Z. Yang, T. Bakas, A.S. -Diaz, C. Charalampopoulos, J. Tsangaris, N. Hadjiliadis, *J. Inorg. Biochem.* (1998), **72,** 133.

[135] H. Barátné-Jankovics, L. Nagy, L. Pellerito, N. Buzás, R. Barbieri. *J. Inorg. Biochem.*, (2002), **92**, 55 .

[136] M. Chauhan, K. Banerjee, F. Arjmand, *Inorg. Chem.*, (2007), **46**, 3072.

[137] C.A. Bolos, K.T. Papazisis, A.H. Kortsaris, S. Voyatzi, D. Zambouli. D.A. Kyriakidis, *J. Inorg. Biochem.*, (2002), **88**, 25.

[138] P. deHoog, C. Boldron, P. Gamez, K. Sliedregt-Bol, I. Rolland, M. Pitie, R. Kiss, B. Meunier, J. Reedijk, *J. Med. Chem.*, (2007), **50,** 3148.

[139] A. Herman, J.M. Tanski, M.F. Tibbetts, C.M. Anderson, *Inorg. Chem.*, (2008), **47**, 274.

[140] W. Seanger, Principles of Nucleic Acid Structure, Berlin, Springer, (1984).

[141] A.L. Harris, X. Yang, A. Hegmans, L. Povirk, J. J. Ryan, L. Kelland, N. P. Farrell, *Inorg. Chem.*, (2005), **44**, 9598.

[142] U. Chaveerach, A. Meenongwa, Y. Trongpanich, C. Soikum, P. Chaveerach, *Polyhedron,* (2010), **29,** 731.

[143] W.J. Geary, Coord. Chem. Rev. (1971), **7**, 81.

[144] J. Marmur, *J. Mol. Biol.*, (1961), **3**, 208.

[145] M.E. Reichmann, S.A. Rice, C.A. Thomas, P. Doty, *J. Am. Chem. Soc.*, (1954) **76**, 3047.

[146] A. Wolfe, G.H. Shimer, T. Meehan, *Biochemistry*, (1987), **26,** 6392.

[147] J. R. Lakowiez, G. Webber, *Biochemistry*, (1973), **12**, 4161.

[148] G.D. Liu, J.P. Liao, Y.Z. Fang, S.S. Huang, G.L. Sheng, R.Q. Yu, *Anal. Sci.*, (2002), **18,** 391.

[149] H.H. Willard, L.L. Merritt jr., J.A. Dean, F.A. Settle jr., Instrumental Method of Analysis, CBS Publishers and Distributors, Delhi, (1986).

[150] A.J. Bard, L.R. Faulkner, Electrochemical Methods; Fundamentals and Applications, Wiley and Sons, New York, (1980).

[151] G. Cohen, H. Eisenberg, *Biopolymers*, (1969), **8**, 45.

[152] A. Kornberg, T.A. Baker, DNA Replication, University Science Books, Sausalito, California, (2006).

[153] S.H. vanRijt, A.F.A. Peacock, R.D.L. Johnstone, S. Parsons, P.J. Sadler, *Inorg. Chem.*, (2009), **48,** 1753.

[154] D. A. Bruce, *J. Chem. Cryst.*, (2003), **33**, 569.

[155] M. Casadesus, M.P. Coogan, E. Davies, L.-L. Ooi, *Inorg. Chim. Acta.*, (2008), **361,** 63.

[156] K.-Y. Choi, M.-J. Kim, D.-S. Kim, Y.-S. Kim, J.-H. Kim, H. Ryu, Y.-M. Lim, S.-G. Kang, U.-S. Shin, K.-C. Lee, C.-P. Hong, *Bull. Korean Chem. Soc.*, (2002), **23,** 1062.

[157] G. Kumar, E.M.R. Kiremire, *Chemistry,* (2007), **16,** 386.

[158] R.K. Dubey, U.K. Dubey, C.M. Mishra, *Ind. J. Chem.*, (2008), **47A**, 1208.

[159] M.S. Nair, R.S. Joseyphus, *Spectrochim. Acta,* (2007), **70,** 749.

[160] M A. Affan, Y.Z. Liew, F.B. Ahmad, M.B. Shamsuddin, B.M. Yamin, *Ind. J. Chem.*, (2007), **46A,** 1063.

[161] M. Nath, S. Goyal, G. Eng, D. Whalen, *Bull. Chem. Soc. Jpn.*, (1996), **69,** 605.

[162] V.-T. Yilmaz, Y. Topcu, F. Yilmaz, C. Thoene, *Polyhedron,* (2001), **20**, 3209.

[163] M.J. Belousoff, M.B. Duriska, B. Graham, S.R. Batten, B. Moubaraki, K.S. Murray, L. Spiccia, *Inorg. Chem.*, (2006), **45,** 3746.

[164] K. Kurdziel, T. Glowiak, J. Jezierska, *Polyhedron,* (2002), **21,** 1857.

[165] B. J. Hathaway, D. E. Billing, *Coord. Chem. Rev.*, (1970), **5,** 143.

[166] S. Chandra, S. Raizada, M. Tyagi, A. Gautam, *Bioinorg. Chem. Appl.*, (2007), **2007**, 51483.

[167] R. Carballo, A. Castineiras, S. Balboa, B. Covelo, J. Niclos, *Polyhedron*, (2002), **21,** 2811.

[168] S.M. Annigeri, A.D. Naik, U.B. Gangadharamath, V.K. Revankar, V.B. Mahalo, *Transition Met. Chem.*, (2002), **27,** 316.

[169] E. Spodine, Y. Moreno, M.T. Garland, O. Pena, R. Baggio, *Inorg. Chim. Acta.*, (2000), **309,** 57.

[170] P.D. Knight, A.J.P. White, C.K. Williams, *Inorg. Chem.*, (2008), **47**, 11711.

[171] T. Ahamad, S.M. Alshehri, *Bioinorg. Chem. Appl.*, (2010), **2010**, 976901.

[172] M. Bera, G.T. Musie, D.R. Powell, *Inorg. Chem. Commun.*, (2008), **11**, 293.

[173] C. Pettinari, F. Caruso, N. Zaffaroni, R. Villa, F. Marchetti, R. Pettinari, C. Phillips, J. Tanski, M. Rossi, *J. Inorg. Biochem.*, (2006), **100**, 58.

[174] Q.S. Li, P. Yang, H.F. Wang, M.L. Guo, *J. Inorg. Biochem.*, (1996), **64,** 181.

[175] J. Liu, H. Zhang, C. Chen, H. Deng, T. Lu, L. Ji, *Dalton Trans.*, (2003), 114.

[176] N. Hoti, D. Zhu, Z.S. Song, Z. Wu, S. Tabassum, M. Wu, *J. Pharmacol. Exp. Ther.*, (2004), **311**, 22.

[177] F. Liu, K.A. Meadows, D.R. McMillan, *J. Am. Chem. Soc.*, (1993), **115,** 6699.

[178] C. Tu, Y. Shao, N, Gan, Q. Xu, Z. Guo, *Inorg. Chem.*, (2004), **43**, 4761.

[179] N. Chitrapriya, V. Mahalingam, M. Zeller, H. Lee, K. Natrajan, *J. Mol. Str.*, Article in Press.

[180] T. Matsubara, K. Hirao, *J. Mol. Str. (Theochem)*, (2002), **581**, 203.

[181] A. Raja, V. Rajindiran, P.U. Maheswari, R. Balamurugan, C.A. Kilner, M.A. Halcrow, M. Palaniandavar, *J. Inorg. Biochem.*, (2005), **99**, 1717.

[182] K. Midorikawa, S. Kawanishi, *FEBS Lett.*, (2001), **495**, 187.

[183] J.H. Kang, W.S. Eum., *Biochim. Biophys. Acta,* (2000), **1524**, 162.

[184] F.-Y. Wu, F.-Y. Xie, Y.-M. Wu, J.-I. Hong, *J. Fluoresc.*, (2008), **18,** 175.

[185] J.B. Lepecq, C. Paoletti, *J. Mol. Biol.*, (1967), **27,** 87.

[186] M.T. Carter, M. Rodriguez, A.J. Bard, *J. Am. Chem. Soc.*, (1989). **111,** 8901.

[187] T.W. Welch, H.H. Thorp, *J. Phys. Chem.*, (1996), **100,** 13829.

[188] M.T. Carter, A.J. Bard, *J. Am. Chem. Soc.*, (1987), **109,** 7528.

[189] Y. Xiong, X.F. He, X.H. Zou, J.Z. Wa, X.M. Chen, L.N. Ji, R.H. Li, J.Y. Zhou, R. Yu, *Dalton Trans.*, (1999), 19.

[190] S. Satyanarayana, J.C. Dabrowiak, J.B. Chaires, *Biochemistry*, (1993), **32**, 2573.

[191] J. Chen, X. Wang, Y. Shao, J. Zhu, Y. Zhu, Y. Li, Q. Xu, Z. Guo, *Inorg. Chem.*, (2007), **46,** 3306.

[192] C.A. Detmer III, F.V. Pamatong, J.R. Bocarsly, *Inorg. Chem.*, (1996), **35**, 6292.

[193] C.A. Detmer III, F.V. Pamatong, J.R. Bocarsly, *Inorg. Chem.*, (1997), **36**, 3676.

[194] E. Trotta, N.D. Grosso, M. Erba, M. Paci, *Biochemistry*, (2000), **39**, 6799.

[195] P. Wittung, P. Nielson, B. Nórden, *J. Am. Chem. Soc.*, (1996), **118**, 7049.

[196] M.S. -Niasari, S.H. Banitaba, *J. Mol. Catal. A: Chemical*, (2003), **201**, 43.

[197] S. Das, S. Pal, *J. Mol. Str.*, (2005), **741**, 183.

[198] S. Chattopadhyay, M.S. Ray, S. Chaudhuri, G. Mikhopadhyay, G. Bocelli, A. Cantoni, A. Ghosh, *Inorg. Chim. Acta.*, (2006), **359**, 1367.

[199] L. Tian, H. Yang, X. Zheng, Z. Ni, D. Yan, L. Tu, J. Jiang, *Appl. Organomet. Chem.*, (2009), **23**, 24.

[200] M. Nath, S. Goyal, G. Eng, D. Whalen, *Bull. Chem. Soc. Jpn.*, (1996), **69**, 605.

[201] H.L. Singh, A.K.Varshney, *Bioinorg. Chem. Appl.*, (2006), **2006**, 23245.

[202] M. Pellei, G.G. Lobbia, M. Mancini, R. Spagna, C. Santini, *J. Organomet. Chem.*, (2006), **691**, 1615.

[203] N. Ancin, O. Celik, S.G. Öztas, S. İde, *Struct. Chem.*, (2007), **18**, 347.

[204] J-D. Lee, S-J Kim, D. Yoo, J. Ko, S. Cho, S.O. Kang, *Organometallics*, (2000), **19**, 1695.

[205] S. Özkar, D. Ülkü, L.T. Yildrim. N. Biricik, B. Gümgüm, *J. Mol. Str.*, (2004), **688**, 207.

[206] J.M. Rivera, D. Guzman, M. Rodriguez, J.F. Lemere, K. Nakatani, R. Santillan, P.G. Lacroix, N. Farfan, *J. Organomet. Chem.*, (2006), **691**, 1722.

[207] R. Shankar, A. Jain, A.P. Singh, G. Kociok-Kohn, K.C. Molloy, *Inorg. Chem.*, (2009), **48**, 3608.

[208] J. Holeček, M. Nádvornik, K. Handlír, A. Lyćka, *J. Organomet. Chem.*, (1986), **315**, 299.

[209] G. Han, P. Yang, *J. Inorg. Biochem.*, (2002), **91**, 230.

[210] V. Barba, E. Vega, R. Luna, H. Höpfl, H.I. Beltŕan, L.S. Z.-Rivera, *J. Organomet. Chem.*, (2007), **692**, 731.

[211] Y. Mantri, S.J. Lippard, M-H. Baik, *J. Am. Chem. Soc.*, (2007), **129**, 5023.

[212] S. Tabassum, C. Pettinari, *J. Organomet. Chem.*, (2006), **691**, 1761.

[213] F. Arjmand, M. Aziz, M. Chauhan, *J. Incl. Phenom. Macrocycl. Chem.*, (2008), **61**, 265.

[214] L. Ghys, M. Biesemans, M. Gielen, A. Garoufis, N. Hadjiliadis, R. Willem, J.C. Martins, *Eur. J. Inorg. Chem.*, (2000), 513.

[215] J.-H. Xu, F.-J. Chen, P.-X. Xi, X.-H. Liu, Z.-Z. Zeng, *J. Photochem. Photobiol. A: Chem.*, (2008), **196**, 77.

[216] F. Liu, K. Wang, G. Bai, Y. Zhang, L. Guo, *Inorg. Chem.*, (2004), **43**, 1799.

[217] F. Arjmand, Mohd. Muddassir, *Chirality*, Article in Press

[218]V.I. Ivanov, L.E. Minchenkova, A.K. Schyolkina, A.I. Polentayer, *Biopolymers,* (1973), **12,** 89.

[219] P. Tamilselvi, M. Palaniandavar, *Inorg. Chim. Acta.*, (2002), **337,** 420.

[220] A. Casini, L. Messori, P. Orioli, M. Gielen, M. Kemme, R. Willem, *J. Inorg. Biochem.*, (2001), **85**, 297.

[221] G.F. deSouza, V.M. Deflon, M.T.P. Gambardella, R.H.P. Francisco, J.D. Ardisson, E. Niquet, *Inorg. Chem.*, (2006), **45,** 4518.

[222] A. Tavman, B. Ülküseven, *Transition Met. Chem.*, (2000), **25,** 324.

[223] M.A. Abdellah, S.K. Hadjikakou, N. Hadjiliadis, M. Kubicki,T. Bakas, N. Kourkoumelis, Y.V. Simos, S. Karkabounas, M.M. Barsan, I.S. Butler, *Bioinorg. Chem. Appl.* (2009), **2009,** 542979.

[224] E. Katsoulakou, M. Tiliakos, G. Papaefstathiou, A. Terzis, C. Raptopoulou, G. Geromichalos, K. Papazisis, R. Papi, A. Pantazaki, D. Kyriakidis, P. Cordopatis, E. M.-Zoupa, *J. Inorg. Biochem.*, (2008), **102**, 1397.

[225] L. Tian, Z. Sheng, X. Zheng, Y. Sun, Y. Yu, B. Qian, X. Liu, *Appl. Organomet. Chem.*, (2006), **20**, 74.

[226] C. Ma, Y. Han, R. Zhang, D. Wang, *Dalton Trans.*, (2004), 1832.

[227] F. Marchetti, C. Pettinari, A. Cingolani, R. Pettinari, M. Rossi, F. Caruso, *J. Organomet. Chem.*, (2002), **645**, 134.

[228] H. Xu, K. Zheng, Y. Chen, Y.Z. Li, L.J. Lin, H. Li, P.X. Zhang, L.N. Ji, *Dalton Trans.*, (2003), 2260.

[229] L.-F. Tan, H. Chao, K.-C. Zhen, J.-J. Fei, F. Wang, Y.-F. Zhou, L.-N. Ji, *Polyhedron,* (2007), **26**, 5458.

[230] T.S. Basu Baul, A. Mizar, A. Lyčka, E. Rivarola, R. Jirásko, M. Holčapek, D. deVos, U. Englert, *J. Organomet. Chem.*, (2006), **691**, 3413.

[231] A. Sebald, Advanced Applications of NMR to Organometallic Chemistry, Solid State NMR Applications in Organotin and Organolead Chemistry, John Wiley and Sons, Chichester, U.K. (1996).

[232] C. Pettinari, Heteronuclear NMR Applications (Ge, Sn, Pb), Encyclopedia of spectroscopy and Spectrometry, J.C. Lindon, Ed:, Academic Press, London, (1999).

[233] M.N. Xanthopoulou, S.K. Hadjikakou, N. Hadjiliadis, *Inorg. Chem.*, (2007), **46**, 1187.

[234] C.D. Nicola, A. Galindo, J.V. Hanna, F. Marchetti, C. Pettinari, R. Pettinari, E. Rivarola, B.W. Skelton, A.H. White, *Inorg. Chem.*, (2005), **44**, 3094.

[235] P.M. Krishna, K.H. Reddy, P.G. Krishna, G.H. Phillip, *Ind. J. Chem*, (2007), **46A**, 904.

[236] S. Kashanian, N. Shahabadi, H. Roshanfekr, K. Shalmashi, K. Omidfar, *Biochemistry (Moscow)*, (2008), **73**, 929.

[237] A. Janscó, L. Nagy, E. Moldrheim, E. Sletten, *Dalton Trans.*, (1999), 1587.

[238] R.W. Gellert, R. Bau, Metal ions in Biological Systems, H. Siegel, Ed:. Marcel Dekker, New York, (1979).

[239] C. Hiort, P. Lincoln, B. Nordén, *J. Am. Chem. Soc.*, (1993), **115**, 3448.

[240] C.V. Kumar, E.H. Asuncion, J.K. Barton, N.J. Turro, *J. Am. Chem Soc.*, (1993), **115**, 8547.

[241] C.V. Kumar, E.H.A. Punzalan, W.B. Tan, *Tetrahedron*, (2007), **56**, 7027.

[242] M.-J.R.P. Queiroz, E.M.S. Castanheira, T.C.T. Lopes, Y.K. Cruz, G. Kirsch. *J. Photochem. Photobiol A: Chem.*, (2007), **190**, 45.

[243] A. Rodger, B. Nordén, Circular Dichroism and Linear Dichroism, Oxford Chemistry Press, UK, (1997).

[244] S. Mahadevan, M. Palaniandavar, *Inorg. Chim. Acta.*, (1997), **254**, 291.

[245] A. Majumder, G.M. Rosair, A. Mallick, N. Chattopadhyay, S. Mitra, *Polyhedron*, (2006), **25**, 1753.

[246] B. Selvakumar, V. Rajendiran, P.U. Maheshwari, H. Stoeckli-Evans, M. Palaniandavar, *J. Inorg. Biochem.*, (2006), **100**, 316.

[247] Y. Li, Z.-Y. Yang, *J. Fluoresc.*, (2010), **20**, 329.

[248] K. Serbest, H. Kayi, M. Er, K. Sancak, I. Değirmencioğlu, *Heteroatom Chem.*, (2008), **19**, 700.

[249] M. Belicchi-Ferrari, F. Bisceglie, G. Pelosi, P. Tarasconi, *Polyhedron*, (2008), **27**, 1361.

[250] R.N. Patel, V.L.N. Gundla, D.N. Patel, *Ind. J. Chem.*, (2008), **47A**, 353.

[251] G. Batra, P. Mathur, *Inorg. Chem.*, (1992), **31**, 1575.

[252] B.J. Hathaway, A.A.G. Tomlinson, *Coord. Chem Rev.*, (1970), **5**, 24.

[253] M.A. Ali, M.T.F. Tarafdar, *J. Inorg. Nucl. Chem.*, (1977), **39**, 1785.

[254] V. Philip, V. Suni, M.R.P. Kurup, M. Nethaji, *Polyhedron*, (2004), **23**, 1225.

[255] M.A. Ibrahim, K.M. El-Mahdy, *Phosphorus, Sulfur, and Silicon*, (2009), **184**, 2958.

[256] S.-H. Hsieh, Y.-P. Kuo, H.-M. Gau, *Dalton Trans.*, (2007), 97.

[257] D.R. McMillan, K.M. McNett, *Chem. Rev.*, (1998), **98**, 1201.

[258] G. Raner, J. Goodisman, J.C. Dabrowiak, *ACS. Symp. Ser.*, American Chemical Society, Washington D.C., (1989), **402**, 74.

[259] L.A. Lipscomb, F.X, Zhou, S.R. Presnell, R.J. Woo, M.E. Peek, R.R. Plaskon, L.D. Williams, *Biochemistry*, (1996), **35**, 2818.

[260] C.L. Liu, J.Y. Zhou, Q.X. Li, L.J. Wang, Z.R. Liao, H.B. Xu, *J. Inorg. Biochem.*, (1999), **75**, 233.

[261] N. Grover, T.W. Welch, T.A. Fairley, M. Cory, H.H. Thorp, *Inorg. Chem.*, (1994), **33**, 3544.

[262] K. Bielawaski, S. Wolczynski, A. Bielawska, *Biol. Pharm. Bull.*, (2001), **24**, 70.

[263] L. Lomozik, A. Gosowska, G. Krzysko, *J. Inorg. Biochem.*, (2006), **100**, 1781.

[264] A. Gosowska, *J. Inorg. Biochem.*, (2005), **8**, 1698.

[265] M.-H. Baik, R.A. Friesner, S.J. Lippard, *J. Am. Chem. Soc.*, (2003), **125**, 14082.

[266] T.M. Fletcher, F.A. Whalmsley, *J. Inorg. Biochem.*, (1997), **68**, 239.

[267] A.H.J. Wang, *Curr. Opin. Struct. Biol.* (1992), **2**, 361.

[268] L. Fin, P.J. Yang, *J. Inorg. Biochem.*, (1997), **68**, 79.

[269] Y. Li, Y. Wu, J. Zhao, P. Yang, *J. Inorg. Biochem.*, (2007), **101**, 283.

[270] M. Roy, T. Bowmick, R. Santhanagopal, S. Ramakumar, A.R. Chakravarty, Dalton Trans, (2009), 4671.

[271] K. Kiridi, A. Garoufis, A. Tsipis, N. Hadjiliadis, H. Dulk, J. Reedijk, *Dalton Trans.*, (2005), 1176.

[272] Y. Jung, S.J. Lippard, *Chem. Rev.*, (2007), **107**, 1387.